

GLOBAL JOURNAL

OF SCIENCE FRONTIER RESEARCH: A

Physics and Space Science

The Modified Interfacial Gravity

IRNSS Satellite Parameter Estimation

Highlights

New Type of Hypothetical Venusian

First Observations of Thermal Surface

Discovering Thoughts, Inventing Future

VOLUME 15

ISSUE 3

VERSION 1.0



GLOBAL JOURNAL OF SCIENCE FRONTIER RESEARCH: A
PHYSICS & SPACE SCIENCE



GLOBAL JOURNAL OF SCIENCE FRONTIER RESEARCH: A
PHYSICS & SPACE SCIENCE

VOLUME 15 ISSUE 3 (VER. 1.0)

OPEN ASSOCIATION OF RESEARCH SOCIETY

© Global Journal of Science
Frontier Research. 2015.

All rights reserved.

This is a special issue published in version 1.0
of "Global Journal of Science Frontier
Research." By Global Journals Inc.

All articles are open access articles distributed
under "Global Journal of Science Frontier
Research"

Reading License, which permits restricted use.
Entire contents are copyright by of "Global
Journal of Science Frontier Research" unless
otherwise noted on specific articles.

No part of this publication may be reproduced
or transmitted in any form or by any means,
electronic or mechanical, including
photocopy, recording, or any information
storage and retrieval system, without written
permission.

The opinions and statements made in this
book are those of the authors concerned.
Ultrapublishing has not verified and neither
confirms nor denies any of the foregoing and
no warranty or fitness is implied.

Engage with the contents herein at your own
risk.

The use of this journal, and the terms and
conditions for our providing information, is
governed by our Disclaimer, Terms and
Conditions and Privacy Policy given on our
website [http://globaljournals.us/terms-and-condition/
menu-1463/](http://globaljournals.us/terms-and-condition/menu-1463/)

By referring / using / reading / any type of
association / referencing this journal, this
signifies and you acknowledge that you have
read them and that you accept and will be
bound by the terms thereof.

All information, journals, this journal,
activities undertaken, materials, services and
our website, terms and conditions, privacy
policy, and this journal is subject to change
anytime without any prior notice.

Incorporation No.: 0423089
License No.: 42125/022010/1186
Registration No.: 430374
Import-Export Code: 1109007027
Employer Identification Number (EIN):
USA Tax ID: 98-0673427

Global Journals Inc.

(A Delaware USA Incorporation with "Good Standing"; Reg. Number: 0423089)

Sponsors: *Open Association of Research Society*
Open Scientific Standards

Publisher's Headquarters office

Global Journals Headquarters
301st Edgewater Place Suite, 100 Edgewater Dr.-Pl,
Wakefield MASSACHUSETTS, Pin: 01880,
United States of America
USA Toll Free: +001-888-839-7392
USA Toll Free Fax: +001-888-839-7392

Offset Typesetting

Global Journals Incorporated
2nd, Lansdowne, Lansdowne Rd., Croydon-Surrey,
Pin: CR9 2ER, United Kingdom

Packaging & Continental Dispatching

Global Journals
E-3130 Sudama Nagar, Near Gopur Square,
Indore, M.P., Pin:452009, India

Find a correspondence nodal officer near you

To find nodal officer of your country, please
email us at local@globaljournals.org

eContacts

Press Inquiries: press@globaljournals.org
Investor Inquiries: investors@globaljournals.org
Technical Support: technology@globaljournals.org
Media & Releases: media@globaljournals.org

Pricing (Including by Air Parcel Charges):

For Authors:

22 USD (B/W) & 50 USD (Color)
Yearly Subscription (Personal & Institutional):
200 USD (B/W) & 250 USD (Color)

INTEGRATED EDITORIAL BOARD
(COMPUTER SCIENCE, ENGINEERING, MEDICAL, MANAGEMENT, NATURAL
SCIENCE, SOCIAL SCIENCE)

John A. Hamilton, "Drew" Jr.,
Ph.D., Professor, Management
Computer Science and Software
Engineering
Director, Information Assurance
Laboratory
Auburn University

Dr. Henry Hexmoor
IEEE senior member since 2004
Ph.D. Computer Science, University at
Buffalo
Department of Computer Science
Southern Illinois University at Carbondale

Dr. Osman Balci, Professor
Department of Computer Science
Virginia Tech, Virginia University
Ph.D. and M.S. Syracuse University,
Syracuse, New York
M.S. and B.S. Bogazici University,
Istanbul, Turkey

Yogita Bajpai
M.Sc. (Computer Science), FICCT
U.S.A. Email:
yogita@computerresearch.org

Dr. T. David A. Forbes
Associate Professor and Range
Nutritionist
Ph.D. Edinburgh University - Animal
Nutrition
M.S. Aberdeen University - Animal
Nutrition
B.A. University of Dublin- Zoology

Dr. Wenying Feng
Professor, Department of Computing &
Information Systems
Department of Mathematics
Trent University, Peterborough,
ON Canada K9J 7B8

Dr. Thomas Wischgoll
Computer Science and Engineering,
Wright State University, Dayton, Ohio
B.S., M.S., Ph.D.
(University of Kaiserslautern)

Dr. Abdurrahman Arslanyilmaz
Computer Science & Information Systems
Department
Youngstown State University
Ph.D., Texas A&M University
University of Missouri, Columbia
Gazi University, Turkey

Dr. Xiaohong He
Professor of International Business
University of Quinnipiac
BS, Jilin Institute of Technology; MA, MS,
PhD,. (University of Texas-Dallas)

Burcin Becerik-Gerber
University of Southern California
Ph.D. in Civil Engineering
DDes from Harvard University
M.S. from University of California, Berkeley
& Istanbul University

Dr. Bart Lambrecht

Director of Research in Accounting and Finance
Professor of Finance
Lancaster University Management School
BA (Antwerp); MPhil, MA, PhD
(Cambridge)

Dr. Carlos García Pont

Associate Professor of Marketing
IESE Business School, University of Navarra
Doctor of Philosophy (Management),
Massachusetts Institute of Technology (MIT)
Master in Business Administration, IESE,
University of Navarra
Degree in Industrial Engineering,
Universitat Politècnica de Catalunya

Dr. Fotini Labropulu

Mathematics - Luther College
University of Regina
Ph.D., M.Sc. in Mathematics
B.A. (Honors) in Mathematics
University of Windsor

Dr. Lynn Lim

Reader in Business and Marketing
Roehampton University, London
BCom, PGDip, MBA (Distinction), PhD,
FHEA

Dr. Mihaly Mezei

ASSOCIATE PROFESSOR
Department of Structural and Chemical
Biology, Mount Sinai School of Medical
Center
Ph.D., Eötvös Loránd University
Postdoctoral Training,
New York University

Dr. Söhnke M. Bartram

Department of Accounting and Finance
Lancaster University Management School
Ph.D. (WHU Koblenz)
MBA/BBA (University of Saarbrücken)

Dr. Miguel Angel Ariño

Professor of Decision Sciences
IESE Business School
Barcelona, Spain (Universidad de Navarra)
CEIBS (China Europe International Business School).
Beijing, Shanghai and Shenzhen
Ph.D. in Mathematics
University of Barcelona
BA in Mathematics (Licenciatura)
University of Barcelona

Philip G. Moscoso

Technology and Operations Management
IESE Business School, University of Navarra
Ph.D in Industrial Engineering and Management, ETH Zurich
M.Sc. in Chemical Engineering, ETH Zurich

Dr. Sanjay Dixit, M.D.

Director, EP Laboratories, Philadelphia VA
Medical Center
Cardiovascular Medicine - Cardiac
Arrhythmia
Univ of Penn School of Medicine

Dr. Han-Xiang Deng

MD., Ph.D
Associate Professor and Research
Department Division of Neuromuscular
Medicine
Department of Neurology and Clinical
Neuroscience
Northwestern University
Feinberg School of Medicine

Dr. Pina C. Sanelli

Associate Professor of Public Health
Weill Cornell Medical College
Associate Attending Radiologist
NewYork-Presbyterian Hospital
MRI, MRA, CT, and CTA
Neuroradiology and Diagnostic
Radiology
M.D., State University of New York at
Buffalo, School of Medicine and
Biomedical Sciences

Dr. Roberto Sanchez

Associate Professor
Department of Structural and Chemical
Biology
Mount Sinai School of Medicine
Ph.D., The Rockefeller University

Dr. Wen-Yih Sun

Professor of Earth and Atmospheric
SciencesPurdue University Director
National Center for Typhoon and
Flooding Research, Taiwan
University Chair Professor
Department of Atmospheric Sciences,
National Central University, Chung-Li,
TaiwanUniversity Chair Professor
Institute of Environmental Engineering,
National Chiao Tung University, Hsin-
chu, Taiwan.Ph.D., MS The University of
Chicago, Geophysical Sciences
BS National Taiwan University,
Atmospheric Sciences
Associate Professor of Radiology

Dr. Michael R. Rudnick

M.D., FACP
Associate Professor of Medicine
Chief, Renal Electrolyte and
Hypertension Division (PMC)
Penn Medicine, University of
Pennsylvania
Presbyterian Medical Center,
Philadelphia
Nephrology and Internal Medicine
Certified by the American Board of
Internal Medicine

Dr. Bassey Benjamin Esu

B.Sc. Marketing; MBA Marketing; Ph.D
Marketing
Lecturer, Department of Marketing,
University of Calabar
Tourism Consultant, Cross River State
Tourism Development Department
Co-ordinator , Sustainable Tourism
Initiative, Calabar, Nigeria

Dr. Aziz M. Barbar, Ph.D.

IEEE Senior Member
Chairperson, Department of Computer
Science
AUST - American University of Science &
Technology
Alfred Naccash Avenue – Ashrafieh

PRESIDENT EDITOR (HON.)

Dr. George Perry, (Neuroscientist)

Dean and Professor, College of Sciences

Denham Harman Research Award (American Aging Association)

ISI Highly Cited Researcher, Iberoamerican Molecular Biology Organization

AAAS Fellow, Correspondent Member of Spanish Royal Academy of Sciences

University of Texas at San Antonio

Postdoctoral Fellow (Department of Cell Biology)

Baylor College of Medicine

Houston, Texas, United States

CHIEF AUTHOR (HON.)

Dr. R.K. Dixit

M.Sc., Ph.D., FICCT

Chief Author, India

Email: authorind@computerresearch.org

DEAN & EDITOR-IN-CHIEF (HON.)

Vivek Dubey(HON.)

MS (Industrial Engineering),

MS (Mechanical Engineering)

University of Wisconsin, FICCT

Editor-in-Chief, USA

editorusa@computerresearch.org

Sangita Dixit

M.Sc., FICCT

Dean & Chancellor (Asia Pacific)

deanind@computerresearch.org

Suyash Dixit

(B.E., Computer Science Engineering), FICCTT

President, Web Administration and

Development , CEO at IOSRD

COO at GAOR & OSS

Er. Suyog Dixit

(M. Tech), BE (HONS. in CSE), FICCT

SAP Certified Consultant

CEO at IOSRD, GAOR & OSS

Technical Dean, Global Journals Inc. (US)

Website: www.suyogdixit.com

Email: suyog@suyogdixit.com

Pritesh Rajvaidya

(MS) Computer Science Department

California State University

BE (Computer Science), FICCT

Technical Dean, USA

Email: pritesh@computerresearch.org

Luis Galárraga

J!Research Project Leader

Saarbrücken, Germany

CONTENTS OF THE ISSUE

- i. Copyright Notice
 - ii. Editorial Board Members
 - iii. Chief Author and Dean
 - iv. Contents of the Issue
-
1. First Observations of Thermal Surface Energy and of the Thermal Evolution Process. *1-49*
 2. The Origin of, Maxwell`S - Gravity`S, Displacement Current. *51-86*
 3. IRNSS Satellite Parameter Estimation using Combination Strategy. *87-95*
 4. New Type of Hypothetical Venusian Fauna Found at the *Venera-14* Landing Site. *97-104*
 5. A Physicist Description of Indigenous Telecobalt Machine Bhahbhatron-II TAW. *105-110*
 6. The Modified Interfacial Gravity: Unifying CDM, MOG, and MOND. *111-117*
 7. Electronic Transport Properties in Bulk ZnO and $Zn_{1-x}Mg_xO$ Using Monte Carlo Simulation. *119-125*
-
- v. Fellows and Auxiliary Memberships
 - vi. Process of Submission of Research Paper
 - vii. Preferred Author Guidelines
 - viii. Index



GLOBAL JOURNAL OF SCIENCE FRONTIER RESEARCH: A
PHYSICS AND SPACE SCIENCE
Volume 15 Issue 3 Version 1.0 Year 2015
Type : Double Blind Peer Reviewed International Research Journal
Publisher: Global Journals Inc. (USA)
Online ISSN: 2249-4626 & Print ISSN: 0975-5896

First Observations of Thermal Surface Energy and of the Thermal Evolution Process

By A. Titov

Yeditepe University, Turkey

Abstract- Using a developed technique of synchronous differential temperature measurements, the existence of the thermal surface energy (TSE) has been demonstrated with a huge signal-to-noise ratio in material artifacts, made of a homogeneous material, when these artefacts are irradiated by an external electromagnetic (EM) field. The TSE, presenting the energy of the oriented motion of the coupled field-particles system inside a solid-state artifact, is shown experimentally to be linearly related to the Poynting vector of the external EM field, and it results in the appearance of the thermal hysteresis effect, which is irreversible in time and has no symmetry in space. The experiments, presented in this paper, have shown that the principle of superposition is not valid for EM fields in case of TSE, so that the *thermal evolution process*, which inevitably includes the changing in time and in space the variations of the thermal surface energy, *is characterized by the infinite number of correlated influence factors.*

Keywords: *surface energy, temperature definition, hysteresis, fourier theory, evolution process.*

GJSFR-A Classification : *FOR Code: M00*



Strictly as per the compliance and regulations of :



First Observations of Thermal Surface Energy and of the Thermal Evolution Process

A. Titov

Abstract- Using a developed technique of synchronous differential temperature measurements, the existence of the thermal surface energy (TSE) has been demonstrated with a huge signal-to-noise ratio in material artifacts, made of a homogeneous material, when these artefacts are irradiated by an external electromagnetic (EM) field. The TSE, presenting the energy of the oriented motion of the coupled field-particles system inside a solid-state artifact, is shown experimentally to be linearly related to the Poynting vector of the external EM field, and it results in the appearance of the thermal hysteresis effect, which is irreversible in time and has no symmetry in space. The experiments, presented in this paper, have shown that the principle of superposition is not valid for EM fields in case of TSE, so that the *thermal evolution process*, which inevitably includes the changing in time and in space the variations of the thermal surface energy, *is characterized by the infinite number of correlated influence factors*. It is shown experimentally that the dependences on time of the thermal evolution process are specific for any particular point on the artifact surface, and that the corresponding hysteresis effect at each point is characterized by its local time. It is found also that the properties of the material artifact, at any time moment in the Universal Coordinated Time, depend crucially on the choice of the observation point on the artifact surface, and *the properties of the artifact at any point are continuously changing in time as a result of its interaction with the external EM field*. The presented studies give an experimental confirmation of Niels Bohr's fundamental observation that, in the general case, the adequate description of material objects in terms of the isotropic and homogeneous concepts of time and space is not possible. The new concept of temperature, presented in the paper, as the energy of the field-particle system of a macroscopic material object, which can be detected by its EM radiation and which includes the oriented motion of this system, is sufficient for the description of the thermal surface energy and extends the notion of temperature to open systems, beyond the approximation of the thermodynamic equilibrium conditions.

Keywords: surface energy, temperature definition, hysteresis, fourier theory, evolution process.

I. INTRODUCTION

In the opening speech at the XVII World Congress of the International Measurement Confederation, held in Rio de Janeiro in 2006, the Director of the National Metrology Institute Prof. A. Brandy was discussing the observation of American scientist "new discoveries are in the next decimal unit", and in this way he was emphasizing the role of precise measurements and

Author: Physics Department, Yeditepe University, Istanbul, Turkey.
e-mail: atitov@yeditepe.edu.tr

Metrology in scientific and industrial progress. The term "discovery" is used in the observation quite intentionally, meaning that with the experimental progress even the well-established physical concepts can be found in contradiction with the results of measurements, which are based on new methods or which realize significantly smaller level of uncertainties. This observation is in agreement with Niels Bohr's views on epistemology, who in accordance with L. Rosenfeld [1] has re-discovered dialectics and who "vividly realized that our proud theories are but temporary resting places of the mind on the unending road to knowledge. Such resting places, however, there must be, where we may taste the joys of knowledge, feel that we have reached a certain harmony between our mental picture of the world and our experience of it". In this respect, we can remind the original N. Bohr observation "*Isolated material particles are abstractions*, their properties being definable and observable only through their interaction with other systems". In 1958 Werner Heisenberg, when discussing the Copenhagen interpretation of Quantum theory, wrote "Our scientific work in physics consists in asking questions about nature in the language that we possess and trying to get an answer from experiment by the means at our disposal... It is understandable that in our scientific relation to nature our own activity becomes very important when *we have to deal with parts of nature into which we can penetrate only by using the most elaborate tools*". From these observations, it is easier to understand N. Bohr's remarks: "We must be clear that when it comes to atoms, language can be used only as in poetry. The poet, too, is not nearly so concerned with describing facts as with creating images and establishing mental connections."

"Physics is to be regarded not so much as the study of something *a priori* given, but rather as the development of methods of ordering and surveying human experience. In this respect our task must be to account for such experience in a manner independent of individual subjective judgment and therefore objective in the sense that it can be unambiguously communicated in ordinary human language."

"What is that we human beings ultimately depend on? We depend on our words. We are suspended in language. Our task is to communicate experience and ideas to others."

"In physics we again and again learn that *our task is not to investigate the essence of things*-we do not

at all know what this would mean; *but to develop those concepts that allow us to speak with each other about the events of nature in a fruitful manner.*"

"There is no quantum world. There is only an abstract quantum physical description. It is wrong to think that the task of physics is to find out how nature *is*. Physics concerns what we can say about Nature."

And quite interesting, but somewhat simplified summary of the ideas of N. Bohr we can find in the University text-book on Physics by D. Giancoly [2]. When discussing the wave-particle duality of light, D. Giancoly writes: "Part of the difficulty stems from how we think. Visual pictures (or models) in our minds are based on what we see in the everyday world. We apply the concepts of waves and particles to light because in the macroscopic world we see that energy is transferred from place to place by these two methods. We cannot see directly whether light is a wave, or particle— so we do *indirect experiments*. To explain the experiments, we apply the models of waves or of particles to the nature of light. *But these are the abstractions of the human mind*. There is no reason why light should conform to these models (or visual images) taken from macroscopic world. *The best we can do is recognize that our knowledge is limited to the indirect experiments*, and that in terms of everyday language and images, light reveals both wave and particle properties." [2a].

The new, revolutionary insights to N. Bohr's epistemology are giving the philosophical observations of Albert Einstein, associated with the last period of his scientific activity: "*No amount of experimentation can ever prove me right; a single experiment can prove me wrong*". This quote is of paramount importance and shows the crucial difference in the roles of the experimental and theoretical studies. Only one experiment can show that the theory is wrong. From the same observation it follows that in accordance with Karl Popper philosophical views no finite number of experiments can prove that the theory is correct, as only one experiment, performed under basically new conditions, can demonstrate the evident inconsistency of the approximations of the theoretical model of this theory with the properties of Nature. In this respect, it is also important to remind two other fundamental philosophical observations of A. Einstein: "I don't believe in mathematics.", and "As far as the laws of mathematics refer to reality, they are not certain; and as far as they are certain, they do not refer to reality".

These observations appear very close to one of the most important Niels Bohr's philosophical statements, which can be even found nowadays in the University text-books. For example, D. Giancoly in [2b] writes: "Perhaps the most important and influential philosopher of quantum mechanics was Bohr. *He argued that a space-time description of actual atoms and electrons is not possible*". The confirmation of this N. Bohr's point of view can be found in the letter of 1926

by Erwin Schrödinger to W. Wien: "*Bohr's standpoint, that a space-time description is impossible, I reject a limine*. Physics does not consist only of atomic research, science does not consist only of physics, and life does not consist only of science. The aim of atomic research is to fit our empirical knowledge concerning it into our other thinking. *All of this other thinking, so far as it concerns the outer world, is active in space and time. If it cannot be fitted into space and time, then it fails in its whole aim and one does not know what purpose it really serves*".

As it is clear from this quote, E. Schrödinger could not accept Niels Bohr's dialectic point of view, which, in Schrödinger's opinion, was in contradiction with the fundamental principles of the theoretical physics, existing at that time. In this respect, it is interesting to pay attention to the opinion of Paul A. M. Dirac, who in his article "*Reminiscences about a Great Physicist*" (published in 1990) wrote about N. Bohr: "*his arguments were mainly of a qualitative nature, and I was not able to really pinpoint the facts behind them. What I wanted was statements which could be expressed in terms of equations, and Bohr's work very seldom provided such statements*. I am really not sure how much later my work was influenced by these lectures of Bohr's... He certainly did not have a direct influence because *he did not stimulate one to think of new equations*". Probably, due to these reasons many theorists prefer to send this Bohr's observation to oblivion, in spite of fact that Albert Einstein (who is known for his "epoch-making contributions to the progress of natural philosophy") has written about Niels Bohr: "Not often in life has a human being caused me such joy by his mere presence as you did." and "*Nobody knows how the stand of our knowledge about the atom would be without him*. Personally, Bohr is one of the amiable colleagues I have met. *He utters his opinions like one perpetually groping and never like one who believes himself to be in possession of the truth*". These A. Einstein's observations are very close to the opinion of Robert Oppenheimer, who describing the process of great synthesis of atomic physics in 1920s, wrote: "It was a heroic time. It was not the doing of any one man; it involved the collaboration of scores of scientists from many different lands. *But from the first to last the deeply creative, subtle and critical spirit of Niels Bohr guided, restrained, deepened and finally transmuted the enterprise*". The estimate of Niels Bohr contribution by Arnold Sommerfeld is quite similar: "The theory of spectral lines will bear the name of Bohr for all time".

An important feature of N. Bohr's method of investigation was pointed out by W. Heisenberg in "*Physics and Philosophy*" (1958), where he wrote: "The first thing Bohr said to me was that it would only then be profitable to work with him if I understood that he was a dilettante. The only way I knew to react to this

unexpected statement was with a polite smile of disbelief. But evidently Bohr was serious. *He explained how he had to approach every new question from a starting point of total ignorance.* It is perhaps better to say that Bohr's strength lay in his formidable intuition and insight rather than erudition". Isidor I. Rabi in the book "*The Physicists*" (1978) adds to this: "When Bohr is about everything is somehow different. Even the dullest gets a fit of brilliancy". An interesting real episode is described in [1], when "one of Bohr's most faithful and eminent disciples, Weisskopf, who, after having discovered, not without effort, the explanation of a tricky case of complementarity put to him by a doubting experimenter, exclaimed, "*Bohr always wins!*".

Naturally, the conclusion under which conditions the space-time description of material systems is valid and in which cases (in accordance with N. Bohr statement) it is not possible, can be given only by the experiment, and it does not depend on how many prominent physicists supported, or rejected this observation. The presented quotes only emphasize specific features and differences of the points of view of several outstanding scientists on the basic philosophical problems of Physics and can help to elucidate the idea of the comparison of the mentioned philosophical standpoints with the results of the presented experimental studies, which are also supporting A. Einstein's observation about a quite special role of the experiment in the comprehension of the properties of Nature.

Speaking about the progress in high-precision experimental studies of the properties of macroscopic material objects, it is worth noting here that with the development of a new methods of optical length measurements by optical interferometry [3a] and with development of optical interferometers with the resolution below 0.05nm [3b, 3c], we have managed to demonstrate in [3d] the *process of gradual changes of the properties of the parts of the measurement system only as a result of electromagnetic interaction between them.* For example, the plots of Figs. 3 and 4 in [3d] characterize the surface deformations of the mono-crystal reference plate, arising in the wringing contact between the gauge block (GB) and the reference plate [4] as a result of electromagnetic interaction between the atoms of the reference plate and the atoms of the gauge block. In Fig.3 of [3d] we show the topography map of the surface deformations of crystalline plate, arising on the area of the plate surface that is not covered by the wringing contact. This map shows the value of the deformations (induced by the wringing contact) as a function of the location of the specified point of the free area of the plate relative to the position of the center of the wrung gauge block. The inset of Fig.3 presents the plots of the magnitudes of the surface deformations as a function of the time interval, elapsed after the realization of the wringing contact. These data

are presented for a couple of points, located symmetrically relative to the GB center. And as it follows from the plots of Figs. 4 and 5 in [3d], the central length of a gauge block [4, 5] is not constant, but presents some function of the time interval elapsed after the realization of the wringing procedure. Besides that, the central length of a GB, the main parameter of a material length standard that is used for the most accurate realization of the Metre [6], is different from the length of a free GB (see Fig.15 in [3e]) as a result of the presence of the surface texture deformations in the wringing contact (see Figs. 12 and 14 in [3e]). Thus, the presented experimental data have clearly demonstrated the existence of the *self-ordering evolution process, when the properties of a material artifact (GB) are gradually changing in time as a result of EM interaction between the two parts of the investigated system (GB and plate),* and the detection method is based on precise length measurements. But interferometric length measurements are closely related to temperature measurements, and in accordance with [5] temperature contribution gives one half of the total uncertainty of the long GB length measurement. For example, figure 4 in [5] shows that the 500mm GB (8 PTB 63) can be regarded as a very stable thermometer, as its length stability of $\sim 10.6\text{nm}$ for the time period of ~ 20 years corresponds to the temperature stability of $\sim 90\mu\text{K/year}$ and with the demonstrated uncertainty in a single measurement series of $\sim 1\text{mK}$. So, the presented above experimental results give a clear indication that the precise temperature measurements can be used for the detailed studies of the thermal self-ordering evolution process when interaction with the electromagnetic (EM) field is used both as a source of evolution process and also as a detection method of the induced variations of the properties of material objects. In this respect it is worthy of note that in recent years there were important advances in precise, traceable temperature measurements of material artifacts [3e-3h] in the temperature range close to 293.15K (20°C). (And all length measurement results should be reduced exactly to this temperature, in accordance with the established international practice). In [3e], for example, the temperature measurements in a water triple-point (WTP) cell [7a] with the random uncertainty of $1\mu\text{K}$ were demonstrated that gave the possibility to detect the evolution process in WTP cells, which are nowadays used for the definition of the temperature unit – Kelvin [7a]. In this case, the thermal evolution process manifests itself as a gradual change of the temperature of the standard (see Fig.8 in [3e]). The observed temperature of the WTP cell appears as a function of the time interval, elapsed after the application of the "thermal shock" that makes the ice mantle free [7a] in that temperature standard. When taking this time dependence into consideration and when comparing

the WTP cell temperatures, measured 1 hour after the application to the cell of the "thermal shock", the agreement between the two WTP cells, produced in Brazil and using the isotope composition of equatorial water [7a], was found to be less than $3\mu\text{K}$ (see Fig.2 in [3f]). Then, the similar approach was applied to the studies of gallium (Ga) standard [7a]: the mean temperature of the last hour of temperature plateau with the total duration of 16 hours in our standard was found to be the most reproducible one, and its time stability on a week interval (characterized by the standard deviation) was found to be about $2\mu\text{K}$ (see Fig.7 in [3e]), when measured by Rosemount standard platinum resistance thermometer [7a] (SPRT, model 162 CE) and a Guildline bridge (Model 9975), and about $12\mu\text{K}$ – for the measurements with a thermistor and high-precision Hp multi-meter (see Fig.9) [3g]. But the WTP and gallium standards are the only two standards that are needed to define traceable temperatures on ITS-90 [7a, 7b] close to 20 degrees C... So, when we combine this information with the possibility to perform the calibration of a couple of SPRT in a double-Dewar system within the uncertainty below $10\mu\text{K}$ (see Figs. 5 and 6 in [3h]) and with the demonstrated time stability of the whole measurement system of $\sim 9.1\mu\text{K}/\text{year}$ (see Fig.1 in [3h]), it is becoming clear that the progress in the reproducibility of the temperature measurements relative to the thermodynamic temperature is about two orders of magnitude, as even the temperature differences between the most complete studies of the primary level constant volume gas thermometers, performed by the groups of R. C. Kemp and D. N. Astrov, are reaching the value of 2.5mK at 250K , and more than 4mK at 200K (see Fig.2 in [8]). So, *there is a unique opportunity to apply in practice N. Bohr's approach of "renovation of the philosophy of science"[1] and to check experimentally if the model assumptions and predictions of some well-established physical theories, such as Thermodynamics [9a, 9b] or Fourier thermal conduction theory (TCT) [9c], are still in agreement with the new advances of experimental physics in the temperature field.*

Such study is acquiring special importance when we recall A. Einstein's warning, made in his classical paper [10] that "*classical thermodynamics can no longer be looked upon as applicable with precision...For the calculation of the free energy, the energy and the entropy of the boundary surface should also be considered*". And in his earlier paper, entitled "A Theory of the Foundations of Thermodynamics" [3], A. Einstein unambiguously defined the fundamental assumptions of thermodynamics, when writing: "*Let the system be isolated, i.e., the system considered should not interact with other systems*". And also there we find: "*Experience shows that after a certain time an isolated system assumes a state in which no perceptible quantity*

of the system undergoes any further changes in time; we call this state the stationary state". So, in accordance with A. Einstein, Thermodynamics deals only with isolated systems, and when all the transient processes have already finished in it. The other very important theoretical observations, fundamental for the understanding of applicability of thermodynamics, can be found in a popular University text-book [9a, 9b], where it is specially emphasized that the basic thermodynamic concept of internal energy is closely related to the theoretical assumptions of adiabatic enclosure [9a] and quasi-static process [9a]. In [9a] it is specially noted that the thermodynamic temperature can be regarded as a function of state, *only if it is assumed that for quasi-static processes the number of the influence parameters is equal to the number of the parameters, which are used for the description of the system under the thermal equilibrium conditions*. In the description of an imaginary experiment (standard for thermodynamic courses), when an ideal gas is located inside the cylinder-piston system with adiabatic isolation [4a], we find the following paragraph on page 48 in [9a]: "*In the limiting case of a quasi-static process, the internal pressure in gas is equal to the external pressure on the piston. Only under these conditions, the internal state of the gas can be characterized by only two parameters (pressure and volume), and only then the process can occur infinitely slow, passing through consecutive equilibrium conditions. In the opposite case, the motion of the piston occurs with acceleration, so that the different parts of the gas move with finite velocities and for description of the internal state of the gas the infinite number of the parameters will be needed*". Thus, it follows from the university text-book that if the process is not quasi-static, the concept of thermodynamic temperature (as a function of state) loses its validity [9a, 9b]. It is also specially noted in [9a] that the thermal conductivity process presents a typical example when a relatively slow process can not be considered as a quasi-static process. This gives a clear indication that the notion of "temperature" in TCT cannot be associated with the thermodynamic temperature. This assertion also follows, naturally, from the assumptions of thermodynamics, indicated by A. Einstein in [11], as the system in TCT is not closed, and the main subject of TCT is the description of the transient process in that system. Unfortunately, in theoretical Physics there is no other definition of temperature except the thermodynamic one.

For the future comparison of the results of our experiments with theory, it is relevant to remind one important observation in [12], dealing with TCT. In the first chapters of this thick text-book, the authors find it necessary to attract the readers attention that the thermal conduction theory, describing the transient processes, is actually based on the result of a *single, one dimensional, steady-state experiment*, with the help

of which the heat flux density in a material artifact is related to the temperature gradient inside the artifact. This remark gives an indication that, most probably, already at that time some discrepancies between TCT and experiments were known. Evidently, only new precise experiments can help to establish the relations between the concept of thermodynamic temperature and the notion of “experimental” temperature, which presents a measure of the thermal energy in a specified part of a material artifact and which has been used by mankind for centuries.

In this paper, using the variation principle (the most general in experimental Physics) we demonstrate the existence of thermal surface energy (TSE). TSE is shown to present the energy of the oriented motion of charged particles inside a solid-state artifact and the energy of the guided electromagnetic (EM) field, which is propagating along the material artifact and which is always accompanying a non-uniform motion of charged particles [13a, 14a]. It is shown that TSE arises when there is an input of the thermal energy (positive or negative) to the system, and the main parameters of TSE (its magnitude and the direction of its increase) are defined by the vector quantity – the Poynting vector of the external EM field, which is produced by an external heat source and the material objects, surrounding the system. So, on one hand, we can say that TSE appears as a result of the EM field pressure [9g] and the specific features of the propagation of the wave momentum [15] (describing the coupled field-particle system [15]) in the vicinity of the boundary of the material artifact. On the other hand, we can also say that the TSE presents a new form of the fundamental collective R. Dicke effect [16], which is known to be related to the interaction of EM field with an ensemble of charged particles [17-19]. In the particular case of the system under consideration, the collective effect corresponds to very low levels of excitation of atomic system [18, 19], when as a result of the effect of trapping of EM radiation in the atomic system, the number of particles in the ensemble becomes a crucial parameter in the description of interaction in the field-particle system [17-19].

The most important results of this study are the following. First, it is experimentally shown that TSE, produced by the Poynting vector of the external heat source, results in the thermal hysteresis effect, which (as the other well-known hysteresis effects [9d, 9e]) is irreversible in time and has no spatial symmetry [9d, 9e]. Second, with very high signal-to-noise ratio it is demonstrated that *the principle of superposition is not valid for TSE*, so that all material artifacts in the presence of a single heat source are found to be in continuous, ever-lasting, non-linear interaction with each other and with the heat source through continuous radiation of EM field, just as a consequence of the existence of the TSE. The main properties of the interaction of EM field with material artifacts –the presence of the hysteresis effect,

or the memory about the pre-history of the system, and the non-linearity of the coupled field –particle system, manifesting itself as the violation of the superposition principle for EM fields, lead to the “self-ordering” evolution process, in which the parameters and properties of each interacting artifact are gradually changing in response to the variations of the resulting EM field, which is produced by all interacting material artifacts. Among the gradually changing parameters and properties of the artifact it is possible to mention some quite general such as the length of an artifact and its aging, as well as some specific ones (such as variations in time and in space of stresses and deformations inside an artifact, particle mass transfer inside it, variations in time and in space of the total-energy density [15] and of the energy flux density [15] of the coupled field-particle system inside the material). The key features of the thermal evolution process are that *the properties of the artifact are specific for any particular point inside the artifact, as well as for the specific time moment, and the number of influence parameters, necessary for the description of the evolution process, is absolutely enormous* under the achieved accuracy level of the experimental studies. When speaking about the general case, we are to note first that the number of material objects, interacting through EM in the Universe, (or the number of influence factors) can be considered as infinite. Second, all of these objects are interacting with the common EM field, which is produced by these objects during the whole precedent time up to the moment of the performance of the particular measurement, and consequently, *all these influence factors are, at least, partially correlated and cannot be regarded as independent ones*. Third, the interaction between the material objects in the evolution process of system depends on the pre-history of each partner, or each object exhibits its specific hysteresis effect. Fourth, in the process of the EM interaction of the objects of the system with external partners, some of these partners can appear as new ones (with basically new physical properties) and some can disappear. Under these conditions, it should be clear that in the general case, the description of any material system, which always depends on the infinite number of correlated variables and which is always under the continuous evolution process, in terms of the existing mathematical tools is not possible. Thus, the *presented experimental studies give a definite indication of the validity of the fundamental philosophical observation of Niels Bohr that the space-time description of material systems in the general case is impossible*. The presented experiments also give the answer to the cited above Erwin Schrödinger’s “other thinking” and to his claim: “The aim of atomic research is to fit our empirical knowledge concerning it *into our other thinking*. All of this other thinking, so far as it concerns the outer world, is active in space and time. If it cannot be fitted into space and time, then it fails in its

whole aim and one does not know what purpose it really serves”.

Among the other fundamental results of this study is the demonstration that the basic assumption of the Fourier TCT that the thermal energy flux in material is determined only by the temperature gradient in it (which was borrowed from the existing at that time experimental physics) is not valid in the general case. It is only *approximately valid* in case of the fixed stationary conditions, when all the transients are finished in the system. Besides that, it follows from the study that *the precise knowledge of the temperature distribution on the surface of a material artifact at some fixed time instant, which is used in formulation of TCT, is impossible to realize experimentally in principle*. So, that the TCT can be regarded as some illustration of the A. Einstein observation that “when the laws of mathematics ... are certain, they do not refer to reality”.

Dealing with the thermodynamics, it is shown experimentally that the concepts of isolated system and of adiabatic enclosure can be treated only as unrealistic theoretical assumptions, which are in contradiction with numerous experimental observations in astronomy, biology (including molecular biology) and zoology. The ideas of the adiabatic enclosure and of the isolated system are in disagreement with the well-known experimental facts that the thermal EM radiation covers the whole spectrum of energies [2d] and all the materials are becoming relatively transparent at high enough frequencies [9g, 9h], so that from the university physics course we can find that the concept of thermodynamic temperature is not appropriate for plasma physics [9a], for example, where adiabatic enclosures do not exist in any approximation [9a]. For precise temperature measurements, achieved nowadays, the concept of thermodynamic temperature as a function of state is obsolete, and must be substituted by the more general concept of *temperature, which includes the energy of the oriented motion of the coupled field-particle system that can be detected through the radiated EM field by different types of thermometers*. Here, thermometers represent the devices, which effectively absorb the propagating EM field and which convert the oriented field propagation into the random motion of the particles of “thermometric fluid”, by changing the resistance in SPRT [7b], for example, and simultaneously transferring the corresponding field impulse to the material surrounding.

It is also shown experimentally (see Fig.11) that that with the existing experimental tools the thermal evolution process can be detected during the time interval of a couple of minutes. It means that the wave momentum density and total-energy density inside the block [15] cannot be regarded as conserved quantities after that time interval.

II. EXPERIMENT

a) *Experimental demonstration of thermal surface energy and of the asymmetry in space of the thermal evolution process*

The main features of our experimental set-up, in which a 100-mm gauge block (GB) is located horizontally on three polished spheres inside a closed Dewar system, can be understood from the inset of Fig.1. The measurement system is located inside a laboratory with precise air temperature control with typical diurnal variations of about 50mK. Two thermistors R6 and R3, equipped with copper adapters covering the whole width of the GB, are located on one of the side surfaces of the GB. Thermistors are, practically, identical and are installed parallel to the gauging surfaces of the GB (Fig.1). A 100-Ohm platinum resistance thermometer (PRT), also equipped with a copper adapter, is located parallel to the adapters of the thermistors at exactly equal distances from them. We use a newly developed multi-channel synchronous detection technique (MSDT) [3f] to measure simultaneously, with high precision the variations of temperatures in the thermistor channels that are induced by the periodic modulation of the current in the PRT. Synchronous measurements of temperatures and of thermal velocities, available from all three thermometers, are realized by the program whose print-screen for the duration of 1.4 period of the modulation cycle is presented in Fig.1. The duration of the cycle is ~140 minutes. One fourth of the cycle duration, the PRT current is kept at the level of 5mA (heating period), and for the left part of the modulation cycle the current is equal to 1mA (cooling period). The PRT is connected to a programmed, high-precision DC bridge Mi-T615 (Canada), so that the accurate temperature measurements of the PRT during the whole modulation cycle are available. Meanwhile, the thermistors R6 and R3 (belonging to channels 1 and 2, respectively) are connected to precision multi-meters HP-3450A, so that synchronous differential temperature measurements between the channels 1 and 2 with the resolution of 1-2 μ K for the time duration of a few minutes can be achieved thanks to high sensitivity of the thermistors relative to PRT. The record in Fig.1 with a faster response time corresponds to the measured variations of the PRT resistance during the modulation cycle. The two other traces show the variations of the resistances of the thermistors, which have negative thermal coefficients. As a consequence of the used geometry, the system is extremely sensitive to any asymmetry in heat fluxes along the surface of the GB in the direction of the longest side of the GB. The key feature of the experiment is that both thermistors are calibrated to measure the temperature of the artifact surface in the close vicinity of its adapter [3i].

With the two cursors of the program (shown in Fig.1 as triangles), we specify the desired part of the record, and the program calculates the mean values of the temperature and of the temperature rate in each channel, using the calibration equations (temperature versus resistance) for each channel that are in advance stored in the program. In two separate windows, the program displays the initial and final moments of the measurement time interval that are defined by the position of the cursors on X-axis of the record. The larger window of the program shows the mean values of the temperature and of the temperature rate, obtained in one of the channels during the specified measurement time interval. The information about the results of the measurements in all of the channels for the sequence of the desired time intervals is written by the same program in a special file. These files contain the data of synchronous differential temperature measurements between the channels 1 and 2 as a function of time. As this information can be presented separately for high and low levels of the modulation current in the PRT, it can be processed using the MSD technique [3f, 3i]. The plots in Figs. 2, 4, 6 of this paper present the examples of the application of the MSD technique to the data of such files. The procedure of the calibration of the PRT and thermistors is described in detail in [3i, 3f] and the application of the MSD technique is outlined in [3h]. Here, we note that the records of Fig.1 correspond to measurements on a steel block with 10-mm separations between the adapters of the thermistors and the adapter of the PRT. The axis of thermistor R6 is located at the distance 4.5mm from the nearest gauging surface. In this case, one of the side surfaces of the thermistor adapter lies in the plane of the gauging surface of the block.

An observation of a paramount importance can be inferred already from the plots of Fig.1: though the separations of thermistors from the heat source are the same, the *induced temperature variations in the thermistor channels are different*. This means that the thermal transfer process is not symmetric in space, similar to the build-up processes of domains in ferromagnetic [4d] or ferroelectric materials [4e] under the application of the external fields. This also means that the basic assumption of the Fourier TCT, defining the energy flux in the material, is in contradiction with the experimental results obtained by the variation principle, the most general and powerful in experimental Physics. This will be demonstrated in detail, with extremely high signal-to-noise ratio when using the MSD technique. But this can be clearly observed even from the unprocessed results of the measurements of Fig.1. Indeed, from the corresponding temperature measurement results of Fig.1 we find that for the last 30 minutes of the cooling part of the cycle at $I=1\text{mA}$, which is presented first in this figure, the mean temperature, recorded by the thermistor R6, was $466\mu\text{K}$ higher than the mean

temperature, obtained from the thermistor R3. For the second modulation cycle, which is shown completely in Fig.1 and which is marked by two cursors, this temperature difference $T[1,2]$ was about $469\mu\text{K}$. Thus, the stability in time of the reference points in Fig.1 was within $4\mu\text{K}$. And it is important to realize that the temperature of the gauge block in the vicinity of the thermistor R6 was *higher* than the temperature of the block in the vicinity of the thermistor R3 for all reference points. And in contrast to the basic approximation of the TCT theory, it follows from Fig.1 that when the current in the PRT was increased to 5mA , the *flux of thermal energy to the unit volumes of the artifact in the vicinity of the R6 thermistor (having already higher temperature) was larger than the energy flux to the unit volumes in the vicinity of the R3 thermistor*, as the temperature rate, recorded by thermistor R6, was definitely larger than the temperature rate, recorded by thermistor R3!

In future, the mean temperature difference between the channels 1 and 2, recorded for the last 30 minutes of the cooling period (at $I=1\text{mA}$), we shall denote by the quantity $T[1,2]$. And all the data points, corresponding to the last 30 minutes of the cooling part of the modulation cycle, we shall call *the reference points*.

Now, the plot of Fig.2 will be used for illustrations of the application of the MSD technique. Here, the experimental conditions are the same as the ones in Fig.1. In Fig.2, the reference points are marked with rectangles. The averaging time for the reference points is chosen to be 5, or 10 minutes. All of these reference points are used to generate the linear fit, which is shown as a solid line and which is very close to abscissa axis. The equation of this fit is presented in Fig.2 in a separate text box. From this equation we find that for the initial time of the record ($X=350\text{min.}$) the fit value is $-0.02\mu\text{K}$, while for the end of the record ($X=480\text{min.}$) it gives the value of $0.11\mu\text{K}$. So, all the values of the reference function, given by the fit equation and representing the systematic offsets, are below $\pm 0.15\mu\text{K}$ for the whole time interval of this observation. The random spread of the data points relative to this fit is also very small: a standard deviation of a single reference point relative to the linear fit is less than $3\mu\text{K}$.

Using this fit as a reference, we can determine very precisely the difference between the simultaneous measurements of temperatures, realized by the channels 1 and 2 during the modulation cycle. This temperature difference, which is measured relative to the fit to the reference points, is denoted here by the quantity $\Delta T[1,2]$. The experimental points of Fig.2, represented by dots, demonstrate the time dependence of the difference in the temperatures of the channels 1 and 2, when *these temperature variations are induced by the increased value of the PRT current ($I=5\text{mA}$) during the heating period of the modulation cycle*. The

measurement time intervals are 2 and 4 minutes at the beginning and at the end of the heating period of the cycle, respectively. It follows from Fig.2 that for all data points of the heating period the quantity $\Delta T[1,2]$ is positive, and the maximum value of $\Delta T[1,2]$ is surpassing by orders the uncertainty of the reference values. For example, the maximum value of the quantity $\Delta T[1,2]$ in Fig.2 is equal to $2620 \pm 3 \mu\text{K}$, while the systematic offset of the reference function is within $\pm 0.15 \mu\text{K}$ and the standard deviation of a single reference point is below $3 \mu\text{K}$.

It should be specially emphasized that the induced temperature difference $\Delta T[1,2]$ is a vector quantity. Its positive value indicates that the amount of thermal energy, delivered from the PRT during the heating period of the cycle to the elementary (unit) volume of the material artifact in the vicinity of the thermistor R6, is larger than the corresponding amount of the thermal energy, delivered to the elementary (unit) volume of the artifact in the vicinity of the thermistor R3. Thus, this experiment has given a first clear demonstration that, in spite of the fact that the thermistors are located on the surface of homogeneous artifact at the same distance from the heat source, the time averaged value of the heat flux of the thermal energy to the elementary volumes of the GB material, located in the vicinity of the nearest gauging surface of the artifact, is substantially higher than the time averaged value of the energy flux to the elementary volumes, located symmetrically relative to the heat source in the bulk material away from the gauging surface. We are to remind here that thermistor R6 is located closer to the gauging surface of the block, and we are analyzing the reaction of the system during the heating period of the modulation cycle when there is a positive net input of energy to the artifact. Thus, from Fig.2 it follows that *the larger average flux of thermal energy to the elementary volumes in the vicinity of the R6 thermistor occurs when for all time intervals of the heating period, the temperature difference between the PRT and R6 is smaller than the difference between the PRT and R3*. Naturally in this case, the projections of temperature gradients along the longer axis of the GB in the direction of the thermistor R6 were definitely smaller than the corresponding projections of the temperature gradients in the direction of the thermistor R3. So, we can infer from Figs. 1 and 2 that *at the initial stages of the heat transfer process there is an additional flux of thermal energy to the elementary volumes of the artifact in the vicinity of its boundary surface, which cannot be related to the thermal gradients in the artifact, as it supposed in TCT*.

Naturally, we can plot the induced temperature variations $\Delta T[1,2]$, which are induced by the current switch from 5mA to 1mA. Such points for the cooling period of the cycle are shown by rhombi. It can be also

inferred from Fig.2 that the excessive thermal energy, which is stored in the vicinity of the gauging surface close to the thermistor R6 during the relatively short part of the heating period of the cycle, is distributed over the whole length of the block, practically homogeneously, at the end of the cooling period of the modulation cycle.

To demonstrate in more detail the main properties of the heat propagation process at its early stages and to find the physical reason for the excessive energy flux, we studied experimentally the variations of the thermal velocities $\Delta V[R6]$ and $\Delta V[R3]$, which were induced by 5mA current and were recorded simultaneously by both thermistors. Thus, this part of our study deals with *synchronous differential thermal velocity measurements*. Here, the mean values of the temperature velocities for both channels ($V[R6]$ and $V[R3]$) for any desired time interval can be found in the way similar to the measurement of the mean values of temperatures. For this it is necessary to specify the desired time interval with the two cursors of the program and to select the appropriate channel. Then the mean value of the thermal velocity will be found in the window of the program (Fig.1) together with the mean temperature value. Both calculations are performed by the program, using the experimentally obtained calibration equations for the responses of the thermistors that have been measured on the GB surface under the analogous external conditions [3i, 3f].

The velocity dependence for the thermistor R6 as a function of the measurement time for two modulations cycles (under the experimental conditions of Fig.1) are presented in Fig.3a. Dots correspond to the heating period of the modulation cycle, while rhombi show the measured values of the thermal velocity for the cooling period of the cycle. The data points for the last 30 minutes of the cooling period, where the slope of the experimental curve is already relatively small, are used as reference points. These points in Fig.3a are shown as rectangles. For all of the reference points of our experiment, with the duration of 16 hours, we find 6-th order polynomial fit using the least squares criteria. The corresponding curve of the fit is shown as a solid line in Fig.3a.

The velocity variations $\Delta V[R6]$, which are induced by the switch of the PRT current from 1mA to 5mA and then back from 5mA to 1mA, are calculated as a difference between the measured values of the thermal velocity in the channel at a specified time and the value of the reference function at the same time. As it follows from Fig.3a, the values of the induced velocity $\Delta V[R6]$ are quite reproducible. For example, the mean maximum value of the quantity $\Delta V[R6]$, averaged over the two cycles presented in Fig.3a, is $1686 \mu\text{K}/\text{min}$. Meanwhile, the scatter of the maximum values, recorded in both cycles relative to the mean value is within $\pm 9 \mu\text{K}/\text{min}$. This scatter can be hardly seen in Fig.3a, as

it is much smaller than the dimensions of the data-points, used in the figure. The time averaging, which is used in the detection of the maximum of the curve in Fig.3a, is only 1 minute. But as a result of the use of the sensitive thermistors, the random uncertainty of the measurements, corresponding to 1 minute averaging time, is quite negligible in comparison with the dimensions of the data-points and does not affect, practically, the position of the points. It should be specially emphasized here that the slow drifts, which are typical for thermistors, are removed, practically completely, in MSD technique by the use of the reference fit, which establishes the recalibration of the thermistors sensitivities every cycle during the time interval, devoted to the measurement of the reference data-points.

The corresponding dependence of the quantity $\Delta V[R6]$, which is averaged over the two cycles of Fig.3a, is presented in Fig.3b. Here again, the dots correspond to the heating period of the modulation cycle, and the rhombi show the obtained values of the thermal velocity $\Delta V[R6]$ for the cooling period of the cycle. The standard deviation of the reference points in Fig.3b relative to the fit is $\sim 10.4 \mu\text{K}/\text{minute}$, and it shows that some systematic cooling of the system at the end of the cooling period of the modulation cycle is still observed. But as the maximum value of the quantity $\Delta V[R6]$ is $\sim 1686 \mu\text{K}/\text{minute}$, it is clear that the measurements of the induced variations of the thermal velocities in this experiment are still performed with huge signal-to-noise ratios.

To demonstrate clearly the fundamental effect of the spatial asymmetry in the delivery of the thermal power to the elementary volumes, located at the same distance from the heat source on a rectangular block, made of homogeneous material, in Fig.3b we present also the induced velocity variations $\Delta V[R3]$, corresponding to the simultaneously measured values in the other channel. For this dependence, the heating period of the cycle is shown by triangles, and the cooling period is presented by circles. Similar to the dependence $\Delta V[R6]$, the maximum value of the induced velocity $\Delta V[R3]$ is observed, approximately, 2.5 minutes after the increase of the modulation current in the PRT. But the value of $\Delta V[R3]$, averaged over the same modulation cycles, is only about $1172 \mu\text{K}/\text{minute}$, instead of $\sim 1686 \mu\text{K}/\text{minute}$ in the other channel. It also follows from Fig.3b that the excessive energy flux to the elementary volumes in the vicinity of thermistor R6 is obtained during the first 15-20 minutes of the heating period of the modulation cycle, and for the rest time interval of the heating period, the induced variations of the thermal velocities in both channels are, practically, equal. In the explicit way, this statement follows from the plot of Fig.3c, where the difference between the quantities $\Delta V[R6]$ and $\Delta V[R3]$, denoted by the quantity

$\Delta V[1,2]$ is presented. From the plots of Figs.1 and 3b it follows that for the last 30-40 minutes of the cooling period of the modulation cycle, the differences $V[1,2]$ between the measured values of thermal velocities $V[R6]$ and $V[R3]$ are usually within $1 \mu\text{K}/\text{minute}$, and the quantity $V[1,2]$ for these points can be used as a reference points (rectangles in Fig.3c), relative to which the induced variations $\Delta V[1,2]$ could be very precisely determined. In this case we can use even a simple linear fit. The equation of this fit, corresponding to the reference points, averaged over two modulation cycles, is presented in the text box of Fig.3c. From the presented fit equation, we can infer that for the time interval between 360 and 440 minutes, the value of the reference function stays in the range of 0.26-0.31 $\mu\text{K}/\text{minute}$. So, for the differential thermal velocity measurements, the contribution to the error budget due to the possible choice of the reference function is, practically, equal to zero. It also means that practically the same results for the quantity $\Delta V[1,2]$ can be obtained by using the linear fit in Fig.3c, or by finding the differences between the quantities $\Delta V[R6]$ and $\Delta V[R3]$ (Fig.3b), calculated with the help of the 6-th order polynomial fits to the reference points in all modulation cycles of a whole measurement series. This is the consequence of a proper choices of the length of the modulation cycle and of the length of its cooling period, so that the mean thermal velocities, recorded by both channels, for the last 30 minutes of the cooling cycle coincide with each other to within a small fraction of $1 \mu\text{K}/\text{minute}$. This observation is supported by the experimental result that the standard deviation of the reference points relative to the linear fit in Fig.3c (that describes the uncertainty of the determination of a single reference point) is equal to $0.83 \mu\text{K}/\text{minute}$. So, the total uncertainty of a single measurement in Fig.3c is by orders of magnitude smaller than the maximum value of the difference in thermal velocities in the channels 1 and 2, which is induced by the variations of the PRT current.

It is also worth reminding here that the difference in thermal velocities $\Delta V[1,2]$, presented in Fig.3c, is also a vector quantity, as it carries the information about the direction along the axis of the block between the positions of thermistors R3 and R6. For example, the positive value of $\Delta V[1,2]$ means that during the heating period of the modulation cycle (presented by dots in Fig.3c) *the thermal power*, delivered to the elementary volume of the artifact material in the vicinity of R6 thermistor, is larger than the thermal power, delivered to the corresponding volume of the artifact in the R3 vicinity. For the cooling period of the cycle, which is shown in Fig.3c by rhombi, the losses of thermal power from the elementary volumes in the vicinity of the R6 thermistor occur faster than from the elementary volumes, located at the same distance

from the heat source but in the direction of the bulk material away, from the gauging surface.

The physical meaning of the thermal power, recorded by thermometers, can be clarified from the basic Poynting theorem of classical electrodynamics [13a, 14b, 15]. In accordance with the integral form of Poynting theorem of classical electrodynamics [13a, 14b, 15], representing the continuity equation for the energy density and for the energy current density of EM field (or Poynting vector, see Eq. (2.13) in [15]), we find: the rate of the change in time of the electromagnetic energy within an artifact volume, plus the time rate of the total work, done by EM fields on charged particles within the artifact volume, are equal to the quantity of EM energy, which is delivered inside the artifact per unit time through its boundary surface by the Poynting vector of EM field [13a]. The differential form of this theorem states that the rate of the change of the total-energy density, written for the particle-field system within the artifact [15], is defined by the divergence of the total-energy current density (see Eq. (2.14), (2.18) in [15]). In other words, *the total power delivered to the elementary volume ($dx dy dz$), is defined by the total-energy flux of the coupled field-particle system [15] that is delivered inside to this elementary volume through its boundary surface.* So, the results of experiments in Fig.3c give a clear indication that the difference in thermal powers (i.e. the difference in the time derivatives of the total field-particle energies that is recorded by the two channels) is the consequence of the additional, systematic flux of energy to the volumes in the vicinity of the gauging surface (nearest to the heat source) relative to the volumes, which are located at the same distance from the heat source but in the opposite direction, away from the boundary of the artifact. From our experiments it can be also inferred (see below) that this additional total-energy current density, arises as a result of the reflection of the propagating wave momentum of the field-particle system from the gauging surface of the artifact, so that the reflected part of the field-particle system results in the appearance of the wave momentum [8] and the total-energy current densities [8], propagating some (relatively small) distance in the direction of the heat source.

It is also clearly seen from the plot of Fig.3c that this additional energy flux does exist only during a short, initial time of the heating period of the modulation cycle, but the additional thermal energy (see Fig.2) is stored in the vicinity of the boundary during the whole heating period. Besides that, the comparison of the dependences on time of the quantity $\Delta V[1,2]$ for the heating and for the cooling periods of the modulation cycle shows that the excessive heating of the elementary volumes in the vicinity of the R6 thermistor, which is observed for the time interval of about 20 minutes after the switch of the current in the PRT from 1mA to 5mA, is followed by the excessive cooling of the

same elementary volumes during approximately the same time interval after the current switch from 5mA to 1mA. The effect changes the sign, but the magnitudes and the dependences on time of the corresponding parts of the process (presented in Fig.3c) are quite similar. The analysis of the numerical results of the measurements, presented in Fig.3c, indicates that for the cooling period of the cycle, after 25 minutes from the current switch in the PRT from 5mA to 1mA the possible deviations of the quantity $\Delta V[1,2]$ stays within $\pm 2\mu\text{K/minute}$. It means that after 25 minutes from the indicated current switch, the cooling processes in the parts of the artifact, located symmetrically relative to the heat source, are becoming, practically, identical, while at the beginning of the cooling period the difference between them exceeds $500\mu\text{K/minute}$, in absolute value.

A somewhat different point of view on the results of Fig.3c, which will be used later in this paper, is based on the observation that the quantity $\Delta V[1,2]$ deals with the differential velocity measurements and also carries the information about the direction along the axis of symmetry of the GB. So, instead of the excessive cooling of the elementary volumes in the vicinity of R6 thermistor after the current switch in the PRT from 5mA to 1mA, we can interpret the same results as a relative excessive heating of the elementary volumes in the vicinity of the thermistor R3. And as the differences between the absolute values of the curves, presented by the dots and by rhombi in Fig.3c, are very small, we can say that during the heating period of the modulation cycle some excessive flux of energy is propagating from the heat source to the elementary volumes, located in the vicinity of the thermistor R6 close to the gauging surface. Meanwhile during the cooling period of the cycle, practically, the same amount of the flux of energy is propagating in the opposite direction from the heat source to the elementary volumes, which are located symmetrically relative to the heat source in the bulk material, in the vicinity of the thermistor R3. Thus, from the results of the studies, presented in Figs. 2 and 3, we can conclude that during the heating period, some excessive thermal energy is stored in the vicinity of the boundary (Fig.2, dots) as a result of a relatively short flux of energy (Fig.3c, dots), while by the end of the cooling period, the thermal energy is distributed almost homogeneously along the surface of the artifact (Fig.2, squares) as a result of a short energy flux (Fig.3c, rhombi), propagating in the opposite direction. Thus, *the positive quantities $\Delta T[1,2]$ and $\Delta V[1,2]$, observed at the beginning of the heating period of the modulation cycle, directly indicate to the existence of the thermal surface energy (TSE), which can be reliably detected by the synchronous differential thermal measurements.*

The other important observation deals with statement that the propagating flux of energy in a material with absorption is always related to the force

density, acting on the material objects inside the elementary volume [15, 9h]. So, during a single modulation cycle, a variable in direction force is acting alternatively in two spatial regions of the artifact, located symmetrically relative to the source of EM field. In this our experimental situation is quite similar to the case of the hysteresis effect in Ferro-electric samples [9e], when the process of the build-up of the sample polarization is observed in the electric field of constant magnitude, but when the field direction is periodically changing in time to the opposite one. In the latter case, every time after the switch of the direction of the electric field, there appears a variable in time force, acting on the elementary volume inside the domain structure, as the domains are polarized predominantly in the direction of the previously existing electrical field. And then, the process of the change of the polarization of the medium starts (as a result of the re-orientation of the domain dipole moments in the new direction of the external electrical field [9e]) that inevitably changes the force, acting on the elementary volume. Thus, the observation method of the hysteresis loop in Ferro-electrics shows the way how to present the hysteresis loop in case the thermal hysteresis effect. Instead of presenting the experimental points as a continuous sweep in time (Fig.2), it is necessary to present the points in two separate time sequences (see Fig.7 below), which correspond to the two directions of the variable forces, acting on two spatially different parts of the system.

But first, we want to present another type of experiment, which unambiguously shows that the quantities $\Delta T[1,2]$ and $\Delta V[1,2]$ describe the thermal surface energy (TSE) by demonstration that the amplitudes of both quantities fall rapidly with the increase of the separation of the thermistor R6 from the gauging surface of the block. Thus, the effects, described in this paper, can be observed only when one of the thermistors is located close to the boundary of the artifact. The other result of paramount importance is the *experimental demonstration that the thermal evolution process, in the general case, is characterized by the spatial asymmetry.*

To prove this, we performed a special experiment, in which our measuring system, which included the PRT and both thermistors, was moved as a whole away from the gauging surface of the steel GB in two equal steps of 4.5mm, each. The separations between the surfaces of the PRT adapter and the corresponding surfaces of the adapters of thermistors were equal to 10 mm. They were installed with the help of a 10mm GB with very high precision. The magnitudes of the quantities $\Delta T[1,2]$ and $\Delta V[1,2]_{\max}$ for the heating period of the cycle are presented in Figs. 4a and 4b as a functions of the separation of the axis of the thermistor R6 from the nearest gauging surface of the block, which will be denoted here by Z. In Fig.4a, the vector quantity

$\Delta T[1,2]$ corresponds to the magnitude of the surface energy, observed 13 minutes after the increase of the modulation current in the PRT. Here, the experimental points, corresponding to the Z-values of 4.5mm, 9mm, 13.5mm and 22mm, are shown as dots. The left data-point in Fig.4a (with the value Z=4.5mm) corresponds to the case when one of the side surfaces of the R6 adaptor lies in the plane of the gauging surface of the block. For this point, the experimental conditions correspond to the plots of Figs. 1-3, and the surface energy, characterized by the quantity $\Delta T[1,2]$, has its maximum value. The right data-point (with the value Z=22mm) corresponds to the symmetric position of the PRT on the side surface of the block. For this point, the magnitude of the quantity $\Delta T[1,2]$ is becoming vanishingly small, as for the larger values of Z the quantity $\Delta T[1,2]$ is becoming negative: in this case the thermistor R3 is becoming closer to the opposite gauging surface of the block, and so, the quantity $\Delta T[1,2]$ changes the sign.

The part of the experimental curve in Fig.4a, corresponding to R6 axis distances less than 14mm, can be approximated by the Gaussian curve $\exp(-(z-z_0)^2/2\sigma^2)$, where z is the distance of the R6 axis from the gauging surface; z_0 is an adjustable parameter (with the value of about 4.43mm), which corresponds to the maximum of the experimental dependence (shown as a solid line in Fig.4a) and takes into account the finite width of the R6 adapter; σ is the sigma value of the Gaussian curve, measured in mm. For the adopted type of the exponential fit, the value of the parameter σ , which describes the characteristic length of decrease of the $\Delta T[1,2]$ magnitude with the increase of the distance from the boundary, is estimated to be about 9.06mm. The corresponding plot of the Gaussian curve, with appropriate magnitude and with the sigma value of 9.06mm, is presented in Fig.4a with rhombi. It covers the Z-values from Z=4.5mm to the σ -value of the curve, representing the magnitude dependence of the Gaussian curve from its maximum to the relative value of 0.606. As it follows from Fig.4a, the thermal surface energy, characterized by the quantity $\Delta T[1,2]$, falls very rapidly with the increase of the distance from the boundary, and so the term "surface" is quite appropriate in this case.

The corresponding dependence of the maximum value of the quantity $\Delta V[1,2]$ (which is clearly observed on the plot of Fig.3c) on the distance of the thermistor R6 from the gauging surface is shown in Fig.4b. Here, the left data-point corresponds to the experimental conditions of Fig.3c. The solid line in Fig.4b is connecting all 4 experimental points, covering Z values in the range from 4.5mm to 22mm. The maximum values of the quantity $\Delta V[1,2]$ in Fig.4b (denoted here as $\Delta V[1,2]_{\max}$) were found from the plots analogous to the one of Fig.3c, but measured in the experiments with

larger values of the separation of the thermistor R6 from the gauging surface. The experimental dependence of Fig.4b can also be accurately approximated by the Gaussian curve from its maximum value to the relative amplitude of 0.606 (which corresponds to 1σ level of the abscissa variable of the Gaussian curve). The approximating part of the Gaussian curve is shown in Fig.4b by rhombi for the relative magnitudes from 1 to 0,606, and by open squares for the abscissa variable beyond 1σ level, i.e. for the R6 separation values in the range of 12-14 mm. The agreement between the fit and the experimental points, lying within 1σ range, is below $1\mu\text{K}/\text{minute}$. Even for the point with Z-value equal to 13mm (where systematic differences are becoming already important), the difference is $3.3\mu\text{K}/\text{minute}$. Here, it should be taken into account that the indicated value of the difference presents less than 1.3% of the measured quantity $\Delta V[1,2]_{\text{max}}$ at this point.

The other important observation concerns the widths of the curves in Figs. 4a and 4b. They are not equal. The width of the curve $\Delta V[1,2]_{\text{max}}$ in Fig.4b is smaller. This result can be immediately obtained from the comparison of the solid curves in these figures. In Fig.4b the experimental points describes a larger part of the corresponding Gaussian curve than the data-points in Fig.4a, corresponding to the same Z-values. The smaller width of the curve $\Delta V[1,2]_{\text{max}}$ means that the energy flux, described by this quantity, falls faster with the R6 separation value from the boundary than the quantity $\Delta T[1,2]_{\text{max}}$. A quantitative description of the widths of the experimental curves in Figs. 4a and 4b can be obtained from the Gaussian approximations of these curves. In Fig.4b the corresponding σ -value is equal to 7.7mm, which is substantially smaller than the σ -value in Fig.4a (9.06mm). The same conclusion will follow from the other experiment, which will be presented at the end of this section.

In Fig. 4a, the magnitude of *the surface energy is presented as a function of the separation Z* of the thermistor R6 from the gauging surface for the fixed value of the time interval after the increase of the modulation current in the PRT. Naturally, this plot has to be complemented by the experimental dependences of *the surface energy as a function of the elapsed time* after the current increase for several fixed values of the separation Z. The corresponding dependences are shown in Fig.4c. The dependence 1 (dots) corresponds to the Z value of 4.5mm, the curve 2 (rhombi) corresponds to Z=9.5mm and the curve 3 (squares) – to Z=13.5mm. If we compare the values of the surface energy obtained for the time intervals of 3 minute and 13 minutes, we shall see that the ratio of magnitudes for the curve 3 is 0.183, for the curve 2 it is equal to 0.299 and for the curve 3, corresponding to the smallest separation of the thermistor R6 from the gauging surface (boundary of the block), it has the maximum value of 0.342. It

means that *not only the magnitude of the surface energy depends on the observation point*, but *the form of the time dependence varies with the change of the observation point*. The decrease of the ratio of the surface energy, observed at fixed time interval (3 minutes) relative to its maximum value, achieved in the experiment, gives a direct indication that the excessive energy flux, responsible for the creation of the thermal surface energy, arrives later to the distances with larger separations from the gauging surface. Consequently, this experiment supports the idea that the excessive energy flux arises as a result of the reflection of the momentum of the coupled field-particle system from the boundary of the artifact. The other fundamental result is that *the thermal evolution process*, arising due to interaction of the external EM field with the ensemble of atoms in a solid-state artifact, *is characterized by the amplitude, depending on the observation point on the artifact surface, and is also characterized by the specific time dependence (or time scale), which is characteristic only for a particular observation point*. As the philosophers claim nowadays, the time and the space concepts are relational ones (see further in Discussions).

The other very important property of the vector quantities $\Delta T[1,2]$ and $\Delta V[1,2]$ is *the lack of spatial symmetry*. As these quantities carry the information about the relative positions of the thermistors, they are to have the asymmetric properties, relative to the center of the larger side surface of the block on which all the thermometers are located. This property follows from the third type of experiments whose results are presented in Figs. 5a-5c. In these experiments we used a 100-mm tungsten carbide (TC) GB, in order to demonstrate also the effect of material properties on the time dependence and on the magnitude of the thermal surface energy (TSE). So, in Fig.5a we present two curves, representing the dependences of the TSE on the time interval after the increase of the modulation current in the PRT and corresponding to two limiting cases. The first curve, marked by squares, corresponds to the external experimental conditions similar to the conditions of Fig.2, and when the axis of the R6 thermistor is located at Z=4.5mm from the nearest gauging surface. The comparison of the corresponding plots on Figs. 2 and 5a shows that the magnitude of the TSE, characterized by quantity $\Delta T[1,2]_{\text{max}}$, has dropped for the TC block (in comparison with the steel artifact) by, approximately, 3 times. It is also clearly seen from these figures that the process for the surface energy build-up is about 3 times faster in the TC block relative to the steel block, having exactly the same form and dimensions.

The second curve in Fig.5a, marked with dots, corresponds to the case when the system of thermometers was shifted as a whole to the opposite gauging surface of the block, so that the separation of

the thermistor R3 was at the distance $Z=4.5\text{mm}$ from the other gauging surface. Both curves 1 and 2 in the figure are reaching the maximum values at the same time (7minutes) after the increase of the PRT current, and the magnitudes of the curves are quite symmetrically located relative to the abscissa axis of the plot. The difference between the curves is that the signs of the quantities $\Delta T[1,2]$ are opposite for both thermometers positions. Now we can plot the experimental points of the curves 1 and 2, corresponding to the time interval of 13 minutes (when the slopes of the dependences are quite small) and add the third point, corresponding to the symmetric positions of the thermistors *relative to the block center*. The obtained dependence is presented in Fig.5b. Here, the TSE is shown as a function of the position of the PRT relative to center of the side surface of the block. From the plot of Fig.5b it follows that the quantity $\Delta T[1,2]$, which is used for the description of the TSE, presents an anti-symmetric function of the displacement relative to the block center, thus presenting another confirmation of the vector character of this quantity.

The total energy of the field-particle system, which affects the readings of the thermistors R6 and R3, consists of a symmetric part (which to about 1.1% uncertainty level is characterized by the R3 temperature record in Fig.1) and anti-symmetric component, represented by the TSE. Thus, directly from the thermistors records of Figs.1 and 5b, one can conclude that, *in the general case, the thermal evolution process of an open system is characterized by the lack of symmetry in space*.

To the same conclusion we can come after the studies of the excessive energy fluxes, described by the quantity $\Delta V[1,2]$ and presented as a function of the time interval elapsed after the increase of the PRT current (Fig.5c). The curve 1 (where data-points are presented by squares) shows the time dependence of the quantity $\Delta V[1,2]$, which corresponds to the displacement of the thermistor R6 from the gauging surface $Z=4.5\text{mm}$. The curve 2 (shown by dots) corresponds to the displacement of the measurement system to the opposite gauging surface, so that the same value of the displacement $Z=4.5\text{mm}$ is observed for the thermistor R3. All the data-points of the curves 1 and 2 lie, practically, symmetrically relative to the abscissa axis. And it shows that $\Delta V[1,2]$ is a vector quantity, anti-symmetric relative to the center of the corresponding side surface of the block. *The total energy flux*, which is presented in Fig.3b for the steel GB, *has clearly no spatial symmetry in the general case* (i.e. for arbitrary position of the heat source relative to the center of the block surface).

The comparison of the plots in Figs. 3c and 5c shows that the maximum value of the excessive energy flux, observed for the heating period of the modulation

cycle, is about $401\mu\text{K}/\text{minute}$ in case TC block. It is definitely smaller than the maximum value of the energy flux in the steel GB, which exceeds $500\mu\text{K}/\text{minute}$ (Fig3c). More substantial is the difference in the time intervals, which are necessary for the realization of the maximum energy flux. In case of the TC block, the time interval is 1.5minutes after the current increase from 1mA to 5mA (Fig.5c), while for the steel block the corresponding interval is about 2.5minutes (Fig.3c). So, when in the observations of the effect the signal-to-noise ratio is of primary importance, we shall use the experiments with steel blocks. Meanwhile, for the detection of a larger portion of the evolution process, the use of TC blocks is more preferable.

The other important feature of the plots in Fig. 5c is the negligible amount of the contribution of random uncertainty in the measurement results. The main contributions are from systematic effects. This is illustrated by the following observations. For example, if the quantity $\Delta V[1,2]$ changes the sign for the time interval from 196 to 194 minutes, then it occurs simultaneously for both curves 1 and 2. If the absolute values of the effects are larger for the time values of 188 and 192 minutes relative to the time values of 190 and 194 minutes, then these observations are valid for both curves in the figure. The analysis of the numerical results of Fig.5c shows that the systematic effects of $5\text{--}7\mu\text{K}/\text{minute}$ can be reliably detected for the TC block under our experimental configuration. This observation will be later used in the analysis of the thermal evolution process in Fig.11.

One can also conclude from Fig.5c that the dependences of $\Delta V[1,2]$ on time are quite complicated and have small "damped periodic oscillations", which are not simply possible for the case of a random force (in accordance with the definition of a random physical quantity given in [10]). Though the data points (presented by squares and dots) belong to absolutely independent experiments, the positions of the data points in Fig.5c are correlated. When the magnitude of the curve 1 increases, then the magnitude of the curve 2, corresponding to the same time interval, also increases. Both curves reach the maximums of their absolute values at a time instant of 1.5 minutes. Only the signs of the two dependences on time are always opposite. The "synchronization" in $\Delta V[1,2]$ time of the two processes is realized in this case, as the abscissa variable in both plots of Fig.5c corresponds to the time interval, elapsed after the current increase from 1mA to 5mA during the heating periods of the modulation cycles in both experiments. The damped oscillations of the curves in Fig.5c, most probably, indicate to the specific features of the propagations of the energy and of the wave momentum [15] in rectangular metallic blocks, when reflections from all artifact boundaries are becoming significant.

From the dependences 1 and 2 of Fig.5c, we can conclude that the largest values of differential thermal powers, delivered to the elementary volumes of the artifact in the vicinity of the thermistors R6 and R3, are observed during the first 5 minutes of the heating period of the cycle. The comparison of the measured values of the induced temperature velocities $\Delta V[R6]$ and $\Delta V[R3]$, realized in each channel during the heating period of the modulation cycle (Fig.3b), shows that for the steel block the maximum value of the ratio of the quantities $\Delta V[R6] / \Delta V[R3]$ as a function of time is equal to 1.39 ± 0.03 . It is observed at the time instant of 2.5 minutes, when the dependence $\Delta V[1,2]$ in Fig.3c reaches its maximum value. For tungsten carbide GB this ratio, describing the maximum ratio of the energy fluxes in two channels, is equal to 1.9 ± 0.07 . But it is observed at a shorter time (1.5 minutes) after the increase of the current in the PRT, and, as it was already mentioned before, the magnitude of $\Delta V[1,2]_{\max}$ in case of tungsten carbide blocks is somewhat smaller in comparison with steel blocks. Thus, the magnitude and dependence on time of the additional energy flux, described by the quantity $\Delta V[1,2]$, are shown experimentally to depend crucially on the artifact material.

The fourth experiment of this study, which is used to clarify further the origin of TSE, establishes the linear relation between the vector quantities $\Delta T[1,2]$ and $\Delta V[1,2]$ and the Poynting vector (S), which characterizes the energy current density [15,13a] and the momentum density [13a,15] of the external EM field. This experiment can be regarded as an experimental check of the validity of the Poynting theorem of classical Electrodynamics, performed with huge signal-to-noise ratio for a wide-band thermal radiation. The main experimental results are shown in Figs. 6a and 6b. In Fig.6a it is demonstrated that the magnitude of the quantity $\Delta T[1,2]$ (and hence the magnitude of TSE) is linearly related to the increments in powers δP , delivered to the GB by the PRT. Actually, in Fig. 6a and 6b we present the results of four independent experiments. The curves marked with number 1 correspond to the displacement $Z=4.5\text{mm}$ of the axis of the R6 thermistor from the gauging surface. The curves 2 correspond to the Z-value of 13.5mm. In Figs.6 the measurements were performed for two different current modulation cycles in the PRT. The first cycle presented a rectangular modulation with DC current values of 1mA and 5mA (as in Fig.1). The other cycle realized the smaller variations of the dissipated energy in the PRT and corresponded to the current values of 1mA and 3mA.

All the data points, shown in Fig.6a, correspond to values of the temperature differences $\Delta T[1,2]$, arising in the channels 1 and 2 during the heating period, exactly 13 minutes after the increase of the modulation current. At this time interval the magnitude of the TSE is

already close to its maximum value (see Fig.2), and the value of the reference function can be very accurately predicted. In Fig.6a we have two increments of the input power, corresponding to 3 power levels. The zero increment of power corresponds to the current in the PRT of 1mA. At this current value (at the end of the cooling period) we define our reference points, relative to which all the differences in the induced temperature variations $\Delta T[1,2]$ in the channels are then measured. From the equation of the reference function in Fig.2, we find that for the time instant of 13 minutes after the current increase, the reference function is about $0.009\mu\text{K}$. This is a quite negligible quantity in comparison with other experimental points of Fig.6a. So, for the zero power increment we plot that vanishingly small quantity, as for the reference function the quantity $\Delta T[1,2]$ is equal, practically, to zero, in agreement with the basic idea of the MSD technique. Then two power increments are plotted as abscissa variables, with the values of $856\mu\text{W}$ and $2568\mu\text{W}$, corresponding to the current variations from 1mA to 3mA and from 1mA to 5mA, respectively. The indicated values of δP take also into account small variations of the resistance of the platinum thermometer (defined as 100 Ohm resistance at 0°C) when it is used close to 20°C , where all our temperature measurements were performed. As in our automatic DC bridge, a digital current control system was used, the power increment δP at $I=5\text{mA}$, with very high precision, was three times larger than the corresponding power increment at $I=3\text{mA}$.

The data point in Fig.6a, belonging to dependence 1 and characterized by the largest value of $\Delta T[1,2]$, corresponds to the experimental conditions of Fig.2, when the PRT current during the heating period was 5mA and one of the surfaces of the R6 adapter was in the plane of the gauging surface of the artifact. The only differences from Fig.2 are that the presented data points in Fig.6a correspond to the mean values of the quantity $\Delta T[1,2]$, obtained by the averaging procedure over all the modulation cycles of long experiments with total duration up to 16 hours, and also here, instead of the linear fit, we used the six order polynomial fit for the reference points of all modulation cycles. The second data point, belonging to dependence 1 and corresponding to the smaller power increment ($\delta P = 856\mu\text{W}$), was obtained as a result of an independent experiment, in which the higher level of the modulation current was 3mA. The stability in time and uncertainty of the measurement procedure in Fig.6a can be estimated from the spread of the data relative to the linear regression line, obtained for the 3 presented experimental points. The equation of the fit is shown in the inset. The maximum deviation of the experimental points for dependence 1 relative to the fit is $0.3\mu\text{K}$. The standard deviation of the data-points is $0.24\mu\text{K}$. These values should be compared with the TSE value of more

than $2500\mu\text{K}$, observed for the power increment of $2568\mu\text{W}$. Consequently, with very high precision it has been demonstrated experimentally, that the TSE magnitude depends linearly on the power, delivered to the artifact by the external heat source. And it has been shown above that the induced temperature variation $\Delta T[1,2]$ is a vector quantity. Among the external influence factors, we have the Poynting vector of the broad-band EM field, radiated by the heat source (PRT), that is also a vector quantity and whose magnitude is linearly related to the power dissipated in the heat source. As the PRT is separated from the block by a layer of isolating, thermo-conducting paste, the tunneling of particles from the PRT is not possible. So, the energy to the charged particles inside the artifact can be delivered only by means of the external EM field [14a], and, in accordance with the integral form of the Poynting theorem of electrodynamics, the power delivered to the field-particle system inside the artifact is defined by the flux of the Poynting vector through the boundary surface of the artifact [13a, 14b, 15]. Thus, *the linear relation between the vector quantity $\Delta T[1,2]$, which describes the thermal surface energy, and the Poynting vector, representing the energy current density of the external EM radiation, has been established experimentally with the signal-to-noise ratio of several thousands.*

Taking into consideration that the fit equation in Fig.6a is linear to a very high accuracy level, we can infer that the TSE value, under the experimental conditions of the dependence 1 and 13 minutes after the increase of the modulation current from zero to 1mA, should be at the level of $\sim 107\mu\text{K}$ (representing 1/8 of the TSE effect for the second point of this series). So, the contribution of TSE due to power dissipation in 100 Ohm PRT at $I=1\text{mA}$ under our experimental conditions is usually substantially smaller than the contributions of the poorly controlled external heat sources, defining the temperature difference $T[1,2]$ at the locations of the thermistors. For example, the total temperature difference between the channels even for the specially selected experimental conditions of Fig.1 is about $470\mu\text{K}$, i.e. more than 4 times higher than the surface energy, produced by the PRT at 1mA. Still, much smaller values of TSE can be very precisely measured as a result of the used combination of the modulation technique with the synchronous differential temperature measurements.

The dependence 2 in Fig.6a, marked with squares, shows the results of the corresponding measurements, when the measuring system, consisting of the PRT and of the pair of thermistors, was moved as a whole away from the gauging surface by 9mm, so that the distance Z of the axis of the thermistor R6 from the nearest gauging surface increased from 4.5 mm to 13.5mm. As the separations between the surfaces of the

PRT adapter and the surfaces of the adapters of the thermistors R6 and R3 were established with the help of a 10mm gauge block, the separations between the adapters were exactly the same in all these experiments. From Fig.6a it follows that the data points of the dependence 2 are also quite close to the corresponding linear fit, passing through the origin and establishing the linear relation between the TSE and the power increment δP . The corresponding fit equation is presented in Fig.6a below the dependence 2. The comparison of the fit equations for the dependences 1 and 2 shows that the increase of the distance of the R6 thermistor from the gauging surface by 9mm resulted in the decrease of the TSE ($\Delta T[1,2]$) magnitude by 1.664 times, when this decrease is characterized by the ratio of the slopes of the dependences 1 and 2.

Similar experimental studies were performed for the maximum value of the additional energy flux, which was characterized by the quantity $\Delta V[1,2]_{\text{max}}$ and which was observed during the initial stages of the heating period of the modulation cycle, similar to the one of Fig.3c. The experimental linear relations between the quantity $\Delta V[1,2]_{\text{max}}$ and the power increments δP , equal to $2568\mu\text{W}$ and $856\mu\text{W}$, are presented in Fig.6b. Here we show two plots, corresponding to the separations of the R6 axis relative to the gauging surface Z equal to 4.5mm and 13,5mm (as in Fig.6a). The equations of the linear regression lines for the experimental dependences 1 and 2 are presented in text boxes of Fig.6b. The decrease of the maximum energy flux with the increase of the separation Z from the gauging surface can be found from the ratio of the slopes of the experimental dependences 1 and 2 of Fig.6b. The obtained ratio is 1.981. This means that the experiment with power modulation of the external energy source has also shown that the maximum value of the energy flux $\Delta V[1,2]_{\text{max}}$ falls with the increase of separation Z from the gauging surface substantially faster than the value of the surface energy $\Delta T[1,2]$, for which the corresponding ratio was 1.664. If we divide the first ratio by the second ratio, we shall obtain the number 1.1905. Here, it can be noted that the conclusion about faster decrease of the energy flux $\Delta V[1,2]_{\text{max}}$ with Z separation from the gauging surface relative to the corresponding decrease of the surface energy $\Delta T[1,2]$ follows from both experiments with modulation cycles of 1mA-5mA and 1mA-3mA. So, the results and conclusions, following from the plots of Figs.4a and 4b, are confirmed by the experiment with the smaller power increment in Figs. 6a and 6b, but the signal-to-noise ratio is smaller in this case.

The result of fundamental importance follows from the linear dependences of Fig.6b, passing through the origin of the X/Y system. It means that the maximum value of the induced energy flux, described by $\Delta V[1,2]_{\text{max}}$, is linearly related to the power increment δP ,

produced by the variations of the Poynting vector of the external EM field. For example, for the dependence 1 in Fig.6b, the standard deviation for all three experimental points is about $0.3\mu\text{K}/\text{minute}$. Meanwhile, the quantity $\Delta V[1,2]_{\text{max}}$ exceeds $500\mu\text{K}/\text{minute}$ for the power increment of $2568\mu\text{W}$. So, from the plots of Fig.6b follows the linear relation between the maximum value of the additional energy flux in the artifact $\Delta V[1,2]_{\text{max}}$ and the Poynting vector of the external EM field, supplying the energy and momentum to the artifact. This relation has been demonstrated experimentally with the signal-to-noise ratio of ~ 1000 .

III. THERMAL HYSTERESIS EFFECT AND EVOLUTION IN TIME OF THERMAL SYSTEM

As it follows from the plots of Figs.1 and 2, the build-up of TSE does not occur instantaneously with the irradiation of the surface of artifact with a broad-band EM field, produced by the step-type increase of the current in the PRT, but there is an easily detected experimentally time delay, whose magnitude increases with the increase of the separation of the thermistor R6 from the gauging surface. Besides the time delay, the experiment shows that the amplitude of TSE is dropping with the increase of the R6 distance from the artifact's boundary (see Fig.4a), and the form of the $\Delta T[1,2]$ dependence on time is also changing with this distance (Figs. 4c and 5a). So, we have a complicated process that evolves in time and varies from point to point inside the artifact, depending also crucially on the material of the artifact. It looks that we have a typical hysteresis effect, as in cases of ferromagnetic [9d] or ferroelectric materials [9e], when the induction inside the artifact does not track instantaneously the changes of the external field, but its build-up depends on the pre-history of the process, when the whole path to the particular state of the system should be indicated.

Additionally, the plots of Figs.5a-5c give a clear proof that the build-up process of the TSE on time is not symmetric in space. And this is again the typical feature of the hysteresis effects in the well studied ferromagnetic and ferroelectric materials. As pointed out in [9e], when an external electric field is applied to a ferroelectric sample (BaTiO_3 , for example), there starts a gradual process of the growth of the domains with the favorable direction of the polarization (when the polarization vector coincides with the direction of the applied field) at the expense of the domains with the unfavorable polarization. This effect as a function of time can be detected experimentally by the observation of the domains in a polarized light. And this type of experiments, which are known for ferromagnetic [9c] and ferroelectric materials [9d], presents a clear experimental proof of the asymmetry in space in case of these hysteresis effects. The other key feature, typical

for the system with hysteresis effect, is the appearance of the *differences in the properties* of the material under the application of the external field that can be considered as the manifestation of the evolution of the material (or the demonstration of the "self-ordering" effect in the material). For example, it has been observed experimentally that in BaTiO_3 crystal, the positive edge of the domain is etched faster by an acid than its negative edge [9e]. These considerations give an indication that the dependencies of Figs.2-6 can be presented as a closed loop of a thermal hysteresis effect, especially, when we notice that the area of the curve above the reference line in Fig.2 defines the amount of energy, radiated by the particular parts of the block into the environment during one modulation cycle, and the area below the reference line defines the energy absorbed by these parts from the environment, so that *the thermal evolution process of Fig.2 has no symmetry in time* in accordance with the Clausius-Thomson-Plank formulations of the second law of Thermodynamics [9b]. The proof can be performed exactly in the same way as it is done for the well-studied hysteresis effects in ferroelectric [9e] and ferromagnetic materials [9d]. Indeed, the key feature of the process in Fig.2 is that it is periodic in time, and the system under the study (the gauge block with the PRT and thermistors) during each cycle realizes the transfer of the energy and of the momentum of the oriented motion of the electrons in the PRT (and of the energy and momentum of the propagating EM field irradiating the block) to the non-oriented thermal energy of the surrounding material objects on the Earth, with the corresponding transmission of the excessive momentum to the environment through the areas of mechanical support of the gauge block. This process is irreversible in time, as the process in the opposite time direction is strictly forbidden by the Clausius-Thomson formulations of the Second Law of Thermodynamics [9b].

After this, it is becoming probably clear that, in accordance with the discussion of the previous section, the indication to the way of the presentation of a closed loop of the thermal hysteresis effect gives the experimental procedure in ferroelectric materials. Instead of presenting the experimental points as a continuous sweep in time, it is necessary to present the points in two separate time sequences, each corresponding to one of the two possible directions of the variable forces, acting on the particles of the system. For materials with absorption, the direction of the EM force, acting on the charged particles, is defined by the direction of the energy propagation in the medium [15, 9g]. As it follows from Fig.3c, and the direction of the energy flux is changed during our modulation cycle. So, to obtain the form of the thermal hysteresis loop it is sufficient to present the data of Fig.2 as a function of the direction of the external force (acting on the field-particle system inside the artifact) by inverting the time for the

cooling period of the cycle. The corresponding plot is shown in Fig.7. Here, the induced temperature variations $\Delta T[1,2]$ for the heating period are presented in the same time scale as in Fig.2. The corresponding data points are shown as dots between the two arrows 1 and 2, indicating to the beginning and to the end of the heating period. The data points for the cooling period of the cycle in Fig.7 are shown by rhombi, corresponding to the path indicated by arrows 2-3-1. Along this path the time variable is $(111 - t)$, which means time inversion relative to the point $t=111$ minute, marked with arrow 2. Between the time interval, indicated by the arrows 2 and 3, the time scale is the same as in Fig.2. For the time interval between the arrows 3-1, where the variations of $\Delta T[1,2]$ are negligible, the data points are presented for much larger time intervals, so that the end of the cooling period coincides with the beginning of the heating period. As the quantity $\Delta T[1,2]$ is measured relative to the mean value of the several reference points at the very end of the cooling period of the cycle, we have a perfectly closed loop, only with some random jitter at a few μK level, which is negligible in comparison with the amplitude of the TSE effect.

The energy, which is radiated by the system during the modulation cycle and which is responsible for heating the environment, is defined by the form of the thermal hysteresis curve. As for the other, well studied hysteresis effects, the TSE process is an irreversible one. To prove this, we shall use the Plank formulation [9b] of the Second Law of the Thermodynamics (the most simple for interpretation), which says that no weight can be lifted in the field of gravity by periodic process when cooling thermal reservoir. We assume that the modulation of the current in the PRT is produced by an electronic switch with negligible losses and rechargeable battery, and the state of the battery charge is continuously monitored by the device, which is used in all portable computers. All the results of the measurements are assumed to be recorded. Then for the normal time direction (or the normal play of the record) we shall observe that the battery is gradually discharged, and the environment is heated by the energy radiated by the gauge block. For the backward play of the record, we shall observe that for the purely periodic process, the energy of the battery is increased only as result of cooling of the environment (thermal reservoir). The energy of the battery can be used to lift some weight. Thus, for the opposite play record (or time direction) we encounter the violation of the Thomson-Plank formulation of the Second Law of Thermodynamics (which presents the result of the analysis of a huge number of experimental facts and is known to have no exemptions). Consequently, such a process is strictly forbidden. So, the thermal evolution process, described by the vector quantity $\Delta T[1,2]$, is irreversible. In other words, it has no symmetry in time,

strictly in accordance with the Weyl idea how to check the symmetry in time of an arbitrary physical process [16].

Thus, experimentally we have demonstrated that *the thermal evolution process*, presented by the experimental plots of Figs. 1-7, is characterized by the lack of symmetries in space and in time and shows clearly hysteresis effect, when the polarization of the medium in the external EM field depends on the pre-history of the system.

Now we shall describe the fifth type of experiments of this study that discovers the other fundamental property of the surface energy, which, together the above mentioned properties of TSE, creates a new concept of the evolution process in physics, which is equivalent to the evolution concept in biology, for example. Experimental dependencies in the following figures show the effect of non-linearity of the material on the thermal evolution process, or, in other words, the invalidity of the superposition principle for the external EM fields in the process of energy and momentum propagations inside the material artifact.

In Fig.8, we show the evolution in time of the magnitude of the TSE, characterized by the quantity $\Delta T[1,2]$. As we were interested in obtaining maximum resolution in the amplitude of the effect, the measurements were performed with the steel block. The TSE magnitudes are presented for the first 13 minutes after the increase of the modulation current to 5mA. The averaging time for each experimental point was 2 minutes. The main differences relative to the experiment of Fig.2 are the following.

First, two additional, auxiliary heat sources (resistors) were located inside the Dewar, symmetrically and at the same distances from the gauging surfaces of the artifact. When one of them was energized, the adjusted value of the stabilized dc current through this resistor could produce a desired temperature difference between the locations of the thermistors R6 and R3. Thus in this experiment, the difference in the induced temperature variations, recorded by the channels 1 and 2, was measured when there was a systematic temperature difference on the artifact surface at the locations of the thermistors belonging to the channels 1 and 2. The temperature difference between the channels, $T[1,2]$, shown as an additional parameter in Fig. 8, was measured as a mean value of the temperature difference between the two thermistors, observed for the last 30 minutes of the cooling period of the modulation cycle. In Fig.8 the range of the variation of the parameter $T[1,2]$ was between -2.46mK and 61.06mK . Second, the separations between the adapters of the PRT and thermistors were increased from 10mm to 13.5mm, in order to study for the steel block the effect of the heat source separations from the thermistors adapters on the TSE amplitude.

As it is clearly seen in Fig.8, the temperature variation $\Delta T[1,2]$, induced by the increase of the current in the PRT, is also affected by the temperature difference $T[1,2]$, which is produced by an independent heat source with a constant dissipated power. It means that the steel gauge block acts as a non-linear device when its surface is irradiated by the EM fields of two independent sources. It also follows from the plots of Fig.8 that for all of the presented time intervals the magnitude of the TSE, represented by the quantity $\Delta T[1,2]$, is increasing with the increase of the temperature difference $T[1,2]$. It means that the larger surface energy is observed when the auxiliary energy source produces excessive heating of the gauging surface in the vicinity of the location of the thermistor R6. It is also clear from Fig.8 that for any data-points, corresponding to the same value of the time interval, the separation between the plots, corresponding to different values of the temperature difference $T[1,2]$, is steadily increasing with the increase of the observation moment. So, we have records of several complicated evolution processes, as each plot in Fig.8 represents a considerable part of the hysteresis loop (similar to the one of Fig.7), and *the parameters of this hysteresis loop can be easily changed by an auxiliary energy source.*

The resolution of the modulation technique is very high and gives the opportunity to observe clearly the difference between the TSE values, resulting from the increase of the temperature difference between $T[1,2]$ by only 4mK. For example, for dependences in Fig.8, corresponding to the temperature differences of 57.1mK and 61.1mK, the systematic differences in $\Delta T[1,2]$ are well above the noise level for all the presented time intervals in the range between 3 and 13 minutes. As the quantity $\Delta T[1,2]$ corresponds to the difference in the temperature variations in the channels 1 and 2, which are induced by the increase of the current in the PRT and *this induced temperature difference is affected by the presence of the other heat source*, this means that *the superposition principle is not valid for the sources of external EM radiation as a result of the existence of the thermal surface energy.* It should be specially emphasized here that *the violation of the superposition principle for EM fields is observed also in a free space, which is not occupied by the material artifacts.* This is a consequence of the fact that the energy, recorded by the thermistor, corresponds to the energy of the oriented motion of the field-particle system, which is radiated by the block into the auto space. When the accuracy of the experiment is sufficient to detect the energy, reemitted by the material objects, the principle of superposition of the EM fields is becoming invalid even for the free space.

From the experiments (presented above) it follows that the thermal evolution process (Figs.2, 7), observed in metallic blocks for periodic power

modulation, is irreversible, or in other words, it has no symmetry in time. This process changes from point to point inside the artifact (Figs.4a, 4b, 6a, 6b) and has no symmetry in space (Figs.3b, 5a, 5b). So, the parameters, characterizing the properties and state of the artifact, should be specified for a particular time instants and for the particular observation points. If in Fig.8, we choose the data points corresponding to measurements, obtained 13 minutes after the increase of the current in the PRT, and plot them as a function of the temperature difference $T[1,2]$ for the locations of the thermistors indicated above, we obtain the plot of Fig.9a. By this plot, we present experimental demonstration of the non-linear properties of the thermal process in steel blocks: the magnitude of the TSE depends not only on the amplitude of the PRT current, but is also affected by the presence of an auxiliary heat source. The non-linearity of the system, which in this case is characterized by the linear dependence of the TSE magnitude on the temperature difference $T[1,2]$, is demonstrated with a huge signal to noise ratio. For this it is sufficient to compare the maximum deviation of the 4 data-points relative to the linear fit (which is $1.75\mu\text{K}$ in Fig.9a) with the total variation of the quantity $\Delta T[1,2]$, exceeding $700\mu\text{K}$. Thus, Fig.9a shows that the non-linearity of the artifact can be measured with the signal-to-noise ratio of several hundreds with the use of modulation technique, in spite of the fact that we are dealing with the next order effect in comparison with the detection of the surface energy as a function power, which is dissipated in the PRT.

In Fig.9a, the equation of the linear fit is presented in a separate text box. When X and Y variables of the plot are both measured in the same units (mK), the quantity R_1 , which is defined as the ratio of absolute values of the vector quantities $\Delta T[1,2]$ and $T[1,2]$, is becoming equal to 1.2%. So, the non-linearity of the system is not that small. But this value characterizes the non-linearity only for the indicated time interval of 13 minutes. As, the plots of Fig.8 describe some portions of the hysteresis loops and the hysteresis effect means some memory in time of the preceding states of the system, the response of the system to the variation of the external EM field, characterized by the non-linearity of the system, inevitably should be some function of time. *Important variations of the non-linearity in time, as a main property of the steel block in the thermal evolution process, follow from the comparison of Figs. 9a and 9b.* In Fig.9b, the induced temperature variations $\Delta T[1,2]$ are presented as a function of temperature difference $T[1,2]$ for the time interval of 3 minutes after the increase of the PRT modulation current. From the equation of the fit in Fig.9b, we find that the value of the ratio R_1 is only 0.25%. So, the non-linearity in this case is 4.8 times less than the one in Fig.9a. If we choose the third time interval as 9 minutes,

we shall find that the ratio R_1 will be 0.95%. When plotting these values as a function of elapsed time, we find that at the beginning of the thermal hysteresis loop, the rate of the increase of the non-linearity value increases rapidly with time, reaches its maximum value and then the rate decreases.

And now we are to explain why in Figs.9 we have such a high signal-to-noise ratio. The answer is simple. In this case we performed special *modeling of the evolution process*. First, we applied a synchronous modulation technique, using the most accurate (square-wave) type of modulation. If, for example, during the total measurement time of ~ 7 hours we have a record of six modulation cycles, then the averaging procedure over all of them keeps, practically, only induced variations for each specified time interval of the quantity $\Delta T[1,2]$. The spurious perturbations of the signal are significantly reduced as a result of effective isolation of the investigated system by the Dewar enclosure, resulting in a very large thermal time constant of the system. The other important factor is the use of the temperature control system, so that when the averaging procedure over several cooling and heating cycles of the temperature control system is realized, the effect of the external temperature perturbations is diminished to the acceptable level. Second, the temperature difference between the locations of the thermistors was produced by the stabilized heat source, which was located inside the Dewar. The effect of the spurious perturbations was about two orders of magnitude smaller. So, even for relatively small signals of Fig.9b, where the total variation of the quantity $T[1,2]$ is about $150\mu\text{K}$, the signal-to-noise ratio is still considerable, as the standard deviation of the points relative to the fit is only $0.22\mu\text{K}$. But the price for this is also clear. In this case we observe the influence on the TSE magnitude only of the static temperature difference $T[1,2]$, represented by the mean value of this quantity over the whole measurement time. The effect of the temperature transients on the TSE can not be observed in this case.

The violation of the superposition principle in combination with hysteresis effect results in important consequences: the presence of an additional heat source can change drastically the evolution process, which can be observed as a result of the energy modulation cycle inside the PRT at any point of the artifact. In more detail this is illustrated by Fig.10, where we present the dependences $\Delta T[1,2]$ versus time for a 100mm tungsten carbide GB, in which the creation of the TSE occurs much faster than in steel blocks. In this case, even during the first 13 minutes after the increase of the modulation current in the PRT, a considerable part of the evolution process can be observed. The separations between the adapters of the thermometers were 14 mm in this case. The other distinguishing feature of the experiments (presented in Fig.10) is that in

all cases the auxiliary heat source irradiates more efficiently the gauging surface, which is far away from the thermistor R6 (belonging to channel 1). So, the external heat source produces the heat flux in the same direction in the vicinity of the thermistor R6 as the PRT does, when the current inside it (during the heating period of the modulation cycle) is increased to the value of 5mA. The dependences 1-3, marked with dots, squares and rhombi, correspond to the mean values of the temperature differences between the channels $T[1,2]$ equal to $-1,17\text{mK}$, $-8,2\text{mK}$ and $-17,2\text{mK}$, respectively. These values were measured at the ends of the cooling periods of several modulation cycles. So, we show here three independent experiments with three different power levels, dissipated by the auxiliary heat source. For each sequence of the data-points, the mean value of the temperature difference between the channels was the additional parameter.

As it is clearly demonstrated by the dependences 1-3, the additional heat source changes significantly the thermal evolution process. The maximum of the curve $\Delta T[1,2]$ versus time is clearly detected for the negative values of the quantity $T[1,2]$. The key features of the evolution process are the variations of the maximum values of the TSE magnitude with the increase of the absolute value of the temperature difference $T[1,2]$, and the shift of the maximum value of the quantity $\Delta T[1,2]$ on the time scale. For example, for the dependences 1-3 the maximum values are, approximately, equal to $915\mu\text{K}$, $863\mu\text{K}$ and $846\mu\text{K}$, respectively. The uncertainty of these measurements is $\sim 2-5\mu\text{K}$. With the increase of the value of the negative temperature difference $T[1,2]$, the position of the maximum value shifts to the smaller time intervals, elapsed after the increase of the modulation current in the PRT. For the dependences 1-3, the corresponding time intervals are, approximately, equal to 7.5, 5.45 and 4.15 minutes, respectively. Thus, we have a record of the evolution process when *the external heat source changes the shape of the dependence of the surface thermal energy on the time elapsed*.

One can see in Fig.10 that the difference between the dependences 1- 3 is steadily increasing with the time increase for the time intervals in the range of 3-13 minutes. For example, for the time intervals 3, 7 and 13 minutes after the increase of the modulation current, the differences between the dependencies 1 and 3 are equal to $13\mu\text{K}$, $123\mu\text{K}$ and $255\mu\text{K}$, respectively. When choosing the data-points of Fig.10, corresponding to the time interval of 13 minutes and plotting them as a function of the temperature difference $T[1,2]$, we obtain (as in Fig.9a) the linear dependence, where the slope for the TC block is somewhat larger than the slope in Fig.9a. The corresponding non-linearity coefficient R_1 is equal to 1.4% in this case. And it is also clear from Fig.10 that the value of the coefficient R_1 will

continue to grow with the further increase of the time interval (at least, in some range).

The other important result follows from Fig.10 when we analyze the presented dependences in the time interval between 0.5-1.5 minutes. The non-linearity ratio R_1 is negative in this range, showing that we have a hysteresis effect of the opposite sign! In this time interval, the auxiliary heat source, producing in advance a stationary energy flux in the direction of the thermistor R6, is increasing the quantity $\Delta T[1,2]$. Or in other words, the additional energy flux, stimulated by the increase of the PRT modulation current, is increased if the steady-state energy flux in the same direction has been created in advance by an auxiliary energy source. Here, it is important to note that for this time interval we have, practically, a pure running wave of the propagating energy, as the reflection from the gauging surface is quite small: the product of the indicated time interval and the mean velocity of the energy propagation in the medium is smaller than the distance from the PRT to the gauging surface. Thus, it is demonstrated experimentally that when the energy reflection from the boundaries is negligible, *the energy flux, which is propagating in a homogeneous medium and which is induced by a step increase of the magnitude of the Poynting vector of the external EM field, is significantly increased, if the energy flux in the same direction has been created in advance by an auxiliary source of EM radiation.* Some preliminary studies of this effect have been reported also in [3f, 3i]. In some cases, this effect can be of primary importance. For example, for the time interval of 0.5 minute after the increase of the modulation current, the quantity $\Delta T[1,2]$, corresponding to the temperature bias $T[1,2]$ of -17.2mK, exceeds by more than 2 times the quantity $\Delta T[1,2]$, observed for the bias of -1.2mK.

Some additional information dealing with this experiment is presented by the plots of Fig.11. Here, we show the differences in the induced temperature velocities $\Delta V[1,2]$ as a function time for the tungsten carbide (dependences 1 and 2) and for the steel block (dependence 3). As it follows from Fig.11, the main parameter, defining the properties of the evolution process, is the type of the material. For the dependence 3, representing the corresponding part of the plot in Fig.3c, the area between the curve and the abscissa axes is much larger than that for the dependence 1, so that the TSE magnitude in steel is about 3 times larger than in tungsten carbide (in agreement with the plots of Figs. 2 and 10). But the process in the TC block evolves much faster, as the maximum value of the additional energy flux in the TC block is observed substantially earlier (Fig.11).

For TC block we show two plots. Dependence 1, represented by dots, corresponds to the temperature difference between the channels $T[1,2]$ of -0.2mK, PRT

current modulation amplitudes 1-5mA and the separations of 14mm between the adapters of all thermometers. Dependence 2, shown by squares, corresponds to the value of the temperature difference $T[1,2]$ of -17.2mK. As there are differences between the dependences 1 and 2, it means that the auxiliary heat source changes the induced variations of the temperature velocity $\Delta V[1,2]$, and consequently the principle of superposition is not valid for EM fields. Here, we are to note that the positive value of the quantity $\Delta V[1,2]$ means that the power, emitted into the outer space by the elementary area of the block surface in the vicinity of the thermistor R6 (close to the gauging surface), is larger than the power, emitted by the elementary area of the block surface in the vicinity of the thermistor R3. The negative value of the quantity $\Delta V[1,2]$ means that the power emission capability of the block surface is larger in vicinity of the thermistor R3. So, the plots of Fig.11 show that *the power emission capability of the block surface is changed by auxiliary heat source both in space and in time.* And the interesting thing is that these variations are observed during a relatively small part of the heating period of the modulation cycle. Probably, the evolution process depends on the enormous quantity of influence parameters. As it follows from Fig.3c, the uncertainty of the measurements are smaller than the dimensions of the symbols used for the presentation of the data-points, and, consequently, the error bars cannot be shown on the plot. The consideration is valid for the experimental curves in Fig.11. So, the comparison of the dependences 1 and 2 in Fig.11 shows that the effect of the auxiliary heat source on the induced thermal velocity difference $\Delta V[1,2]$ is well beyond the uncertainty of the experiment. For example, for the time interval of 0.5 minute the negative value of the quantity $T[1,2]$ increases the velocity difference. Meanwhile in the range of intervals from 1.5 to 13 minutes, the negative value of $T[1,2]$ diminishes the value of the quantity $\Delta V[1,2]$, thus reducing the excessive energy flux density associated with the TSE. A complicated form of the difference between the dependences 1 and 2 gives an indication that even for our experiment, when the mean value of the temperature difference $T[1,2]$ and the PRT modulation current value characterize sufficiently accurately the external experimental conditions, the number of internal influence parameters is enormous. As it will be shown in the next section of the paper, the cycle-averaged rate of the conversion into heat of the energy of the oriented motion of the field-particle system [15] is linearly related to the total force density [15], acting on the field-particle system inside the material with arbitrary level of absorption. So, if in Fig.3 the quantity $\Delta V[1,2]$ is changing the sign at the beginning of the heating and cooling periods of the modulation cycle, then there are the corresponding variations in the

energy flux densities in time and in space that immediately result in the differences in the total force densities in time and in space. But the variation of the force, acting on the elementary volume of the medium, means that force results in deformations and stresses in the medium, which change the properties of the medium and which lead to the creation of a non-uniform medium in the presence of the EM field. So, it is not astonishing that the non-linearity parameter, which is one of the fundamental in Electrodynamics and which is characterizing the response of the medium to the EM field, is also changing in time and in space (see Figs. 8-10).

For the steel block, it is natural to expect that the process of the propagation of the field-particle system is crucially affected by the presence of the domain structure. So, in the list of influence factors we are to include the size of each domain, its orientation relative to axis of the block and its position relative to the gauging surfaces. The dislocations inside the domain structure are also inevitably affecting the propagation of the free electrons and displacement of the ions of the lattice. So, among the internal influence factors we are to include the position, orientation and the size of each dislocation. Thus the number of influence parameters, affecting the thermal evolution process in a steel block, is always enormous. But, similar situation with enormous number of influence factors is observed in case of ferromagnetic materials, which have been studied experimentally for many decades. And it is known from the book of Ch. Kittel that the description of the hysteresis effect in ferromagnetic materials presents too complicated problem for theoretical physics [16a]. Even larger number of internal influence factors is typical for tungsten carbide gauge block. The domain structure is not present in that material and the positions of all atoms are to be specified (the nearest order does not exist in this case).

The enormous number of internal influence factors in case of the thermal evolution process should be added to the huge number of external factors, which define the magnitude and direction of the resulting Poynting vector of the EM field at each point of the surface of the gauge block under investigation. When we use an auxiliary heat source, its radiated energy is partially transmitted through the side walls of the Dewar and part of it propagates along the walls in the direction of the Dewar axis, so that the mean temperature of the gauge block over the time interval of the modulation cycle is, practically, constant. To solve the problem, it would be necessary to write the equations for the continuity of energy, momentum and angular momentum, but the solution is not possible as, for the realized accuracy of the experiment, it is necessary to take into account the radiated energy of the Sun that propagates through turbulent atmosphere and the walls of the building. And the description only of turbulent

atmosphere requires an infinite number of macroscopic parameters [9a]. Besides that, when the energy, radiated by the Sun reaches any material object it produces the surface energy and some part of the energy is reemitted as a result of the oriented motion of the field-particle system. So, *the resultant Poynting vector of the EM field, irradiating the Dewar surface, is the vector sum of the contributions of the enormous number of material objects, which cannot be considered as independent, as all of these objects are interacting with the common EM field* [17-19]. The same considerations are valid for the investigated gauge blocks, as the Dewar (or any other experimental set-up) cannot produce adiabatic isolation of the system. Thus, for the investigated material objects, for which evolution process, as shown experimentally, is characterized by the hysteresis effects, produced by the infinite number of correlated influence factors, it is very doubtful that the description of the corresponding process can be realized in terms of mathematical tools, specially developed and only quite adequate for the description of relatively simple cases of Newtonian mechanics. Indeed, as it follows from the fundamental principle of thermodynamics even for a specific theoretical model of an ideal gas, the presentation of the evolution process by a continuous line on the pressure versus volume diagram is only possible for the (so-called) quasi-static processes of the isolated systems [9b], that is only for the sequence of thermally equilibrium states, following each other without any transient intermediate processes. The experimental observation of the evolution processes in thermal systems gives sufficient proofs for the validity of the Niels Bohr statement that the description of arbitrary system in terms of time and space is not possible in the general case. This is a direct consequence of the famous incompleteness theorem of Kurt Gödel in mathematics. In the described experiments it is shown that the interaction of the EM field with the ensemble of atoms of a solid-state artifact results in a clearly observed hysteresis effect, while the theoretical physics, equipped with the standard mathematics (specially developed for the description of Newtonian systems with the finite number of independent variables), *has not been able, so far, to describe adequately the "simplest case" of the hysteresis effect in ferromagnetic materials in a constant magnetic field. Thus, the description in the general case of the evolution process, characterized by the infinite number of interacting material objects, which produce the common Poynting vector over the whole space and consequently cannot be regarded as independent, is far beyond the possibilities of all Modern Physics, as even its basic concepts of isotropic time and of isotropic space (borrowed from mathematics) are in dramatic contradiction with all Natural sciences* (see Discussions).

Besides that, our experiments have demonstrated that the time dependence of the thermal

evolution process and the magnitude of the surface energy are specific for a particular point inside the artifact, and that both quantities can be significantly changed by the auxiliary external heat source (see Figs. 3-11). *As philosophers say nowadays, the time and space concepts are relational ones* (see Discussions). On the other hand, the very fact of the existence of the thermal hysteresis effect means that there is a time scale, which is characteristic to each material object and which is defined by its own evolution process. The two time scales, corresponding to any two material objects, are inevitably somewhat different: among the huge number of internal parameters, characterizing each object, there will be some difference. Besides that, the driving source of each thermal evolution process is the Poynting vector of the resultant common EM field, is also somewhat different as a result of spatial difference in the locations of the two objects. On the same reasons, the record of the evolution process of a particular material object in time scales of two clocks (including quantum atomic clocks) will be always somewhat different. This is the consequence of a well-established experimental fact that the Allan variance as a function of the averaging time for any quantum clock starts to increase (after reaching the “flicker floor”) [20], or in other words *the time scales of the two clocks start to deviate in unpredictable manner when the observation time exceeds the flicker floor averaging time. Thus, the processes in material objects cannot be synchronized in time, and this is the manifestation of the fact that isolated systems do not exist in Nature. All these are experimental proofs to the Niels Bohr’s famous observation that “Isolated material particles are abstractions, their properties being definable and observable only through their interaction with other systems”.*

IV. CONCLUSIONS AND DISCUSSIONS

Before starting discussions, it is worth noting that the main parameter, affecting the indications of a resistance thermometer (thermistor) is the energy of the external EM field, irradiating the surface of the thermometer. This field is mainly produced by the irregular motion of the charged particles and the EM field inside the artifact, which is in contact with the thermistor. As the adapter of the thermistor is isolated from the artifact by nonconductive paste and charged particles cannot tunnel through the gap of $\sim 0.1\text{mm}$ between the adapter and the artifact, the only way for the energy transfer is the radiation of the EM field, with the following absorption of it in the thermistor adapter. The part of the EM energy, absorbed in the thermistor, changes the number of carriers in the valence and in conductance bands, thus effectively changing the recorded resistance value of the sensor. This is the consequence of the Poynting’s theorem of

Electrodynamics [13a, 14a], which says that the rate of change of the electromagnetic energy plus the total rate of doing work by the fields over the charged particles within the volume of a material artifact is equal to the flux of the Poynting vector (see eq.(6.109) in [13]), S , entering the volume of the artifact through its boundary surface (see eq.(6.111) in [13]). So, the vector S describes the energy-flux density of EM field [13], or the energy current density (as it is called in [15]). For the dielectric material with arbitrary level of losses, the continuity equation for the total energy density for the coupled EM field and dielectric lattice, under the approximations made in [15], can be presented in the form (see eq.(2.17) in [15]):

$$\frac{\partial}{\partial t} W + m\Gamma\left(\frac{\partial}{\partial t} s\right)^2 = -\nabla S \quad \dots(1)$$

Here, W presents the total energy density, which contains in addition to the EM field energy density, the kinetic and potential energy densities of the optic vibrational mode; s is the relative spatial displacement field of two ions in the primitive unit cell; m is the reduced mass of two ions in the primitive unit cell, and Γ is the damping rate of the optical mode.

The rate of the energy variations, described by the first two terms in Eq. (1), can be detected by thermistors and corresponds to the experimentally measured thermal velocities at the specified points of the material artifact ($\Delta V[1]$ and $\Delta V[2]$). Indeed, the reading of the thermometer depends on the power absorbed from the EM field, as in accordance with the Poynting’s theorem, the power, radiated by the material artifact, is defined by the total rate of the energy loss of the EM field and of the energy loss of the optical mode, which is directly coupled to the EM field [15]. The second term in Eq. (1) describes the rate of loss of the energy of the optical mode, which is converted into heat as a result of intrinsic non-linearity of the system [15]. And this contribution is also detected by thermistors, as all the thermometers are traditionally used to characterize the random part of the thermal energy of the material artifacts. So, if in Fig.3 we see that the quantity $\Delta V[1,2]$ is not equal to zero during a short interval of time after the change of the PRT current, it means that there is an additional energy flux (positive or negative) to the elementary volumes $(dx)(dy)(dz)$ in the vicinity of the thermometer R6 relative to the elementary volumes in the vicinity of the thermometer R3. And in accordance with the continuity equation in the differential form [13a, 15], these energy fluxes arrive inside these volumes through their boundary surfaces as a result of the total-energy current density S [15], which is present at a particular point of the artifact and describes the interacting field-particle system. As the difference in the induced temperature velocities $\Delta V[1,2]$ is not equal to zero, it means that the total-energy current densities [15] at two different locations inside the

artifact, located symmetrically relative to the energy source, are also different at that time moments. And this difference in the energy current densities S , representing the oriented motion of the coupled field-particle system inside the artifact, is shown experimentally to be linearly related to the energy current density of the EM field, irradiating the surface of the artifact (section 2.1). Thus, *the oriented motion of the energy and momentum of the field-particle system, which is stimulated and supported by the Poynting vector of the external EM field, is the physical reason for the existence of the thermal surface energy $\Delta T[1,2]$.*

Simultaneously, the above presented experimental studies have clearly demonstrated that *the basic assumption of the Fourier thermal conductivity theory (TCT), which is borrowed from the steady-state experiments and which states that the thermal energy flux is defined by the temperature gradient [9c], is not valid for any period of the heat transfer process.* Especially, it is not true for the “transients” of the propagation process of the thermal energy. As it follows from Figs.1-3, for the heating period of the cycle, the maximum energy fluxes to the unit volumes inside the steel artifact, which are located symmetrically, but in the opposite directions relative to the energy source, differ by $\sim 40\%$ and the energy flux to the vicinity of the R6 sensor is larger. But the temperature in the system was adjusted in such a way that the temperature of the artifact surface, close to R6 sensor, was already somewhat higher than the temperature, close to R3 sensor, just before the increase of the modulation current. During the whole heating period of the modulation cycle, the induced temperature difference $\Delta T[1,2]$ continues to increase and at the end of the heating period, characterized by the equal thermal fluxes (see Fig.3), the largest induced temperature difference $\Delta T[1,2]$ of about $\sim 2.5\text{mK}$ is observed. Meanwhile, at the end of the cooling period of the modulation cycle, the energy fluxes to the unit volumes in the vicinities of both sensors are again, practically, equal, but the temperature difference between the PRT and the thermistor R6 is somewhat smaller (by approximately 0.47mK) than the temperature difference between the PRT and the thermistor R3. From this it follows that *the TCT can be expected to give reasonable agreement with the temperature measurements of moderate precision only for the steady-state periods of the heat transfer process, but the TCT predictions about the initial periods of the heat transfer are very doubtful.*

The other very important observation, which is necessary for the interpretation of the presented experimental studies, follows from the solid-state physics [16b]. It is known that for a charged particle inside the solid-state, the conserved quantity is the total momentum, which consists of the kinetic momentum of the translational motion of the charged particle and the

potential momentum of the EM field [16b]. As pointed out by Ch. Kittel, this requirement on the total momentum of the field-particle system is correct, because it results in the proper equation for the Lorentz force acting on the charged particle [16b].

This is in agreement with the conservation laws of electrodynamics [13a, 14c, 15]. The electromagnetic momentum density \mathbf{G}_{EM} (in accordance with eq. (6.118) [13a]) is given by:

$$\mathbf{G}_{EM} = \mathbf{S} / c^2 \quad \dots (2)$$

where c is the velocity of light in vacuum. The continuity equation of Electrodynamics in the integral form (see eq. (6.122) in [13a]) states that the first derivative in time of the total momentum of the field-particle system in the artifact volume, consisting of the EM momentum and the momentum of the charged particles, is defined by the flow through the boundary surface inside the artifact volume of the EM momentum current density, given by the Maxwell stress tensor (see eq.(6.120) in [13a]). Thus, from the fundamentals of Electrodynamics and the Solid-state Physics it follows that the “conserved” quantities of the field-particle system inside material artifact can be only the total momentum and the total energy densities (Poynting’s theorem, section 3 above) of the field-particle system. So, in agreement with the presented experimental studies, the temperature, as a physical parameter, which characterizes the variations of the internal energy of a macroscopic elementary volume inside the artifact that can be detected by EM radiation, should inevitably correspond to the variations of the total energy of the field-particle system. Thus, the total energy has to include the energy of EM field in addition to the energy of the charged particles. And the experimental result of the primary importance of these studies is that *the internal energy includes both: the energy of the random type of the motion of the field-particle system (with the mean values of the linear momentum and angular momentum equal to zero) and the energy of the systematic part ($\Delta T[1,2]$), which describes the oriented propagation inside the medium of the thermal energy with the corresponding wave-momentum [15].* In this respect our experiments present the necessary confirmation of the theoretical studies of R. Loudon, L. Allen and D. F. Nelson [15], dealing with the propagation of the energy and momentum through an absorbing dielectric with an arbitrary level of losses. The essential features of the theory [15] are the inclusion of the contributions from EM field and from dielectric medium to the total energy density W and to the wave momentum density, and taking into account the Röntgen term in the current density in the Maxwell equations. The Röntgen term changes drastically the relation between the magnetic field \mathbf{H} and magnetic induction \mathbf{B} (by introducing the term, depending on the

polarization of the medium \mathbf{P} , which is induced by electrical field). In accordance with [15], the wave-momentum density consists of the EM field momentum \mathbf{G}_{EM} and the pseudomomentum density \mathbf{G}_{psm} , found to be equal to $[\mathbf{P} \times \mathbf{B}]$ plus a dispersive term, which accounts for the thermal losses in the system. The main results in [15] are illustrated by the one-dimensional case of a plain transverse EM wave, propagating in z-direction of dielectric material with arbitrary losses. The intensity of the EM field in z-direction is assumed to fall exponentially with the characteristic length L , as a result of the gradual conversion of the energy of the optical mode into heat (see eq.(3.11) in [15]).

As pointed out in section 2.1, our measurement procedure is sensitive to the variations of temperature only in one z-direction, along the longer side of the GB. Also, from the experimental plots of Fig.12 in [3c] we can infer that a thermal wave, induced by power dissipation in the PRT located on the surface of a long (900mm) steel block, can be quite well approximated by inhomogeneous plane wave, if its amplitude and attenuation coefficient in the direction of the propagation are obtained from experiment. But for the plane transverse EM wave, propagating along the dielectric medium with arbitrary large losses [15], all the basic solutions (including the energy of the system which is converted into heat) can be obtained in a closed form as a function of the total-energy current density (see eq. (2.18) in [15]). So, from the temperature measurements, described in this paper, we can define quite accurately the variable part of the total-energy density of the field-particle system, W :

- a) the induced temperature variations along the artifact can be precisely measured;
- b) the thermal capacity of steel at room temperature is well known;
- c) the distribution of temperature in the vertical direction inside the GB (at some distance from the heat source) is quite homogeneous;
- d) the thickness of the block (9mm) is much smaller than its length;
- e) the adapters of thermometers cover the whole width of the GB.

Additionally, from the experiments presented here, the *velocity of the energy propagation* inside the steel GB *can be found*, so that we can have a reliable estimation of the basic processes inside the artifact. For example, for the plane TEM wave (in accordance with [15]), the cycled-averaged value of the total-energy current density $\langle S \rangle$ (which has the only nonzero component in the direction of the energy propagation z) is related to the cycle-averaged energy density $\langle W \rangle$ (see eq.(2.19) in [15]) by a simple relation (4.16):

$$\langle S_z \rangle = v_e \langle W \rangle \quad \dots (3)$$

where, v_e is the velocity vector of the energy propagation in the material. This is a standard relation between the energy current density and the energy density that describes quite precisely an arbitrary medium with absorption [9f]. And all the parameters on the right side of eq.(3) can be accurately enough measured experimentally for any particular point of the artifact. Meanwhile, the total energy density W can not be properly calculated by theory by using the parameters of the external EM field irradiating the object, as the *constitutive relations for the medium are not known* [13b].

For the wave vector k in the medium, given by the usual expression [15]:

$$k = [\eta + i\kappa] \omega / c \quad \dots (4)$$

where ω is the EM field frequency; c is speed of light; η is the refraction index of the medium; and κ is the extinction coefficient, the expression for the energy velocity v_e , in accordance with eq.(4.16) in [15], is

$$v_e = c / (\eta + c/(L\Gamma)) \quad \dots (5)$$

Here, Γ is the parameter showing how fast the energy of the optical mode is converted into heat through Rayleigh dissipation function, and $L = c / (2 \omega \kappa)$ is the characteristic length of the decay of the intensity of the EM field with the distance along the propagation direction. The parameters η and κ in different materials can be precisely determined from the studies of optical reflections from the surfaces [3g]. For example, for steel gauge blocks in red light the refractive index η is 2.2 and $\kappa=3.4$; for tungsten carbide GB, $\eta=3.4$ and $\kappa=2.4$ [3b]. These values are in agreement with very accurate measurements of the phase change at optical reflection by optical interferometry [3a]. The velocity value v_e of the energy propagation in steel can be estimated from the present studies, when using the dependencies of $\Delta T[1,2]$, obtained for different distances from the gauging surface. (These studies are similar to the ones resulting in the plots of Fig.5). From these studies the velocity v_e is found to be of the order of 10mm per minute for the steel block.

We can have also a reliable estimation of the wave momentum density \mathbf{G} in the medium, which consists of the momentum density of the EM field and of the pseudomomentum density of the medium (see Eq. (3.21) in [15]). Pseudomomentum contains the contribution of the polarization, which is induced in the medium by the propagating EM field. In accordance with equation (4.32) in [15], the cycle-averaged value of the wave momentum density \mathbf{G} in the propagation direction z of the plane wave is also related to the Poynting vector of EM field inside the medium and is given by the expression:

$$\langle G_z \rangle = v_e \langle W \rangle / (v_p v_{wm}) \quad \dots (6)$$

where $v_p=c/\eta$ is the phase velocity of EM field and the velocity v_{wm} of the wave momentum current density is

$$v_{wm} = c / (\eta + c/(L\Gamma) + \kappa^2 / \eta) \quad \dots (7)$$

It follows from equations (3) and (5) that in case when $v_e \ll c$, the velocities v_e and v_{wm} are, practically, equal. So, in accordance with Eq. (6), the value of the z-component of the wave momentum density G_z is, approximately, equal to the ratio of the energy density $\langle W \rangle$ and the value of the phase velocity v_p . Both parameters can be quite precisely determined from the experiments.

For the plane, transverse EM wave, the cycle-averaged values of the wave momentum current density T_{ji} , defined by equations (3.18) and (3.24) in [15], presents the sum, taken with the sign minus, of the Maxwell stress tensor [13a] and the product of the corresponding components of the EM field and of the arising polarization of the medium. The quantity T_{ji} describes the values of stresses and shears, acting on the unit areas inside the artifact material [14b]. For example, the component T_{zz} is given by the relation [15]:

$$- \langle T_{zz} \rangle = \langle W \rangle (v_e / v_p) \quad \dots (8)$$

Under the same approximations, the total force density $\langle F_t \rangle$, consisting of the Lorentz force density (which is acting on the particles) and of the time derivative of the EM field momentum density [15], can be presented by the expression:

$$\langle F_t \rangle = [(1 + \eta^2 + \kappa^2) / (2\eta^2 L)] \langle W \rangle (v_e / v_p) \quad \dots (9)$$

Meanwhile, the cycle-averaged rate of the energy conversion into heat $\langle R_H \rangle$ in accordance with continuity equation (2.17) in [15], written for the energy density of the coupled field-particle system, can be presented in a form:

$$\langle R_H \rangle = \langle S_z \rangle / L = v_e \langle W \rangle / L \quad \dots (10)$$

So, from equations (9) and (10) it follows that the cycle-averaged rate of the energy conversion into heat $\langle R_H \rangle$ is linearly related to the total force density $\langle F_t \rangle$ for dielectric material with arbitrary level of losses [15]. So, *the propagation of thermal energy and momentum are always accompanied by stresses and deformations in the material that can be estimated from the experimental data.*

But the theoretical model in [15] uses an approximation of a simple Lorentz oscillator, which is characterized by an instantaneous, linear response to the external EM field. So, the hysteresis effect, which forms the basis of the thermal evolution process, is beyond the scope of this theory. In this respect it can be noted here that the thermal hysteresis effect in the bulk material was first observed for the external heat source in a 900mm steel GB (see Fig.9 in [3f]). Also, from the

experimental dependence of Fig.8 in [3h]) it follows that the heat energy (described by the energy density W) in a homogeneous, well thermally isolated material artifact can propagate large distances with very small damping. It means that when in the experiments presented here, the gauge block surface is irradiated by an EM field of the PRT, then, in accordance with [15], the wave momentum density G of a coupled field-particle system should be detectable at any point of a 100mm block. But if the total momentum, consisting of the momentum of the charged particles and the momentum of the EM field, is not equal to zero, then some part of the total momentum will be inevitably reflected from the boundary, and the reflected total-energy and momentum densities will produce an additional energy flux to the unit volumes of the artifact in the vicinity of the boundary. From this we can conclude that the general theoretical observation of A. Einstein about the importance of taking into account the surface energy has been confirmed experimentally for a particular case of the thermal surface energy $\Delta T[1,2]$ (see Figs.2-5).

Here, we are to note also that the *velocity error studies* in thermal systems, described in [3a, 3b] and performed under thermally non-equilibrium conditions, do present a particular kind of the of the thermal hysteresis effect, when we studied the propagation of the oriented part of the thermal energy in the bulk material under the influence of an external heat source. There, the energy transfer was studied in a specially designed system, in which the energy propagation vector lied along the same line both for heating and cooling periods of the evolution process (as a result of the spatial symmetry of the system), and the time constant of the system exceeded 20 hours. When the input of the thermal energy to such system is constant and when the quasi steady-state phase of the thermal process is realized ($V_1=V_2=V$), then the temperature difference between the locations of two thermometers inside the material artifact can be described by the velocity error correction $V\tau$, where τ is the propagation time of the thermal signal between the locations of the thermometers [3a-3c].

It is also worthy of note here that under the approximation of a plane TEM field, adopted in section IV of [15], the z-component of the wave momentum can be described by equation (6), and the rate of the energy conversion into heat by equation (10). The parameters $\langle W \rangle$ and L , which enter these equations and correspond to the wave, reflected from the gauging surface and propagating in the z-direction away from the boundary, can be determined quite accurately from the experimental plots of Figs. 2a, 2b, 6 and 7. Indeed, these plots are obtained from the differential energy measurements, performed synchronously at the specified time intervals for several distances from the gauging surface, and the averaging procedure of the

results of the measurements in x,y-directions has been used. From these plots it follows, for example, that the energy density $\langle W \rangle$ is changing continuously in time and in space and represent one of the parameters of the evolution process, which is irreversible in time, has no symmetry in space and exhibits a clearly detectable hysteresis effect. Some other parameters of this process are: rate of energy conversion into heat R_H , the wave momentum density \mathbf{G} , the total force density \mathbf{F}_t and tensor quantity \mathbf{T}_{zz} , which corresponds to the force acting in z-direction on the unit area inside the material that is oriented in the same direction. All these parameters, which can be approximately described by the relations (6),(8-10), correspond to the new properties of the artifact medium that are acquired as a result of interaction with the external energy and momentum sources of the environment. All of these parameters of the evolution do not simply exist under the thermal equilibrium conditions. So, we have an evolution process, when the properties of a material artifact, representing the part of the interacting system are changed in response to the variations of the external conditions. Such process in literature is sometimes called as a "self-ordering" process, but it is much more appropriate to call this process as *synthesis*, as in this meaning it was first introduced into philosophy by the XVIII century German philosophers H. M. Chalybäus and J. G. Fichte and is commonly used nowadays in Chemistry. Indeed, *the thermal evolution process is the simplest one, when the material artifact changes its properties and characteristics (see Figs.9a and 9b) as a result of the exchange with the environment of only three material quantities: linear momentum, angular momentum and the energy, which are delivered to the object by the external EM field.*

In general, the irreversible in time changes of the properties of the material objects, subjected to hysteresis evolution process, are well known in many fields of Natural Science. Some example results in case of ferroelectric and ferromagnetic materials were presented above in section 2.2. But, probably, the most spectacular and well studied example is our planet [21]. As a result of interaction with material objects of the Universe and evolution processes in the Earth, the pole of the planet is in continuous motion with respect to the Earths crust, with well-detected daily, unpredictable wobble of the pole, with the presence of the quasi-periodic components (characterized by the durations 1.0 and 1.2 years) and with the relatively slow secular drift of the pole along the meridian 80° [21]. When these pole variations are combined with the variations of the magnitude of the angular velocity of the Earth's rotation that have "random", quasi-periodic and secular components, the total effect, obtained during 50 years of continuous observations, is equal to -34 seconds relative to the time scale of atomic standards [21]. So, as a result of unpredictable, systematic changes in the

Earth's rotation, the amount of the energy, received from the Sun by the objects on the Earth's surface is continuously changing, and as a consequence of the violation of the superposition principle for the thermal surface energy, all the thermal processes on the Earth are definitely irreversible in time. For example, the measurement of Fig.1, performed for the duration of several days, presents a *spiral type curve*, for which the form and amplitude of each cycle is slightly different as a result of some input of momentum and energy from the time irreversible environment, and also as a result of constant changes of the properties of the particular artifact. Even without the realization of the square-wave modulation of the energy by the PRT, we shall have the same spiral type of the thermal evolution process of the system as a result of the daily, seasonal and secular variations of the level of EM radiation of the Sun on the Earth's surface. Naturally in this case, the span of the spiral will be much smaller, as a sophisticated air temperature control system was used in our experiments and the effective thermal isolation of the artifact from the environment was realized inside the Dewar. Summarizing this part, we can conclude that *the demonstration of the thermal evolution process in the form of a spiral under the influence of the infinite number of the continuously changing parameters presents an experimental confirmation of the basic concepts of the dialectics of the Ancient Greek philosopher Heraclitus of Ephesus (6-5 centuries BCE).*

It should be also noted here that the time irreversible evolution processes of material objects are well known in Astronomy for many years. So, that the concept of the arrow of time was introduced in 1927 by the British astronomer Arthur Eddington. According to A. Eddington, the distinguished direction of the time can be determined by the study of organizations of material objects in the Universe. Thus, the lack of symmetry in time, demonstrated here for the thermal evolution process, is an agreement with the experimental studies of ferromagnetic [9d] and ferroelectric materials [9e], is an agreement with the huge number of astronomical observations (including the studies of the Earth's rotation process [21]) and with all biological studies, naturally including the fundamental discovery of Ch. Darwin and A. R. Wallace [22].

From the presented studies we can conclude that the discovery of the thermal surface energy has a fundamental impact on the Electrodynamics in general. Indeed, as described by N. Ramsey theoretically and first shown experimentally by P. Kusch, the process of interaction of the EM field with the quantum system is always nonlinear [23]. So, from our experimental results and the equation (V, 55) in [23] it follows that *if in the "thermal" range of energies of EM field for the process of interaction of the field with matter is irreversible in time and exhibits hysteresis effect, then the hysteresis effects should be observed in the whole range of energies of the*

EM radiation, if the proper accuracy of measurements can be realized in the corresponding range. Here, it is also worth noting that our experimental demonstration of the invalidity of the superposition principle for thermal systems is in agreement with the experiment of P. Kusch [23], showing the fundamental property of nonlinearity of atomic systems that are exposed to EM radiation. P. Kusch used atomic beams, monochromatic EM radiation, and performed the analysis of the spectral response of the system. While for the thermal broadband radiation and metallic artifacts (used in our studies), the amplitude analysis of the interaction of the two energy sources with material artifact is preferable, and it is definitely simpler from the point of view of the interpretation of the results of the measurements. But both approaches can be considered as complementary for the studies of the nonlinearity of the field-particle system.

It should be also specially emphasized that the violations of symmetries in space, which are clearly demonstrated by the plots of Figs. 1-3 and 6 in case of thermal evolution processes, are also known from other fields of Natural science. Similar effects were reported earlier in the experimental studies of the hysteresis effects in ferromagnetic [9d] and ferroelectric [9e] materials, as discussed above in section 2.2. The lack of spatial symmetry is well known in biology, and many examples can be found in the University text-book [24]. Here, we find: "Proteins consist of chains of amino acids. The one that comes from the living thing is called *L-alanine*. All proteins use *L-alanine* exclusively [24]". So, in biology the violations of symmetries in time and space are well established facts, and the importance of the prehistory of the system on its future evolution is clearly realized. In theoretical physics it is acknowledged nowadays that the law of conservation of parity, following from quantum-mechanical equations of the weak decays under reflection [24], is in obvious contradiction with numerous experimental observations. And one of the first experimental observations of the violation of the reflection symmetry was performed using β -disintegration of radioactive isotope of cobalt in strong magnetic fields at low temperatures [24]. As pointed out by R. Feynman himself: "*Fundamentally, the law of reflection symmetry, at this level in physics, is incorrect*" [24]. But in accordance with the approach of K. Popper and A. Einstein (that are generally accepted by the physical community nowadays), if a theory is in contradiction with a single experiment it should be considered as the falsified one (or the wrong one).

The violations of symmetries in time and in space are known in Astronomy for a long time. Relatively recent astronomical studies of the radiation levels in the Universe, performed with radio-telescopes, clearly demonstrated the anisotropy of the Universe [25]. Here, it is worth noting that our experimental observations of violations of symmetries in time and in space in case of

thermal evolution processes are in agreement with more general asymmetries [26, 27], which have been predicted and explained theoretically by the prominent Russian physicist A. D. Sakharov in case of the physics of elementary particles [27].

It should be specially emphasized that the results of our studies and conclusions are in deep agreement with the fundamental discovery of Charles Darwin and Alfred Russel Wallace, first formulated in their article "On the Tendencies of Species to form Varieties, and by Perpetuation of Varieties and Species by Natural Means of Selection" [22]. In this paper, the effect of the long-term influence of the surrounding Nature on the evolution process of living species (organisms) has been unambiguously established for the first time. In this paper, we have demonstrated that basically similar *thermal evolution process, with the continuous creation of the new properties of the material object, does occur continuously in non-living material objects under the influence of infinite number of material objects, which are (at least) partially correlated and which produce a common Poynting vector, interacting with the investigated material artifact*. Naturally, in case of living objects the evolution process due to interaction with the outside Nature is much more spectacular, as besides the energy and momenta, the living objects absorb from environment different material objects, starting with atoms and molecules and finishing with different gasses, liquids and dissolved minerals. The evolution process in living organisms has more manifestations, can be observed even with "naked eye", but its detection requires usually very long observation time intervals. Meanwhile, in the presented experiments on the thermal evolution process, as a result of the use of the sophisticated measurement procedure, the change of the properties of the material artifact can be clearly detected within a couple of minutes (see Figs. 10 and 11).

It can be also emphasized that *in case of our very precise experiments with water triple point (WTP) cells [3a], when the ensemble of different isotopes is located in the field of gravity, each isotope has different temperatures of phase transitions, and the whole system is exposed to super-cooling in the process of creation of the ice mantle, the thermal evolution process is much more complicated than in metallic blocks, and has, at least, three different time scales*. For example, the record, presented by the plot of Fig.8a in [3a], demonstrates the part of the evolution process with the smallest time scale. It is associated with the gradual changes of the isotopic composition and chemical impurities in a thin water layer between the ice mantle and the thermometric well in a short period of time after the thermal shock, which makes possible the ice mantle to rotate freely relative to the thermometric well. As in case of the WTP cells, the temperature measured by thermometer differs by less than 0.2mK from the

temperature of the triple point in water (due to hydrostatic pressure effect), the sensitivity of temperature on different influence factors is much higher than in metallic blocks. So, the thermal differential measurements are not necessary, and the study of the evolution process can be performed with the use of only one thermometer. It is also worth noting here that the evolution process in WTP cells has two additional hysteresis effects, which are detected at longer observation times. The first effect is associated with origin of the water (arctic or equatorial) [7a], and the second (with much smaller characteristic time) depends on time interval, elapsed after the creation of ice-mantle, and the pre-history of keeping the cell and its use in temperature calibrations.

As pointed out above, the thermal hysteresis effect has many common features with hysteresis effects in ferromagnetic and ferroelectric materials, associated with the change of the direction of the constant magnetic or electric fields. But as in our experiments we study the interaction of EM radiation with the ensemble of atoms, which are forming material artifacts, we can establish correspondence between our experimental results and the standard technique of laser cooling of the ensemble of the free moving neutral atoms [28] that is currently used in all modern time and frequency fountain standards [20]. It is known from laser cooling experiments that if the frequency of the laser light is red-shifted (i.e. lower than the mean frequency emitted by a stationary atom), then the free atoms are cooled, and when the frequency is blue-shifted, the atoms are heated. If we have an atomic beam propagating in vacuum device, then the blue-shifted resonant radiation of sufficient intensity can easily remove the atoms from the measurement zone. Similar effects are demonstrated here by the plots of Figs.3a-3b. If the average energy of the external thermal radiation is higher than the average energy, radiated thermally by the artifact, then the temperature of the artifact is rising and there is the excessive energy flux and the excessive force, acting on the charged particles absorbing radiation, in the direction of the nearest gauging surface. If the average energy of the external radiation is lower (frequency is red-shifted) relative to the average energy value of the emitted radiation, then the artifact is cooled, and the energy flux and the force are directed from the gauging surface. These properties are properly described by expressions (8) and (9), which show that the direction of the stresses in the artifact and the direction of the force, acting on the unit volume inside it, are both defined by the direction of the energy propagation vector. And as the energy density inside the artifact, in accordance with presented experimental studies, is changing significantly in space for a particular specified moment of time (Fig.4a), and is changing in time for the specified positions in space (Fig. 5a), then the forces and the stresses in the artifact, described by

the equations (9) and (8), are continuously changing in the evolution process both in space and in time. But the forces, acting on the unit volumes, are responsible for the mass transfer of the particles inside the artifact, and the stresses and shears are responsible for the deformations inside it. Thus, the one dimensional theory of [15] cannot describe in detail 3-dimensional experiment, but it clearly predicts that propagation of energy and momentum inside the artifact is inevitably accompanied by the complicated processes of material deformations and free carriers mass transfer, both evolving in time and in space. So, any adequate thermal conduction theory has to describe in detail the mass transfer and deformation processes, which are always the necessary components of the thermal evolution process.

As it follows from the previous discussion, the *rigid body approximation* is not sufficient for the precise description of the propagation of energy and momentum in thermal processes. On the other hand, the force of the EM pressure, which also changes with distance L and in time, does produce the systematic motion of free electrons in the artifact as a result of the momentum acquisition of the EM field in the process of the EM energy absorption. And the systematic motion of free electrons in the presence of the external force results in the *mass transfer* in the thermal evolution process that must be taken into account in an adequate heat conduction theory. The systematic motion of electrons also results in the additional lattice deformations, which can be understood and described theoretically on the basis of the electron-lattice interaction [29]. Most probably, the lattice deformations are responsible for the fast, negative part of the dependence $\Delta V[1,2]$ on time, shown in Fig.3c. It follows from Fig.3c that the forms, magnitudes and time scales are, practically, equal for the heating and cooling periods of the modulation cycle. The total time of the observation of the effect in the induced differential thermal velocities $\Delta V[1,2]$ is about 25 minutes. It is much shorter than the time interval of several hours, which is necessary for the acquisition of the steady-state condition between the block and the environment (see the R3 temperature dependence in Fig.1). At the beginning of the heating period of the cycle, the electrons are moving in a systematic way, as a result of the uncompensated force, associated with the absorption of energy and momentum of the field-particle system. At the beginning of the cooling period, when the external force is switched off (or diminished), the electrons have to return to their steady-state, equilibrium positions as a result of the uncompensated force, produced by the deformed lattice whose magnitude has been tuned to compensate the higher level of the forces, acting on the unit volumes inside the artifact and described approximately by eq. (9).

In general, the process of the gradual changes of the properties of the material standards in the presence of stresses and deformations is known in many fields of physics, where accurate measurements are available. For example, in interferometric length measurements, the measured length of the material standard (gauge block) is found to depend on the level of deformations [3b, 3c], arising in the wringing procedure of the reference plate to the gauging surface of the block. So traditionally for optical interferometry, the length of the gauge block is defined in the wrung condition. Also, to minimize the effect of deformations, arising in the field of gravity, on the optical length measurements, the support of a long gauge block inside the optical comparator is performed at the special (Airy) points. Using modern fringe-pattern analyzing interferometers it is possible to study the process of the build-up of the wringing deformations of the surface of the reference plate in time and in space [3c]. As a common practice, the length measurements by optical interferometry in international comparisons are realized after a certain time interval, when the variations of the measured length in time due to the wringing procedure are becoming less, or comparable with the total uncertainty of the length measurement. The method, resulting in the crucial decrease of the wringing deformations on the result of the interferometric length measurement, has been also developed [3a].

The effect of the presence of stresses in the solid state parts of temperature standards on their performance is also well known. In WTP cells, the temperature standards that are used for the definition of the unit of temperature – Kelvin, the stresses in the ice mantle, which are produced in the process of the ice crystallization from the super-cooled very clean water, can produce the systematic shifts to lower temperatures. These shifts are usually much larger than the resolution of modern temperature-measuring equipment. So, the WTP cells are suitable for the accurate comparisons only after the relaxation of stresses, by keeping the standard for several days at the temperatures, which are slightly below the triple point value. In temperature standards, using the phase transition in pure metals, the effect of deformations and stresses on the reproduced temperature can be an order of magnitude larger than in the WTP cell. But probably, the most spectacular demonstration of the effect of stresses on the properties of the matter is known from material science. It is found that in mechanical tests, performed under the multiple mechanical deformations variable in time, metallic and plastic artifacts demonstrate specific hysteresis effect: they are getting “tired” and dismantle to smaller pieces when subjected to stresses, an order of magnitude smaller than stresses, which they can withstand at the beginning of the test. As the mechanical perturbations have EM origin, then combining the observation of the

material science with the result of this study that the propagating EM field inevitably produces stresses and deformations inside the irradiated material artifact, we can infer that all the material processes under the typical Earth’s conditions should be considered as transient: there is a period of creation and growth of material object, there is a period of time when its properties and parameters are changing very slowly, and there is a period of relatively fast decline and demolishing of the object. In this we can see common features with the evolution of the living species known in Biology. And it is worth special note that all these experimental observations are in agreement with the principles of dialectics of Heraclitus, which were concisely formulated by his disciples in the form: “everything is continuously flowing and changing; no person steps in the same currents (river) twice; no one can experience the state of death twice”.

We can also consider that our experimental results present some clarification to the famous philosophical triad (thesis – antithesis - synthesis), which was introduced by the German philosopher H. M. Chalybäus and then was greatly elaborated by J. G. Fichte. In the presented thermal measurements, thesis and antithesis, which are to describe the opposite properties of the entity that coexist simultaneously in a material object, correspond to the two types of internal energy. The first type of the internal energy, which is characterized by the mean value of the momentum of the field-particle system equal to zero, represent the result of a long-term evolution process of the hysteresis type under the influence of a huge number of external sources of EM radiation. This type of internal energy can be quite precisely described by a random quantity. The other type of the internal energy, complementary to the first one, corresponds to the thermal surface energy and represents the oriented motion of the field-particle system under the influence of a few, closely located heat sources. This type of energy is characterized by the total momentum, which is not equal to zero. As it follows from equations (2)-(10), the properties and parameters of the material object for these two types of motion of the field-particle system are also opposite, complementary to each other. There are two observations of primary importance, which are to be mentioned in this respect. First, in each elementary process of absorption or emission of the EM energy by free electrons inside the metallic blocks, the laws of conservation of energy and momentum are realized with tremendous accuracy, so that these two types of thermal energy should be considered as independent for short time observations. Second, as the skin depth for the external EM field, irradiating the surface of material artifact, is by orders of magnitude smaller than the characteristic length of the observation of the reflected wave from the boundary surface of the artifact (see Fig.5), these elementary processes are repeated a huge number of times [3d],

so that at time intervals of about 15 minutes after the increase of the PRT current, the physical laws of conservations of energy and momentum are no more valid for the blocks, as a consequence of the fact that the system is an open one. During this time interval, the absorbed momentum and energy of the external EM field are sufficient to realize a complicated pattern of lattice deformations and stresses inside the artifact, and to produce systematic displacements of free electrons. In accordance with the equations (2)-(10), the external field will produce a continuously changing in time and in space the distributions of wave-momentum and energy densities inside the artifact, which correspond to the oriented motion of the field-particle system and which can be observed simultaneously with the distribution of the thermal energy of the random type. Thus, the thermal evolution process, or the thermal synthesis (when following the terminology of J. Fichte), can be observed when the physical laws of the conservations of energy and momentum are no more valid, as the blocks (as any material objects in the Universe) present typical examples of the open systems. In this respect, our experiments present a spectacular illustration to the basic ideas of Heraclitus, who is famous for his insistence on ever-present changes in the Universe (“All entities move and nothing remain still.”) and his cryptic utterances that “Ever-newer waters flow on those who step into the same stream”, and “All entities come to be in accordance with this Logos”. (Here, the term Logos corresponds to the present day concept of the Law of Nature).

It is also worth noting here, that there is an experimental observation of primary importance from the point of view of basic concepts, which has no analogue in Fichtean dialectics. But the corresponding philosophical concept can be found in the Ancient Indian (Jain) philosophy. It is known that the fundamental Jain doctrine (Anekantavada) states that all entities have infinite number of modes of existence and qualities, and, consequently, these entities cannot be completely perceived in all their aspects and manifestations by human beings as a result of the inherent, intrinsic limitations of a human person. Only the Kevalis – the omniscient beings – can comprehend the object in all its aspects and manifestations, while human beings are capable of knowing only some part of it. Consequently, no one view can claim to represent the absolute truth. This fundamental doctrine is clearly in agreement with the presented experimental studies. Indeed, it has been shown experimentally that for the TSE the principle of superposition is not valid, and this result is in agreement with P. Kusch experiments [23], demonstrating that quantum systems, interacting with EM field, are basically nonlinear systems. As a result of the TSE existence and the non-validity of the superposition principle, all the energy sources of the Universe are in continuous interaction with each other

through hysteresis type evolution processes. And for the description of the TSE, as a part of this process, the Poynting vector, representing the vector sum of the corresponding vectors of all the external EM fields, has to be specified for each point of the artifact surface and for all the preceeding time moments, as the properties and parameters of the wave-momentum, propagating inside the artifact, are defined by the Poynting vector of the external field and the material (constitutive) relations for the artifact medium [6b, 8] (which have to be treated as evolution processes and which cannot be described by standard mathematical functions due to the presence of the hysteresis effect). Correspondingly, the energy and momentum of the EM field, radiated by the artifact, depend, in particular, on the wave-momentum and energy distributions, existing inside the artifact for the specified time moment, and thus depend on the prehistory of the interaction between the external field and the artifact. As the radiated field amplitude is dropping with distance [6, 7], among the influence parameters for the resultant Poynting vector of the external field (even in the simplest case of a free space) we are to include all the distances from the energy sources to the artifact, the mutual orientations between each energy source and the artifact, mutual angles of observation and energy excitation levels of all the sources. So, for the achieved level of temperature measurements (of about $1\mu\text{K}$), the number of energy sources, which are to be taken into account, is becoming enormous. Consequently, the number of the influence parameters, which increases much faster than the number of sources, is approaching infinity, even in a free space. In the standard case of the propagation of the part of thermal energy in a turbulent atmosphere, when the propagating energy represents the coupled field-particle system and the particles are also participating in the macroscopic turbulent motion in the field of gravity with the dissipation of energy and with the important mass transfer on the macroscopic level, the number of influence parameters should be considered as infinite one [4a]. The infinite number of influence factors inevitably results in the infinite number of modes of existence of a thermal system and in the infinite number of the manifestations of the thermal evolution process. Thus, in accordance with the Jain philosophy (which is kept in the memory of the mankind for several thousands of years) and in accordance with the results of the present experimental studies, the thermal evolution process has infinite number of influence factors, cannot be perceived in all aspects and in all of its manifestations by any human being, and, consequently, cannot be adequately described by any experiment. The experiment, under these conditions, is fundamentally incomplete, covering only a few of the influence factors. *And the most important result of this experimental study is that the original evolution process of the artifact is in irreversible way damaged by the*

presence of the measuring instrument, with which the artifact forms a new coupled, interacting system. And this is one of the experimental confirmations of the famous observation of N. Bohr that isolated system is a mere abstraction of theoretical physics.

Finally, we shall perform in a concise way the comparison of our experimental results with the main conclusions of the series of theoretical papers [17-19], dealing with the interaction of the EM field with an ensemble of atoms or molecules. It was R. H. Dicke, who first pointed out that the standard theoretical treatment of spontaneous radiation by a dilute gas of molecules, in which it is considered that separate molecules radiate independently of each other, "is wrong in principle and many of the results obtained from it are incorrect"[17]. In accordance with [17-19], the parameters of the radiation process critically depend on the pre-history of the system and the type of its excitation. In [17] we find an important observation: "consider a gas of two-level molecules, all excited", when "an intermolecular spacing is large compared with the radiation wavelength. Assume that a photon is emitted in the \mathbf{k} direction". Then it follows from [17] that "the radiation probability in the direction \mathbf{k} has twice the probability, averaged over all other directions" that "corresponds to the ordinary, incoherent spontaneous radiation of a single molecule". Thus, such system of molecules has an angular correlation between the successively emitted photons [17].

In [17] it is specially emphasized that if the dimensions of the molecular system are large in comparison with the wavelength of the resonant radiation, *the coherent spontaneous decay of the system is still possible, but only in the single direction*, as "the polarization of the emitted or absorbed radiation is uniquely given by the direction of propagation". It is pointed out in [17] that if "in the present case the incident radiation is assumed to be plane with the propagation vector \mathbf{k} , then after the excitation, the gas radiates coherently in the \mathbf{k} direction". Because of the difference in the selection rules for coherent and incoherent spontaneous radiation (see equations (51) and (52) in [17]), "radiation in directions other than \mathbf{k} tends to destroy the coherence with respect to the direction \mathbf{k} " [9]. So, the *theoretical description of an ensemble of molecules, interacting with EM field [17], shows that the coupled field-particle system is the anisotropic one, and the considerations of space symmetry are not valid for it*. This is in strict agreement with our experimental results (see Figs.1-6).

The other basic property of the Dicke's ensemble of molecules, following from the theoretical analysis in [17,18], is the irreversible in time evolution process, described by the coherent spontaneous emission. In accordance with [18], the evolution of the ensemble of two-level atoms in equivalent positions can be described by the motion of the super Bloch vector \mathbf{R}

on the Bloch sphere, when in the process of this motion the length value R of this vector is kept constant. The X- and Y- components of \mathbf{R} are related to the dipole moment of the transition and its time derivative, and describe (in combination with the field amplitudes) the interaction process in time between the field and the ensemble of atoms. The projection of the vector \mathbf{R} on the Z-axis describes the dependence of the total energy of the atomic system in time, which is measured in terms of the energy difference $h\omega$ between the two levels of the unperturbed molecular transition. As the quantity R^2 is conserved in the process of the coherent spontaneous radiation [17, 18], its length value R is defined solely by the initial excitation of the system [18, 19]. It is demonstrated in [18] that "the rate of change of the super Bloch vector \mathbf{R} is R times as rapid as the rate of change of the vector describing an isolated single atom". Under the approximations of [18], the expression for the total energy of the atomic system can be obtained in a closed form. The energy of the atomic ensemble decays in time as a negative of the hyperbolic tangent (see Eq. (35) in [18]), where the corresponding time scale is equal to $\tau_0/(2R)$ and τ_0 represents the time of incoherent spontaneous decay of an isolated atom. The theoretical models in [17, 18] correspond to open systems, and the coherent spontaneous radiation process is inevitably terminated, when the vector \mathbf{R} acquires the $-Z$ direction on the Bloch sphere, which corresponds to the zero value of the total dipole moment of the system [18]. In that state, in the general case, some part of the excitation energy is still trapped in the atomic system (as a consequence of the conservation of R^2). Thus, "the system of atoms can no longer radiate coherently, and the remaining energy will be dissipated by whatever incoherent processes are available to the atoms" [18]. So, when comparing this property of the solution in [18] with our studies of the interaction of the EM field with ensembles of atoms, forming rectangular metallic blocks, we can see that in both cases the processes are irreversible in time. And the lack of symmetry in time for all natural processes is nowadays explicitly formulated in the University textbooks [2c]. It is interesting that this property of Nature immediately follows from the fundamentals of Ancient Greek and Indian philosophies that are kept in the memory of the mankind for thousands of years.

The other very important property of the theoretical solution of [18, 19], which has a complete experimental confirmation of our studies, deals with the huge number of influence factors, which determine the process of coherent spontaneous radiation. The EM field, which is acting on an arbitrary atom in the ensemble, is produced by all other atoms, and the expression for the near field of an ensemble of dipoles (see Eqs. (10)-(11) in [18]) depends explicitly on all the distances and on all the mutual orientations between the

specified atom and its partners. So, in accordance with [18], among the parameters, characterizing the system, we have all the separations between the atoms and their mutual orientations, that is, approximately, $2N$ influence parameters (where N is the total number of atoms in the ensemble). But as it is also necessary to specify initial conditions, and the super Bloch vector is defined as a vector sum of the Bloch vectors of individual atoms (in accordance with Eq. (19)-(20) in [18]), this procedure requires additionally $3N$ influence factors. If the number of atoms N is much larger than 1 (as it is in the majority of practical cases), then the number of influence parameters, in accordance with [18], in fast way approaches infinity. In the real experiments on the thermal evolution process the number of influence parameters is even greater, as for the experiments with material objects, performed in a free space, the additional information about the forms of material objects, properties of material properties and the solid angles, at which each object is seen from the positions of its partners, are expected to be added to the enumerated influence factors of the theoretical paper. At the resolution level of about $1\mu\text{K}$ (typical for the presented experiments), when the propagation in a turbulent atmosphere of the Earth of the wave-momentum, generated by the EM radiation of the Sun, had to be taken into account, the number of influence parameters in the thermal evolution process can be considered as infinite [9a]. So, the theories of [17, 18] and our experimental studies are presenting a clear support from the physical point of view to one of fundamentals of the Jain philosophy that the number of modes of existence of the processes in Nature is infinite, and so, no human being is capable to perceive such process in all of its manifestations.

In conclusion, we would like to discuss the N. Bohr observation that *in the general case* the theoretical description of the material objects, interacting with the surrounding material objects through different fields, is not possible. Here, it is necessary to remind again the letter of E. Schrödinger to W. Wien: "*Bohr's standpoint, that a space-time description is impossible, I reject a limine... The aim of atomic research is to fit our empirical knowledge concerning it into our other thinking. All of this other thinking, so far as it concerns the outer world, is active in space and time.* If it cannot be fitted into space and time, then it fails in its whole aim and one does not know what purpose it really serves". From the following short analysis it can be concluded that none of the E. Schrödinger's contributions to the Natural sciences can present a slightest trace of refutation to the fundamental N. Bohr's "standpoint". Indeed, the theoretical model for the Schrödinger's equation is an isolated stationary atom, and it is natural that the solution presents a set of stationary energy levels, specific for each type of atom. As in accordance with the solution, the atom can stay indefinitely long in each state, M. Born gave the

statistical interpretation of the wave function, so that in case of a hydrogen atom, the square of the modulus of the wave function in the arbitrary point of space corresponds to the probability of finding the electron, bound to the proton, in the elementary volume, corresponding to that point of space. But in accordance with N. Bohr observation "Isolated material particles are abstractions, their properties being definable and observable only through their interaction with other systems". So, the solutions of the Schrödinger's equation should be compared with spectroscopic studies. And from numerous experiments in the field of optical spectroscopy it definitely follows that in hydrogen atom, for example, only the ground state is stable, and all others decay through spontaneous radiation to the ground state. For the first excited state in hydrogen, which is connected to the ground state by the electrical dipole transition, the life-time is about 1.5ns, and for the similar higher excited states the life-time is further dramatically reduced. Such short time intervals, representing the whole life-time, cannot be measured for a single isolated atom, as the modern electronic counters can have the necessary time resolution of about 1ns for the electrical pulses, which have not only a shorter rise time but which possess the electrical power, producing $\sim 20\text{mA}$ current on 50 Ohms input of the counter that makes the signal observable against the background noise level. Also it should be taken into account that in mathematics, the concept of probability was introduced by C. F. Gauss for the description of *stationary processes*, as the measurement of the probability distribution with the infinite resolution, which is assumed for the presentation of the distribution function as a continuous one, requires an infinite time of the measurement process. Besides that, for the existence of the probability function it is necessary that any new procedure of the measurement of the probability function for any real process should give the identical results with the previous determinations. This is also only possible for stationary processes.

The discrepancies between the solutions of the Schrödinger's equation (supported by the statistical interpretation of M. Born) and the numerous experiments in the field of optical spectroscopy were so important, that in the year 1949 N. Bohr considered it necessary to publish in his article "Discussions with Einstein on Epistemological Problems in Atomic Physics" the following statement: "...evidently the interpretation of the spectral laws implies that an atom in an excited state in general will have the possibility of transitions with photon emission to one or another of its lower energy states. In fact, *the very idea of stationary states is incompatible with any directive for the choice between such transitions and leaves room only for the notion of the relative probabilities of the individual transition processes*".

There is also another fundamental discrepancy between the solutions of the Schrödinger's equation and the historic Stern – Gerlach experiment, performed before the publication of the Schrödinger's theory. In this experiment it was demonstrated that the beams of silver or hydrogen atoms in their ground state were splitted into two lines by inhomogeneous magnetic field, while the Schrödinger's theory predicted no splitting. In 1925 Uhlenbeck and Goudsmit showed that the splitting in the Stern – Gerlach experiment and the fine structure of atoms in spectroscopic studies could be explained by the intrinsic angular momentum of the electron, which they called spin. And this new quantum number is not present in the Schrödinger's equation. But in accordance with Carl Popper – Albert Einstein principle, if a theory is in contradiction even with a single experiment, the theory should be considered as the falsified one.

Still, there is the general contradiction of the Schrödinger's equation with the properties of Nature. As the equation is of the first order in respect to time, the knowledge of the wave function at some arbitrary time moment is sufficient for the prediction of the state of the system at any past or even future time moment. This is in dramatic contradiction with numerous experimental observations in various natural sciences, such as biology (including the discovery of the evolution process by Ch. Darwin and A. R. Wallace in 1858), geology or astronomy, for example, including the arrow of time by Arthur Eddington of 1927 or fundamental Edwin Hubble experiment of 1929. Lee Smolin, in his book "Time reborn" writes: "The central principle is that time must be real and physical laws must evolve in that real time" [30a]. It is pointed out there that the idea of evolving laws is not new, and the American philosopher Ch. S. Pierce wrote in 1891: "Now the only possible way of accounting for the laws of nature and for uniformity in general is to suppose them the results of evolution". The same idea was expressed later by the famous British physicist Paul Dirac in a more general way [30a]: "At the beginning of time the laws of Nature were probably very different from what they are now. Thus, we should consider the laws of Nature as continually changing with epoch, instead of as holding uniformly throughout space-time." It is specially noted in [30b] that for "complex systems, involving large numbers of atoms, we must deal with the laws of thermodynamics, which are not reversible in time". And there is a special emphasis in [30b] that "many laws in physics are time-reversible. One is Newtonian mechanics, another is general relativity, still another is quantum mechanics". In this respect, of primary importance is the record of the conversation with A. Einstein by the Viennese philosopher R. Carnap [30c]: "Once Einstein said that the problem of the Now worried him seriously. He explained that the experience of the Now means something special for man, something essentially different from the past and future, but **this**

important difference does not and cannot occur within physics. That this experience cannot be grasped by science seemed to him a matter of painful but inevitable resignation". After this citation there can be no ambiguity about the meaning of Albert Einstein's historical observation: "No amount of experimentation can ever prove me right; a single experiment can prove me wrong". This is a rigorous refutation of all "Modern Physics", which is based on the fundamentally wrong, illusionary concepts of "symmetrical" space and "symmetrical" time, typical both for Relativity theories and Quantum mechanics. It was evidently clear to A. Einstein that the concept of space-time, introduced into his theories, was not only in contradiction with the principles of thermodynamics or E. Hubble experiment, but it was in the obvious disagreement with the natural processes, studied in many Natural sciences, such as Biology, Geology, Paleontology, Astronomy or even in some parts of Classical Physics (ferromagnetism, for example). And from the very formulation of A. Einstein statement it follows that every natural process depends on the infinite number of influence parameters, and so, in agreement with K. Popper observation, only the infinite number of experiments, performed under all possible conditions, can only prove the validity of a theory. To realize clearly what advancement in physics presented A. Einstein's statement, it is sufficient to compare it with some observations of R. Feynman made more than 10 years later. In the course of University physics he writes that "all electrons are the same, all protons are the same, all positive pions are the same; and so on" [24b]. And on the next page we read: "Apparently it is true that the fundamental physical laws, on a microscopic and fundamental level, are completely reversible in time". Only much later, R. Feynman has changed crucially his point of view, musing in an interview [30a]: "The only field which has not admitted any evolutionary question is physics. Here are the laws, we say,...but how did they get that way, in time? So, it might turn out that they are not same all the time and that there is a historical, evolutionary question".

In the recent book [31], published by B. Greene, we can find: "The concept of symmetry's breaking, and its realization through the electroweak Higgs field, clearly plays a central role in particle physics and cosmology. Like the aether, a condensed Higgs field permeates space, sweeps through everything material, and as a nonremovable feature of empty space, it redefines our conception of nothigness" [31]. In [30a] we find a more general observation: "There can be no absolute time that ticks on blindly whatever happens in the world. Time must be consequence of change; without alteration in the world there is no time. Philosophers say that time is relational – it is an aspect of relations, such as causality, that govern change. Similarly, space must be relational; indeed, every property of an object must be a reflection of dynamical relations between it and other things in the

world". Further, in [30c] we find: "Leibniz's principle of *the identity of the indiscernibles* follows from the basic idea that physical properties of bodies are relational. What about two electrons, one of which is in the atom in the bedspread, the other on top of the mountain on the dark side of the moon? These are not identical particles, because their location is one of their properties. From a relational point of view, they are distinguishable by having distinguishable surroundings". It is clear that this statement is supported by the experiments of P. Kusch of the year 1954, when the non-linear character of interaction between EM field and atomic beam was established, using spectral type of measurements. It is in agreement with our studies, in which the non-linear properties were demonstrated with high precision in interaction of the ensemble of atoms in the solid state with EM field, resulting in a clearly observed hysteresis effect.

Also, in [30d] we read: "Darwinian evolutionary biology is the prototype of thinking in time, because at its heart is the realization that natural properties developing in time can lead to creation of genuinely novel structures". This observation is in complete agreement with our studies. As in natural selection in biology, in our experiments there is always infinite number of external parameters (as discussed in detail above). *The Poynting vector of the external field is the result of the interaction between the numerous material objects during the whole preceding time epoch, including the instant of the last measurement point in the series.* The EM field, re-emitted by the each object, depends on its own pre-history, simply as a consequence of the existence of the surface energy and the accompanying hysteresis effect. The evolution process in the studied artifact presents the synthesis process, occurring under the influence of infinite number of internal and external influence factors. *And the basic result of this study is the experimental demonstration that thermal evolution process, or thermal synthesis, means the appearance of the new properties in the object, which were not present in the parts of it before the open system absorbed the momentum and energy of the external EM field.* This is an experimental proof for the particular case of electromagnetic fields of more general principle of *driven self-organization* [30c]: "Flows of energy through open systems tend to drive them to states of higher organization". We can say that our experimental result presents an additional confirmation of the fundamental observation, known to the mankind thousands of years since the time of Ancient Buddhism, that the properties and the structure of material objects are defined by the processes, occurring inside and outside this object. We can also emphasize that the specific character of the time dependence, observed at any point of the artifact in its evolution process, gives a clear experimental indication that processes cannot be synchronized. This is in agreement with the well-known

observation in medicine that the person dies when some vital organ (heart, for example) stops to function normally, and there are no "normal" cases when all the body of the person starts to disintegrate simultaneously to small parts just as a result of the general ageing of the organism of the person. From these observations it is becoming evident that the unambiguous, accurate description of material processes by mathematics in term of imaginary reference system, consisting of homogeneously spaced three "coordinate" axis's and one homogeneous "time" axis, with the assumed possibility to make infinitely accurate projection even of a point object (electron in a hydrogen atom, for example) on each axis, which is commonly used in theoretical physics, is only a primitive illusion. This expectation contradicts the fundamental Kurt Gödel incompleteness theorem, which says that "Any effectively generated theory, capable of expressing elementary arithmetic, cannot be both consistent and complete", and the observation of C. F. Gauss that the queen of mathematics is arithmetic. From the physics point of view this should be absolutely clear. Indeed, mathematics is incapable of description of the synthesis process under the influence of infinite number of external parameters, which are, at least, partially correlated and the properties of the object under consideration are continuously changing in time and in space. So, the mathematical description can be only applicable for relatively short periods of time, only when the properties of the object can be considered as invariable. And this time period can be only established from the comparisons with the corresponding experiment. In many cases the mathematical description is simply not possible. For example, in the studies of ferromagnetic properties of materials, the theoretical physics is unable to present any description of the process, resulting in the observation of the well-established experimentally hysteresis loops in different materials. The other important example follows from astronomical observations. Since 1887 it is known that the pole is moving with respect to the Earth [21]. These motions cannot be predicted theoretically; their measurement requires a continuous monitoring which started in 1900 [21]. Nowadays, besides regular optical measurements, the information about the daily rotation of the Earth relative to stars is obtained from laser ranging to the satellites and to the Moon, from very long baseline radio-interferometry of quasars and from the Doppler shift measurements between the clocks on the satellites and on the ground stations. And in spite of a huge number of experimental data, the theoretical predictions of the Earth's rotation with the precision, comparable with the uncertainty of the indicated experimental observations is found to be impossible [21]. The result is clear: the change in the properties of the Earth can be observed on the daily time interval. Something similar is observed in the presented studies.

The time of propagation of a thermal signal, measured at its half-amplitude value (due to significant dispersion in velocities), exceeds 30 minutes in a 1m steel gauge block. Meanwhile, the variation of the properties of the block under the application of the external EM field, is recorded in 1-2 minutes. Taking these observations into account, it is not very surprising the comparison in [30] that in theoretical physics, mathematics appears nowadays not as a queen, but as an ordinary room maiden.

The long term irregularities of the Earth's rotation were demonstrated in the first half of the 20-th century, by comparison with the orbital motion of planets in the Solar system (called Ephemeris Time) [21]. Since the middle of the last century the rotation of the Earth was in detail studied relative to the International Atomic Time (TAI) scale, and since January 1958 up to January 2011, 34 leap seconds have been added to the Universal Coordinated Time, which has the dimension of TAI second, to keep in agreement with the Earth's rotation to within 1 second. And it was found that sometimes, the leap seconds had to be added every consecutive year, and sometimes this interval (by unknown reasons) was increased to 7 years [21]. Combining these results with the presented experimental studies of the thermal evolution process, we are coming to the experimental confirmation of N. Bohr – A. Einstein statement that the material objects and the processes in Nature cannot be adequately described in terms of the time-space concepts of Modern Physics. The historic statement of A. Einstein that “No amount of experimentation can ever prove me right...” should be, probably, complemented by an important observation that in all natural process the enormous number of influence factors cannot be regarded as independent ones, as all material objects are participating in the generation of the resultant field, which reflects the process of interaction between them in all the preceding time epochs up to the moment of the last measurement or observation. Thus, the hysteresis effect presents one of the main, characteristic features of the evolution processes in Nature. The famous observation of Paul Dirac that “we should consider the laws of Nature as continually changing with epoch, instead of as holding uniformly throughout space-time” presents another, relatively late admission of the importance of N. Bohr – A. Einstein idea that the description of processes of Nature in terms of the existing space-time concepts of Modern Physics is not possible. Only, instead of K. Popper terminology (which was used by A. Einstein), P. Dirac preferred to use the notions of the 19th century American philosopher Ch. S. Pierce.

V. ACKNOWLEDGEMENTS

The author gratefully acknowledge financial support of the studies at INMETRO by the CNPq of Brazil and a fruitful cooperation with Igor Malinovsky during that period. The technical and moral support of our studies by the staff of INMETRO is highly appreciated and will never be forgotten. The author is grateful to members of Physical department of the Yeditepe University (Turkey) for useful discussions and for the afforded possibility to present some results of this study at the International Conferences.

REFERENCES RÉFÉRENCES REFERENCIAS

1. L. Rosenfeld, “Niels Bohr's contribution to epistemology”, *Physics Today*, **v.16**, No.10, pp. 47-53, (1963).
2. D. G. Giancoly “Physics for Scientists and Engineers”, Prentice Hall, 3-ed., pp.958-959 (2000) [2a]; 3-ed., p.981 (2000) [2b]; 4-ed., p.543 (2009) [2c], p. (2009) [2d].
3. A. Titov, I. Malinovsky, H. Belaidi, R.S. França, C.A. Massone, “Advances in interferometric length measurements of short gauge blocks”, *Metrologia*, **37**, (2), pp. 155-164 (2000) [3a];
 - a) Malinovsky, A. Titov, J.A. Dutra, H. Belaidi, R.S. França, C.A. Massone, “Towards sub-nanometer uncertainty in interferometric length measurements of short gauge blocks.” *Applied Optics*, **38**, No.1, pp.101-112 (2000) [3b];
 - b) A. Titov, I. Malinovsky, “Advances and new techniques in length measurements by optical interferometry”, pp. 1-6, XVIII IMEKO WORLD CONGRESS, September, 17 – 22, 2006, Rio de Janeiro, Brazil [3c];
 - c) A. Titov, I. Malinovsky and C. A. Massone, “Wringing deformation effects in basic length measurements by optical interferometry”, *Proc. SPIE*, **5190**, *Recent Developments in Traceable Dimensional Metrology*, ed. by J.E.Decker, N.Brown, pp. 43-53, San Diego, CA, USA, 4-6 August, (2003) [3d];
 - d) A. Titov, I. Malinovsky and C. A. Massone, “Scientific basis for traceable dimensional measurements in a nanometer range: methods and concepts”, *Proc. SPIE*, vol. **4401** *Recent Developments in Traceable Dimensional Measurements*., eds. J. E. Decker & N. Brown, pp. 33-43, (2001) [3e];
 - e) A. Titov, I. Malinovsky, “Nanometrology and high-precision temperature measurements under varying in time temperature conditions”, *Proc. SPIE*, **5879**, *Recent Developments in Traceable Dimensional Metrology*, ed. by J. E. Decker, Gwo-Sheng Peng, pp. 587902-1 – 587902-10,

- San Diego, CA, USA, 31 July-1 August, (2005) [3f];
- f) A. Titov, I. Malinovsky, H. Belaïdi, R. S. França, M. Erin, "Primary level gauge block interferometers for realization of the SI length unit", Proc. SPIE, **5190**, *Recent Developments in Traceable Dimensional Metrology*, ed. by J.E.Decker, N.Brown, pp. 24-33, San Diego, CA, USA, 4-6 August, (2003) [3g];
 - g) A. Titov, I. Malinovsky, "New techniques and advances in high-precision temperature measurements of material artefacts", *Can. J. of Scientific and Industrial Research*, vol.2, no.2, pp. 59-81(2011) [3h];
 - h) A. Titov, I. Malinovsky, M. Erin, H. Belaïdi, R. S. França, "Precise certification of the temperature measuring system of the original Kösters interferometer and ways of its improvement", *Proc. SPIE*, **5879**, *Recent Developments in Traceable Dimensional Metrology*, ed. by J. E. Decker, Gwo-Sheng Peng, pp. 587904-1 – 587904-10, San Diego, CA, USA, 31 July-1 August, (2005) [3i].
4. E. Engelhard "Precise Interferometric Measurement of Gage Blocks", Proc. "Metrology of Gage Blocks", Symposium on Gage Blocks, August 1955, NBS, Circ.581, pp.1-20, 1957.
 5. H. Darnedde, "High-precision Calibration of Long Gauge Blocks Using the Vacuum Wavelength comparator", *Metrologia*, **V. 29**, pp. 349-359, (1992).
 6. "Documents Concerning the New Definition of the Metre", *Metrologia*, V.19, pp. 163-177, (1984).
 7. J. V. Nicholas and D. R. White, "Traceable Temperatures", J. Wiley and Sons, 2-nd ed., pp. 96-111 (2000) [7a]; pp. 203-220 [7b]; pp. 13-18 [7c].
 8. R. L. Rusby, *et al*, "A review of progress in the measurement of thermodynamic temperature", TEMPERATURE. Its Measurement and Control in Science and Industry, J. F. Schooley, Ed., Vol. 6, pp.9-14, American Institute of Physics, New York, (1993).
 9. D. V. Sivukhin, "General Course of Physics", *Physmatlit*, Moscow, (2008):
 "Thermodynamics", **V2**, pp.44-71 ([9a]);
 "Thermodynamics", **V2**, pp. 85-110 [9b];
 "Thermodynamics", **V2**, pp.162-182 [9c];
 "Electricity", **V3**, pp.293-317 [9d];
 "Electricity", **V3**, pp. 159-172, [9e];
 "Electricity", **V3**, pp. 613-621 [9f];
 "Optics", **V.4**, pp. 466-480 [9g];
 "Optics", **V.4**, pp. 466-480 [9h].
 10. Einstein, "Investigations on the Theory of the Brownian Motion", *Annalen der Physik*, **v.17**, No.3, pp.549-566, (1905).
 11. A. Einstein, Theory of the Foundations of Thermodynamics", *Annalen der Physik*, **v.11**, pp.170-187, (1903).
 12. E. R. G. Eckert and R. M. Drake, Jr., "Analysis of heat and mass transfer", International Student Edition, McGraw-Hill, Kogakusha Ltd, Tokyo, pp. 38-56, 1972.
 13. J. D. Jackson, "Classical Electrodynamics", J. Willey and Sons, 1999, 3-ed, p.239-262 [13a]; p. 14 [13b].
 14. D. J. Griffiths, "Introduction to Electrodynamics", Prentice Hall, 3-ed, 1999, pp.435-460 [14a]; p.346-348 [14b].
 15. R. Loudon, L. Allen and D. F. Nelson, "Propagation of electromagnetic energy and momentum in absorbing dielectric", *Phys. Rev. E*, **55**, 1071 (1997).
 16. C. Kittel, "Introduction to Solid State Physics", Wiley and Sons, 8-ed., pp.323-355 [16a]; p. 661 [16b] (2005).
 17. R. H. Dicke, "Coherence in Spontaneous Radiation Processes", *Phys. Rev.*, **93**, 99 (1954).
 18. C. R. Stroud, Jr. and J. H. Eberly, W. L. Lama and L. Mandel, "Superradiant Effects in Systems of Two-Level Atoms", *Phys. Rev. A*, **5**, 1094 (1972).
 19. F. W. Cummings and Ali Dorri, "Exact solution for spontaneous emission in the presence of N atoms", *Phys. Rev. A*, **28**, 2282 (1983).
 20. V. Gerginov *et al*, "Uncertainty evaluation of the caesium fountain clock PTB-CSF2", *Metrologia*, **47**, p.65 (2010).
 21. B. Guinot, "Solar time, legal time, time in use", *Metrologia*, **48**, pp. S181-S185 (2011).
 22. Ch. Darwin and A. R. Wallace, "On the Tendencies of Species to form Varieties, and by Perpetuation of Varieties and Species by Natural Means of Selection", *Journal of the Proceedings of Linnean Society of London, Zoology* **3**, **3** (9), pp.46-50 (1858).
 23. N. F. Ramsey, "Molecular beams", Oxford, Clarendon Press, pp. 115-144 (1963).
 24. R. P. Feynman, R. B. Leighton and M. Sands, "The Feynman Lectures on Physics", Addison-Wesley, 1-ed, **V.1**, Ch.52, pp.1-12 (1964).
 25. G. Smoot, M. Gorenstein, and R. A. Muller, "Detection of anisotropy in the cosmic background radiation", *Phys. Rev. Lett.* **39**, 898-903 (1977).
 26. A. D. Sakharov, "Violation of CP Symmetry, C-Asymmetry and Baryon Asymmetry of the Universe", *JETP Lett.* **5**, 24 (1967).
 27. A. D. Sakharov, "Topological structure of elementary particles and CPT asymmetry", in "Problems in theoretical physics", dedicated to the memory of I.E. Tamm: Nauka, Moscow, pp.243-247, (1972).
 28. D. J. Wineland, R. E. Drullinger and F. L. Walls, *Phys. Rev. Lett.*, **40**, 1639 (1978).
 29. J. Bardeen, L. N. Cooper, and J. R. Schrieffer, *Phys. Rev.* **108**, 1175 (1957).

30. Lee Smolin, "Time reborn", Houghton Muffin Harcourt, Boston – New York (2013), pp. XXV-XXVI [30a]; pp. 52-53 [30b]; pp. 214-219 [30c]; pp. 27-29.
31. B. Greene, "The fabric of the cosmos: space, time and the texture of reality", p. 268, Alfred A. Knopf, New York (2006).

FIGURE CAPTIONS

Fig.1. Simultaneous records of the resistance variations of the platinum resistance thermometer (PRT) and of the two thermistors R6 and R3, which are located symmetrically relative to the PRT on the surface of the gauge block (see insert). During the modulation cycle, the current in the PRT is kept at the level of 5mA for $\frac{1}{4}$ of the modulation period, and it is kept at 1mA for the rest part of the period. As the sensitivities of the thermistors are equal, these records demonstrate that the induced temperature variations in the channels are different for the asymmetric PRT position relative to the gauging surfaces. The location of one of the gauging surfaces of the block is shown by an arrow. (See text for other details).

Fig.2. The dependence on time of the thermal surface energy (TSE), represented by the difference in the induced temperature variations $\Delta T[1,2]$, recorded in the two thermistor channels 1 and 2 during one modulation cycle. Dots and rhombi show the experimental points, obtained during the heating and cooling periods of the modulation cycle, respectively. Squares correspond to the reference points for the two adjacent cycles, and the linear fit to these points is shown as a solid line, with the corresponding expression presented in the inset.

Fig.3a. The thermal velocity dependence $V[R6]$ as a function of time is presented for two modulation cycles under the experimental conditions of Fig.1. The experimental points corresponding to the heating period are shown as dots, while the cooling period is presented by rhombi and the reference points, corresponding to the last 30 minutes at $I=1mA$, are shown as rectangles. The solid line presents a 6-th order polynomial fit to all reference points for all modulation cycles in that experiment.

Fig.3b. The variations in time of the quantities $\Delta V[R6]$ and $\Delta V[R3]$, which are measured relative to their 6-th order fits and which are averaged over a couple of modulation cycles of Fig.3a. The values of $\Delta V[R6]$ and $\Delta V[R3]$ are shown as dots and triangles, respectively, for the heating period of the modulation cycle, and as rhombi and circles, respectively, for the cooling period of the cycle. The reference points are shown as squares.

Fig.3c. Variations in time of the difference between the induced temperature velocities in the channels 1 and 2, $\Delta V[1,2]$, observed during the heating period of the modulation cycle (dots) and during the cooling period

of the cycle (rhombi). The reference points are shown as squares. The linear fit equation is presented in the inset.

Fig.4a. The dependence of the maximum value of the quantity $\Delta T[1,2]$ on the separation value of the axis of the thermistor R6 from the nearest gauging surface. The zero value of the quantity $\Delta V[1,2]$ corresponds to the symmetric position of the PRT on the block surface. Rhombi show the values of the Gaussian fit to the experimental points.

Fig.4b. The dependence of the maximum value of the quantity $\Delta V[1,2]$ on the separation of the axis of the thermistor R6 from the nearest gauging surface. The zero value of the quantity $\Delta V[1,2]$ corresponds to the symmetric position of the PRT on the block surface. (See text for other details).

Fig.4c. The dependences of the vector quantity $\Delta T[1,2]$ on time for the separations of the R6 thermistor from the gauging surface of 4.5mm (dots), 9mm (rhombi) and 13.5mm (squares). The reference points are shown as triangles.

Fig.5a. The dependences of the surface energy $\Delta T[1,2]$ on time, obtained for a tungsten carbide block when the R6 thermistor is close to the gauging surface of the block (curve 1), and when the R3 thermistor is close to the opposite gauging surface (curve 2).

Fig.5b. The dependence of the maximum value of the quantity $\Delta T[1,2]$ on the displacement of the PRT relative to the center of the gauge block surface.

Fig.5c. The dependences of the quantity $\Delta V[1,2]$ on the time interval, elapsed after the increase of the PRT modulation current, for two opposite cases of the thermistors positions: dependence 1 (shown by squares) corresponds to the separation of the R6 thermistor of 4.5mm from one of the gauging surfaces of the block, while the dependence 2 (shown by dots) corresponds to the case when the measuring system as a whole was shifted along the surface of the block, so that the separation of 4.5mm of the thermistor R3 from the other gauging surface was realized.

Fig.6a. The effect of the PRT power increment on the quantity $\Delta T[1,2]$. Dependences 1 and 2 correspond to the separations of the R6 axis from the nearest gauging surface of $L=4.5mm$ (dots) and $L=13.5mm$ (squares), respectively. These plots establish the linear relation for the heating period of the modulation cycle between the two vector quantities: the Poynting vector of the external EM field and the quantity $\Delta T[1,2]$, characterizing the TSE. The decrease of the magnitude of the TSE with the increase of the R6 separation from the nearest gauging surface is clearly demonstrated by the dependences (1) and (2). (See text for other details).

Fig.6b. The effect of the PRT power increment on the maximum value of the quantity $\Delta V[1,2]$. Dependences 1 and 2 correspond to the separations of the R6 axis from

the nearest gauging surface of $L=4.5\text{mm}$ (dots) and $L=13.5\text{mm}$ (squares), respectively. These plots establish the linear relation for the heating period of the modulation cycle between the Poynting vector of the external EM field and the maximum value of the additional energy flux in the gauge block, described by the quantity $\Delta V[1,2]$.

Fig.7. The thermal hysteresis loop for the quantity $\Delta T[1,2]$ that corresponds to the temperature records of Figs. 1 and 2. The heating period of the cycle (between the arrows 1 and 2) is shown by dots, while the cooling period of the modulation cycle (between the arrows 2, 3 and 1) is presented by rhombi. (See text for other details).

Fig.8. The records of the build-up in time of the thermal surface energy in a steel GB during the first 13 minutes of the heating period of the modulation cycle when the temperature differences between the channels $T[1,2]$, equal to 2.46mK (dots), 9.12mK (rhombi), 57.1mK (triangles) and 61.06mK (squares), were realized with the help of an auxiliary energy source in the Dewar. These dependences show that the principle of superposition is not valid for the external EM fields, and that the external energy source changes the dependence on time of the thermal evolution process, which is irreversible in time and specific for a particular point of the artifact.

Fig.9a. The dependence of the quantity $\Delta T[1,2]$, measured 13 minutes after the increase of the PRT modulation current in steel gauge block, on the temperature difference $T[1,2]$ between the positions of the thermistors R6 and R3. The maximum deviation of the measured values relative to the fit is $1.75\mu\text{K}$ and the standard deviation for a single measurement is $1.34\mu\text{K}$. (See text for other details).

Fig.9b. The dependence of the quantity $\Delta T[1,2]$, measured 3 minutes after the increase of the PRT modulation current in steel gauge block, on the temperature difference $T[1,2]$ between the positions of the thermistors R6 and R3.

Fig.10. The dependencies of the quantity $\Delta T[1,2]$ on time for the first 13 minutes of the heating period that were obtained for the tungsten carbide gauge block for the temperature differences $T[1,2]$ of -1.72mK (dependence 1; dots), -7.2mK (dependence 2; squares) and -12mK (dependence 3; rhombi).

Fig.11. The dependencies of the quantity $\Delta V[1,2]$ on time for the first 13 minutes of the heating period that were obtained for the tungsten carbide gauge block (dependences 1 and 2) and for the steel block (3) for the temperature differences between the locations of the thermistors $T[1,2]$ of $-0,2\text{mK}$ (dependence 1; dots) and -17.2mK (dependence 2; squares). Note that the thermal evolution process is described by a complicated function of time, which is specific for the selected points

inside the artifact, and whose form and magnitude depend on the direction and magnitude of the constant heat flux, created in advance by an auxiliary heat source. (See text for other details).

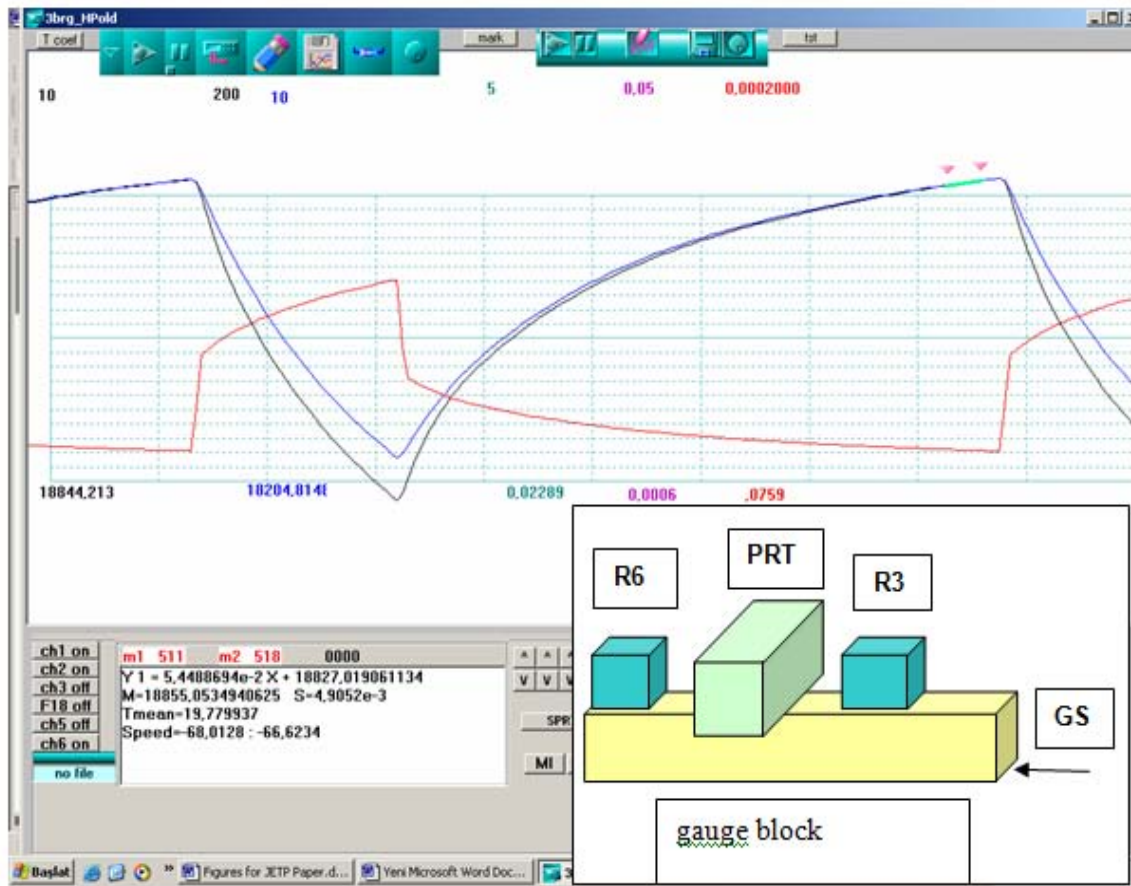


Fig.1 : Simultaneous records of the resistance variations of the platinum resistance thermometer (PRT) and of the two thermistors R6 and R3, which are located symmetrically relative to the PRT on the surface of the gauge block (see insert). During the modulation cycle, the current in the PRT is kept at the level of 5mA for $\frac{1}{4}$ of the modulation period, and it is kept at 1mA for the rest part of the period. As the sensitivities of the thermistors are equal, these records demonstrate that the induced temperature variations in the channels are different for the asymmetric PRT position relative to the gauging surfaces. The location of one of the gauging surfaces of the block is shown by an arrow. (See text for other details)

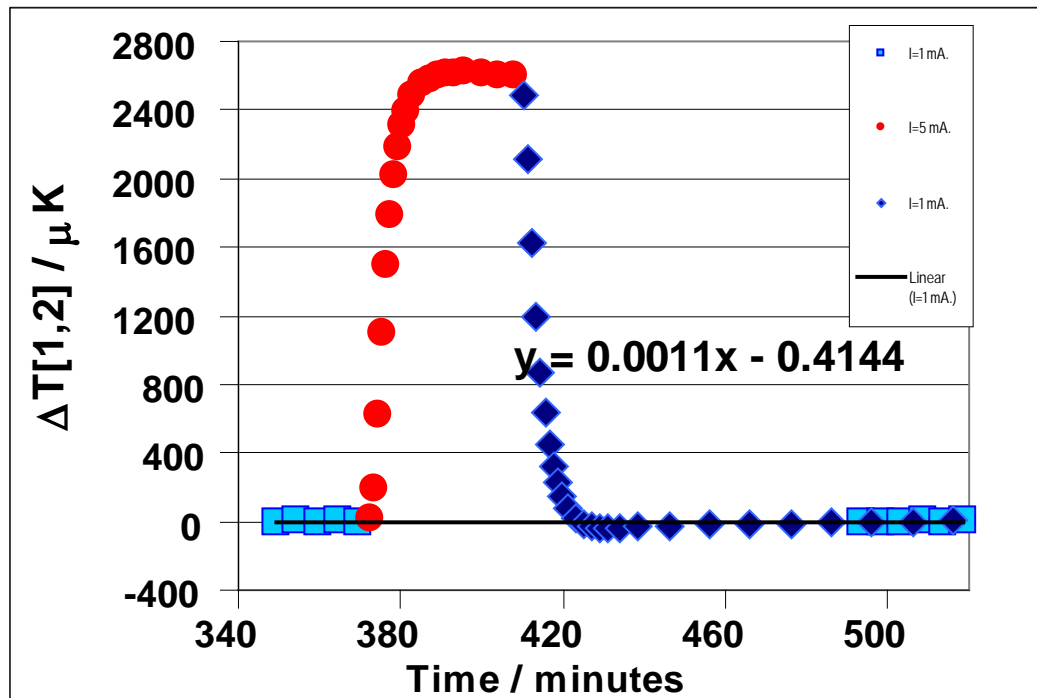


Fig. 2 : The dependence on time of the thermal surface energy (TSE), represented by the difference in the induced temperature variations $\Delta T[1,2]$, recorded in the two thermistor channels 1 and 2 during one modulation cycle. Dots and rhombi show the experimental points, obtained during the heating and cooling periods of the modulation cycle, respectively. Squares correspond to the reference points for the two adjacent cycles, and the linear fit to these points is shown as a solid line, with the corresponding expression presented in the inset

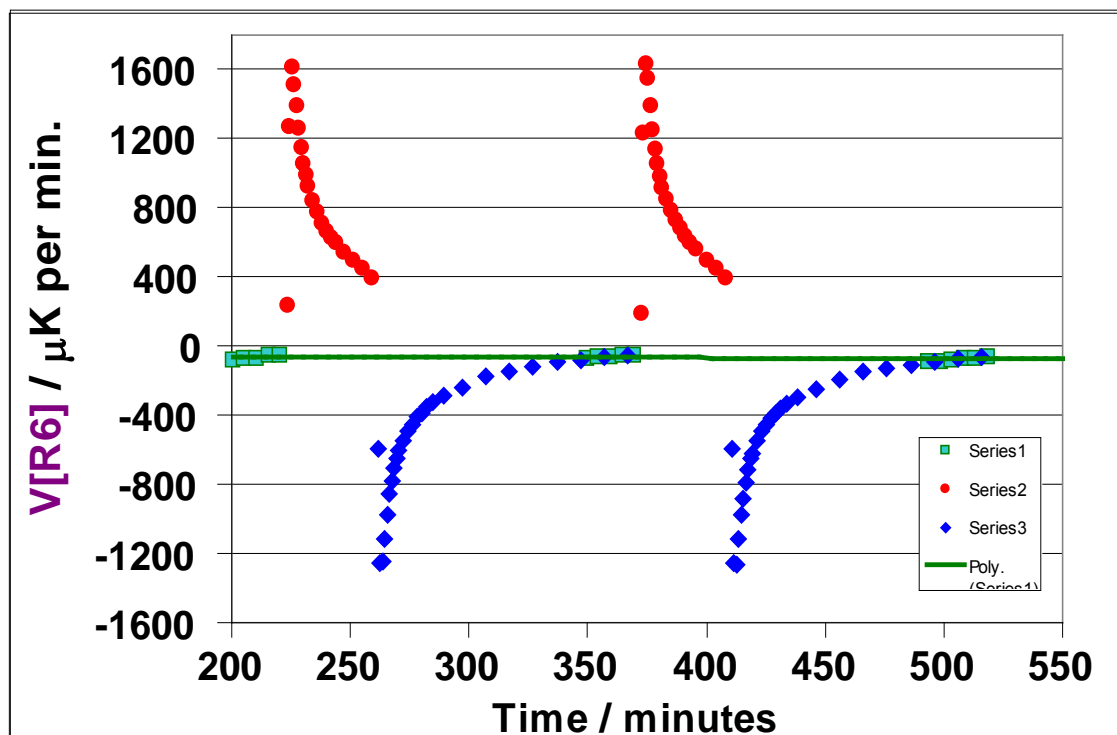


Fig. 3a : The thermal velocity dependence $V[R6]$ as a function of time is presented for two modulation cycles under the experimental conditions of Fig.1. The experimental points corresponding to the heating period are shown as dots, while the cooling period is presented by rhombi and the reference points, corresponding to the last 30 minutes at $I=1\text{mA}$, are shown as rectangles. The solid line presents a 6-th order polynomial fit to all reference points for all modulation cycles in that experiment

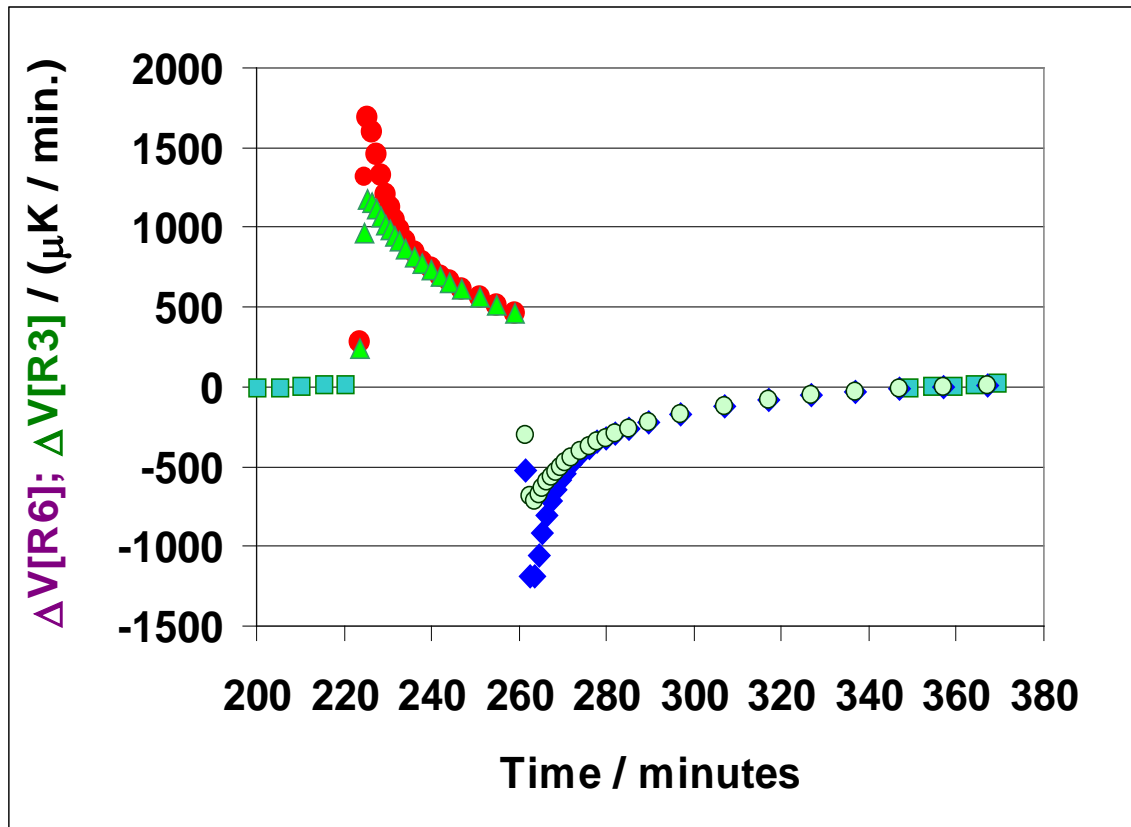


Fig. 3b : The variations in time of the quantities $\Delta V[R6]$ and $\Delta V[R3]$, which are measured relative to their 6-th order fits and which are averaged over a couple of modulation cycles of Fig.3a. The values of $\Delta V[R6]$ and $\Delta V[R3]$ are shown as dots and triangles, respectively, for the heating period of the modulation cycle, and as rhombi and circles, respectively, for the cooling period of the cycle. The reference points are shown as squares

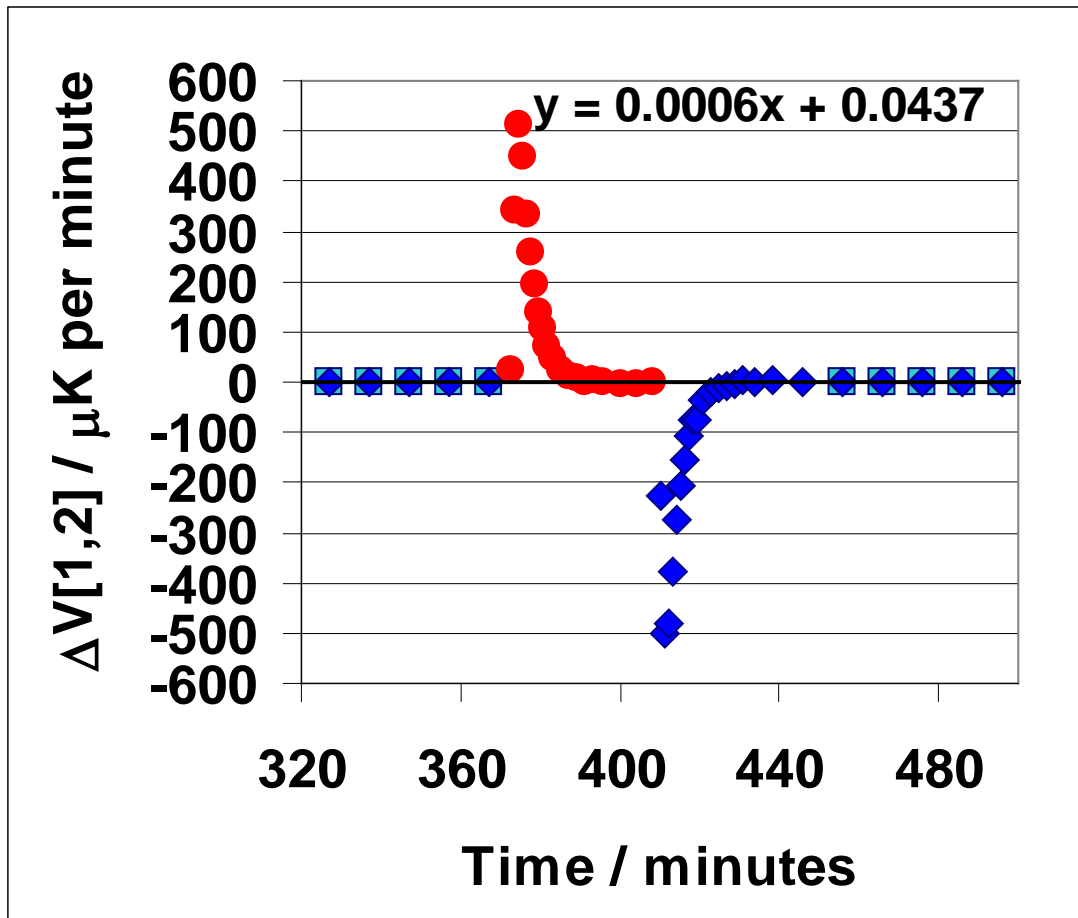


Fig. 3c : Variations in time of the difference between the induced temperature velocities in the channels 1 and 2, $\Delta V[1,2]$, observed during the heating period of the modulation cycle (dots) and during the cooling period of the cycle (rhombi). The reference points are shown as squares. The linear fit equation is presented in the inset

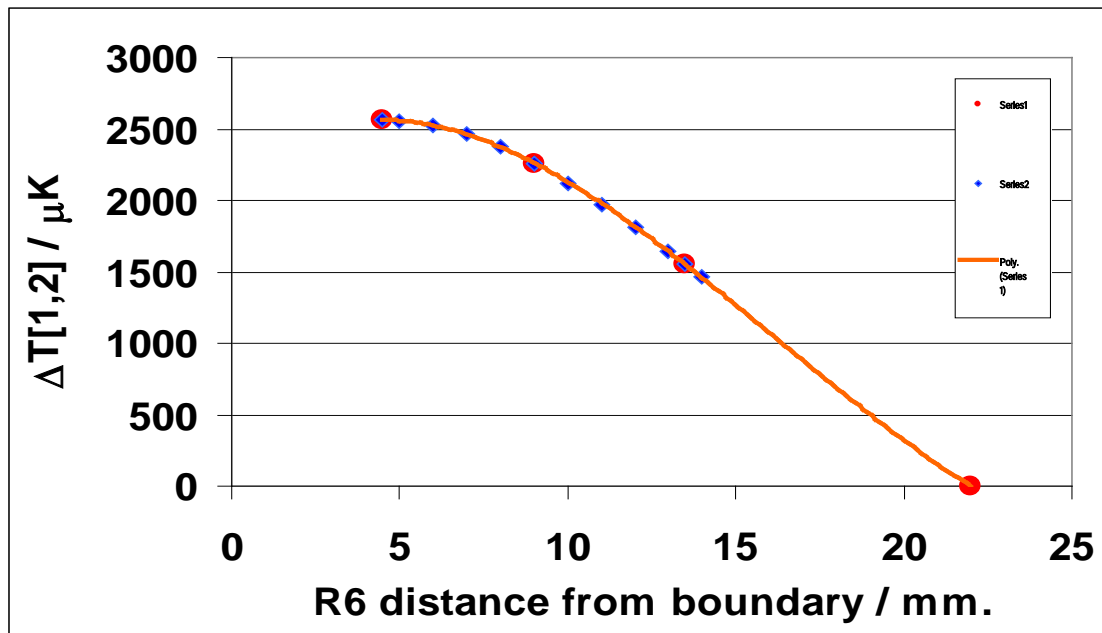


Fig. 4a : The dependence of the maximum value of the quantity $\Delta T[1,2]$ on the separation value of the axis of the thermistor R6 from the nearest gauging surface. The zero value of the quantity $\Delta V[1,2]$ corresponds to the symmetric position of the PRT on the block surface. Rhombi show the values of the Gaussian fit to the experimental points

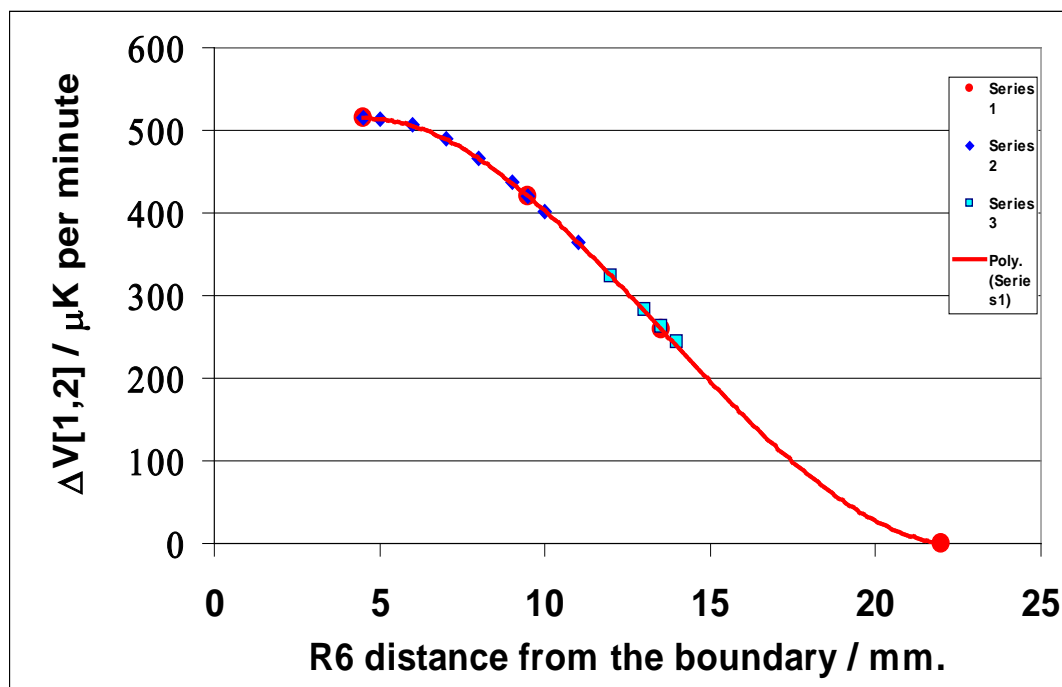


Fig. 4b : The dependence of the maximum value of the quantity $\Delta V[1,2]$ on the separation of the axis of the thermistor R6 from the nearest gauging surface. The zero value of the quantity $\Delta V[1,2]$ corresponds to the symmetric position of the PRT on the block surface. (See text for other details)

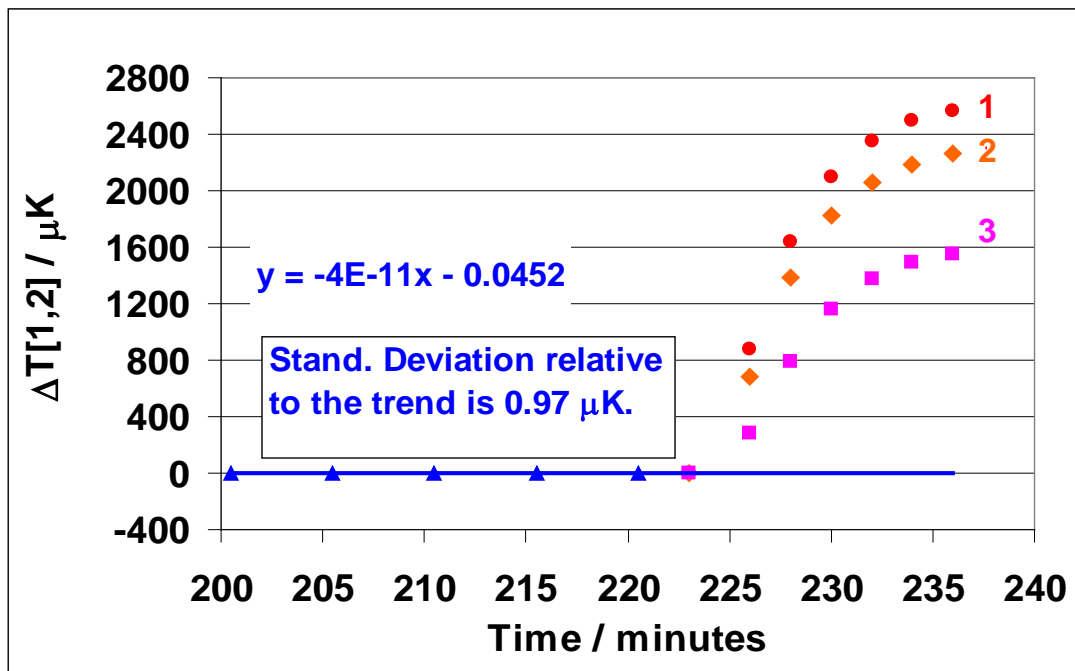


Fig. 4c : The dependences of the vector quantity $\Delta T[1,2]$ on time for the separations of the R6 thermistor from the gauging surface of 4.5mm (dots), 9mm (rhombi) and 13.5mm (squares). The reference points are shown as triangles

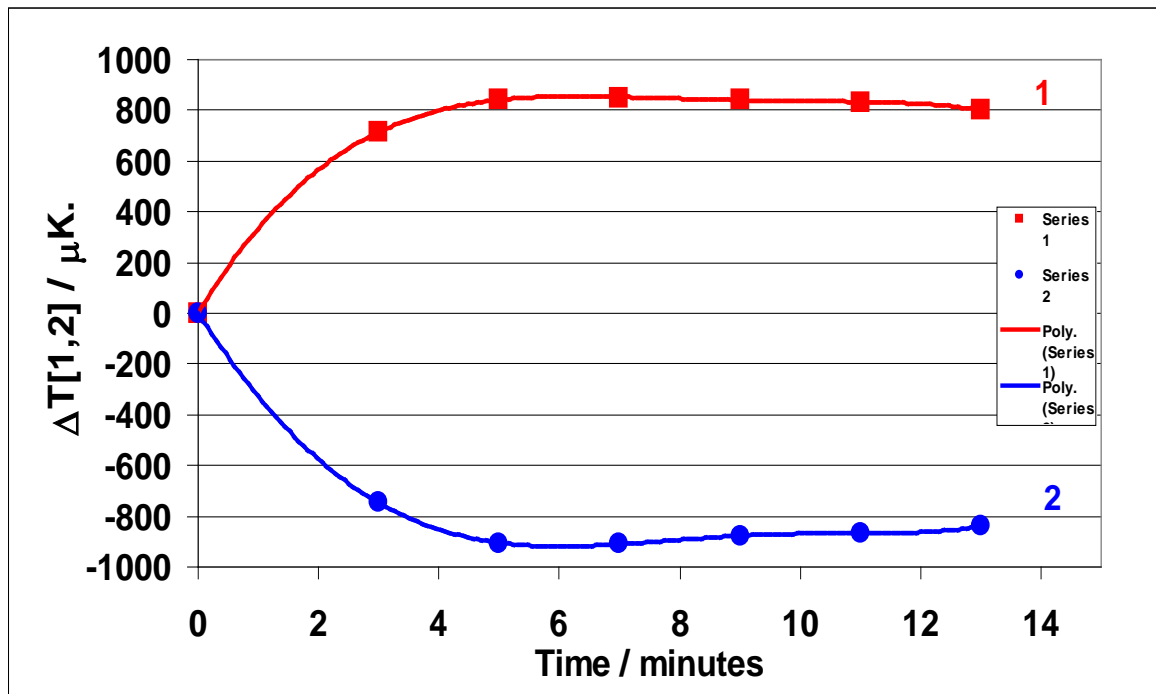


Fig. 5a : The dependences of the surface energy $\Delta T[1,2]$ on time, obtained for a tungsten carbide block when the R6 thermistor is close to the gauging surface of the block (curve 1), and when the R3 thermistor is close to the opposite gauging surface (curve 2)

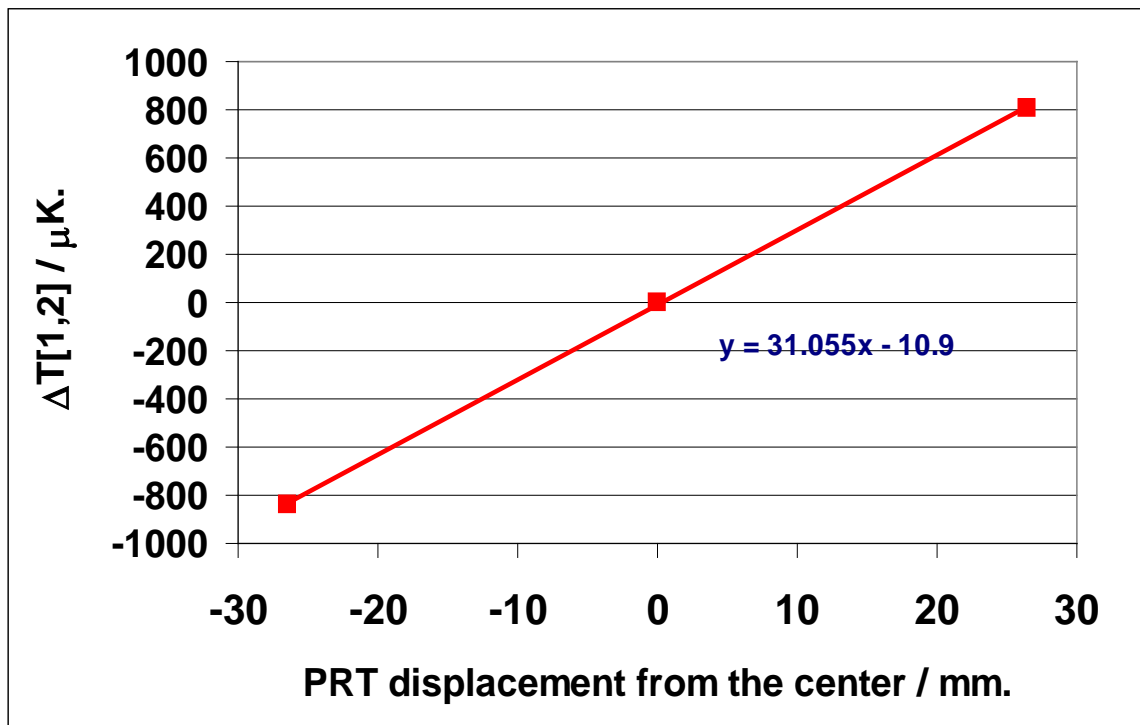


Fig. 5b : The dependence of the maximum value of the quantity $\Delta T[1,2]$ on the displacement of the PRT relative to the center of the gauge block surface

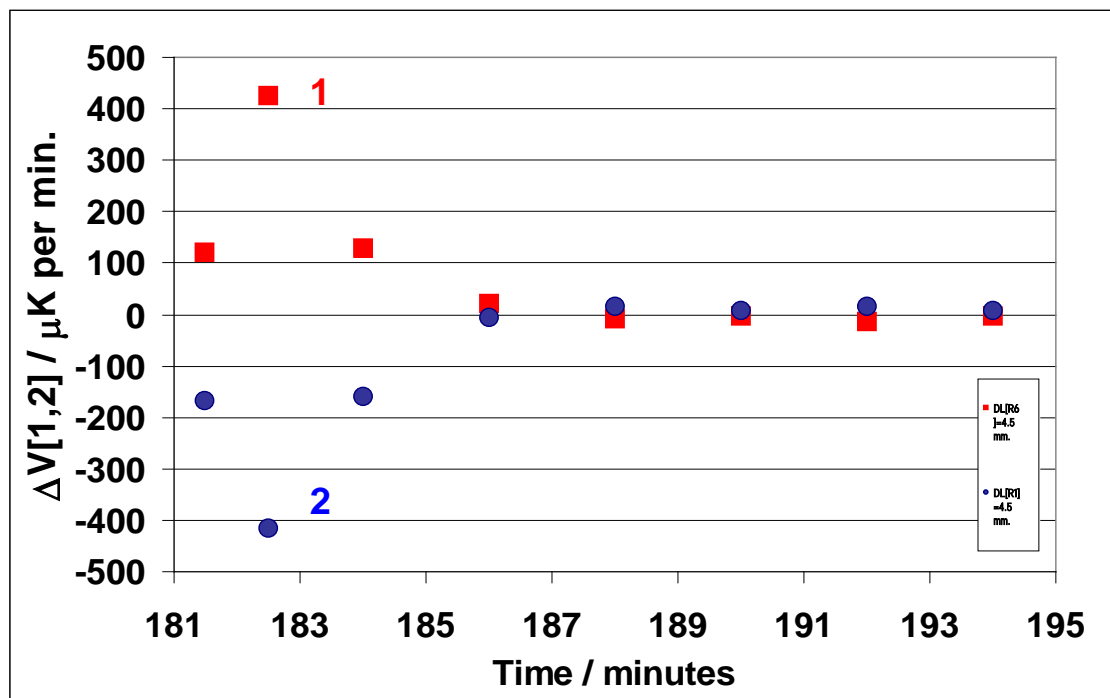


Fig. 5c : The dependences of the quantity $\Delta V[1,2]$ on the time interval, elapsed after the increase of the PRT modulation current, for two opposite cases of the thermistors positions: dependence 1 (shown by squares) corresponds to the separation of the R6 thermistor of 4.5mm from one of the gauging surfaces of the block, while the dependence 2 (shown by dots) corresponds to the case when the measuring system as a whole was shifted along the surface of the block, so that the separation of 4.5mm of the thermistor R3 from the other gauging surface was realized

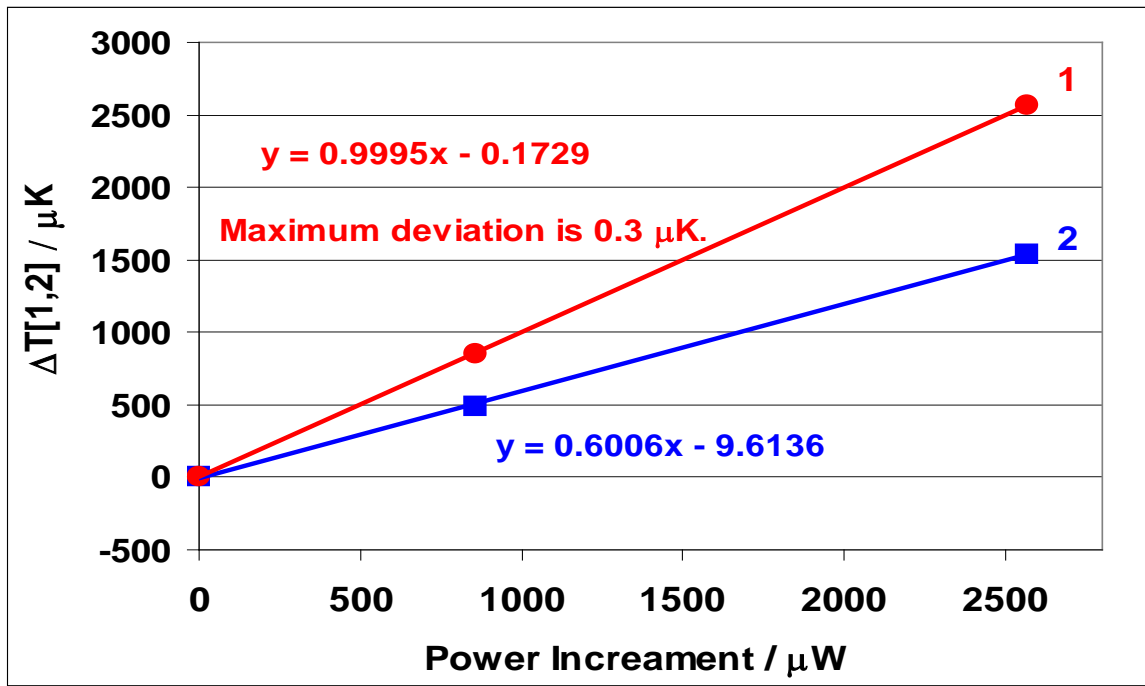


Fig. 6a : The effect of the PRT power increment on the quantity $\Delta T[1,2]$. Dependences 1 and 2 correspond to the separations of the R6 axis from the nearest gauging surface of $L=4.5\text{mm}$ (dots) and $L=13.5\text{mm}$ (squares), respectively. These plots establish the linear relation for the heating period of the modulation cycle between the two vector quantities: the Poynting vector of the external EM field and the quantity $\Delta T[1,2]$, characterizing the TSE. The decrease of the magnitude of the TSE with the increase of the R6 separation from the nearest gauging surface is clearly demonstrated by the dependences (1) and (2). (See text for other details)

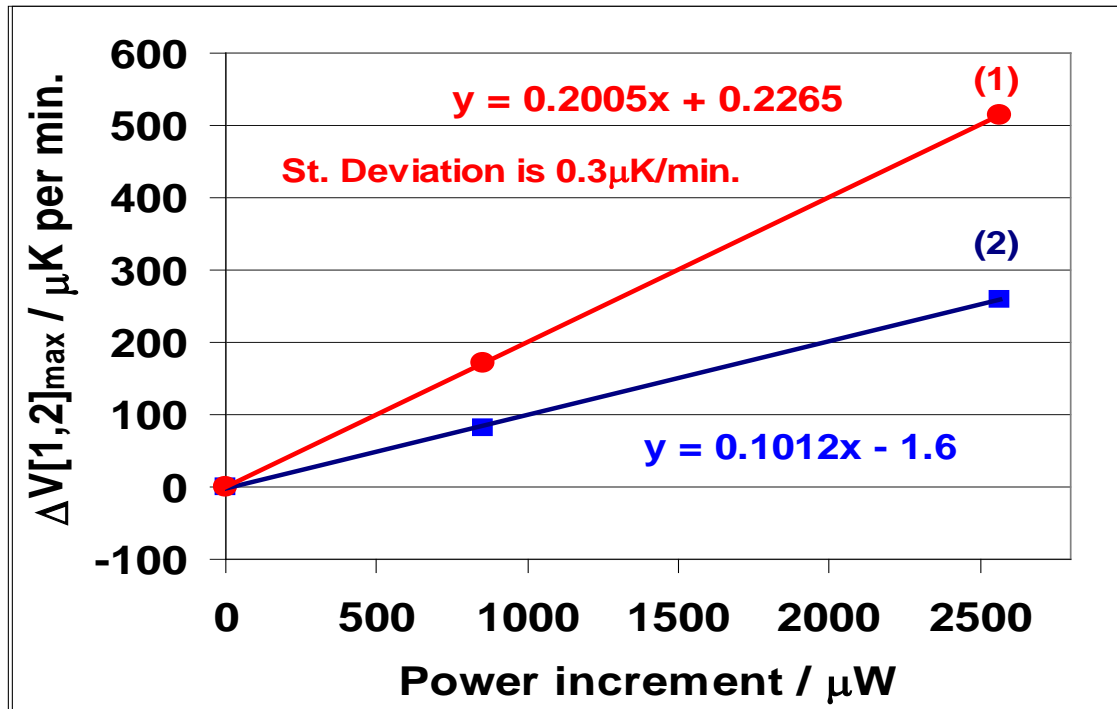


Fig. 6b : The effect of the PRT power increment on the maximum value of the quantity $\Delta V[1,2]$. Dependences 1 and 2 correspond to the separations of the R6 axis from the nearest gauging surface of $L=4.5\text{mm}$ (dots) and $L=13.5\text{mm}$ (squares), respectively. These plots establish the linear relation for the heating period of the modulation cycle between the Poynting vector of the external EM field and the maximum value of the additional energy flux in the gauge block, described by the quantity $\Delta V[1,2]$

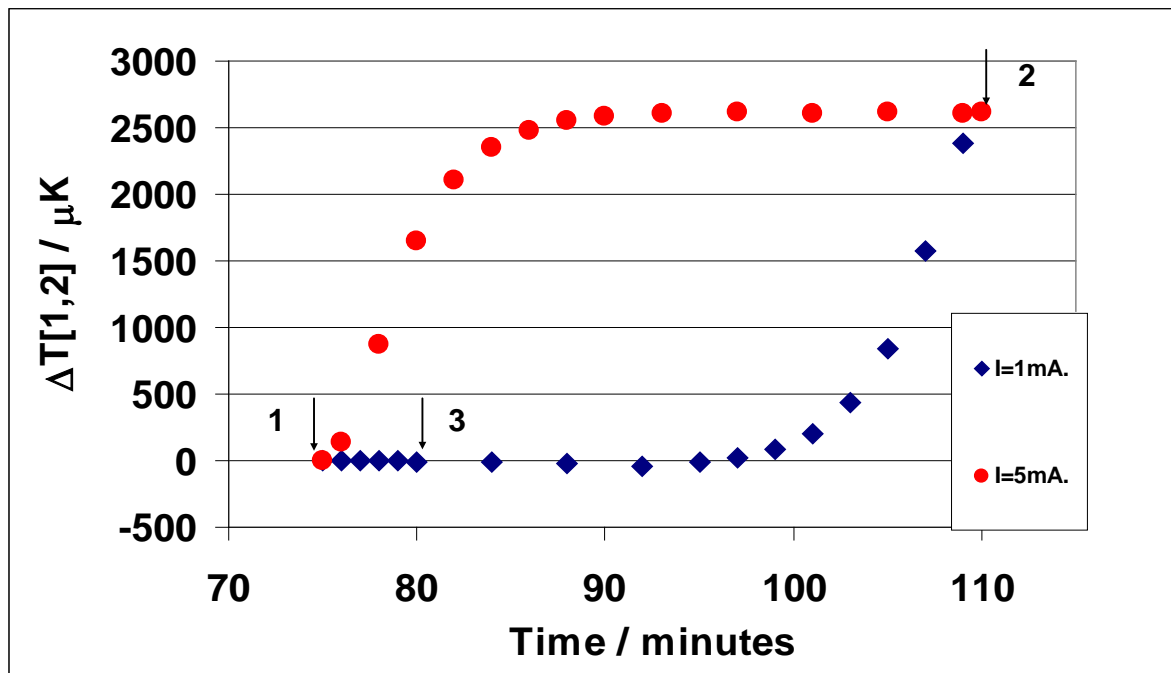


Fig. 7 : The thermal hysteresis loop for the quantity $\Delta T[1,2]$ that corresponds to the temperature records of Figs. 1 and 2. The heating period of the cycle (between the arrows 1 and 2) is shown by dots, while the cooling period of the modulation cycle (between the arrows 2, 3 and 1) is presented by rhombi. (See text for other details)

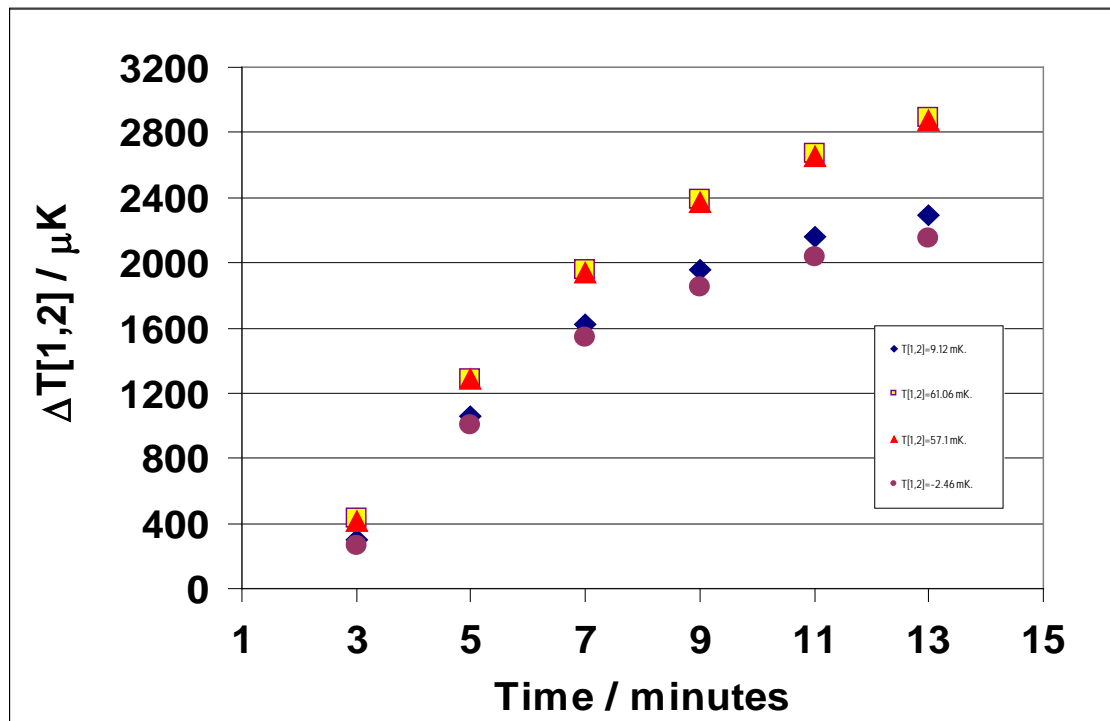


Fig. 8 : The records of the build-up in time of the thermal surface energy in a steel GB during the first 13 minutes of the heating period of the modulation cycle when the temperature differences between the channels $T[1,2]$, equal to 2.46mK (dots), 9.12mK (rhombi), 57.1mK (triangles) and 61.06mK (squares), were realized with the help of an auxiliary energy source in the Dewar. These dependences show that the principle of superposition is not valid for the external EM fields

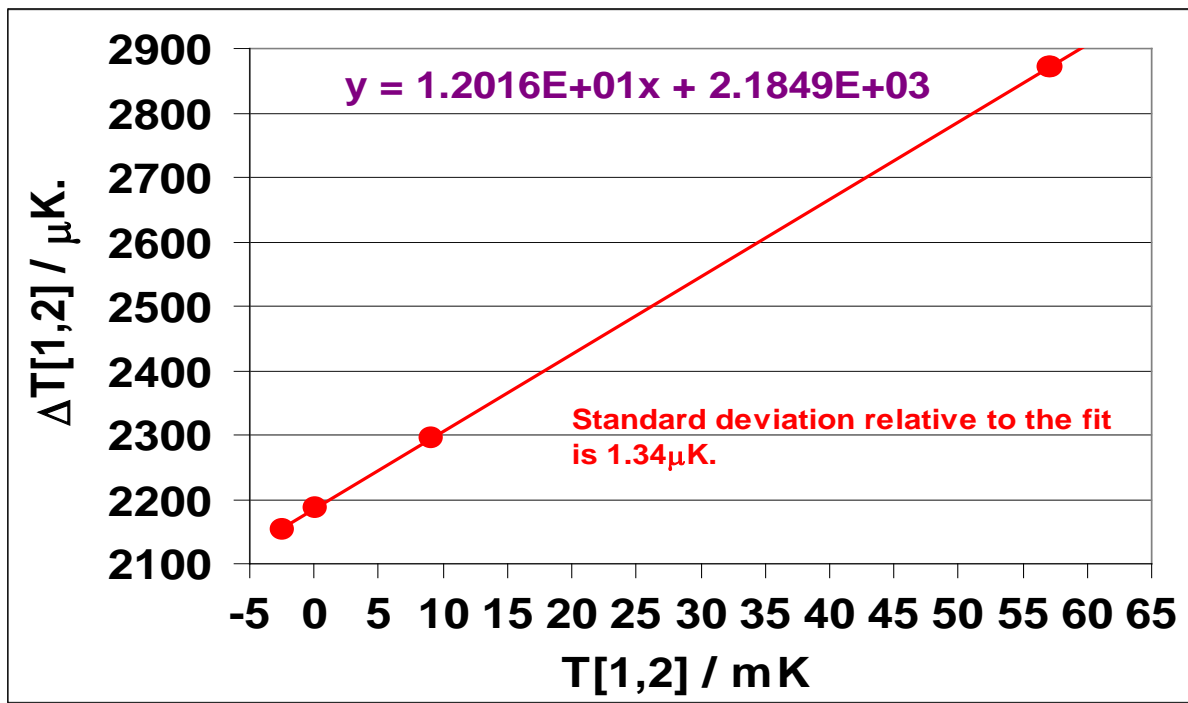


Fig. 9a : The dependence of the quantity $\Delta T[1,2]$, measured 13 minutes after the increase of the PRT modulation current in steel gauge block, on the temperature difference $T[1,2]$ between the positions of the thermistors R6 and R3. The maximum deviation of the measured values relative to the fit is 1.75 μK and the standard deviation for a single measurement is 1.34 μK . (See text for other details)

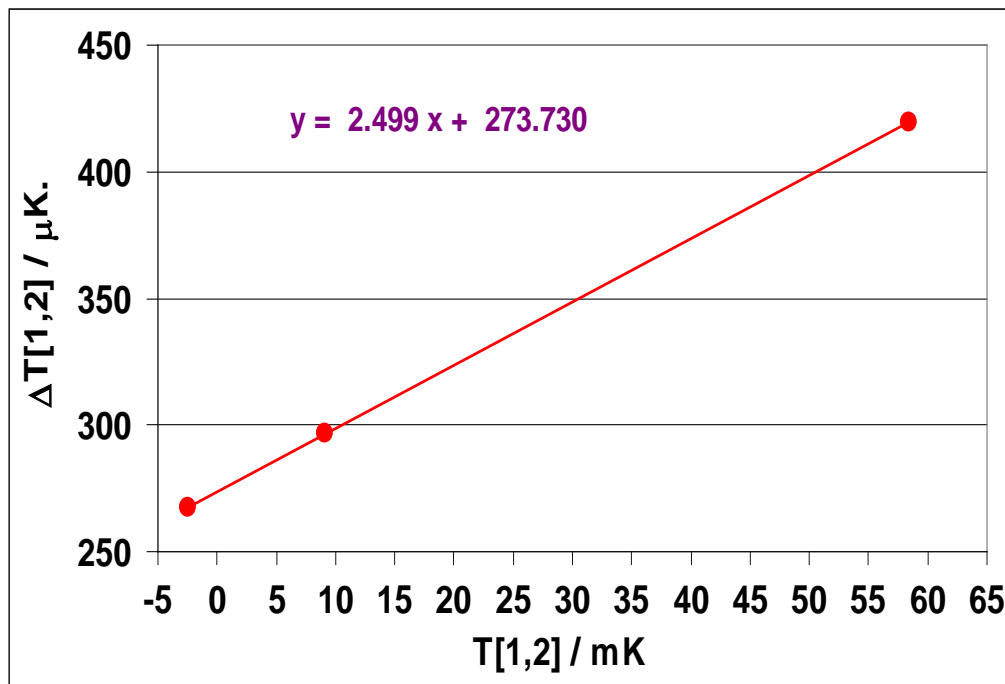


Fig. 9a : The dependence of the quantity $\Delta T[1,2]$, measured 3 minutes after the increase of the PRT modulation current in steel gauge block, on the temperature difference $T[1,2]$ between the positions of the thermistors R6 and R3

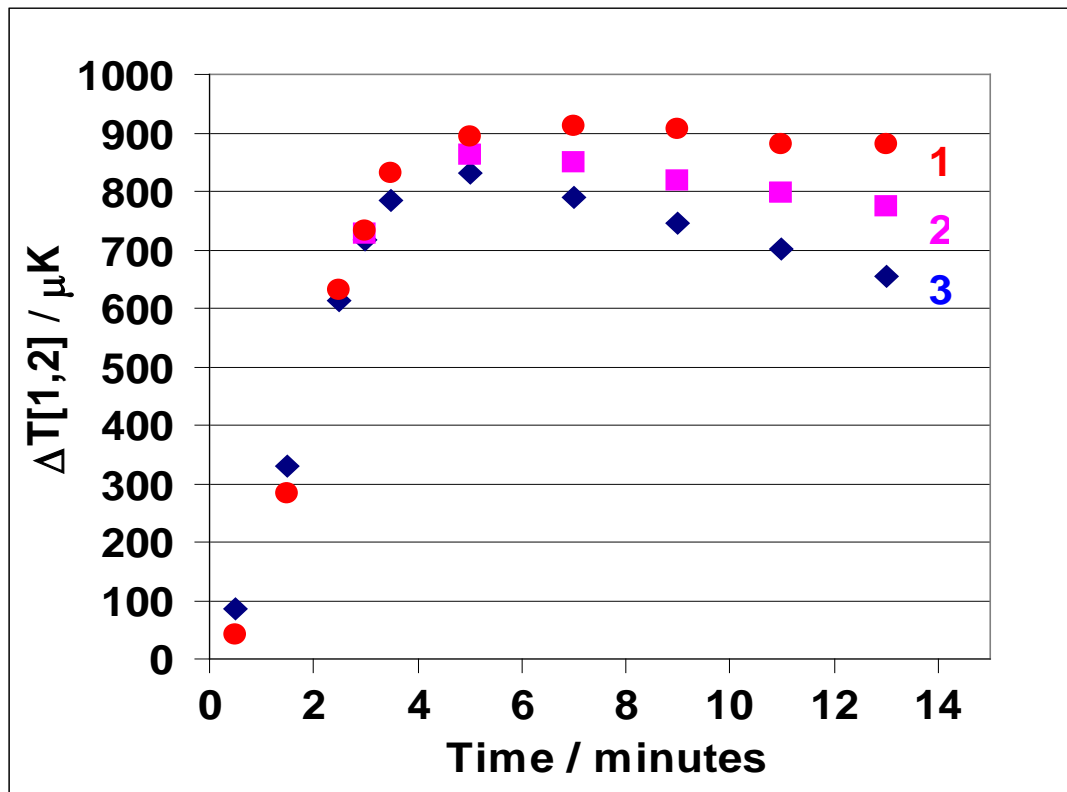


Fig.10 : The dependencies of the quantity $\Delta T[1,2]$ on time for the first 13 minutes of the heating period that were obtained for the tungsten carbide gauge block for the temperature differences $T[1,2]$ of -1.72mK (dependence 1; dots), -7.2mK (dependence 2; squares) and -12mK (dependence 3; rhombi)

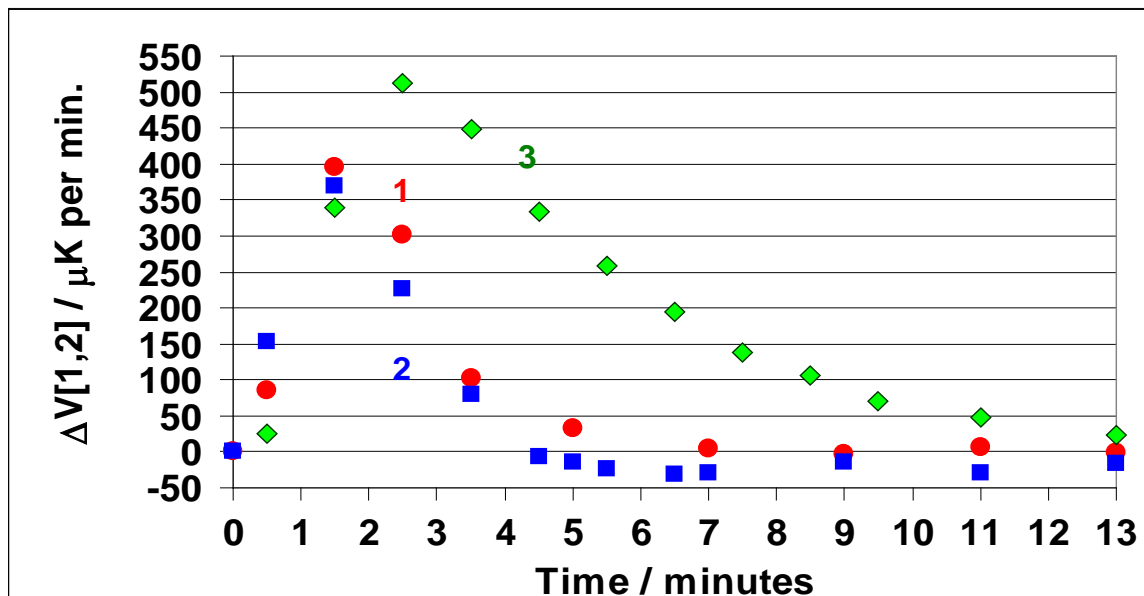


Fig. 11 : The dependencies of the quantity $\Delta V[1,2]$ on time for the first 13 minutes of the heating period that were obtained for the tungsten carbide gauge block (curves 1 and 2) and for the steel block (3) for the temperature differences between the locations of the thermistors $T[1,2]$ of -0,2mK (dependence 1; dots) and -17.2mK (dependence 2; squares). Note that the thermal evolution process is described by a complicated function of time, which is specific for the selected points inside the artifact and whose form and magnitude depend on the direction and magnitude of the constant heat flux, created in advance by an auxiliary heat source. (See text for other details)



This page is intentionally left blank



GLOBAL JOURNAL OF SCIENCE FRONTIER RESEARCH: A
PHYSICS AND SPACE SCIENCE
Volume 15 Issue 3 Version 1.0 Year 2015
Type : Double Blind Peer Reviewed International Research Journal
Publisher: Global Journals Inc. (USA)
Online ISSN: 2249-4626 & Print ISSN: 0975-5896

The Origin of, Maxwell`S - Gravity`S, Displacement Current

By Markos Georgallides

Abstract- Waves need a media to travel and carry energy. A standing wave is an oscillation pattern with a stationary outline (*envelope*) that results either from the superposition of two identical waves travelling opposite directions or from an inner equilibrium vibration. A given particle that is bound (*confined*) in a certain region of space is a standing wave and vibrates within the constraints of the envelope function $y = 2A.\sin(kx).\cos.(wt)$. Light is both, a particle and a wave.[39]. Since quaternion, as work is constant then $W = q = (\lambda, \pm\lambda \times \nabla i) = \text{Force (P)}$ acting on wavelength (λ) = Normal stress σ acting on area A is, $(\sigma.A) \times \lambda$, and for $A = 0$ then becomes the linear Momentum = $\bar{v} \times \lambda$ (*since Stationary energy becomes Kinetic*) and $W = \bar{v} \times \lambda$, .i.e. Work = Travelling Energy and because when converted into, velocity, \bar{v} , in wavelength λ as background media, then this is the reason that doesn` t collapse by radiating away its or their energy.

Keywords: the origin of maxwell`s-gravity`s displacement current, the inner structure of gravity , the inner structure of moving particles, equilibrium of quantized space and spin by the opposite cycloidal motion in quantized anti-space . the quanta of space and energy.

GJSFR-A Classification : FOR Code: M10



Strictly as per the compliance and regulations of :



The Origin of, Maxwell's - Gravity's, Displacement Current

Markos Georgallides

Abstract- Waves need a media to travel and carry energy. A standing wave is an oscillation pattern with a stationary outline (*envelope*) that results either from the superposition of two identical waves travelling opposite directions or from an inner equilibrium vibration. A given particle that is bound (*confined*) in a certain region of space is a standing wave and vibrates within the constraints of the envelope function $y = 2A.\sin(kx).\cos(\omega t)$. Light is both, a particle and a wave.[39]. Since quaternion, as work is constant then $W = q = (\lambda, \pm \Delta x \nabla i) = \text{Force (P) acting on wavelength } (\lambda) = \text{Normal stress } \sigma \text{ acting on area } A \text{ is, } (\sigma.A)\lambda$, and for $A = 0$ then becomes the linear Momentum $= \bar{v}\lambda$. (*since Stationary energy becomes Kinetic*) and $W = \bar{v}\lambda$, i.e. Work = Travelling Energy and because when converted into, velocity, \bar{v} , in wavelength λ as background media, then this is the reason that doesn't collapse by radiating away its or their energy. Work as Vibration is confined in its wavelength as a Damper, *absorber*, and is retained unchanged when travelling. The How and when is widely analyzed.

Since also a stationary wave consists of two transverse waves then is not interpreted as an equal mixture of the two, but an inner equilibrium on monad λ . It was shown that Energy-Space universe (*the beyond Planck's length, Gravity's and Spaces' levels*) is [PNS] and Space Anti-Space as work is $\rightarrow W = \int P.ds = 0$, which is the cause of Spaces existence with the only two quantized magnitudes $\lambda, \bar{\lambda}$, on Monads AB as the breakages $[s^2 = \pm (\bar{w}.r)^2]$ in Inertial systems consisting the {MFMF = Background medium Field and $[\nabla i = 2.(\bar{w}.r)^2]$ } the Gravity force. Momentum as velocity \rightarrow [velocity $= \bar{v}.g$ = the breakage $[2.(\bar{w}.r)^2]$], *is the cross product of two velocity vectors, \bar{v}_1, \bar{v}_2 , which form with the two side-by-side Medium breakages $\rightarrow [| + (\bar{w}.r)^2 | \leftrightarrow | - (\bar{w}.r)^2 | = |\lambda|]$ the Intrinsic and Stationary Electromagnetic Field of gravity's (The Electric $E \perp$ Magnetic P , following the cycloid motion) in Medium $|\lambda|$. Breakages and Particles with velocity, \bar{v} , being the units of matter with Electric charge, $q = \lambda.m$, as their physical property is, when placed in prior referred Electromagnetic Field $E \perp P$, where like charges repel and unlike charges attract, experience a force as Lorentz force, and this is called Gravity-Force, and equal to $\rightarrow F_g = q.[E + \bar{v} \times P] \leftarrow$ while Background-medium, is the Gravity-Field $= Gf = [E + \bar{c} \times P]$ in the medium $\{ds = |\lambda| = [2.(\bar{w}.r)^2] = [+ (\bar{w}.r)^2] \leftrightarrow [- (\bar{w}.r)^2] \}$, i.e. the Quantized-Space is the medium ds , which is also Quantized-Energy of two (\pm) breakages $= |\lambda|$, on which is exerted a Thrust as Velocity \bar{c} which is decomposed into the two equal velocity vectors, \bar{v}_1, \bar{v}_2 and moving on two transverse cycloid trajectories, which create an Intrinsic Stationary Electromagnetic wave $E, P \rightarrow$ the Gravity field $[E + \bar{c} \times P] \leftarrow$, into where motion (E, P) and spin is balanced from the anti- cycloidal motion (evolute) of*

the Anti - Quantized-Space ($-ds$). Gravity force is exerted on breakages $[\leftrightarrow \pm (\bar{w}.r)^2 = \text{The Material points forming dipoles}]$ as velocity vector, \bar{c} , which is decomposed into two reverse velocities following the cycloidal motion, and consisting the intrinsic Stationary Electro-magnetic Wave of gravity, and which is binding the points of this Homogenous- Isotropic, Rest and mass-less nature Field. This is the Space-Energy unification Universe in Inertial systems consisted of this [MFMF] Field and Gravity's inner Displacement current force and consist the Absolute frames in nature. The known relation $c^2.\epsilon.\mu = 1$ between the speed of light, and Permittivity - Permeability in free space is proved, and the immense confusion in the basic ideas regarding the Quantized Energy-Space, *The Quanta*, vanishes.

Keywords: *the origin of maxwell's-gravity's displacement current, the inner structure of gravity, the inner structure of moving particles, equilibrium of quantized space and spin by the opposite cycloidal motion in quantized anti-space. the quanta of space and energy.*

I. INTRODUCTION

Point, which is nothing and has not any Position may be anywhere in Space, therefore, the Primary point A being nothing also in no Space, is the only Point and nowhere, i.e. Primary Point is the only Space and from this all the others which have Position, therefore it is the only Space and so to exist point A at a second point B somewhere else point A must move towards point B, where then $A \equiv B$. Point B is the Primary Anti-Space which Equilibrium point A, [PNS] = $[A \equiv B]$. The position of points in [PNS] creates the infinite dipole and all quantum quantities which acquire Potential difference and an Intrinsic moment $\pm \bar{\lambda}$ in the three Spatial dimensions (x, y, z) and on the infinite points of the (i) Layers at these points, which exist from the other Layers of Primary Space, Anti-Space and Sub-Space, and this is because Spaces = monads = quaternion [9]. Since Primary point A is the only Space then on this exists the Principle of Virtual Displacements $W = \int P.ds = 0$ or $[ds.(PA + PB) = 0]$, i.e. for any $ds > 0$ Impulse $P = (PA + PB) = 0$, $[ds.(PA + PB) = 0]$, Therefore, Each Unit $AB = ds > 0$, exists by this Inner Impulse (P) and so $PA + PB = 0$ i.e. The Position and Dimension of all Points which are connected across the Universe and that of Spaces exists, because of this equilibrium Static Inner Impulse, on the contrary should be one point only (Primary Point A = Black Hole $\rightarrow ds = 0$ and $P = \infty$).

Author: Larnaca, Cyprus.

e-mail: georgallides.marcos@cytanet.com.cy

All points may exist with $P = 0 \rightarrow (PNS)$ and also with $P \neq 0, (PA + PB = 0)$, for all points in Spaces and Anti-Spaces, therefore [PNS] is self-created, and because at each point may exist also with $P \neq 0$, then [PNS] is a (perfectly Homogenous, Isotropic and Elastic Medium) Field with infinite points which have a \pm Charge with $P = 0 \rightarrow P = \Lambda \rightarrow \infty$

Since points A, B of [PNS] coincide with the infinite Points, of the infinite Spaces, Anti-Spaces and Sub-Spaces of [PNS] and exists rotational energy $\pm \Lambda$ and since Motion may occur at all Bounded Sub-Spaces ($\pm \Lambda, \lambda$), then this Relative motion is happening between all points belong in g to [PNS] and to those points belonging to the other Sub-Spaces ($A \equiv B$). The Infinite points in [PNS] form infinite Units (monads) $AiBi = d\bar{s}$, which equilibrium by the Primary Anti-Space by an Inner Impulse (P) at edges A, B where $PiA + PiB \neq 0$, and $ds = 0 \rightarrow N \rightarrow \infty$.

Monad (Unit) $\bar{A}\bar{B}$ is the ENTITY and $[A, B - \bar{P}\bar{A}, \bar{P}\bar{B}]$ is the LAW, so Entities are embodied with the Laws.

Entity is quaternion $\bar{A}\bar{B}$, and law $|AB| =$ length of points A, B and imaginary part forces, $\bar{P}\bar{A}, \bar{P}\bar{B}$ or fields.

By definition $i = \sqrt{-1}$ and $(-1)^2 = -1$ i.e. $[Energy]^2 = -[Space] =$ Anti-space and since also exists $\Lambda \times \Lambda = -(-1)^2 = \pm \Lambda \cdot \nabla i$, the basic equation of quaternion becomes $[-(\Lambda \times \Lambda)/m \pm \Lambda \times \nabla i] = [\lambda, \pm \Lambda \times \nabla i]$ i.e. wavelength $\lambda = -(\Lambda \times \Lambda)/m$ where $m =$ a constant depending on reactions to present or other conditions.

Applying this in energy cavities there $\hat{\wedge} - i [(\pi/2) \cdot b]^2 = e^{-i \cdot (\frac{2\pi}{\lambda}) \cdot b} = e^{-i \cdot (\pi) \cdot b} \rightarrow$ i.e. The massive mechanism Diffraction and the Energy mechanism Diffraction are Interchangeable, $e^{-i \cdot (1,78 \cdot 10^7)^2} = e^{-i \cdot (3,56 \cdot 10^{14})}$, and for Relativity massive Energy $(\Lambda \times \Lambda) = (-m \cdot i) \times (-m \cdot i) = m(i)^2 = -m \cdot (\bar{v})^2 = -m\bar{v}^2$, where imaginary part $i = \bar{v}$, i.e. Space acquires energy as velocity.

Applying quaternion equation $[-\nabla \Lambda, \nabla \times \Lambda] = 0$ for point, O, and constant velocity, c.e., then $[-\nabla c, \nabla \times c] = 0$ where $[-\nabla c] \perp [\nabla \times c]$ meaning that it is a mechanism that instantly transports breakage masses dynamically and perpendicularly to all Inertial frames Layers. [26]

II. COMPLEX NUMBERS - QUATERNION

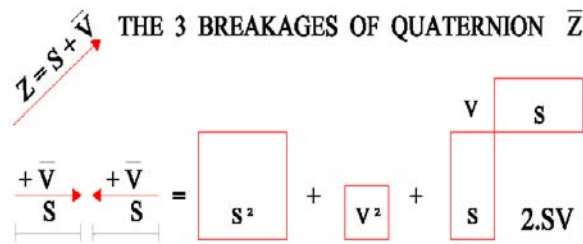


Fig.1 : The Action of quaternion $\bar{z} \cdot \bar{z} = [s + \bar{v} \cdot \nabla i]^2 \rightarrow \bar{z} \cdot \bar{z} = [s + \bar{v} \cdot \nabla i]^2 = s^2 - |\bar{v}|^2 + [2\bar{w}] \cdot |s| \cdot |r| \cdot \nabla i \cdot \bar{w}$

- Quaternion Actions: Action (©) of a quaternion $\bar{z} = s + \bar{v} \cdot i = s + \bar{v} \cdot \nabla i$ on point P (a, x, y, z) is $a\bar{z}' = \bar{z}p\bar{z}'$ (screw = helicoidally motion) and for $a \neq 0$ then z and $a \cdot z = az$ which have the same action $\bar{z}p\bar{z}'$, meaning that quaternion is homogeneous in nature. Action of a Unit quaternion on a scalar, s , is $\bar{z}s = \bar{z}s\bar{z}' = s$. Action of a Unit quaternion \bar{z} on a vector ($\bar{v} \cdot \nabla i$) is $\bar{z}\bar{v}\bar{z}'$

i.e. another vector \bar{v}' (quaternion) $\bar{v}' = (0, \bar{v}' \cdot \nabla i)$, and of vector type $\bar{v}' \cdot \nabla i = \bar{z} + 2\bar{v} \cdot (\bar{v} \times \bar{z}) + 2\bar{v} \times (\bar{v} \times \bar{z})$.

Every quaternion, q, is equal to its versor, V(q), multiplied by its tensor (norm), and for versor $V(q) = e^{(0+\pi i)} \rightarrow$ then $|V(q)| = \sqrt{3}$ and $q = V(q) \cdot \sqrt{3} \cdot \pi$.

Action (©) of a quaternion $\bar{z} = s + \bar{v} \cdot i = s + \bar{v} \cdot \nabla i$ on itself is the Binomial type i.e.

$$(s + \bar{v} \cdot \nabla i)(s + \bar{v} \cdot \nabla i) = [s + \bar{v} \cdot \nabla i]^2 = s^2 + |\bar{v}|^2 \cdot \nabla i^2 + 2|s| \cdot \bar{v} \cdot \nabla i = s^2 - |\bar{v}|^2 + 2|s| \cdot |\bar{w} \cdot r| \cdot \nabla i = s^2 - |\bar{v}|^2 + [2\bar{w}] \cdot |s| \cdot |r| \cdot \nabla i$$

where,

$s^2 \rightarrow$ is the real part of the new quaternion and it is a Positive Scalar magnitude.

$-|\bar{w}|^2 \rightarrow$ the always negative Anti-space which is always a Negative Scalar magnitude.

$[2\bar{w}] \cdot |s| \cdot |r| \cdot \nabla i \rightarrow$ the double angular velocity term which is a Vector magnitude.

III. THE METHOD

The Balancing of Space \rightarrow Anti-Space, in Sub-Space common - Circle

THE TWO OPPOSITE EQUILIBRIUM MOMENTUM ELLIPSOIDS

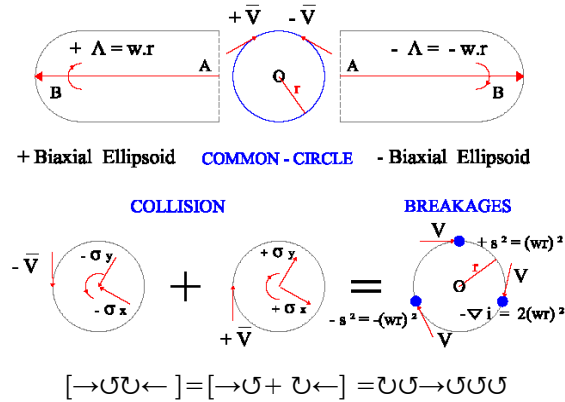


Fig. 2 : Equilibrium vorticity (vortices) ±Λ (Rotating energy) σv Collision on common circle [CC] → vσ ← Thrust on Breakages = v, σv.

The work W, of the two opposite dipole AB, BA with planes is equal to $W = [n.P.ds] = [\lambda = \Lambda \Lambda, \Lambda x \Lambda]$ where,

λ . = displacement of A to B and it is a scalar magnitude called wavelength of dipole A|B.

Λ = the amount of rotation on dipole AB, (this is angular momentum L, and it is a vector parallel to a, axis .

Momentum $\pm \Lambda = r.m.v = r.m.wr = mr^2.w$, where, r, is the radius and angular velocity $\bar{w} = (\text{spin})$ which maps velocity vector \bar{v} , on the perpendicular to a, axis plane with the two components $\bar{v} \perp \bar{v} B$. Tangential velocity $\bar{v} = \bar{w}.r$ is a quaternion $\bar{v} = \bar{w}.r = \bar{z} = [s + \bar{v}.\nabla i]$ where $s = |\bar{v}.E| = |\bar{r}.\bar{w}|$ and $\bar{v}.\nabla i = |\bar{w}x\bar{r}| = |\bar{w}|.|r| \perp |\bar{w}|.r$ where the two opposite biaxial ellipsoid equilibrium.

$$(s + \bar{v}.\nabla i)(s + \bar{v}.\nabla i) = [s + \bar{v}.\nabla i]^2 = s^2 + |\bar{v}|^2.\nabla i^2 + 2|s|x\bar{v}.\nabla i = s^2 - |\bar{v}|^2 + 2|s|x|\bar{w}.r|. \nabla i = s^2 - |\bar{v}|^2 + [2\bar{w}].|s| |r|. \nabla i \dots \tag{3-a}$$

where, $[+s^2] \rightarrow s^2 = (w.r)^2$, is the real part of a new quaternion which is, the positive Scalar product, of Space from the same scalar product, s, s, with $1/2, 3/2, \dots$, spin, and represents the, Space, part of quaternion, the min. Space-Quanta.

$[-s^2] \rightarrow -|\bar{v}|^2 = |\bar{w}.\bar{r}|^2 = -[|\bar{w}|.|\bar{r}|]^2 = -(w.r)^2 \rightarrow$ is the always, the negative Scalar product, of Anti-space from the dot product of, w.:, r.: vectors, with $-1/2, -3/2, \dots$, spin, and represents the, Anti-Space, part of quaternion, the min. Anti-Space Quanta..

$[\nabla i] \rightarrow 2.|s|x|\bar{w}.\bar{r}|.\nabla i = 2|wr|.|\nabla i| = 2.(w.r)^2 \rightarrow$ is a vector of, the velocity vector product, from the cross product of \bar{w}, \bar{r} vectors with double angular velocity term and represents the, Velocity vector product, of quaternion giving 1,3,5, spin, the min. Energy -Quanta. i.e.

In the recovery equilibrium (a surface of a cylinder with 2r diameter), and because velocity vector is on the circumference, the infinite breakages Identify with

In a spherical cave the Biaxial Ellipsoid ($\sigma x = \sigma y$) exists as momentum + Λ on caves of diameter 2r with parallel circles $\rightarrow 0$. The Biaxial Anti-Ellipsoid ($-\sigma x = -\sigma y$) exists as equal and opposite momentum - Λ on the same diameter 2r with anti-parallel circles $\rightarrow 0$. Equilibrium of the two Ellipsoids $\pm \Lambda$, presupposes a Stabilizer system attached to Ellipsoids such that opposite Momentum is distributed to the Center of Mass of the total system and, recover equilibrium, which is the center of the spherical cave. The Biaxial Ellipsoid and Anti-Ellipsoid are inversely directed and rotated in the same circle, so the two opposite velocity vectors collide. This collision of the two opposite velocity vectors is the Action (Thrust) of the two quaternion and it is, Action of quaternion's

points A,B,C(of the extreme triangles ABC of Space ABC) and with points AE, BE, CE(of the extreme triangles AE.BE.CE of Anti-Space) all, on the same circumference of the prior formulation and are rotated with the same angular velocity vector \bar{w} . The inversely directionally rotated Energy $\pm \bar{\Lambda}$ equilibrium into the common circle, so Spaces and Anti-Spaces meet in this circle which is the common Sub-space. Extreme Spaces (the Extreme triangles ABC) meet Anti-Spaces (the Extreme triangles AE.BE.CE), through the only Gateway which is the Plane Geometrical Formulation Mechanism (mould) of the [STPL] line, or as cylinder.[17]

The \rightarrow [Space, Anti- Space equilibrium, $\pm \bar{\Lambda}$, Absolute System [S] \leftarrow], as Angular momentum $\bar{\Lambda} = \Omega = m.vr$, is Crushed out into Fragments and, becoming the three Breakages $[s^2 = (wr)^2]$, $[-s^2 = -(wr)^2]$, $[\nabla i = 2(wr)^2]$, and after clashed with the velocity vector \bar{v} of [S], (unless succeed to escape unclashed through centre O in STPL line and this because $\bar{v} = 0$), are Thrown OFF this System [S], conveyed into the Linear

momentum, the Inertial and Energy-Space, the Relative [STPL] System [R] as Particles

$$\text{Fermions} \rightarrow [\pm \bar{v}.s] \text{ and Bosons} \rightarrow [\bar{v}.\nabla i] .$$

IV. GEOMETRICAL MOULDS

a) STPL → The Navel Cord of Galaxies

It was shown [16] that Projective and Perspective geometry are Extrema in Euclidean

geometry and [STPL] line their boundaries, becoming from common Space and Anti-space. Energy, *Motion*, follows this Euclidean mould, because this Proposition, *Principle*, belongs to geometry`s, and not to Energy`s which is only motion.

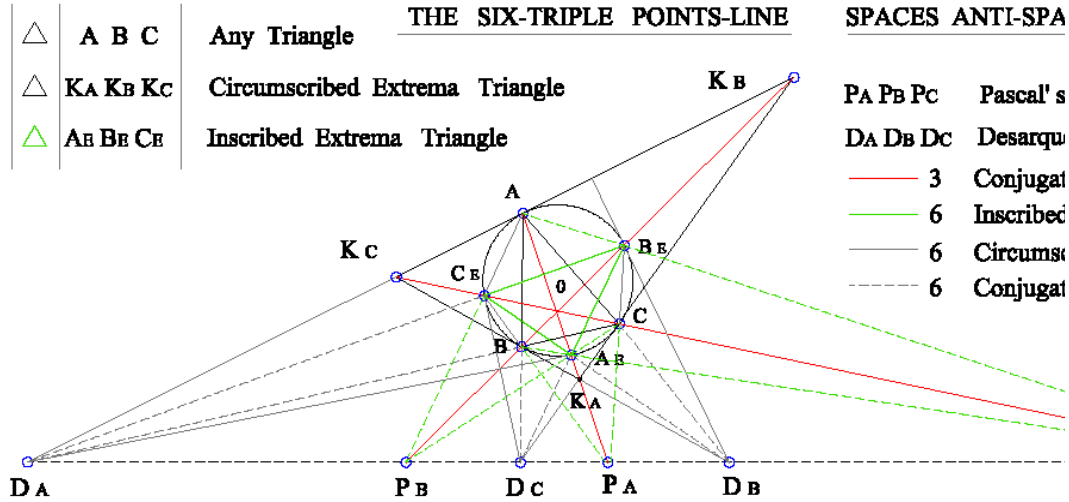


Fig. 3 : DA, DB, DC, ↔ PA, PB, PC = The Six Triple Points Line [STPL]

Un-clashed Fragments through center O, consist the Medium-Field Material-Fragment → [± s²] = [MFMF] as base for all motions, and Gravity as force [∇i], while the clashed with the constant velocity, c̄, consist the Dark matter [± c̄.s] and the Dark energy [c̄.∇i]. or from,

$$\text{Breakages} [\pm s^2 = \pm (wr)^2] - [\nabla i = 2(wr)^2.]$$

$$A.. [\pm \bar{v}.s^2] \rightarrow \text{Fermions} \text{ --- } [\bar{v}.\nabla i] \rightarrow \text{Bosons}$$

$$B.. [\pm s^2] \rightarrow \text{[MFMF] Field} - [\nabla i] \rightarrow \text{Gravity force}$$

$$C.. [\pm \bar{c}.s^2] \rightarrow \text{Dark matter} [\bar{c}.\nabla i] \rightarrow \text{Dark energy}$$

$$\rightarrow A.. [\pm \bar{v}.s^2] \rightarrow \text{Fermions} \text{ --- } [\bar{v}.\nabla i] \rightarrow \text{Bosons}$$

Thrust ($\bar{v} = \bar{w}.r$) continually acting on the Breakages $[s^2, -|\bar{v}|^2, [2\bar{w}].|s|.|r| = 2(\bar{w}.r)^2]$ produces the $[1-1 +2].\bar{w}^3.|\bar{r}|^3$ magnitudes $(w.r)^3$, which is a Positive Scalar magnitude, with Positive or zero electric charge and with, 1/2 or 1, spin. [30] $[2\bar{w}].|s|.|\bar{r}|\nabla i$

1. Positive breakage Quantity $|\bar{v}|^2 = |\bar{w}x\bar{r}|^2 = |\bar{w}.r|^2 \rightarrow$ Being at Space points A,B,C then Action magnitudes Q at coinciding points DA, DB, DC - PA,PB,PC Produces Leptons and Quarks, and carry them on [STPL] line.
2. Negative breakage Quantity $-|\bar{v}|^2 = -|\bar{w}x\bar{r}|^2 = -|\bar{w}.r|^2 \rightarrow$ Being at Space points A,B,C then Action magnitudes Q at coinciding points DA, DB, DC-

PA,PB,PC Produces Anti-Leptons and Anti-Quarks, and carry them on [STPL] line.

3. Positive breakage Quantity $[2\bar{w}].|s|.|\bar{r}|\nabla i = 2w.(sr).\nabla i = 2w.(r^2.w).\nabla i = 2w.r^2w.\nabla i \rightarrow$ Bosons, being at Space points A,B,C then Action magnitudes Q at coinciding points DA, DB, DC - PA,PB,PC Produces Bosons, and carry them on [STPL] line.
4. Breakage Quantities $[\pm s^2 = \pm (wr)^2]$, being at, O, commons` circle center and shackd OFF into [STPL], and this because of $v=0$, formulate the [MFMF] Field, which consist the base of all motions.
5. Breakage Quantities $\nabla i = 2(wr)^2]$ being at, O, commons` circle center and shackd OFF into [STPL], and this because of $v=0$, formulate the Gravity force.
6. Breakage Quantities $[\pm \bar{c}.s^2]$ and $[\bar{c}.\nabla i]$, the clashed with the constant velocity, c̄, formulate in [STPL] cylinder Dark matter and Dark Energy respectively.

b) Cycloid → The Inner motion of monads

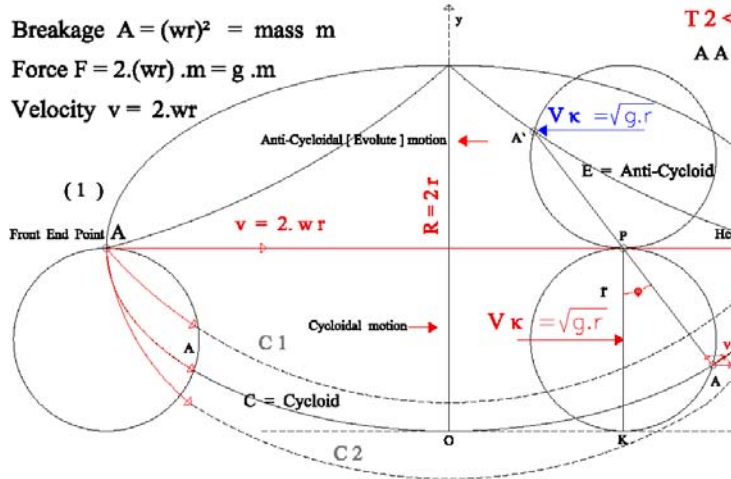


Fig. 4 : The Cycloid motion of material point $A1 \rightarrow A2 = |AA|$, The Brachistochrone Curve $A1 \rightarrow A2$

• Properties

Cycloid is the curve described (traced) by a point on the circumference of a circle of radius, r , as this rolls along a straight line without slipping. In an orthogonal coordinate system (x,y) the equations of motion are $x = r(t-\sin.t)$, $y = r(1-\cos.t)$ where $t =$ time.

The area between the curve and the straight line is $A=3\pi r^2$ and the arc length $l = 8r$. Differential equation of the curve $(dy/dx)^2 = y/(2r-y)$ is also satisfied .

Motion on a cycloid is such that, as long as a particle moves under gravity, g , then the total period of oscillation is $T = 4\pi/g$ which does not depend on speed of rolling, (Huygens cycloid pendulum). The arc length $l=8r$ is completed for faster, as one revolution in less time than the slower one, meaning that, On cycloid all points of y axis reach $x-x$ axis at the same time, regardless of the height from which they begin (isochrones). This property is used for breakages to reach STPL line isochrones. Evolutes also of a cycloid are a cycloid itself, (apart from coordinate shift). Velocity vector of a motion is directed along the tangent and is the sum of the velocity vectors of the constituent motion, thus at each point of a cycloid, the line joining that point, to the point that circle is, then at the top of the generative circle is tangent to the cycloid and the line joining point that is to that of bottom (of circle) is normal to the cycloid. [5]

Evolutes of a cycloid is the balancing cycloid, Anti-cycloid.

For trajectory element $ds^2 = dx^2 + dy^2$ and $ds = \sqrt{2r/y}.dy$ and $s = 2.\sqrt{2ry} + C$ and with a coordinate system $(y=0, s=0)$ then $C= 0$ and $s = \sqrt{2r}.y = 4r.\sin \phi$. (F-4).

Since velocity \bar{v} is tangent to the point then component $\bar{v}.\sin\phi$ is $\sin\phi = s/4r$, and then equation of motion becomes $\rightarrow [ds^2 / dt^2] = - (g/4r).s$ which is a harmonic oscillation with total time period $T = 4\pi\sqrt{r/g}$

which is independent of any amplitude (Displacement, Energy). i.e. On cycloid, all moving points on y axis reach $x-x$ axis at the same time (isochrones motion) regardless of the height from which they begin (they do not depend on the oscillation amplitudes), or if, a particle of mass $m = |(wr)^2|$ tied to a fix point A executes a Simple harmonic motion under the action (Thrust) of the tangential velocity $\bar{v} = \bar{\omega}.r$, and since \rightarrow linear momentum $\bar{p} =$ Breakage \times Velocity $= |\bar{\omega}.r|.2(\bar{\omega}.r)^2 = 2(\bar{\omega}.r)^3 = 2g.m$, then it follows a cycloid's trajectory with a Total time period $T = 4\pi\sqrt{r/g} = R_c.\gamma/c$ which is dependent on angular velocity only and it is the Spin of particle $|AA|$.

• Remarks

Breakage \times Velocity $= m_c.v = (\bar{\omega}.r)^2.(\bar{\omega}.r)$ and force

$$F = [(\bar{\omega}.r)^2.(\bar{\omega}.r)] = 2.(\bar{\omega}.r)^2.(\bar{\omega}.r) = 2m_g$$

This property is used to show that the wavelength of norm $|\bar{v}|$, of vectors, \bar{v} , is a Stationary wave, with the two edges as Energy material nodes, Cycloidally carried on wavelength $|\lambda| = 2|A1-A2|$ twice the norm.

This rolling circle has a constant velocity \bar{v} . $r = \sqrt{rg}$ Period $T = \frac{2\pi r}{\sqrt{gr}} = \frac{2\pi\sqrt{r}}{\sqrt{g}} = 2\pi \frac{\sqrt{R}}{\sqrt{2g}} = \pi.\sqrt{2}.\sqrt{\frac{R}{g}}$ and Area of moving circle $A = \pi.r^2 = \pi.(2r.\cos\phi)^2 = \pi R^2.\cos^2\phi$.

Thrust is the velocity vector $\bar{v} = \bar{\omega}.r$ on the circumference of common circle of the inversely rotating Space, anti-Space becoming from the rotational energy vector $\pm\Lambda$ of PNS. The wave length of norm of velocity $|\bar{v}|$ is the static equilibrium position vector of amplitude, ds , of dipole $|AB| = |\bar{v}| = ds$ and in terms of the static deflection, ds , then $T = 1/f = 2\pi/\omega$ where $ds =$

$$z = \bar{v} = A.e^{i.\omega.t} = \bar{v}. \cos.\omega.t + i.\bar{v}.\sin.\omega.t$$

i.e. Breakages acquire different velocities and different energy, and because are following cycloid trajectories, thus, need the same time (isochrones) to reach [STPL] line. Simultaneity is a property of Absolute system and the intrinsic property of vectors and Poinso'tsellipsoid now becomes a \rightarrow <Cycloidal ellipsoid >, since $onc1(T1) >c> c2(T2)$.

Any material point [Medium-Field Material-Fragment] $\rightarrow[\pm s^2]=|\bar{w}x\bar{r}|^2 \rightarrow$ [MFMF] Field following trajectory, in=(c1), or, out=(c2), Cycloid=(c)=|A1-A2| needs more or less time $T(2)<T= 4\pi v(r/g)<T(1)$ to reach end A2. And since frequency $f = 1/T$ and energy $E = h.f$ then Cycloid motion Controls constancy of Energy by changing velocity, $\bar{v} = \bar{w}.r$, and period, T, of monads.

Breakage quantity $2.(wr)^2$ under the tangential action $\bar{v}=wr$ becomes $2.(wr)^3$ acting on point A $\rightarrow 2wr.m$

$\Delta = OAD_A \gg OA = 1, AD_A = V, OD_A = C$
 $sec.\phi = 1/\sqrt{1-\sin^2\phi} = 1/\sqrt{1-(v/c)^2}$
 Lorentz factor $\gamma = sec.\phi = 1/\sqrt{1-\sin^2\phi} = 1/\sqrt{1-(v/c)^2}$

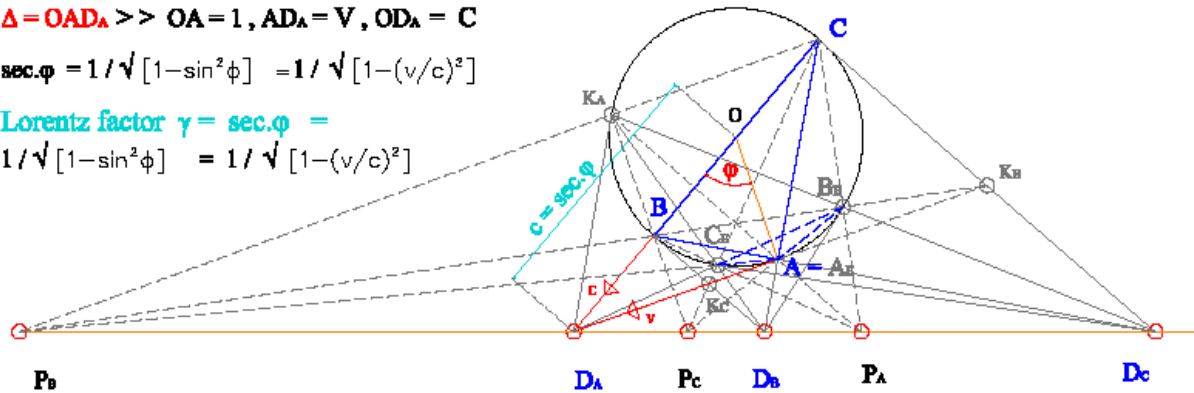


Fig.5 : The Geometrical expression of Lorentz factor , γ , where $sec.\phi = \gamma = ODA:ADA = \pm 1 / [\sqrt{1 - (v/c)^2}]$

Geometry does not need the meter, time, to perform any logic because it is the logic. Motion (quantization of energy) occurs as mould (Tensor) on a geometrical formation, because in motion interferes the meter of time, so material points [real, imaginary] = $[x,y,z -\nabla i = \Lambda = r.mv = r^2mw = r.m.(s/t)]$ acquire different meters of time independently of any system.

Since in, common circle, exist the constant tangential to, r, circle velocities, \bar{v} , and on center O wherer = 0, Coriolis, Centrifugal and Centripetal forces are present, then the corresponding velocities equilibrium and Centrifugal velocity, $\bar{v}=\bar{w}r$, is a constant, \bar{c} , because acceleration $[d\bar{v}/dt=d(\bar{w}r/dt)=0]$ is zero, i.e. constancy exists a Priori in all Inertial Systems and is not needed any other propositions. Breakages $[\pm(w.r)^2, 2(w.r)^2]$ on circumference \rightarrow formulate Particles which are deported in STPL line, while on center O breakages \rightarrow vanish and deported in STPL cylinder are formulating the Rest Medium Field and Gravity force, the Dark matter and Dark energy, as follows,

Consider $O(x,y,z, c = O.DA)$ being an Absolute Cartesian coordinate system with constant velocity, \bar{c} , due to the tangential velocity $\bar{v} = A.DA$ of the same system and $O'(x',y',z', \bar{v}')$ being another one Cartesian

of common circle. The same also for points A,B,C of Space and AE,BE,CE of Anti-Space. Because all velocity vectors AA, BB, CC carry material points A,B,C at points DA, DB, DC in time, t, isochrones, then material points follow a cycloid with period the norm of wavelength of velocities $|AA|, |BB|, |CC|$.

This Simultaneity is succeeded by Lorentz factor where transformations between Inertial frames that preserve the velocity of light will not preserve simultaneously. The Geometrical expression of this transformation (it is the base Mould, of natural Universe) follows.

c) $OD_A = sec\phi \rightarrow$ Lorentz Factor γ

The Absolute's System constancy of velocity, c, and Simultaneity.

coordinate system on [STPL] line and as direction DA, PA. F-5, F-8

Question?? When and how the two systems keep Centrifugal velocity $|O.DA| =$ constant independently of any changes of velocity, \bar{v} , of the system??

A first answer is that the two vectors $|\bar{O}, DA|, |\bar{A}, DA|$ must have the same edge DA with not any set restrictions, or their interior period $T = 4\pi v(r/g)$ to be the same for all equal vectors, which happens to the Cycloid motion on wavelength of norm $|\bar{c}|$ and $|\bar{v}|$ of their stationary wave with common period T. A second is the prior referred, where Centrifugal velocity, $\bar{v} = \bar{w}r$, is always a constant \bar{c} , because acceleration $[d\bar{v}/dt=d(\bar{w}r/dt)=0]$ is zero since \bar{w} is always constant.

Since $r = OA$ may be any cave of rotation, then is considered a unit length ($OA=1$) and circle (O, OA) as unit circle. In triangle $\Delta [O,A,DA]$, $\{OA=1\}$, $\{A,DA = \bar{v}\}$, $\{O,DA = \bar{c}\}$ and $\sin\phi = (\bar{v}/\bar{c})$ and $O,DA = sec.\phi = 1 : (\cos.\phi) = \pm 1 / (\sqrt{1 - \sin^2\phi})$ and issues, $sec.\phi = \pm 1 / [\sqrt{1 - (v/c)^2}] = c / \sqrt{c^2 - v^2}$, i.e. velocity \bar{O}, DA is constant independently of the position [either circle (O,OA) or magnitude \bar{A}, DA and direction] $\rightarrow A.DA$ of velocity $\bar{A}, DA = \bar{v}$ and this mould valid for all points on [STPL] line, cylinder, so $sec.\phi$ is identical to the, γ , Lorentz's

factor or $\rightarrow \sec.\phi = \gamma = \pm 1 / \sqrt{1 - (v/c)^2} = c / \sqrt{c^2 - v^2}$,and represents the Geometrical expression of Lorentz's factor, the master key of all universe, and STPL line - cylinder is the Navel Cord of Galaxies.

• *Remarks*

a. The two velocity vectors \bar{v}, \bar{c} coincide at, DA, point, therefore, the meter of their changes is the same and equal to, t, and $\bar{O}, DA = c, \bar{A}, DA = \bar{v}.t$, i.e. on constant velocity vector \bar{O} , DA point O removes from position O to position DA. The same also for point A which removes from position A to DA. This removal is <Isochrones> because the two velocity vectors coincide at edge DA , which means that points O,A of this System remove to point DA at the same time(isochrones), independently of oscillation amplitude on the cycloid.

Since acceleration, a, for a quaternion $z = (s + \bar{v}.\nabla i)j = a = [d^2z/dt^2] = (d/dt, \bar{w}).(-\bar{w}z, dz/dt + \bar{w}xz) = 0$, and this because $\bar{w} = \text{constant}$, therefore velocity $\bar{v} = \text{constant}$.

When the element $d\bar{s} = \bar{A}, DA = \bar{v}.t = \lambda T = \text{constant} = \bar{c}.T$ then $ds^2 = dx^2 + dy^2 + dz^2 = (cT)^2$ being a spatial equation .

Since quaternion = [Energy]² = - [Space] = Anti-space = $[-(\Delta x \Lambda) / m, \pm \Delta x \nabla i] = [\lambda, \pm \Delta x \nabla i] \rightarrow$ is meaning that the massive mechanism Diffraction and the Energy mechanism Diffraction are Interchangeable.

A Particle with wavelength $\lambda = (1)-(2)$ and spin say, $h/2$, is consisted of two parts, The one because of the translational motion of speed \bar{v} , and the second of the, *common circle*, self-rotation velocity $V_c = \lambda^2/T = \lambda^2.f = \sqrt{1 - (v/c)^2}.f = f.[1 - (v/c)^2]$. Energy $[\Delta x \nabla i] = (J1)$ as velocity vector, \bar{v} , is the cross product of two velocity vectors, $\bar{v}1, \bar{v}2$ or $\rightarrow \bar{v} = \bar{v}1 \times \bar{v}2$, with head at point (1) and analyzed , in a perpendicular to (1)-(2) directional, plane, into the two orthogonal velocity vectors $\bar{v}1, \bar{v}2$ which heads are at point (1). Energy J1 is carried to point (2) by following the cycloid motion in $\lambda = (1)-(2)$ as follows , in F-4.

b. Following the above logic, the vector-quaternion Norm is kept constant by an intrinsic (in wavelength norm) isochrones (harmonic oscillation) because of the cycloid motion, and independently of amplitudes (displacements, or strengths).

i.e. Quaternion $q = [\lambda, \pm \Delta \nabla i]$ with norm, wavelength $|\lambda|$ is a Standing wave (a plane Stationary wave) which preserve the constant position of magnitude $|\lambda|$ with the two edges as nodes independently of amplitude , with a period $T = [\gamma \lambda / 2c]$, $\Lambda = r.m\bar{v} = r\bar{p} = r.m(\bar{v}r)^2 = mr^2.\bar{v}^2$ depending on, \bar{w} , only (it is spin) and thus forming the spherical standing waves . F-5.

V. CONCLUSION

Applying all equations of Mechanics and Physics in Common circle (c) of radius r_c , angular

velocity $\bar{w}c$, then velocity on radius is $\bar{v}c = \bar{w}c.r_c$, and the reaction to this motion which is mass m_c , is, $m_c = v_c.v_c = v_c^2 = (w_c.r_c)^2$. Linear momentum $\bar{p} = m\bar{v}c$ and the resultant rotational energy $\Lambda = r_c.p_c = r_c.m_c.\bar{v}.c$, and then since work on circle is $W = p_c.L = p_c.(2\pi.r_c) = m_c.v_c.2\pi.r_c = \Lambda$, by solving to, r_c , and for constant velocity $v_c = c$ then,

$$r_c = \Lambda / 2\pi.m_c.v_c = \Lambda / 2\pi.m_c \dots (a)$$

Applying equation (a) for the fundamental particles (monads) OFF the common circle, then magnitudes are transformed as,

$$\text{mass}(m) \rightarrow m_c . \gamma = m . [\sqrt{1 - (v/c)^2}] \dots \dots \dots (b)$$

$$\text{radius, } r_c, \text{ of cycloid helix} \rightarrow r_c = \Lambda / 2\pi.\gamma.m_c \dots (c)$$

which is the quantization of \rightarrow Energy as Space and as Energy cavity.

Since, $m = E/c^2 = hf/c^2 = h/T.c^2$ (Einstein's de Broglie's), $\text{Radius } R_c = 2r_c = 2. \Lambda / 2\pi.\gamma.m.c = [h / 2\pi.c\gamma (m = E/c^2 = hf / c^2)] = c / 2\pi.\gamma.f = [c.T / 2\pi.\gamma] = [2c / w.\gamma][2c^3 / w(c^2 - v^2)]$ and

$$(r_c) = c / w.\gamma \dots \dots \dots (d)$$

$$\text{Period } T_c = 4\pi.\sqrt{r_c} / g = \pi.\sqrt{R_c} / g \dots \dots \dots (e)$$

$\text{Length } L_c = \bar{v}r_c.T_c = [\sqrt{g.r_c}].[4\pi.\sqrt{r_c}/g] = 4\pi.(r_c) = 4\pi(c/w.\gamma) = A1 - A2$, is the wavelength $\lambda = L_c \rightarrow$ from which

$$\text{Constant velocity} \rightarrow \bar{c} = w.\gamma.r_c = w.\gamma.(\lambda/4\pi) = \gamma L_c(f_c)/2 \dots (f)$$

Where,

$\Lambda = h = \text{Rotational Energy (Spin)}$,

$\bar{v} = \text{Velocity of particle in Inertia System [R]}$,

$\bar{v}r = \sqrt{g}$. $r_c = \text{The Rolling circle center constant velocity}$,

$\bar{c} = \text{The constant velocity of the System, (of Light)}$,

$R_c = 2.(r_c) = \text{The radius of, Cycloid helix}$,

$g = \text{Gravity's force} \rightarrow 2.(wr)^2$, acceleration,

$T_c = \text{The intrinsic Cycloid period, } \pi.\sqrt{R_c/g}$

$\bar{c} = \gamma.L_c(f_c)/2 = \text{The relation between constancy (c) of Light, Laurence factor is } (\gamma)$, Wavelength ($\lambda = L_c$), and the Cycloid helix rolling circle frequency (f_c) \rightarrow [39].

a) *Material Points and Energy Fields [QUANTA]*

The Quantization of Energy in space is the stationary Electromagnetic wave in monad and quantization of Space ds is the work W in breakages $^2 = \lambda$, The Energy-Space Quanta.

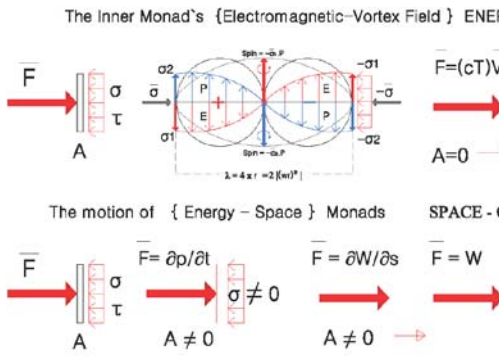


Fig. 6 : The Quantization of Work as Force ,(Energy) = [E , P]and as Space (Wavelength) = [λ] .

From work equation $W = [\lambda, \pm \Delta \nabla i]$ where, λ = the Wavelength of quaternion=monad and $\pm \Delta \nabla i = \Delta = p = M \cdot \bar{c} = [\lambda | \Delta |] \cdot \bar{c} = (\lambda m) \cdot \bar{c} = (\lambda m) \cdot \bar{w} \cdot r = \bar{w} \cdot [\lambda(m \cdot r)] = \bar{w} \cdot [\lambda(\bar{v})] = \bar{w} \cdot [(cT) \cdot \bar{v}] =$ the Energy, \bar{w} , is the angular velocity or the spin, \bar{c} is the constant velocity equal to that of light, \bar{v} is the velocity of monad, T is the period in wavelength's monad.

Quantization of Energy confined in a monad say (\bar{v}) , (it is the inner structure of monad) is the Stationary wave of the Real part $|\lambda|$ of \bar{v} , due to the Electric Displacement field $(|\bar{v}| = \epsilon \cdot E + P)$, alternately in terms of The Electric field $E = \partial P / \partial t$ and The Magnetic field $P = \partial E / \partial t$, ϵ is the Permittivity as a measure of how much the wavelength opposes E-field.

Object in mechanics, is the Quantized Material point(1) at Euclidean point (1), which is now Breakage $\pm [(\bar{w} \cdot r)^2]$ magnitude, in the Rest, Homogenously, Quantized mass-less Field $\{\pm [(\bar{w} \cdot r)^2]\}$ and consists the required coordinate System and the base for all motions and forces. This rest Space system (the Base) is [MFMF] Field with the less space distance $ds = |\bar{w} \cdot \bar{r}|^2$ extended beyond Planck's length, the Space Quanta.

Object in mechanics may be also the Quantized Energy as wavelength $\lambda = (1)-(2)$ in [Medium-Field Material Fragment $\rightarrow [\pm s^2] = |\bar{w} \cdot \bar{r}|^2 =$ [MFMF] Field \leftarrow] which is a standing wave in cavity (1)-(2) with scalar breakage $\{ | +(\bar{w} \cdot r)^2 | \leftrightarrow | -(\bar{w} \cdot r)^2 | \}$ as medium (1)-(2) field, and $(J1 = \bar{v})$ the Energy as velocity at point (1) and carried to point (2) by following the isochrones cycloid motion from point (1) to (2). Velocity, \bar{v} , during shifting, and because $A=0$, is analyzed into two transverse velocity vectors $\bar{v}1, \bar{v}2$, which undergo vibrations and cause two waves which are the two Quantized Electric and Magnetic isochrones components because follow cycloid trajectories. The Energy Quanta, in Space Quanta.

General Relativity is dependent on one axiom, that of Galilean Relativity and on doubtful non-Euclidean geometries without any physical meaning and reality, and this because these are extreme of the Euclidean [38]. Now, the immense confusion in basic ideas

regarding Quantized Energy-Space, The Energy and Space Quanta, vanishes.

Question, When maximum velocity occurs in Common circle???. From Fig-5 maximum velocity occurs when the two velocities \bar{c}, \bar{v} are perpendicular between them, where then dispersion follows Pythagoras theorem and the consultant Quantized Space, r, becomes $r = \sqrt{v^2 + c^2}$.

The total Rotating energy is $\rightarrow \pm \bar{\Lambda} = \bar{p} \cdot r = (M \cdot c) \cdot r = (M \cdot c) \cdot \sqrt{v^2 + c^2}$ and $[\pm \bar{\Lambda}]^2 = p^2 \cdot r^2 = M^2 \cdot c^2 \cdot (v^2 + c^2) = (M^2 \cdot v^2) \cdot c^2 + M^2 \cdot c^4 = (p^2 \cdot c^2) + M^2 \cdot c^4 = [p \cdot c]^2 + [m_0 \cdot c^2]^2$, which is the known relativistic energy-momentum equation of Lorentz transformations equation.

VI. BEYOND GRAVITY FORCES

a) Gravity's Medium Field-Gravity-Force

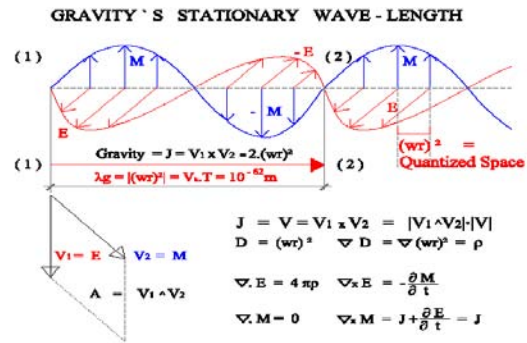


Fig 7 : $[\pm s^2] \rightarrow$ [MFMF]Field , $[\nabla i] \rightarrow$ Gravity force . Gravity Transport mechanism in cave $\lambda = 10^{-62}m$ and through breakage $\lambda_g = (1)-(2) = [\pm s^2 = \pm |(\bar{w} \cdot r)^2]$ as the Medium Field of Material Fragment, [MFMF] $\rightarrow (1)-(2), \bar{w}$,

Properties

Since, Distance = Velocity. Time, then $\lambda = v \cdot T$

The un-clashed through center, O, Fragments $s^2 = \pm |(\bar{w} \cdot r)^2|$ occupy the minimum quantized space $|s^2|$ and fill all [STPL] cylinder and thus consist the Rest, Homogenous, Isotropic Base of all motions. On this Base moves force $[2 \cdot |(\bar{w} \cdot r)^2 | \nabla i]$, the rotational Gravity Momentum force and all other clashed or un-clashed fragments of the cylinder consisting the Relative System [R] to Absolute, Space, Anti-Space, $\pm \bar{\Lambda}$, System [S].

Time T interfere with the calculations in reference frame only and does not into the motionless frame.[26]

Since work in [PNS] is $W = [\int_A^B P \cdot ds] = 0$ and is stored on points A,B as quaternion $z_0 = [\lambda, \Delta \nabla i]$ then forces (the spin $\bar{\Lambda}$) are conservative and because work from conservative forces between points is independent

of the taken path and on a closed loop is zero, $\text{curl} = 0$ and Force becomes from the Potential function gradient, and also from the equilibrium of Spaces Anti-spaces, where then Spin rotations, $\bar{\Lambda}$ - $\bar{\Lambda}$, are in inverted order of rotation and vice-versa, and then even function $f(\Lambda) = f(-\Lambda)$, odd function is $-f(\Lambda) = f(-\Lambda)$ and their sum $f(\Lambda) + f(-\Lambda) = 0$, i.e.

Mapping (graph) of Even function $f(A)$, is always symmetrical about A axis (i.e. a mirror) and of Odd symmetrical about the origin and this is the interpretation of the Wave Nature of Spaces, [PNS].

Differential operator of even order quaternion plus differential operator of odd order quaternion is zero:

It is the Mapping (graph) of Even function $f(\Lambda)$ and of Odd $f(-\Lambda)$ and is the interpretation of the Wave nature of Spaces and all the others (i.e. The Physical Universe behaves as a simple harmonic oscillator). Because functions $f(\Lambda)$, $f(-\Lambda)$ are Stationary and only their sum creates their conjugation operation through mould \bar{z}_0 , so their sum is zero and independently of time (negation truth)as, even function

$$f(\Lambda) \rightarrow (\partial/\partial t, \nabla) \odot (\lambda = s^2, \Lambda \nabla) = -\nabla, x\Lambda = \text{eo odd function } f(-\Lambda) \rightarrow (\partial/\partial t, \nabla) \odot (\lambda = s^2, -\Lambda \nabla) = \nabla \Lambda, -\nabla x \Lambda = \text{eo even} + \text{odd} = 0 \rightarrow (-\nabla \Lambda, \nabla x \Lambda) + (\nabla \Lambda, -\nabla x \Lambda) = [0, 0 + 0] = 0$$

$$\text{even-odd} = 0 \rightarrow (-\nabla \Lambda, \nabla x \Lambda) - (\nabla \Lambda, -\nabla x \Lambda) = 2.[-\Lambda \nabla, \nabla x \Lambda] \text{ i.e. is doubled.}$$

In Calculus when a function is recognized in terms of the Even and Odd functions then $x(\tau) = E(\tau) + O(\tau)$. Because an even function $E(\tau)$ is symmetric about the origin then $E(\tau) = E(-\tau)$, i.e. $\cos. wt = \cos(-wt)$ and because an Odd function satisfies the relationship $O(\tau) = -O(-\tau)$ then $\sin. wt = -\sin(-wt)$ and then $\int_{-\tau/2}^{\tau/2} E(\tau). \sin. wt. dt = 0$ and $\int_{-\tau/2}^{\tau/2} O(\tau). \cos. wt. dt = 0$

Quaternion of the Primary Space dipole is $\bar{z}_0 = [s, \bar{v}n, \nabla i] = [\lambda, \Lambda \nabla i]$ and it is the only one Physical existing truth monad ($\bar{z}_0 = 1$) and (eo = 0) the only Physical non-existing equilibrium monad, This negation truth = the equilibrium of the two equal and opposite momentum $p = \pm \bar{\Lambda}$, on points and by using the additive form of Binary quaternion then

$$[\nabla \lambda, 0] + [0, -\nabla x \bar{\Lambda}] = [\nabla \lambda, -\nabla x \bar{\Lambda}] = 0 \text{ i.e.}$$

non-existence (0) becomes existence with [PNS] motionless dynamic mould ($\bar{z}_0 = 1$), and it is Done everywhere, following Boolean logic operations with all combinational rules and laws, as follows,

$$\rightarrow \text{Element } [\bar{z}_0 = 1], \text{Element } [eo = 0] \leftarrow$$

$$\text{Conjunction } [z \times \bar{z}_0 \rightarrow 0] - \text{Conjugation } [\bar{z}_0 \odot 0] -$$

Quaternion $[\bar{z}_0 \equiv eo] \rightarrow 0, z_0, 0, z_0 - 0, 0, z_0, z_0 - z_0, 0, z_0, z_0 - 0, z_0, z_0, 0 - z_0, 0, 0, z_0$, so Quaternion's $\leftrightarrow \bar{z}_0 = [\lambda, \pm \Lambda \nabla i]$, $\bar{z}_0' = [\lambda^2 - |\bar{\Lambda}|^2]$, $eo = [\Lambda \nabla, -\nabla x \bar{\Lambda}]$. All above are the three fundamental equations of [PNS], unifying the known homogenous Euclidean geometry ($\lambda = \lambda \nabla$) and the source term Energy ($d\bar{s}.dP = \lambda. \Lambda =$

constant $K_{1,2,3}$ with motion Λ), and imbedding in them all conservation physical laws with the only two quantized magnitudes λ , $\bar{\Lambda}$ on Monad $\bar{A}\bar{B}$ which are λ = the length of geometry primary dipole (wavelength of dipole AB) which is a scalar magnitude, $\bar{\Lambda}$ = the spin of dipole, source term, the amount of rotation on dipole $\bar{A}\bar{B}$, equal to angular momentum vector $\bar{p} = \bar{\Lambda} = \bar{w}$. $\lambda = m.v = d/ds \{ \int_A^B P. ds \}$, and

Time = The conversion factor, t, equal to Zero.

The mechanism of Energy Transport as (\bar{v}) through its quantized wavelength $|\lambda = \bar{v}.T|$, is a property of any standing wave, into the Medium $|\lambda| = (1)-(2)$, and involves the Absorption and Reemission of the wave quantized energy $J = (J_1) = (J_2)$ by the two neighbor edges (1) and (2) of the medium. The Absorption of energy causes, J_1 , within edge (1) to undergo vibrations as $[ds^2/dt^2] = -(g/4r)$. s which causes a new wave with the same frequency (because $f = E/h$) as the first wave but delaying the motion through the medium until Reemission by travelling, J_1 to J_2 , through this small region of space between edges (1) and (2) and once the energy of wave is reemitted by its neighbor edge (2) then mechanism is recycled. This mechanism is succeeded by the intrinsic property of the waves (\rightarrow quaternion's, monads, vectors, Tensors) which is, the Stationary wave nature of Spaces, and works as follows, \rightarrow It was shown in [27] that on dipole $AB = [\lambda m, \Lambda]$ under the influence of Space Anti-Space force $sd P = PB-PA$ are created from forces $dP//$ Space lines the Static Force Field, E, from forces $dP \perp$ Space lines the Static Force Field, P, where $P \perp E$, which then experience on any moving dipole AB with velocity \bar{v} , a total force $F = F E + F P = (\lambda m). E + (\lambda m). \bar{v} \times P$ which combination of the two types result in a helical motion, with stability demand $\rightarrow E = -(\bar{v} \times P) = -(\bar{v}.P) \perp$ which is the alternative conservation of momentum $\Lambda^2/2\lambda m$, in the two perpendicular fields E, P.

In case $(\lambda m) = q$ then total force

$$F = F E + F P = q.E + q. \bar{v} \times P = q.[E + \bar{v} \times P] \rightarrow$$

which is Lorentz force in the Electro magnetic crossed fields E and P with electric charge $q = \lambda m$ and are the two beyond Gravity Fields, interpreting the fundamental cause (effect) of motion, in small and large scales.

Gravity Force F_g , Gravity field G_f :

Equilibrium of Space Anti-space forces creates energy as velocity vector \bar{v} which is decomposed in two cross product velocity vector fields (Electric and Magnetic) into which breakage $2(\bar{w}.r)^2$ as charge q , causes the Lorentz force in this small scale [27].

The standing waves in cavity (1) - (2) with the scalar breakage $|\pm(\bar{w}.r)^2|$ as medium (1)-(2) = $|\pm(\bar{w}.r)^2|$ Field, and Energy $[\Lambda x \nabla i] = (J_1) = 2.(\bar{w}.r)^2$ as velocity \bar{v} only at point (1), [and this because Work as Force in extreme case where zero area ($A=0$) becomes velocity \bar{v}], need the same time (different velocities and

different energy on (1) are isochrones and this because are following cycloid trajectories in medium (1)-(2) to reach edge (2). Energy (J1) as velocity vector, \bar{v} , is the cross product of two velocity vectors \bar{v}_1, \bar{v}_2 or $\bar{v} = \bar{v}_1 \times \bar{v}_2$, with head at point (1) and analyzed, in a perpendicular to (1)-(2) directional, plane, into the two orthogonal velocity vectors \bar{v}_1, \bar{v}_2 which heads are at point (1). Energy J1 is carried to point (2) by following the cycloid motion (1)-(2).

During contracting (shifting), velocity vectors \bar{v}_1, \bar{v}_2 , being vectors, undergo vibrations (expand as oscillation) which causes two waves that represent the two Electric and Magnetic perpendicular components (The combination of vibration (O) and oscillation (\rightarrow) is what determines the frequency rate, the cyclic pattern of scalar waves) until reaching point (2) which is the Reemission of the wave and it is the new head of velocity, \bar{v} , where then mechanism is recycled. These scalar waves are standing waves that flash on and off. Since wavelength, λ , as distance (1)-(2) is equal to product velocity (v).period (T) then $\lambda = \bar{v} T$.

Medium in cavity $\lambda = (1)-(2)$, is breakage $|\pm(\bar{w}.r)^2|$ and Energy (J1) is momentum as velocity vector $\bar{v} = 2(\bar{w}.r)^2$, so this velocity vector fits to the scalar magnitude $[|(\bar{w}.r)^2| = (1)-(2)]$ which is the force in all Inertial systems and is called GRAVITY or Momentum GM. Because any particle of mass, $m = 2(wr)^2$ tied to a fix point (1) executes a Simple harmonic motion in Medium (1)-(2) which is breakage $|\pm(\bar{w}.r)^2|$, then $GM = 2(\bar{w}.r)^2$, is a Force also and it is the intrinsic Stationary velocity vector, which is binding points of this Homogenous- Isotropic, Rest and mass-less nature Field $\pm(\bar{w}.r)^2$.

What is then Gravity Force F_g and what is Gravity field G_f ? Since Gravity, momentum, is $\rightarrow 2(\bar{w}.r)^2$ and medium $|\pm(\bar{w}.r)^2|$, then is consisted of very penetrating material in the same material where dipole breakage $\pm(\bar{w}.r)^2$ formulate infinite dipole that rotate and thus configuration becomes attractive and, is the why Gravity is always attractive.

Since Gravity Force is equally scattered in all universe and as a Rest force is affective, attractive to massive Energy, (matter \rightarrow Dark matter, Dark energy, the fundamental particles Fermions and Bosons etc.) as Gravitational Force is differing from, Electromagnetic Force, which is one of the interaction of other forces of the [STPL] cylinder, so Gravity Force is as \rightarrow The Effective process of Gravity Force $F_g \rightarrow$ Breakage $|[s^2 = \pm(\bar{w}.r)^2|$ represents the Infinite Space, Anti - Space and is spread in all dimensions as the Rest and simple harmonic Oscillating Dipole $\rightarrow (1)-(2) = \{|[s^2]| \leftrightarrow 2[s^2] \leftrightarrow |[-s^2]| \}$ where, $[\pm s^2] \rightarrow$ is the Field-Length of Medium, and $2[s^2] \leftrightarrow$ is the Gravity as momentum $(m\bar{v}.g)m = 1 \rightarrow$ and this because exists zero resistance to motion and happens,

a. Momentum as velocity $\bar{v}.g =$ the breakage $2(\bar{w}.r)^2$, is the cross product of two velocity vectors $\bar{v}_1 \perp \bar{v}_2$

and is forming the two Fields on Medium $|(\bar{w}.r)^2|$, which is a Stationary Wave in medium $s^2 = |(\bar{w}.r)^2|$.

b. Velocity, $\bar{v}.g$, is binding the Medium, the breakage $|(\bar{w}.r)^2|$, through the Electric (E) and Magnetic (P) curled fields, following the cycloid motion.

c. Breakages and Particles with velocity, \bar{v} , being the units of matter with Electric charge, $q = \lambda m$, as their physical property is, when placed in prior referred Electromagnetic Field $E \perp P$ experience a force as Lorentz's Force and this is called Gravity equal to \rightarrow Gravity - Force $F_g = q.[E + \bar{v} \times P] \leftarrow$ and the Homogeneous Gravity - Field $G_f = [E + \bar{v} \times P] \leftarrow$

b) Dark matter - Dark Energy

C.. $[\pm \bar{c}.s^2] \rightarrow$ Dark matter and $[\bar{c}.\nabla i] \rightarrow$ Dark energy

Thrust ($\bar{v} = \bar{w}.r$) on circumference of, common circle, is continually acting on the three Breakages $+ [(\bar{w}.r)^2]$, $- [(\bar{w}.r)^2]$, $2[(\bar{w}.r)^2]$, producing the fundamental particles Leptons and Bosons with $\frac{1}{2}$ and 1 spin.

It has been referred that in case Thrust ($\bar{v} = \bar{w}.r$) is not acting on the Breakages, (it is the case where $r=0$ where then Thrust $= \bar{v} = \bar{w}.r = 0$) the un-clashed through center, O, Fragments $s^2 \pm |(\bar{w}.r)^2|$ which occupy the minimum quantized space $|s^2|$ are deported and fill all [STPL] cylinder which is the Base of all motions.

Constant velocity \bar{c} is acting in [R] system only, off the common circle and when acting on Breakages $\pm [(\bar{w}.r)^2]$ produce Dark matter $\pm \bar{c}.[(\bar{w}.r)^2]$ being the opposite in Relative [R] system and this because of equilibrium of masses, and when acting on Breakages $2[(\bar{w}.r)^2]$ produce Dark energy $2\bar{c}[(\bar{w}.r)^2]$ which is an active force in all Relative parallel frames which are the Inertial frames. Because it is of the same homogenous material, is interacting with gravity only and since is of negative pressure is acting repulsively.

On the same Base, $([(\bar{w}.r)^2] \rightarrow$ moves force $[|(\bar{w}.r)^2| \nabla i] = 2[(\bar{w}.r)^2]$ as Intrinsic Stationary wave in $2|(\bar{w}.r)^2|$ cavity, and it is the Gravity and all other clashed or un-clashed fragments of the cylinder, consisting the Relative System [R] to the Absolute, Space, Anti-Space, $\pm \bar{\Lambda}$, System [S].

In case that Thrust, \bar{c} , is not acting on the Breakages they are then resting in STPL cylinder and continually existing as Gravity Field $\pm [(\bar{w}.r)^2]$ and force called Gravity $2.[(\bar{w}.r)^2]$.

Because power of $(\bar{w}.r)^2$ is 2 so is a homogenous form of repulsively acting energy, not very dense, in STPL cylinder which permeates all of space interacting with gravity only and following acceleration of universe. Because of the velocities retardations (birefringence of STPL) red shifts must be observed at distance. Dark matter $\bar{c}.[\pm(\bar{w}.r)^2]$ having energy density properties defects in STPL cylinder.

c) *Relative Motion*

Because properties in and on [STPL] line are relative to the only one equilibrium and Absolute system $\pm \Lambda = r.m\bar{v} = r.m.\bar{w}.r = mr^2.\bar{w}$, so exists that

what is called Relativity. As Absolute System let it be [S] $\equiv \{DA-O\}$ and as the Relative (Reference, Affine) System, [R] $\equiv \{DA-PA\}$. Fig-8 Relative motion of [S] $\equiv \{DA-O\}$, [R] $\equiv \{DA-PA\}$ Systems

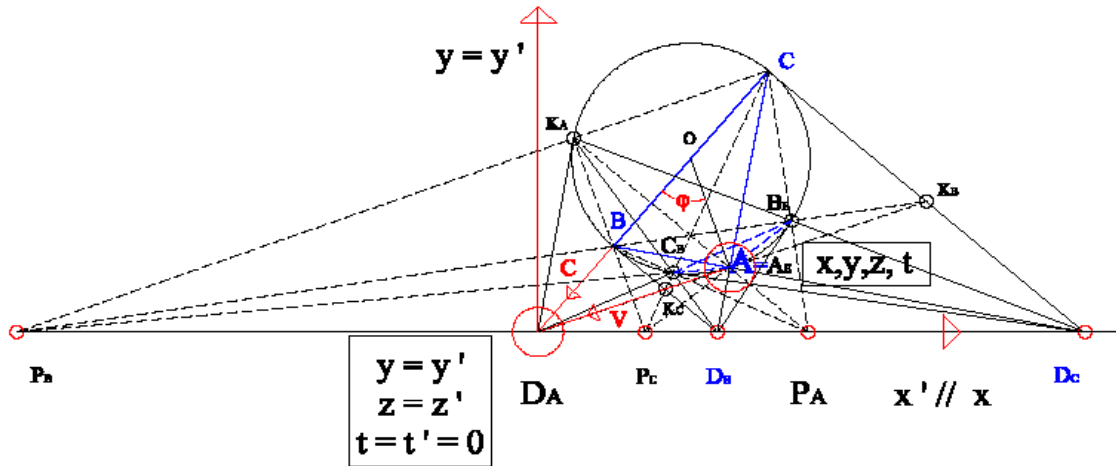


Fig.8 : Reference System $\{DA-PA\} \equiv [R](x',y',z',t)$ moves with velocity \bar{v} , parallel to, $x-x'$, axis with respect to the fixed and Absolute System $\{DA-O\} \equiv [S](x,y,z,t)$.

It was shown (4-2), that in $\{DA-O\}$, (x,y,z,t) , System \bar{c}, \bar{v} , vectors are isochrones i.e. period $T = L/V = 2\pi R/V = 2\pi/[c/r_c] = 2\pi/[v/r_v] \rightarrow c/r_c = v/r_v \rightarrow c.r_v = v.r_c$, where r_v, r_c are the radius of their intrinsic rolling circles. This relation is geometrically expressed as $\text{assec.} \phi = O.DA : A.DA = \gamma = \pm 1/\sqrt{1-(v/c)^2} = c/\sqrt{c^2 - v^2}$ and it is a Cycloid property equal to Lorentz's γ , factor.

Newton's laws are true into Reference System $\{DA-PA\}$

Considering $\{DA-O\}, (x, y, z, t)$, as the fixed frame [S] of the coordinate system in the Gravity cave ($d=2r$) and point A(x, y, z) is fixed on circle (O,OA) and is rotating with a velocity $\bar{v} = \bar{w}r$ and of angular velocity $\bar{w} = 2\pi/T$ where period of rotation, T, is constant also.

Since acceleration for a quaternion $z = (s + \bar{v}.\nabla i)$ is $a = [d^2z/dt^2] = (ds/dt.\bar{v}.\nabla i) + s.d(\bar{v}.\nabla i)/dt = 0 + s.d(wr)/dt = 0 + 0$, and this because $\bar{w} = \text{constant}$ for both, therefore, velocity $\bar{v} = \text{constant}$, i.e. \rightarrow Centrifugal velocity of Absolute system [S] is any constant, \bar{c} , and thus is not needed to accept apriori this constancy of velocity $\bar{c} = 0 \rightarrow \bar{v} \rightarrow \infty$ on circle (O,OA) to exist in frame, so automatically is defined the conversion factor $t = \text{time}$, between the conventional time units (second) and length units (meter = A.DA) or as $\bar{c}.r_v = \bar{v}.r_c \rightarrow \bar{c}(v)(T/2\pi) = \bar{v}(c)(T/2\pi) \rightarrow \bar{c}(v)/w = \bar{v}(c)/w$ which is happening with the same, w, without any restrictions.

This is why conversion factor, $t = \text{time}$, has not any essence in all universe but this aim only.

Because [STPL] line of the fixed frame is becoming from this system [S], then this relative frame [R] is common to the fixed one (common DA) and let it be $[R](x', y', z', t')$.

From figure F-8, $\sin \phi = (\bar{v}/\bar{c})$ meaning that the Relative system, [R] (x', y', z', t') , (Affine Frame) is the

projection of Absolute Frame [S] $\equiv \{DA-O\}-(x, y, z, t)$ where exists as Simultaneity for all motions, i.e. $[R] \equiv \{DA-A\} \equiv [(x', y', z', t')] = [S] \equiv \{DA-O\} \equiv (x, y, z, t) . \gamma$

Considering point DA as the common center and [STPL] as the $x-x'$ axis of the two systems, then becomes $DA(x, y=y', z=z', t)$ and for all linear systems $DA(x', y' = y, z' = z, t')$ respectively.

This specific state of constancy, i.e., the Centrifugal velocity of Absolute system [S] to be a constant, \bar{c} , and the rectilinear motion with respect to one another, defines the natural Inertial frames, uniformity of Space and motion and the same meter of their changes (Time).

Since points O, A remove to point DA isochrones by their intrinsic property motion, which is \rightarrow wavelengths are a Stationary wave \leftarrow , following Lorentz's factor, γ , then this following, happens also to all frames which make this motion, and so issues $\{DA-O\} = \gamma.\{DA-A\} \dots (F-8)$.

On this system DA $(x', y'=y, z'=z, t')$ are conveyed, the Breakages $[\pm(wr)^2, 2(wr)^2]$ of (O,OA) circle after the colliding with the rotating velocity $\bar{v} = \bar{w}.r$ of [S] system, and are the fundamental particles, Fermions and Bosons, or by escaping consisting the Rest Field and Gravity, or Dark matter and Dark Energy, as analytically is shown.

Remarks

- Material point A $\equiv \pm |(\bar{w}.r)^2|$ of the Fixed System $\{DA-O\}$ travels with velocity \bar{v} at point DA, so geometrical distance A.DA in the Relative System $[R] \equiv \{DA-PA\}$ is $A.DA = x' + \bar{v}t'$, and because of the isochrones motion in the Fixed System $[S] \equiv \{DA-O\}$ it is

$$x = (x' + \bar{v}.t').\gamma \text{ or } x = (x' + \bar{v}.t')\gamma = [x' + \bar{v}.t'] : [\sqrt{1-(v/c)^2}] \dots \quad (7a)$$

Inversely, using (7a) where $[S] \equiv \{DA-A\} \equiv \{DA-O\}$ / γ , then if Material point A of the Fixed System $\{DA-O\}$ travels with velocity \bar{v} at point DA, the geometrical distance A.DA in the Fixed System $[S] \equiv \{DA-O\}$ is $\rightarrow A.DA = x - \bar{v}.t$ and in the Relative System $[R] \equiv \{DA-PA\}$ it is

$$x' = (x - vt).\gamma = [x - vt] : [\sqrt{1-(v/c)^2}] \dots \quad (7b)$$

b. Conversion factor t = time, between the conventional time units (second) and length units (meter) and because of the isochrones motion of vectors $\bar{c} = O$,

$$c = x/t = x'/t', \text{ and time } t = x/c, t' = x'/c$$

$$\text{ort} = (x' + vt') / c.(\sqrt{1-(v/c)^2}) = (x'/c) + (v/c).t' : N$$

$$= [(t' + (v/c^2).x') : N = [t' + (v/c^2)x'] : [\sqrt{1-(v/c)^2}] \dots \quad (7c)$$

From relation $t' = x'/c = (x-vt).\gamma/c = [t - (v/c^2)x] : N = [t - (v/c^2).x] : [\sqrt{1-(v/c)^2}] \dots \quad (7d)$

i.e. equations,

$$x = (x' + v.t').\gamma = [x' + v.t'] : [\sqrt{1-(v/c)^2}] \dots \quad (7a)$$

$$t = (x' + vt').\gamma/c = [t' + (v/c^2).x'] : [\sqrt{1-(v/c)^2}] \dots \quad (7c)$$

$$y = y', z = z'$$

$$x' = (x - vt).\gamma = [x - vt] : [\sqrt{1-(v/c)^2}] \dots \quad (7b)$$

$$t' = (x - vt).\gamma/c = [t - (v/c^2).x] : [\sqrt{1-(v/c)^2}] \dots \quad (7d)$$

$$y' = y, z' = z$$

which are the known equations of Relativity.

c. For constant velocity $c = \infty$ equations become

$$x = x' + v.t', y = y', z = z', t = t',$$

and inversely

$$x' = x - v.t, y' = y, z' = z, t' = t.$$

issuing in [PNS] Spaces.

Breakages $[(wr)^2, -|wr|^2, 2(\bar{w}.r)^2]$, being masses off the system [S], under the Action of the constant velocity \bar{c} , which is not changed, are multiplied by Lorentz factor, γ , where then the new masses are,

$$m' = m.\gamma = 2(wr)^2\gamma = 2(wr)^2/[\sqrt{1-(v/c)^2}] = 2m/[\sqrt{1-(v/c)^2}]$$

The embedded energy to Breakages, masses, is as

$$E = mv^2/2 = \{2m/[\sqrt{1-(v/c)^2}]\}.c^2/2 = mc^2/[\sqrt{1-(v/c)^2}]$$

which is the known formula of Einstein in GR.

• For $t = 0$ then $\sin\phi = vt/c = 0$ independently of velocities, v, c , where $\sec.\phi = \pm 1 / [\sqrt{1 - 0^2}] = \pm 1$ and since $\sin\phi = vt/c = 0$ and when $c = \infty$ also, then Systems

$$[S] \rightarrow x = x' + v.t', y = y', z = z', t = t',$$

$$[R] \rightarrow x' = x - v.t, y' = y, z' = z, t' = t$$

$$m' = m.\gamma = 2m/[\sqrt{1-(v/c)^2}] \text{ and } E = mc^2/[\sqrt{1-(v/c)^2}]$$

DA and $\bar{v} = A, DA$, then vectors $O, \bar{DA} = \bar{c}.t$ and $A, \bar{DA} = v.t'$ reach point DA simultaneously. This Geometrically means that conversion factor t , on \bar{c} , is projected on \bar{v} , and so,

$$t - t.\sin\phi = t - t(v/c) = (1-v/c).t = (c - v).t / c.$$

From above Question, and because $\bar{w} =$ constant where then Centrifugal velocity $\bar{v} = \bar{c}$ is also constant and such that velocity, \bar{c} , is kept the same in two reference frames, valid \rightarrow

i.e. [PNS] Space is such that, velocities, \bar{v}, \bar{c} , exist independently of the Zero conversion factor, t , and of the constant velocity being $c = \infty$, and mass $M = 2m$, that of Space and the equilibrium Anti-Space, and infinite energy $E = mc^2 = \infty$ equilibrium from opposite energy of Anti-Space.

• For $t = c/v$ or, $v = c$, then $\sin\phi = vc/vc = 1$ and $\sec.\phi = \pm 1 / [\sqrt{1 - 1^2}] = \pm \infty$, and the Systems \rightarrow

$$[S] \rightarrow x = x' + v.t', y = y', z = z', t = t',$$

$$[R] \rightarrow x' = x - v.t, y' = y, z' = z, t' = t$$

$m' = m\gamma = \infty$ and $E = \infty$, independently of velocities v, c but from their relation only, i.e. it is a NEW Space where velocities, v, c , dependent on their relation only and conversion factor, t , also.

• For $t = 1$ then $\sin\phi = vt/c = v/c$ and $\sec.\phi = \pm 1 / [\sqrt{1 - (v/c)^2}] = \pm 1$ and the Systems \rightarrow

$$[S] \rightarrow x = [x' + v.t'] / [\sqrt{1-(v/c)^2}], y = y', z = z', t = t',$$

$$[R] \rightarrow x' = [x - vt] / [\sqrt{1-(v/c)^2}], y' = y, z' = z, t' = t$$

$$m' = m.\gamma = 2m/[\sqrt{1-(v/c)^2}] \text{ and } E = mc^2/[\sqrt{1-(v/c)^2}]$$

i.e. it is a Space where velocities, \bar{v}, \bar{c} , exist and dependent on the conversion factor, t , and the constant velocity \bar{c} mass $m' = 2m/[\sqrt{1-(v/c)^2}]$ and energy $E = mc^2/[\sqrt{1-(v/c)^2}]$.

• For $t = \text{any}, t$, then $\sin\phi = vt/c$ and $\sec.\phi = \pm 1 / [\sqrt{1 - (vt/c)^2}]$ and the Systems are \rightarrow

$$[S] \rightarrow x = [x' + v.t'] / [\sqrt{1-(vt/c)^2}], y = y', z = z', t = t',$$

$$[R] \rightarrow x' = [x - vt] / [\sqrt{1-(vt/c)^2}], y' = y, z' = z, t' = t$$

$$m' = m.\gamma = 2m/[\sqrt{1-(vt/c)^2}] \text{ and } E = mc^2/[\sqrt{1-(vt/c)^2}]$$

i.e. it is a Space where velocities \bar{v}, \bar{c} , exist and dependent on the conversion factor, t , and the constant velocity, \bar{c} , and mass $m' = 2m/[\sqrt{1-(v/c)^2}]$ and energy $E = mc^2/[\sqrt{1-(v/c)^2}]$. Momentum $\bar{p} = m\bar{v} = \bar{h}$ and Energy

$E = mc^2 = h.f$ possess the double helix structures (the screw motion).

General Relativity as referred is dependent on one axiom, that of Galilean Relativity and also on dispute non-Euclidean geometries without any physical meaning and reality.

Gravity force is exerted on breakages $[\pm(\bar{w}.r)^2 = \text{Material points} = \text{Dipole of the two } \pm\text{quantized energy-spaces } (\bar{w}.r)^2]$ as velocity vector, \bar{c} , which is then decomposed into two reverse velocities following the cycloidal motion, and consisting the intrinsic Stationary Electro-magnetic Wave of gravity, and which is binding points of this Homogenous- Isotropic, Rest and mass-less nature Field. The total dispersion Rotating energy of dipoles is $[\pm\bar{\Lambda}]^2 = [p.c]^2 + [m_0.c^2]^2$, which is the known relativistic energy- momentum equation of Lorentz transformation equations.

VII. PHOTO ELASTICITY

In Photo elasticity, the speed of light (vector \bar{v}) through a Homogenous and Isotropic material, (transparency, outstanding toughness, dimensional stability, mold ability, very low shrink rate, etc.), varies as a function of the direction and magnitude of the applied or residual stresses.

Light through a Polarizing filter (a Plane cavity of thickness L) blocks spatial components except those in the plane of vibration, (the norm of stationary wave) and if through a second Plane cavity, then the components of the light wave vibrate in that plane only. Polarized light passing through different Flat caves (stressed material), splits into two wave fronts travelling at different velocities, each parallel to a direction of principal stress but perpendicular to each other. (This is the Birefringence property of stress material with two indices, n_1, n_2 , of refraction).

The components of the light waves interfere with each other to produce a color spectrum as this happens in < common circle >.

[Retardation, $\bar{\delta}$, ($1.nm=10^{-9}$) is the phase difference between the two light vectors through the material at different velocities (fast, slow) and divided by the material thickness (L) is proportional to the difference between the two indices of refraction i.e. $\bar{\delta}/L = n_2 - n_1 = C.(\sigma_1 - \sigma_2)$ where σ_1, σ_2 , are the Principal stresses.

Retardation, $\bar{\delta}$, determines color bands or fringes (A fringe N is each integer multiple of the wavelength) where the areas of lowest orientation and stress appear black followed by gray and white and as Retardation and stress (σ) go up then the colors cycle through a more or less repeating pattern and the Intensity of the colors diminishes (decreases).

Because the colors repeat at different levels of retardation and stress, then is tracked as color band sequence from the black (very high energy) or white (very low energy) regions and are repeated periodically

following the whole fringe of the colors, as Black Gray, Violet [$f=668-789\text{THz}$ and $\lambda=380-450\text{nm}$], Blue [$f = 606-668\text{THz}$ and $\lambda=450-495\text{nm}$], Green [$f = 526 - 606 \text{THz}$ and $\lambda=495-570\text{nm}$], Yellow [$f = 508 - 526 \text{THz}$ and $\lambda=570-590\text{nm}$], Orange [$f = 484 - 508 \text{THz}$ and $\lambda=590-620\text{nm}$], Red [$f = 400 - 484 \text{THz}$ and $\lambda = 620-750\text{nm}$] as the (1st order fringe), Blue-green, -yellow, Orange (dark-yellow), Red, Violet (2nd order fringe).

Meaning that White light is the Mixture (Diffraction) of all frequencies, a vector with Low energy $E = h. f$ at Red (Red-shift) \rightarrow low $f = 400-484\text{THz}$, long $\lambda = 620-750\text{nm}$ (Blue-shift) \rightarrow high $f = 606-668\text{THz}$, short $\lambda = 450-495\text{nm}$ and High energy since $E = h.f$ at Blue.

Wave nature of light is proved by Young's Double Slit experiment where energy is carried by the dark fringes and Particle nature by Compton's Photoelectric Effect experiment with energy carried through the emission of electrons.

In this way Light is PARTICLE as Photon, $\lambda=380-780\text{nm} = (3,8-7,8).10^{-7}\text{m}$ and WAVE, as The Stationary Wave in, Λ , meaning that, since Photon is the only Electric Displacement field $D = \epsilon.E + B$, then in the rate of change is alternately in terms of The Electric field ($\partial B/\partial t$) and The Magnetic field ($\partial E/\partial t$). This is called the Dual Nature of light or Wave-Particle Duality.

Because GR was confined in Planck's length cavity (cleft, slit) of $\bar{h} \approx 1,054.10^{-34}\text{Js}$ failed to perceive the infinite cavities of nature being beyond Planck's level and which are wavelengths, λ , of monads \equiv quaternion $\equiv q = [s + \bar{v}. \nabla i]$. [31-36]

Energy confined in a monad [The inner structure of monad] is the Stationary wave on the Real part [$|s| = \lambda = \text{wavelength}$], and the Electric Displacement field ($\bar{v} = \epsilon . E + B$), alternately in terms of The Electric field $E = \partial B/\partial t$ and The Magnetic field $B = (\partial E/\partial t)(F-12)$.

Common circle is not empty space because of different angular velocity vector, $\bar{v} = \bar{w}.r$, and because of the malty refractivity and birefringence behaves as crystal with single or double or multi refractivity and in the absence of applied Torques produces a color Spectrum which is, the Color Forces \rightarrow Gluon Red, Gluon Green, Gluon Blue...

Stability is obtained by the opposite momentum $-\bar{\Lambda}$ where $E = -(\bar{v} \times B) = -(\bar{v}.B) \perp \rightarrow$ or and $B \perp E$ and for monad Evolutes.

The two perpendicular Static force fields E and Static force field B of Space-Anti-Space, experience on any moving dipole $\bar{AB} = [\lambda, \Lambda]$ with velocity \bar{v} (momentum $\bar{\Lambda} = m.\bar{v}$ only is exerting the velocity vector \bar{v} to the dipole λ) a total force $F = F E + F B = (\Lambda m). E + (\Lambda m). \bar{v} \times B$ which combination of the two types result in a helical motion and generally to any Space Configuration (the Continuum) extensive property, as Kinetic (the 3-current motion) and Potential (the

perpendicular Stored curl fields E,B) energy, by displacement (the magnitude of a vector from initial to the subsequent position) and rotation of equation as [25].

The Total Energy State of a quaternion is $\rightarrow ET = \sqrt{[m.vE]^2 + [\Lambda.vB + \Lambda \times vB]^2} = \sqrt{[m.vE]^2 + E^2} = \sqrt{[m.v.E]^2 + |\sqrt{p1.v.B1}|^2 + |\sqrt{p2.v.B2}|^2 + |\sqrt{p3.v.B3}|^2}$. i.e. a moving Energy cuboids (axbxc), rectangular parallelepiped, with the space diagonal length equal to $E = \sqrt{a^2+b^2+c^2}$ where $\rightarrow a = |p1.vB1|$, $b = |p2.vB2|$, $c = |p3.vB3|$ and when $vE = 0$ then $ET = \Lambda.vB + \Lambda \times vB \rightarrow$ which is the accelerating removing energy Λ toward $s\bar{v}B$ is $m = 0$, and then $ET = \Lambda\bar{v}B + \Lambda \times \bar{v}B \rightarrow$ which is the linearly removing energy Λ towards $\bar{v}B$, and for $\bar{v}B = 0$, then $ET = m.vE^2 \rightarrow$ which is the Kinetic energy in Newtonian mechanics towards $\bar{v}E$. [23-26].

a) Conclusions

Any moving monad [$z = s + \bar{v}$] is transformed into \rightarrow

1. In Elastic material Configuration , as Strain Energy and is absorbed as Support Reactions and displacement field [$\nabla \epsilon (\bar{u}, \bar{v}, \bar{w})$] upon the deformed placement, (where these alterations of shape by pressure or stress is the equilibrium state of the Configuration [26] , and then equations of Elasticity are, $G.\nabla^2.\epsilon + [m.G / (m-2)]. \nabla[\nabla . \epsilon] = F$) or in isotropic material [$\mu.\nabla^2.\epsilon + (\lambda+\mu).\nabla(\nabla.\epsilon) + F = 0$]. [22-23].
2. In Solid material Configuration, as Kinetic (Energy of motion \bar{v}) and Potential (Stored Energy) energy by displacement (the magnitude of a vector from initial to subsequent position) and rotation, on the principal axis (through center of mass of the Solid) as ellipsoid, which is mapped out, by the nib of vector $(\delta\bar{r}.c) = [\bar{v}.c + \bar{w}.r\bar{n}] \delta t$,as the Inertia ellipsoid [Poinot's ellipsoid construction] in [S] frame which instantaneously rotates around vector axis \bar{w}, ϕ with the constant polar distance $\bar{w}.Fe / |Fe|$ and the constant angles θ_s, θ_b , traced on, Reference [R] cone and on [S] cone, which are rolling around the common axis of \bar{w} vector without slipping, and if Fe , is the Diagonal of the Energy Cuboids with dimensions a,b,c which follow Pythagoras conservation law, then the three magnitudes (J, E, B) of Energy-state follow Cuboids (Cycloid), Plane, or Linear Diagonal direction, and If Potential Energy is zero, then vector \bar{w} is on the surface of the Inertia Ellipsoid. [23-27-28].
3. In Quaternion Extensive Configuration, as New Quaternion's (with Scalar and Vector magnitudes). Points in Primary Space [PNS] carry A priori the work $W = \int A-B [Pds] = 0$, where magnitudes P, d \bar{s} can be varied leaving work unaltered. The Diffusion (decomposition) of Energy is as the mechanism of Energy Transport as (\bar{v}), through its quantized wavelength $|\lambda|$, which is a property of any standing wave , into the Medium $|\lambda|$

= (1) - (2), and involves the Absorption and Reemission of the wave quantized energy $J = (J1)=(J2)$ as Electric and Magnetic field of Electric Displacement by the two neighbor edges (1) and (2) of the medium following Cycloid motion .[37-39]

4. In Space conserved Extensive property Continuum (Spatial Configuration), as Kinetic (3-current motion) and Potential (perpendicular Stored curl fields) Energy by Cycloid motion (the magnitude of wavelength vector $|\lambda|$), from initial (1) to subsequent position (2), as $|\lambda| = (1)-(2)$.During shifting Energy as velocity vector, \bar{v} , (and this because extreme case happens for zero application area) is decomposed into two velocity vectors $\bar{v}1, \bar{v}2$, being vectors, undergo vibrations which causes two waves that represent the two Electric and Magnetic perpendicular components until reaching point (2) which is the Reemission of the wave and it is the new head of velocity, \bar{v} , where then mechanism is recycled .[39-40].
5. The dynamics of any System = Work = Total Energy, is transferred as generalized force Q_n as, $Q_n = \partial W / \partial (\delta \bar{q}_n)$, $(\delta \bar{q}_n) = \bar{v}_n . \delta t = [\bar{v}c + \bar{w}.r\bar{n}] \delta t =$ (Translational + rotational velocity). δt as velocity and $Q_n = [\bar{v}c. \partial T / \partial t + \bar{w}.r\bar{n}.(\partial T / \partial t)] \rightarrow$ Translational kinetic energy + Rotational kinetic energy as Energy . [40].
6. The ultimate Constituents of Monads ($s, \bar{v}, \bar{v}i$) is the real part, $|s|$, and the Magnitude of Imaginary part as Vector $\bar{v} = \bar{v}i$, decomposed into velocity vectors $\bar{v}1, \bar{v}2$. [STPL] cylinder is a Geometrical Mechanism (Mould) which transfers the two Quantities of the breakable monads from one Level (Confinement) to another Level using Quantities or the Breakages of collision between monads .This Mechanism is not the Origin of monads, but it is the Mould (the Regulative Universe Valve) . It was shown that into Gravity cave $Lg = 2.r = e^{-i.(-9.\pi/2)b} = 3,969.10^{-62}m$, is inversely balancing the Common circle , of Space, Anti-Space .

For rotations Space, with velocities $[\bar{v}g = \bar{w}r]$ that of light, \bar{c} , tending to zero in cave $Lc > Lg$ then exist velocities $[\bar{v}c > c]$ tending to infinity. The hidden pattern of universe is, STPL line, which is off the Spaces and connect them (it maintains, conserve and support all universe), so may say, it is *The Naval Cord (string) of Galaxies*. [33-34]. i.e.

In Common Circle (the Sub-Space) of the rotating Space Anti-Space $[\pm \Lambda]$, with maximum angular Velocity Vector, $\bar{v} = \bar{w}.r$ on circumference, [in the absence of applied Torques and because of the Birefringence property of stress continuum with different indices, n, of refraction, which this creates the Retardation, δ , and determining Color Bands or Fringes] is Produced a color Spectrum which is, the *<Color Forces>* \rightarrow Gluon Red, Gluon Green, Gluon Blue.

When tangential velocity $\bar{v} = \bar{\omega}.r$ on circumference of a circle, r , is in another of radius $R > r$, then the new tangential velocity $\bar{v} = \bar{\omega}.R$ is greater than \bar{v} and when \bar{v} is the speed of light, then the new \bar{v} are velocities greater than that of light.

7. In Black holes Energy scale $[|\lambda| \cdot \Lambda = k \cdot 1]$ there are infinite high frequency small amplitude vacuum fluctuations at Planck energy density of 10^{113} J/m^3 that exert action (pressure) on the moving Spaces dipole and their Stability is always achieved by Anti-space in the rotational equilibrium.
8. Dipole vectors are quaternion's (versors) of *waving nature*, i.e., one wavelength $|\lambda|$ in circumference in energy levels, that conserve energy by transferring the Total kinetic energy T into angular momentum $L = \bar{r}m\bar{v} = \bar{r} \cdot \bar{p} = \bar{r}\Lambda$, as constant mass $m \pm [(\bar{\omega}.r)^2]$. Different versors with different Energy (scalar) possess the same angular momentum. A Composition of Scalar Fields (s) and Vector Fields (\bar{v}) of a frame to a new unit, maps the alterations of Unit by rotation only and transforms scalar magnitudes (particle properties) to vectors (wave properties) and vice-versa, and so, all particle-like properties are both of waves and particles. In Planck Scale, when the electron is being accelerated by gravity which exists in all energy levels as above, gravity is still exerting its force, so Electrodynamics can be derived from Newton's second law. [31-36].

b) General Remarks

From breakages $\rightarrow v.[(\bar{\omega}.r)^2]$, $-v.[(\bar{\omega}.r)^2]$, $2.(\bar{\omega}.r)^2$ on, *common circle*, are produced *Particles* \rightarrow *The Fermions* $\pm(\bar{\omega}.r)[(\bar{\omega}.r)^2]$ and *Bosons* $\pm 2.(\bar{\omega}.r)[(\bar{\omega}.r)^2]$ which are conveyed in STPL cylinder. [35]

From the constant velocity \bar{c} , on centre O , of *common circle*, are produced \rightarrow *Dark matter* $\rightarrow [\pm c.[(\bar{\omega}.r)^2]]$ and \rightarrow *Dark Energy* $\rightarrow [(2c) \times (\bar{\omega}.r)^2]$ in STPL cylinder,

From breakages $\rightarrow [\pm[(\bar{\omega}.r)^2]] \rightarrow$ *The Medium Field material* $\rightarrow \pm[(\bar{\omega}.r)^2]$ and \rightarrow *the Gravity force* $\rightarrow [2.(\bar{\omega}.r)^2]$. [36]

From, vector analysis, multiplication of a Scalar (s) magnitude and a vector (\bar{v}) magnitude is $\rightarrow s \cdot \bar{v} = \text{vector}$,

Dot product of two vectors, $v1 \cdot v2 = \text{yields a scalar}$

Cross product of two vectors $v1 \times v2 = \text{yields a vector}$

Breakage $(\bar{\omega}.r)^2 = |(\bar{\omega}.r)| \cdot |(\bar{\omega}.r)|$ is the *massive real part* therefore is a Scalar magnitude. *the min. Space-Quanta*.

Breakage $-(\bar{\omega}.r)^2 = -(\bar{\omega}.r) \cdot (\bar{\omega}.r)$ is the *massive energy part* therefore is a Scalar magnitude. *the min. Anti-Space Quanta*.

Breakage $2.(\bar{\omega}.r)^2 = 2|(\bar{\omega}.r)| \cdot |(\bar{\omega}.r)|$ is a *Force acting on the minimum quantized quantity of rotating Energy (i.e. the Spin)*, and it is a *Vector*. *the min. Energy Quanta*.

Two perpendicular vectors produce zero work and since Dark-energy vector is perpendicular to, Gravity - vector, *then Gravity is affecting on all particles except that of Dark-energy Gravity is affecting on (-) Field-Medium only for the equilibrium of spaces.*

Electromagnetic waves are created by the vibration of an electric charge. This vibration creates a wave which has both an Electric and a Magnetic perpendicular component.

The mechanism, of *Energy Transport through a Medium*, involves the *Absorption and Reemission* of the wave energy by two neighbor atoms (1) and (2) of medium. The Absorption of energy causes the electrons within the atoms (1) to undergo vibrations which causes a new wave with the same frequency (because $f=E/h$) as the first wave but delaying the motion through the medium until Reemission *by travelling through a small region of space between atoms (1) and (2)* and once the energy of wave is reemitted by its neighbor atom (2) then mechanism is recycled. This mechanism is succeeded by the intrinsic property of waves (= quaternion's, monads, vectors) which is the Stationary wave nature of spaces.

Breakage $\pm(\bar{\omega}.r)^2 = s^2$, is the *Medium, mediator*, filling all Space (*STPL cylinder*) is massive, mass less without viscosity, incompressible and continuous in very small scale, motionless because inactive, without exerting any pressure on other breakages, Homogenous and Isotropic *i.e. Breakage* $\pm(\bar{\omega}.r)^2$ is a *Rest, Neutral, Homogenous and Isotropic material and also the mediator of all fields - changes such that these cannot exceed the constant velocity, \bar{c} , on which motions may happen.*

Assuming the postulate of Relativity was valid without restrictions, this would imply that all forces of nature must be invariant under Lorentz transformations in order that principle be rigorously and universally true.

Since acceleration for a quaternion $z = (s + \bar{v} \cdot \nabla)$ is $a = [d^2z/dt^2] = (d/dt) \cdot (wz, dz/dt + wxz) = 0$, and this because $\bar{\omega} = \text{constant}$, therefore velocity $\bar{v} = \text{constant a priori}$.

c) Properties of Space-Energy Configuration

1. All universe is Isotropic and Homogenous in all reference frames of points (*in spatial and Temporal domain*) and work (W) is quantized on points as spin $\pm(\bar{p})$ and from this equilibrium of the quantized angular momentum, independently of time, is capable of forming the wave nature of Spaces, following the Boolean logic and distorting momentum $\bar{p} = \Lambda s$ as energy, *on the intrinsic orientation position of points*, on all points of the microscopic and macroscopic homogeneity as $(\partial/\partial \bar{\omega}) \otimes (-\lambda \bar{p}, \nabla \times \Lambda) = [0, \Lambda]$.
2. Momentum $\bar{p} = \Lambda s$ on the infinite dipole $AiBi$ with a momentum lever equal to zero (0) or equal to

wavelength λ create *linear motion*, while with a momentum lever $\neq 0$ creates the *rotational motion* (Euler, Coriolis, Centrifugal) $\rightarrow m \cdot [(d^2\vec{r}/dt^2) + m \cdot [d\vec{\omega}/dt \times \vec{r} + 2\vec{\omega} \times (d\vec{r}/dt) + \vec{\omega} \times (\vec{\omega} \times \vec{r})]$ where momentum $m \vec{p} = m \cdot r \vec{\omega}$ and mass m is a constant equal to, *the Reaction to the motion*, or as Inertia (I) which are a natural property of dipole and both are conserved vice versa. Forces $dP = PA - PB$ parallel to the Space, Anti-Space lines $[S] \perp [AS]$, create a Static force field B , and when Forces dP are perpendicular to the Space Anti-Space lines, create a Static force field E , which experience *Lorentz force* and it is the fundamental interpretation cause of motion, in small and large scales. On all dipole of wavelength λ , and momentum Λ , their product $\lambda \cdot \Lambda = k_{1,2,3}$ constant for each energy level. The fundamental force in universe is the total kinetic energy $T = 1/2 \vec{\omega} L = \Sigma (L^2/2I)$, a repulsive force following Pythagoras conservation law such that both T and L be conserved (when T decreases then this lost energy is transferred to angular momentum L and vice versa, in L by changing angular velocity vector $\vec{\omega}$, differently is needed a speed faster than that of light. *Energy is conserved on three perpendicular fields* J, E, B , on dipole such that the kinetic energy to be the diagonal of the cuboids.

3. The action of a quaternion on point is equivalent as -energy density and pressure- the state of stress at a point on the deformed placement or new configuration which is on the directional axis of the point. Gravity exists upon the point axis as $[d\vec{\omega}/dt \times \vec{r} + 2\vec{\omega} \times (d\vec{r}/dt) + \vec{\omega} \times (\vec{\omega} \times \vec{r})]$ where angular velocity is $\vec{\omega} = |\vec{\Lambda}| / |\vec{r}| = k/(\lambda m)$ and so exerts a direct action between two events, i.e. *Stationary points of [PNS] are rotating dipole and may be pictured as wave existing in the infinite points of Spaces and exerting an action (pressure) on the moving Spaces, dipole.* The Stability is achieved by the Anti-space.
4. In Black hole Energy scale ($\lambda \cdot \Lambda = k_1$) there are infinite high frequency small amplitude vacuum fluctuations at Planck energy density of 10^{113} J/m³ that exert action (pressure) on the moving Spaces dipole and their Stability is achieved by Anti-space also. A wide analysis for gravity force and gravity medium is shown in Maxwell's Displacement field which follows.
5. Dipole vectors are quaternion's (versors) of waving nature, i.e., one wave length in circumference in energy levels, that conserve energy by transferring Total kinetic energy T into angular momentum $L = \vec{r} m \vec{v} = \vec{r} p = \vec{r} \Lambda$, where mass $m =$ is a Constant. Different versors with different Energy (scalar) possess the same angular momentum. A Composition of Scalar Fields (s) and Vector Fields (\vec{v}) of a frame, to a new unit which maps the alterations of Unit by rotation only and transforms

scalar magnitudes (particle properties) to vectors (*wave properties*) and vice-versa, and so, has all particle-like properties of wave and particles. In Planck Scale, when the electron is being accelerated by gravity which exists in all energy levels as above, the gravity is still exerting its force. Matter is only built out of the primary dipole $AiBi$. properties of wave and particles. In Planck Scale, when the Matter is only built out of the primary dipole $AiBi$.

VIII. MAXWELL'S ELECTRIC DISPLACEMENT FIELD

a) General

{Quaternion \leftrightarrow dipole as work} $\vec{z}o = [ds = \lambda, \pm \Lambda \times \nabla i]$, $\vec{z}'o = [\lambda^2 - |\vec{\Lambda}|^2]$, $\vec{e}o = [\Lambda \nabla, -\nabla \times \Lambda]$ are the three fundamental equations of [PNS]. In dipole AB , $\vec{AB} = \lambda m$ is considered as Matter (*the reaction to velocity motion*) and it is the always communicator (*medium*) of the Bounded Impulses $P\vec{A}$, $P\vec{B}$, *The equilibrium and Bounded Primary Space-Anti-Space of Monad* AB or as $P[A \rightarrow (\lambda = \vec{v} \cdot T) \leftarrow B] = 0$, and thus unifying the known homogenous Euclidean geometry ($\Lambda \nabla$) and the source term energy ($d\vec{s} \cdot dP = \Lambda \Lambda = W$) with motion Λ imbedding in them all conservation physical laws with the only two quantized magnitudes, λ, Λ of Monad \vec{AB} and equal to the angular momentum vector $\vec{p} = \Lambda = \vec{\omega} \cdot \lambda = m \vec{v} = d/ds \{ \int A-B [Pds] \}$, and Time, T , to be the conventional factor, t , equal to zero. The three jointed cases of, ESM, Energy-Space -Monads are inter-transformed in space as follows,

$$E \rightarrow P\vec{A} > 0, dF > 0, ds = 0, P\vec{B} = 0, \rightarrow \sigma, \tau \neq 0$$

$$S \rightarrow P\vec{A} > 0, dF = 0, ds = \lambda > 0 \rightarrow \sigma, \tau \equiv m\vec{v}, P\vec{B} = 0,$$

$$M \rightarrow P\vec{A} > 0, dF = 0, ds = \lambda > 0 \rightarrow \sigma, \tau \equiv m\vec{c}, P\vec{B} > 0 \rightarrow \sigma, \tau = m\vec{v}$$

where $P = \vec{P}A =$ Force executed at point A of area dF , space $d\vec{s} = |\lambda| m =$ displacement of point A to B and equal to work done $= \int_A^B Pds$, and equal to main stresses σ, τ on area dF , and equal to velocity \vec{v} , t , is the conventional factor of time (t), and mass the reaction to the motion \rightarrow factor (m).

All bodies possessing mass and Elasticity are capable of vibration and are of two classes.

Free vibration takes place when a system oscillates under the action of forces inherent in the system itself with frequencies established by its mass and stiffness distribution.

Forced vibration takes place under the excitation of external forces in the system, and if the frequency of excitation coincides with one of its natural frequencies, a condition of <resonance> is encountered, resulting to any oscillation.

Periodic motion is when motion is repeated in equal intervals of time T (period of oscillation) and is designated by the time function $x(t) = x(t+T) = x = A \cdot \sin(2\pi \cdot t/T) = A \cdot \sin \omega t, \dots$

where A=the amplitude of oscillation measured from equilibrium position and motion is repeated when $t = T$.

Quantity $(2\pi/T) = \omega =$ circular frequency, $f = 1/T =$ frequency.

$$\text{Velocity } \dot{x} = \omega A \cdot \sin(\omega t + \pi/2) \text{ and}$$

Acceleration $\ddot{x} = \omega^2 A \cdot \sin(\omega t + \pi)$, which are also harmonic with the same frequency of oscillation, and when evaluated lead to the displacement x , by $\pi/2$ and π radians respectively and the system reveals at $\ddot{x} = -\omega^2 A$, so that *In harmonic motion acceleration* to be proportional to the displacement and directed to the origin, and because also Newton's second law of motion states that the acceleration is proportional to the force, then harmonic motion can be expected with force varying as kx . (which is Hook's law $F=kx$ and k , the stiffness coefficient, directed in centrifugal velocity vector \bar{v}_r , on radius r).

Because velocity vector is composed of the centrifugal velocity \bar{v}_r , and the rotational velocity \bar{v}_q , perpendicular to displacement, x , and because viscous damping represented by a dashpot, is described by a force proportional to the velocity as holds $F=c\dot{x}$ where, c , is the damping coefficient, then it is directional to velocity \bar{v}_q .

b) *The Electromagnetic fields E,P of monads (S):*

Free vibration on monads $AB = q = [s + \bar{v}\nabla i]$ oscillating under the action (thrust) inherent in itself, subject to *damping* because energy is dissipated by the *stiffness*, k , of monad and *constant of proportionality*, c , regarding motion of *mass*, m , when placed into motion, oscillation will take place at the natural frequency, f_n , which is a property of monad.

The homogenous differential equation

$$m\ddot{x} + c\dot{x} + kx = 0 \dots \quad (1)$$

corresponds physically to the free damped vibration, where is $x =$ the displacement, $\dot{x} =$ velocity of monad with general solution given by the equation $\rightarrow x = A \cdot e^{s_1 \cdot t} + B \cdot e^{s_2 \cdot t}$ where

$$s_{1,2} = -[c/2m] \pm \sqrt{[c/2m]^2 - (k/m)} \text{ and } S = \sqrt{(k/m) - [c/2m]^2},$$

and for initial conditions $x(0), \dot{x}(0) \rightarrow A, B$ then displacement

$$x = e^{-i \cdot (c/2m)t} \cdot [A \cdot e^{S \cdot t} + B \cdot e^{-S \cdot t}] \text{ and oscillatory}$$

$$x = e^{\pm i \sqrt{(k/m) - [c/2m]^2} t} = \cos \sqrt{[c/2m]^2 - (k/m)} \pm i \cdot \sin \sqrt{[c/2m]^2 - (k/m)} \cdot (2)$$

For $[c/2m]^2 > [k/m]$ no oscillations are possible, *over-damped*,

For $[c/2m]^2 < [k/m]$ exponent becomes an imaginary number and terms are oscillatory, *under-damped*, and this because ψ

For $[c/2m]^2 = [k/m]$ then oscillatory, non-oscillatory and radical motion is zero, *critical dumping*
 $C_c = 2m\sqrt{[k/m]} = 2m\omega_n = 2\sqrt{km}$.

Equalization of mass m from pairs $C_c = 2\sqrt{km} C_c^2 = 4km$ then $m = C_c^2 / 4k$ and from $2m\sqrt{[k/m]} = 2m\omega_n \rightarrow k = m\omega^2$ then $m = k/\omega^2 = C_c^2 / 4k$, or $\rightarrow 2k = \omega \cdot C_c = 2\pi \cdot f \cdot C_c$ a relation between Stiffness, circular frequency and damping coefficient The Electromagnetic fields of monads :

1 : Monads 2 : Equilibrium of Plane Cycloidal motion 3 : Thales theorem

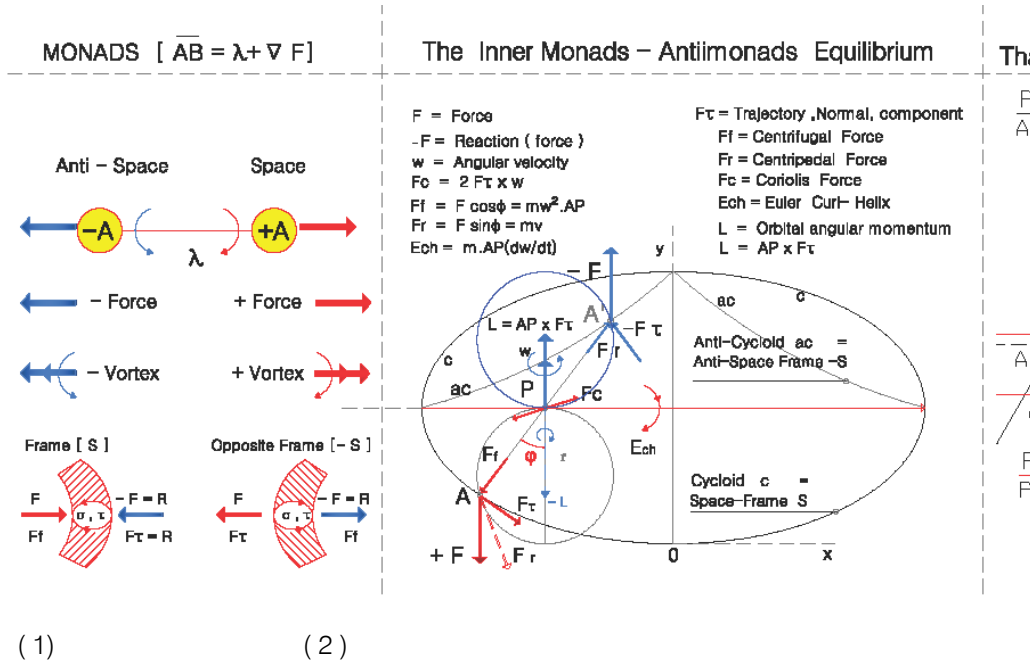


Fig. 9 : The inner structure of a Stationary Wavelength $\lambda=2\pi r$ executing a Free vibration, and under Equilibrium of forces in Cycloid, Anti-cycloid

Any damping can then be expressed in terms of the critical damping by the non-dimensional number $\zeta = C/C_c$ and S in terms of ζ , $[\frac{c}{2m}] = \zeta [\frac{C_c}{2m}] = \zeta w_n$, is $S = [-\zeta \pm \sqrt{(\zeta^2-1)}].w_n$ and differential equation of motion

$$x = e^{-\zeta.w_n.t} . [A.e^{i\sqrt{(1-\zeta^2)}.w_n.t} + B.e^{-i\sqrt{(1-\zeta^2)}.w_n.t} = e^{-\zeta.w_n.t} . \{ [\dot{x}(0) + \zeta.w_n.x(0)].\sin\sqrt{(1-\zeta^2)}.w_n.t] / [w_n.\sqrt{(1-\zeta^2)}] + x(0).\cos\sqrt{(1-\zeta^2)}.w_n.t \} \dots(3a)$$

which indicates that the frequency of the damped oscillation is equal to

$$w_d = \frac{2\pi}{\tau_d} = w_n.\sqrt{(1-\zeta^2)}$$

For $\zeta > 1$ is the Non-oscillatory motion, *Over-damped case* with the two roots increasing and decreasing with general solution $x = A.e^{[-\zeta + \sqrt{\zeta^2-1}].w_n.t} + B.e^{[-\zeta - \sqrt{\zeta^2-1}].w_n.t}$ where

$$x = e^{-w_n.t} . [A + B.t] = e^{-w_n.t} . \{ x(0) + [\dot{x}(0) + x(0).w_n].t \}$$

i.e. a double root $S_1 = S_2 = -w_n$ which is according to the Newton's second law, the deformation of the real part, $|s|$, which is $k.|s| = -w = -mg$ and frequency $f_n = (1/2\pi).\sqrt{g/|s|} = 2\pi\sqrt{m/k}$ depending on the mass and stiffness of monad, being its properties. This critical damping occurs on monads, which is their inner motion. For $\zeta = 0$ differential equation reduces to $s^2 + 2/w_n = \pm i$ and the roots on the imaginary axis correspond to un-damped case.

Conservation of energy in an, free vibration un-damped system, energy is partly kinetic T (stored in the

becomes $\ddot{x} + 2\zeta w_n \dot{x} + w_n^2 x = 0$ and the general solution is given by the three equations,

For $\zeta < 1$ is the Oscillatory motion, *Under-damped case*.

$$A = \{ \dot{x}(0) + [\zeta + \sqrt{(\zeta^2-1)}].w_n.x(0) \} / [2w_n.\sqrt{(\zeta^2-1)}]$$

$$B = \{ -\dot{x}(0) - [\zeta - \sqrt{(\zeta^2-1)}].w_n.x(0) \} / [2w_n.\sqrt{(\zeta^2-1)}] \dots (3b)$$

For $\zeta = 1$ is the Internally Isochronal oscillatory motion, *The critical damped motion case* and displacement, x, is as

mass by virtue of its velocity and for mass-less in velocity vector) and partly potential U (stored in the form of strain energy in elastic deformation of work done in a force field), and is Quantized.

The principle of virtual work states that, in an equilibrium system under the action of a set of forces is given a virtual displacement, the virtual work done by the forces will be zero.

Coulomb damping results from the sliding of two dry surfaces where damping force is equal to the product of the normal force and the coefficient of

friction, μ , independent and opposite of the velocity valuing only for half-cycle intervals.

Viscous damping force F_d determines an decay of amplitude $X_2 - X_1 = 4.F_d / k$ and the frequency of oscillation $w_n = \sqrt{k/m}$ equal to that of the un-damped system, and in case of two masses with stiffness k_1, k_2 then $k = k_1 + k_2$.

Energy dissipated by damping is the amount of loss of energy from the oscillatory system which results in the decay of amplitude of free vibration determined under conditions of cyclic oscillations. The force displacement curve will enclose an area, *hysteresis loop*, that is proportional to the energy lost per cycle. Considering the simplest case of energy dissipation, *that of a spring-mass system with viscous damping*, then is Damping force $F_d = c.\dot{x} = \pm c.w.\sqrt{A^2 - x^2}$ with

$$P = F(dx/dt) = (w.X_o.F_o). \sin(wt+\phi). \cos wt = (w.X_o.F_o). [\cos\phi.\sin wt.\cos wt + \sin\phi.\cos^2 wt] = w.X_o.F_o/2 [\sin\phi + \sin(2wt+\phi)]$$

where,

The first term is a constant, representing the steady flow of work per unit time.

The second term is a sine wave of twice the frequency which represents the fluctuation component of power, the average value of which is zero over any interval of time that is a multiple of the period.

d) *Lagrange`s Equations*

In reviewing the method of virtual work, the equation is $\delta W = \sum_i [F_i.\delta r_i] = 0$ where F_i are applied forces excluding the constraint forces and internal forces of frictionless joints and δr_i are the virtual displacements. By including D`Alembert`s inertial forces $-m.\ddot{r}_i$, the procedure is extended to dynamical problems by the equation $\delta W = \sum_i [F_i - m_i\ddot{r}_i].\delta r_i = 0$.

This equation leads to Lagrange`s equation when the displacement, \bar{r} , is expressed in terms of the generalized coordinates. The difference between, $\delta \bar{r}_i$, and, $d\bar{r}_i$, takes place in the time, dt , whereas, $\delta \bar{r}_i$, is an arbitrary number that maybe equal to, $d\bar{r}_i$, but is assigned instantaneously irrespective of time, ensuring compatibility of displacement.

For kinetic Energy, E , as a function of the generalized coordinates displacements, x , and the generalized velocity, \dot{x}_i , whereas Potential energy, U , is a function of, x , is,

$(d/dt)(\partial E/\partial \dot{x}_i) - (\partial E/\partial x_i) + (\partial U/\partial x_i) = 0$ and for $i = 1$ and for a system without potential ($U=0$) then ,

$$(d/dt)(\partial E/\partial \dot{x}) - (\partial E/\partial x) = 0 \quad \dots(L1)$$

Note: The elastic behavior of a system can be expressed in terms of the stiffness, k , or the flexibility, af , as,

• *Stiffness formulation*

Force, F , = Stiffness, k , .displacement, x , $F=k.x$ and $[k=N/m]$

steady-state displacement, x , and velocity \dot{x} , natural frequency $w_n = \sqrt{k/m}$ and constant $c = 2\zeta\sqrt{k/m} = 2\zeta w_n$, where ζ = the dumping ratio. For A = maximum amplitude, then Dumping Force is graphically represented as $\rightarrow [F_d / c.w.A]^2 + [x/A]^2 = 1$, i.e. an Ellipse with F_d , x , plotted in vertical and horizontal axis of velocity vector and equal to the area enclosed by the ellipse, and if added to F_d the force, $k.x$, of the lossless spring (pressure) then the hysteresis loop is rotated through F_d axis. (Voigt model). Quantized Energy is the enclosed by ellipse

c) *Power of a Free force*

The Power developed by a free force $F = F_o.\sin(wt+\phi)$ acting on a displacement $x = x_o.\sin(wt)$, where Power (P) is the rate of doing work, which is the product of the force, F , and velocity, $\dot{x} = w.r$, so Power is,

• *Flexibility formulation*

Displacement, x , = { Flexibility , af ,}. { force, F ,} $\rightarrow x = af.F$ and in measures $[af = m/N]$

e) *Work*

Work, W , by a force, F , exerted on an object which moves with distance times, dx , in the direction $x-x$ of the force is $W = F.dx$, and in the special case of a constant force, the work maybe calculated by multiplying, the distance times dx . the component of force $F.\cos\phi$ or $W = (F.\cos\phi).dx$.

Since the component $F.\cos\phi$ of force F when acting in the perpendicular direction $y-y$ ($dy \perp dx$) of the motion $x-x$, produces zero work, therefore, Work, *Kinetic Energy*, produced as *Stiffness*, k , in the dx Formulation, is stored in the perpendicular $y-y$ direction as *Flexibility* =, af , in the, dy , Formulation.

The Analogues in Gravity:

Work W by a constant force $F = 2(wr)^2$, or by the constant velocity, c , exerted on an object [$breakage (wr)^2$] which moves with a distance times $dx = |(wr)^2|$, and because Surface is zero is calculated in two perpendicular Formulations ($dx \perp dy$) as,

Stiffness $k = N/m \rightarrow$ velocity vector $v1 \rightarrow$ Electric field E

Flexibility $af = m/N \rightarrow$ velocity vector $v2 \rightarrow$ Magnetic field P

The why Energy is transformed into velocity, and velocity to a field is explained through Extrema Principle.

f) *Gravitational field and Newton`s 2nd Law in a Non-inertial rotating Frame:[25-26]*

When conjugation is done between $eo = [-\nabla\lambda, \nabla x\lambda] = 0$ and a quaternion of the differential time operator $\partial/\partial t$ and 3D angular speed vector, \bar{w} , then \rightarrow

$(\partial/\partial t, \bar{w}) \odot (-\lambda \nabla, \nabla \times \Lambda) = d/dt(-\nabla \lambda) + \bar{w} \cdot \nabla \times \Lambda, d/dt(\nabla \times \Lambda) + \bar{w} \cdot \nabla \lambda - \bar{w} \times \nabla \times \Lambda = 0 - \bar{w} \cdot \Lambda, 0 + \bar{w} \cdot \lambda + \bar{w} \cdot \Lambda = 0, \bar{w} \cdot \Lambda$
or, $(\partial/\partial t, \bar{w}) \odot (-\lambda \nabla, \nabla \times \Lambda) = (0, \bar{w} \cdot \lambda) = [0, \Lambda]$

Equation implies that the new quaternion which maps the alterations of, *negation truth Unit*, by rotation only, transforms only vector term magnitudes and since \bar{w} is velocity then $\bar{w} \cdot \lambda$ is momentum, \bar{p} , i.e. *negation truth Unit* $eo = [-\lambda \nabla, \nabla \times \Lambda] = 0$ is a machine that instantly transfers Inertial mass as *momentum* $\Lambda = \bar{w} \cdot \lambda = p = m \cdot \bar{v} = m \cdot (\bar{w} \bar{r}) = (m \bar{r}) \cdot \bar{w} = (m \lambda) \cdot \bar{w} = (J) \cdot \bar{w}$ to all points, in Inertial or not, frames Layers K1,2,3 $= \lambda \cdot \Lambda$ and over spaces, *NOT as said with Big-Bang*, but of this reason only.

Since Λ is constant and Wavelength (λ) may be equal to 0, then angular velocity $\bar{w} \rightarrow \infty$ meaning that, this is also happening to all Inertial or not Frames. Label 'gravity' probably is referred to something heavy. Conjugation between the quaternion of the differential

$$eo \rightarrow (eo)^2 = [\nabla \lambda, \Lambda \times \nabla]^2 = [\lambda^2 - \Lambda^2 \pm 2\lambda \cdot \Lambda \nabla^2] = \lambda^2 - \Lambda^2 \pm 2\lambda \cdot \Lambda = \lambda^2 - \Lambda^2 \pm 2\lambda \times \Lambda = [\lambda^2 - \Lambda^2] = [\lambda^2 - (i^2 + j^2 + k^2) |\Lambda^2|]$$

since λ, Λ are axially. *The upper relation was used by Special relativity [Minkowski metric (g $\mu\nu$)] for Events to be represented as 4-vectors for all scalar operations, without knowing that this is (eo)², which equilibrium the two opposite and spherical rotations of Space, Anti-space transformations vorticity magnitudes $\pm |\Lambda|$ to all other 4-vectors $\bar{z} = [s, \bar{v} \cdot \nabla]$. Conjugation of $\bar{z} \odot (eo)^2 = [sn, \bar{z} \cdot \nabla] \cdot [\lambda^2 - \Lambda^2] = \lambda^2 \cdot sn - \Lambda^2 \times \bar{v} \cdot \nabla$, $-sn \cdot \Lambda^2 - \lambda^2 \cdot \bar{v} \cdot \nabla - (\bar{v} \cdot \nabla \times \Lambda^2) \nabla$ may give an explanation to linear central force and to Newton's inverse square law. Newton law of motion for a material point is - Force = mass \times acceleration (a) - in an Inertial frame $a = d^2r/dt^2$. By twice applying the transformation from stationary to rotating frame, absolute acceleration, a, is written as $a = d^2r/dt^2 = |d/dt| \cdot |dr/dt| = |d/dt| \cdot [(dr/dt) + wxr] = (d^2r/dt^2) + |dw/dt| \times r + 2wx(dr/dt) + wx(wxr)$ or $a = |dw/dt| \times r + 2wx(dr/dt) + wx(wxr) = [a - d^2r/dt^2] \rightarrow$ i.e.*

Apparent acceleration's terms of, a, are independent of mass and a first interpretation is because *acceleration is the hypothetical external reaction to the motion* which does not happen in the stationary [PNS] but of action on points only.

time operator $\partial/\partial t$ and 3D angular speed vector, \bar{w} and the Position quaternion $\bar{z} = (r = 0, \bar{z})$ is the velocity $(\partial/\partial t, \bar{w}) \odot (0, \bar{z}) = (-\bar{w} \cdot \bar{z}, \bar{w} \times \bar{z} + d\bar{z}/dt)$ and

$$(\partial/\partial t, \bar{w}) \odot (-\bar{w} \cdot \bar{z}, \bar{w} \times \bar{z} + d\bar{z}/dt) = (-d\bar{w}/dt \cdot d\bar{z}, d^2\bar{z}/dt^2 + 2 \cdot \bar{w} \times d\bar{z}/dt + d\bar{w}/dt \times \bar{z} - \bar{w} \cdot \bar{z} \cdot \bar{w})$$

and which is the acceleration transforming both scalar and vector parts. Time (t), which is a phenomenological reference concept of alterations and it is the only element in the scalar of an event of a Position quaternion, does not exist in, eo, unit, where Energy is related as momentum Λ , so \rightarrow *Universe is a Space-Energy Configuration Frame* \leftarrow and not Space-Time as in GR believed.

Force field is the derivative of the potential of Newton's scalar field equation $\nabla^2 \Phi = 4\pi G \rho$ and for vacuum is $\Phi = GM / \sqrt{(x^2 + y^2 + z^2)}$ which is the same as the square quaternion of

Momentum, $\bar{p} = m \cdot \bar{v}$, on points in [PNS] is expressed by constant m and angular velocity, \bar{w} , and since m is hypothetical magnitude *representing the reaction to the motion*, then $\bar{p} = m \times$ angular velocity $= m \times \bar{w}$.

Conjugating on points then $[0, \Lambda] \odot [\bar{r}, i] = 0 - \Lambda \bar{r}, 0 + \Lambda r + \Lambda \times \bar{r} = -|\bar{\Lambda}| \cdot |\bar{r}|, \bar{r} \bar{\Lambda} + \bar{\Lambda} \times \bar{r}$ and Rearranging then becomes \rightarrow

$$[0, \bar{\Lambda}] \odot [r + \bar{r}, i] = -|\bar{\Lambda}| \cdot |\bar{r}| + |\bar{r}| \cdot \bar{\Lambda} + \bar{\Lambda} \times \bar{r} = |r| \cdot \bar{\Lambda} + |\bar{\Lambda}| \cdot |\bar{r}| + \bar{\Lambda} \times \bar{r} = \bar{w} \cdot |r| + |\bar{\Lambda}| \cdot |\bar{r}| + \bar{\Lambda} \times \bar{r}$$

and because by replacing $\Lambda = m \bar{w}$ then Velocity on Points $P(r, \bar{r}, \nabla i) = m [\bar{w} \cdot |r| + \bar{w} \cdot \bar{r} + \bar{w} \times \bar{r}]$ and since for points in motionless Frame [PNS] momentum Λ and the position vector of point vector, \bar{r} , apply on the same stationary point, then $\bar{w} \cdot |r| = 0$ (*this in motionless [PNS] only*) and the variation at point which is the same as the variation of, \bar{r} , therefore, $|\bar{\Lambda}| \cdot |\bar{r}|$ is equal to $d\bar{r}$, else $+ |\bar{\Lambda}| \cdot |\bar{r}|$, i.e. Angular velocity $\bar{w} = |\bar{\Lambda}| / |\bar{r}| = k / (\lambda m)$, is the effect of momentum $\Lambda = m \bar{w}$ on points as velocity magnitude, and so quaternion of the differential time operator $\partial/\partial t$ to 3D angular speed vector \bar{w} is the Apparent acceleration at Point and as,

$\gamma = \partial/\partial t [d\vec{r} + \vec{\Lambda} \cdot |\vec{r}| + \vec{\Lambda}x\vec{r}] = \partial/\partial t [d\vec{r}/dt + \vec{\omega} \cdot \vec{r} + \vec{\omega}x\vec{r}] \cdot m$
 $= m \cdot (d/dt) [d\vec{r}/dt + \vec{\omega} \cdot \vec{r} + \vec{\omega}x\vec{r}] = m \cdot (d/dt) [d\vec{r}/dt + \vec{\omega}x\vec{r}]$,
 which is $\rightarrow \gamma = m \cdot d/dt [d\vec{r}/dt + \vec{\omega}x\vec{r}] = m \cdot [(d^2\vec{r}/dt^2) + \vec{\omega} \cdot d\vec{r}/dt + 2 \cdot \vec{\omega}x(d\vec{r}/dt) + \vec{\omega}x(\vec{\omega}x\vec{r})]$ where exists,
 $m \cdot (d\vec{r}/dt) \cdot \vec{v} =$ Centrifugal Energy ($m \cdot \omega^2 r$),
 $\vec{v} =$ Position Velocity $= [d\vec{r}/dt + (\vec{\omega} \cdot \vec{r}) + (\vec{\omega}x\vec{r})]$
 $m \cdot (d\vec{r}/dt) \times \vec{v} =$ Coriolis Energy ($2m \cdot \omega \cdot v = 2m\omega^2 r$),
 $\vec{a} =$ Position Acceleration $= d\vec{v}/dt$
 $m \cdot \vec{r} \times \vec{a} =$ Euler's Energy ($m \cdot \omega \cdot r$),
 $m =$ Constant \Rightarrow The hypothetical Reaction tom. $\vec{r} \times \vec{a} =$
 Any other Energy in the motion.
 $(d^2\vec{r}/dt^2) =$ Linear acceleration of position point.
 $|d\vec{\omega}/dt| \times \vec{r} =$ Euler intrinsic acceleration of position point
 $2\vec{\omega}x(d\vec{r}/dt) =$ Coriolis intrinsic acceleration of position point
 $\vec{\omega}x(\vec{\omega}x\vec{r}) =$ Centrifugal intrinsic acceleration of position point.

Remarks:

The effecton, (γ) , is The Gravity in Inertial Frames of Planck's Scale matter conjugation, of momentum ($\Lambda = m\vec{v}$) on Points $P(r, \vec{r}, \nabla i)$ of [PNS] $\rightarrow z o = [\lambda, \pm \Lambda \nabla i] = |z o| \cdot e^{\wedge} \text{arc.cos} |\lambda/z o| \cdot [\vec{\Lambda} \cdot \nabla i / |\Lambda|] = |z o| \cdot e^{\wedge} \theta \cdot \vec{\Lambda} \nabla i$ it is the Gravity in Scale Frames, which is harmonically oscillated to all points of infinite spaces in [PNS] as New Quaternion $(-|\vec{\Lambda}| \cdot |\vec{r}|, r\vec{\Lambda} + \vec{\Lambda}x\vec{r})$ and oriented on the directional axis of the points (is on the unit quaternion of the points) as the Diagonal of an Energy Cuboid (Poinso't's ellipsoid) or Cube, which decomposition follows Pythagoras conservation law, Total Energy $\rightarrow W = \int A \cdot B [P.ds] = T = \sqrt{J^2 + E^2 + B^2}$ where the three orthogonal magnitudes (J,E,B), $J \approx d\vec{r}/dt = \vec{r}$, $E \approx \vec{\omega} \cdot \vec{r} = \vec{v}E$, $B \approx \vec{\omega}x\vec{r} = \vec{v}B$ of Energy-state follow Cuboidal, Plane, or Linear Diagonal direction as the normal quaternion $\rightarrow [-|\vec{\Lambda}| \cdot |\vec{r}|, r(\vec{\Lambda} + \vec{\Lambda}x\vec{r})] / (\Lambda r \sqrt{3})$. Stability is obtained by the opposite rotational momentum $-\vec{\Lambda}$ where $E = -(\vec{v}xB) = -(\vec{v} \cdot B) \perp \rightarrow$ or $B \perp E$ The two perpendicular Static force fields E and Static force field B of Space-Anti-Space, experience on any moving dipole $\vec{A}B = [\lambda, \Lambda]$ with velocity \vec{v} (only the momentum $\vec{\Lambda} = m\vec{v}$ is exerting the velocity vector \vec{v} to the dipole λ) a total force $F = F E + F B = (\lambda m) \cdot E + (\lambda m) \cdot \vec{v}xB$ which combination of the two types result in

a helical motion and generally to any Space Configuration (Continuum) extensive property, as Kinetic(3-current motion) and Potential (the perpendicular Stored curl fields E, B) energy, by displacement (the magnitude of a vector from initial to the subsequent position) and rotation.

g) Equations of motion of a, Plane frame, [R] :

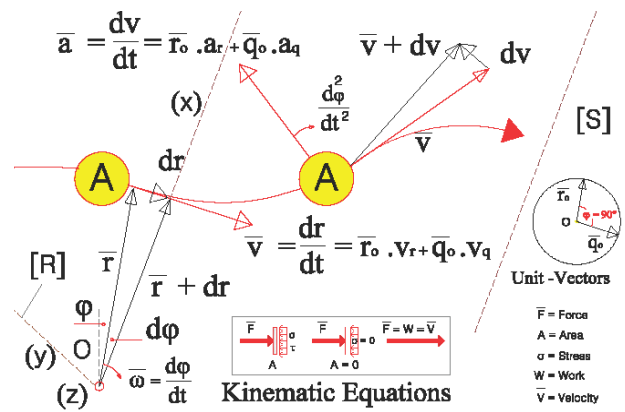


Fig. 10 : The Kinematic equations of motion in a Plane Frame and the Extreme case where Area is Zero, Point motion.

Let be point O the origin and radius $\vec{r}(t) = OA$ the instantaneous position of the moving Point A of a frame S, $\vec{v} = v(t)$ the instantaneous velocity and $\vec{a} = a(t)$ the instantaneous acceleration having the general coordinate independent definitions, $\vec{v} = dr/dt$, $\vec{a} = d\vec{v}/dt = d^2r/dt^2$.

$\vec{r}_0 =$ The unit-vector in direction r and $\vec{q}_0 =$ the unit vector in tangential to the angle ϕ (transverse), so $\vec{r} = \vec{r}_0 \cdot r$.

Differentiating radius, $d\vec{r} = \vec{r}_0 \cdot dr + d\vec{r}_0 \cdot r$ and since $\vec{v} = d\vec{r}/dt$ then $\vec{v} = d\vec{r}/dt = \vec{r}_0 \cdot dr/dt + d\vec{r}_0/dt \cdot r \dots (1)$

Since motion in the transverse position is $d\vec{r}_0 = \vec{q}_0 \cdot d\phi$, so \vec{v} becomes $\vec{v} = d\vec{r}/dt = \vec{r}_0 \cdot dr/dt + \vec{q}_0 \cdot r \cdot d\phi/dt = \vec{r}_0 \cdot vr + \vec{q}_0 \cdot vq \dots (2)$ where $vr = dr/dt$, $vq = r \cdot d\phi/dt$.

i.e. the total velocity, \vec{v} , is composed of the centrifugal velocity $\vec{v}r$, on radius r, and the rotational velocity $\vec{v}q$, perpendicular to OA, (the tangential to the angle). F-10

Derivative of (2) is acceleration $\vec{a} = d\vec{v}/dt = \vec{r}_0 \cdot r \cdot dvr/dt + dr/dt \cdot vr + \vec{q}_0 \cdot vq/dt + d\vec{q}_0/dt \cdot vq$ and since $d\vec{q}_0 = -\vec{r}_0 \cdot d\phi$, and $dvr/dt = (dr/dt) \cdot (d\phi/dt)$

$/dt) + r.(d^2\phi/dt^2)$ then, $\bar{a} = d\bar{v}/dt = \bar{r}\omega.ar + \bar{q}\omega.aq$, where, $ar = d^2r/dt^2 - r.(d\phi/dt)^2$ and $aq = r.d^2r/dt^2 + 2(dr/dt)(d\phi/dt) = d/dt(r^2.d\phi/dt) \bar{v}$.i.e. the total acceleration, \bar{a} , is composed of the centrifugal acceleration, \bar{ar} on radius r and the rotational acceleration, \bar{aq} , perpendicular to OA (tangential to angle).

where, $\bar{ar} = |v|.(d/dt)[\frac{\bar{v}}{|v|}]$ and $\bar{aq} = [\frac{\bar{v}}{|v|}].d|v|/dt$

Considering a moving frame [R] with center point O and \bar{r} as the direction axis, x, y, axis in the plane of motion and, z, axis perpendicular to x, y then the absolute velocity \bar{v} is composed of the following elements \rightarrow

$\bar{r}\omega.(dr/dt) \rightarrow$ Is a part of the absolute velocity \bar{v} relative to system [S] on OA axis, where $(d\phi/dt) = 0$, with which point A, participates in [R] frame centrifugal motion.

$\bar{q}\omega.r.(d\phi/dt) \rightarrow$ Is a part of the absolute velocity \bar{v} relative to system [S] perpendicular to OA axis where $(dr/dt) = 0$, with which point A, participates in [R] frame rotational motion, and absolute acceleration, \bar{a} , which is composed of, $\bar{r}\omega = r.(d^2r/dt^2) \rightarrow$ The relative to system [S] component acceleration where $(d\phi/dt) = 0$, with which point A, participates in [R] frame centrifugal motion.

$\bar{q}\omega.r.(d^2\phi/dt^2) - \bar{r}\omega.r.(d\phi/dt)^2 \rightarrow$ The relative to system [S] component rotational and centrifugal acceleration where $(dr/dt) = 0$, with which point A participates in [R] frame motion $\bar{q}\omega.2.(dr/dt).(d\phi/dt) \rightarrow$ Coriolis acceleration, The relative to system [S] supplementary acceleration components of both centrifugal and rotational acceleration \bar{a} , where $(dr/dt) \neq 0, (d\phi/dt) \neq 0$, of point A participation in [R] frame.

Coriolis force $\rightarrow [Cf]$.i.e. this force Cf is perpendicular to \bar{w}, \bar{v} vectors and thus perpendicular to radius $\bar{r} = OA$ which also is acting in the Plane of the motion and is equal to $\rightarrow Cf = \bar{q}\omega.2.(dr/dt).(d\phi/dt) = 2[\bar{w}.\bar{v}] = 2[|\bar{w}|^2.r]$.

From equation $d\bar{v} = \bar{a}.dt$ then $v.dv = \bar{a}.\bar{v}.dt = a.d\bar{r} = d(v^2/2)$ and when multiplied with mass becomes $m\bar{a}.d\bar{r} = d(mv^2/2) = Pd\bar{r} = dL$ and $L = mv^2/2 =$ kinetic energy. i.e. work W executed on a material point A by a force \bar{P} on instantaneous displacement $d\bar{r}$, is manifested

as change of kinetic energy and since also centripetal force $m.\bar{ar}$ is perpendicular to the trajectory then executes zero work. The executed work is produced by force $P =$ thrust = velocity in any time moment and is equal to the time change of kinetic energy, or $\rightarrow dL/dt = \bar{P}.(dr/dt) = (\bar{P}.\bar{v} = \bar{P}.[\bar{r}\omega.vr + \bar{q}\omega.vq] = \bar{P}.\bar{q}\omega.aq$. Work executed by Coriolis force is conserved as a curl helix on a surface perpendicular to the plane of motion.

h) *Extremes Principle or Extrema*

All Principles are holding on any Point A.

For two points A, B not coinciding, exists Principle of Inequality which consists another quality. Any two points exist in their Position under one Principle, *Equality of Stability, (Virtual displacement which presupposes Work in a Restrained System)*. [16-17]. This Equilibrium presupposes homogenous Space and Symmetrical Anti-Space.

For two points A, B which coincide, exists the *Principle of Superposition* which is a Steady State containing Extrema for each point separately.

Extrema, for a point A is the Point, for a straight line the infinite points on opposite line, either these coincide or not or these are in infinite, and for a Plane the opposite infinite lines and points with all combinations and Symmetrical ones, .i.e. all Properties of Euclidean geometry, compactly exist in Extreme opposite, Points, Lines, Planes, circles by following anode or descend sequence.

Since Extreme is holding on Points, lines, Surfaces, Volumes, bodies etc., therefore all their compact Properties (*Principles of Equality, Arithmetic and Scalar, Geometric Segments and Vectors, Proportionality, Qualitative, Quantities, Inequality, Perspectivity etc.*), exist also in the common opposite context *magnitude to direction*, therefore in Superposition the magnitude AB is equal and constant in both directions, or any other direction $\neq 0, [|A,B| - P\bar{A}, P\bar{B}]$.i.e.

Any Segment \bar{AB} between two points A, B consist a Vector, described by the magnitude AB, and directions $\bar{A}B, B\bar{A}$ and in case of Superposition $\bar{A}A, A\bar{A}$, where Properties of Vectors, Proportionality, Symmetry, etc. exist either on edges A, B or on segment AB as \rightarrow

A quantity to Anti-quantity, a monad to Anti-monad, and since it is either a scalar or a vector and by their distinct definitions, Scalars, are quantities that are fully described by a magnitude or numerical value alone in *Anti-Scalars. Energy* which is motion to Anti-motion, .i.e. to the Anti-trajectory.

According to Thales theorem, F-9.3 if two intersecting lines PA, PB are intercepted by a pair of Parallels $AB//A'B'$, then ratios $PA/AA', PB/BB', PA/PA'$,

PB/ PB' of lines, or ratios in similar triangles PAB, PA'B' are equal or ratio $\lambda = [PA / AA'] = [PB / BB']$. In case line A' B' coincides with AB, then AA' = AA, BB' = BB, i.e. exist Extreme and then $\lambda = [PA/AA] = [PB/BB]$, (Principle of Superposition), where property of scalar exists on common segment AB.

Vectors are Imaginary quantities that are fully described by a constant magnitude and change direction in order to keep their constant numerical value or move to *Anti-Space*.

Strain (ϵ) = change of length / length \rightarrow It is the relative change in shape or size of an object due to externally-applied forces. Young modulus (E) = tensile stress / tensile Strain.

$$\sigma_{1,2} = (\sigma_1 + \sigma_2)/2 \pm (1/2) \cdot \sqrt{(\sigma_1 - \sigma_2)^2 + 4 \cdot \tau_{12}} \text{ and } \rightarrow \tan \theta = 2 \cdot \tau_{12} / (\sigma_1 - \sigma_2) \dots \quad (a)$$

When surface becomes a point [This is extreme case where surface is interchanged as line or line-segment, it is the same as the infinite small, ds, in Calculus], then $\sigma_2=0$ and τ_{12} very small. Since force

$$\sigma_{1,2} = \sigma_1 / 2 \pm (1/2) \cdot \sqrt{\sigma_1^2 + 4 \cdot \tau_{12}^2} = \sigma_1 / 2 [1 \pm (\sqrt{5})].. \quad (b)$$

i.e. Stress σ on a point is manifested as $\sigma = P / dF$ and as $dF = 0 \rightarrow \bar{\sigma} = P / [dF \rightarrow 0]$ becomes momentum $m\bar{v}$

Since Stationary force P exists independently of the acting area then for zero surface (a point) stresses P/F vanish, and Stationary force P becomes a Moving

$$\sigma_1 = \bar{v}_1 = (\sigma_1) / 2 (1 + \sqrt{5}) \text{ and } \sigma_2 = \bar{v}_2 = (\sigma_2) / 2 (1 - \sqrt{5})... \quad (c)$$

$\sigma = P / dF = 0 \rightarrow \bar{P} = m \cdot \bar{a} \rightarrow \bar{v} = \{\bar{v}_1 \perp \bar{v}_2\} = \{\bar{\sigma}_1 \perp \bar{\sigma}_2\} = \text{Constant}$, where,

$\bar{v}_1 \rightarrow$ represents the *Inward compressible* radial velocity and

$\bar{v}_2 = \bar{v}_1 \rightarrow$ represents the *Transverse Outward stretchable* radial velocity of point, which is transformed into,

$\sigma_1 \rightarrow$ representing the *Inward compressible* radial pressure

$\sigma_2 = \sigma_1 \rightarrow$ representing the *Transverse Outward stretchable* radial pressure of material point,

m = the reaction to the change of velocity motion (the mass),

\bar{a} = the change of velocity motion (the acceleration), (F10) i.e.

Force P in a material body appears as Kinetic energy, in an elastic surface is appearing as *Principal and Shear stress*, in a material line or segment as *tension*, in Euclid line becomes *velocity on line or, a Free Velocity moving Line-Segment*, or a *moving Vector (quaternion=monad)*. The *minimum Quantized Energy, Quanta = 2s²*, is diffused through the *minimum Quantized Space, Quanta s²*, in all quantized spaces, which are

Stress (σ) = E. Strain = E. ϵ , Strain = Stress / E = $\epsilon = \epsilon(u,v,w)$ G = shear modulus = E.m²(m +1) where m = Poisson's ratio = 1/ μ = 10/3. [26-27]

Volume and, Surface, Plane stress:

A material is said to be under Plane stress if the stress-vector is zero across a particular surface, i.e. $\sigma_3 = 0$ or $\sigma_z = \tau_{yz} = \tau_{xz} = 0$

From mathematical theory of Elasticity a surface, F, under pressure, p, due to a transverse force, P, is $p = P/F$ pervaded in all, and around surface and if force direction forms an angle θ , then Principal stresses σ_1, σ_2 and Shear stresses τ_{12} areas,

P is a vector, then as in cross-product to a right-handed coordinate system where exists $\sigma_2=0$ and $\tau_{12} = \sigma_1$, equation (a) becomes

force \bar{P} and exists as momentum $m\bar{v}$ with $m=1$ (*Extreme hypothetical Reaction to the motion*) i.e. the velocity \bar{v} at this point and which is decomposed in the two perpendicular velocities \bar{v}_1, \bar{v}_2 , where then equation (b) is transformed as,

Particles, [MFMF] Field, moving Vectors, free velocity monads, Material lines \rightarrow Surfaces and Bodies.

Since also it is a moving energy then diffusion (decomposition) of stored energy follows Pythagoras theorem in a New Configuration with Scalar and Vector magnitudes such that satisfy the principle of conservation of linear momentum.

Points in Space carry A priori the work $W = \int A - B [PdS] = 0$, where magnitudes P, dS can be varied leaving work unaltered.

Using the work formulas of elasticity then In and On Surface work W is,

$$W = [(\sigma_1^2 + \sigma_2^2) / 2 - (\sigma_1 \cdot \sigma_2) / m] / EF$$

$$W_v = [(\sigma_1^2 + \sigma_2^2 - \sigma_1 \cdot \sigma_2) / 6 \cdot GF] \text{ where,}$$

σ_1, σ_2 , Are the Principle stresses, W_i is the work Inward radial surface,

W_v , Is the work Onward radial surface (*the transverse*)

Placing equation (c) in above work equations then become,

$$W = [P^2 / 4 \cdot EF^2] \cdot (6 + 4/m)$$

$$W_v = [2P^2 / 3 \cdot GF^2] \text{ and for } m=4 \text{ and } G = 2E/5$$

$$W = (7/4) \cdot [P^2 / EF^2]$$

$$Wv = (5/3) \cdot [P^2 / EF^2] \dots \quad (d)$$

Fig.(11) The two, opposite signed, Fragments s^2 where on this, Force $[\nabla i = 2(wr)^2]$ as velocity $\vec{v} = \vec{c}$, The $= \pm |(\vec{w} \cdot r)^2|$ consist the under Gravity primary Dipole, Thrust, cause Gravity's Electromagnetic Field $E \perp P$

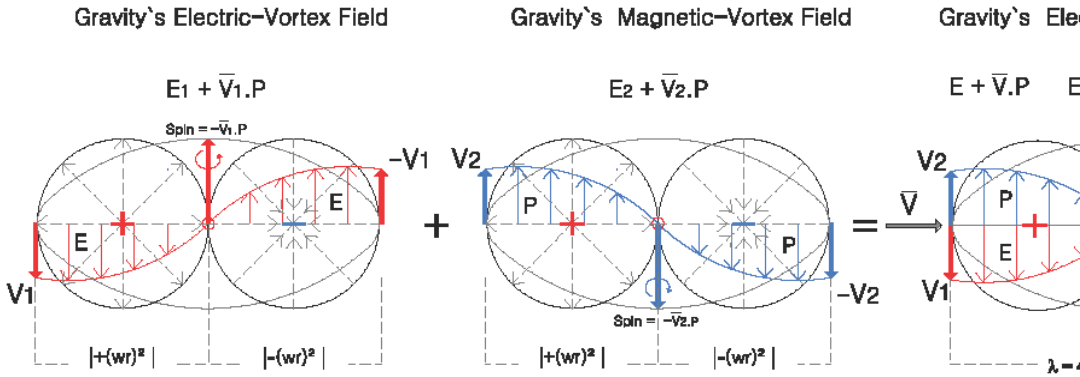


Fig. 11 : Fragments $[+(|wr|^2) \leftrightarrow -(wr)^2]$ as Dipole are joined by Gravity Force that causes the Electromagnetic Gravity-Field E, P

Since principal stresses σ_1, σ_2 are equal to the corresponding transverse velocities v_1, v_2 which are the Cross product of a vector \vec{v} , so, $\vec{v}_1 = (\vec{v}_1 / 2) \cdot [1 + \sqrt{5}]$ $\rightarrow \vec{v}_2 = (\vec{v}_2 / 2) \cdot [1 - \sqrt{5}]$ being Odd and Even functions of points.

The Norm is $|\vec{v}| \cdot |\vec{v}| = v^2 = (v_1 / 2) \cdot [1 + \sqrt{5}] \cdot (v_2 / 2) \cdot [1 - \sqrt{5}] = (v_1 \cdot v_2 / 4) \cdot (1 - 5) = -v_1 \cdot v_2$ or $\vec{v}^2 = -\vec{v}_1 \cdot \vec{v}_2$ and the analogous,

$$\sigma^2 = -\sigma_1 \cdot \sigma_2 \dots \dots \quad (e)$$

i.e. Extreme equation (e), joints at points the Principal stresses σ and velocities \vec{v} into the quaternion type $\vec{z} = \vec{\sigma} = \vec{v}$ which is $\vec{z} = [\lambda, \pm \Lambda \nabla i]$, the conjugate quaternion $\vec{z}' = [\lambda^2 - |\Lambda|^2]$ and defines the deep relation between, Energy as velocity (\vec{v}) and stress (σ) into both, Space as velocity $|\vec{v}_1| \perp |\vec{v}_2|$ or stresses $\sigma_1 \perp \sigma_2$, and into the transverse equilibrium Anti-space as velocity $-|\vec{v}_1| \perp |\vec{v}_2|$ or stresses $-\sigma_1 \perp -\sigma_2$.

This property of equation (e) in inner monad's wavelength (λ) where $dF=0$ results to the equation $c^2 = \sigma^2 = \sigma_1 \cdot \sigma_2 = v_1 \cdot v_2$ and it is a relation between constancy of velocity and main stresses. Furthermore σ_1 is a measure of how much in medium, the wavelength λ of monads where with (+), (-) dipole moment creates the inner Electric and Magnetic Fields E, P, opposes to any external E, B field and σ_2 is a measure of the inner vortex density (w) of medium which opposes also to any external E, B field. The inner Electromagnetic field of monads is produced from the two transverse moving velocity vectors \vec{v}_1, \vec{v}_2 on the two cycloids and consist Space-Quanta. Fig.11

From electromagnetic theory,

Permittivity (ϵ), is a Dielectric constant multiplier which affects the propagation of Electric fields, and it is a measure of how much the molecules oppose the external E-field due to a single point charge $q[C]$ at a distance R and exists, Electric flux density $D =$ multiplier (ϵ) .Electric field E.

Permeability (μ), is a measure (a scalar field) of the inner vortex density $w[\nabla \times \vec{v}]$ oppose the external B-field due to a moving electric charge q and exists, $H =$ The pure vorticity (Spin), $B =$ The weighted vorticity that is weighted for the density of the vortex [MFMF] field, issuing $B = \mu H$. By definition $\epsilon = 1/q = 1/\sigma_1$ and $\mu = 1/w = 1/\sigma_2$ where then $c^2 = v^2 = \sigma^2 = \sigma_1 \cdot \sigma_2 = v_1 \cdot v_2 = (1/\epsilon) \cdot (1/\mu) = \frac{1}{\epsilon \cdot \mu}$ or, $c^2 \cdot \epsilon \cdot \mu = 1$ which is the known relation between the speed of light and Permittivity, Permeability, in free space medium ... [40]

i) Stability of Whirling in monads

The two perpendicular velocities \vec{v}_1, \vec{v}_2 (The thrusts) F-12 follow the cycloid shaft (1)-(2) with center O and are synchronous and acquire equal speed of rotation, w , and equal to the whirling speed $\hat{\theta}$ and thus exist $\hat{\theta} = w$. Equilibrium of whirling presupposes the balancing of Space, Anti-space opposite equal motion. On intergrading the speed is obtained $\phi = w t$, where ϕ is the phase angle between moving shaft center O, of AA' , OA is the eccentricity from (1)-(2) axis, and O the geometric center of $|\vec{v}| = r \rightarrow R$ which is constant. Since $\hat{\theta} = w = \text{constant}$ then $\ddot{\theta} = \dot{r} = \ddot{r} = 0$ and the problem reduces to that of one degree of freedom with mass $m = \epsilon = \mu = 1$ for monads. By using the general

equations of whirling then $\rightarrow (\frac{c}{m} - w^2).R = e.w^2.\cos\phi$, $\frac{c}{m}.w.R = e.w^2.\sin\phi$ and by division the next equation is obtained,

$\tan\phi = (\frac{c}{m} w.R) : (\frac{k}{m} - w^2) = [2\zeta\frac{w}{w_c}] : [1 - (\frac{w}{w_c})^2]$ where $w_c = \sqrt{k/m}$ is the critical speed, $\zeta = \frac{c}{c_c}$, $e = OA$ is the eccentricity and from Pythagoras theorem $\cos\phi = (\frac{k}{m} - w^2) : \sqrt{(\frac{k}{m} - w^2)^2 + (\frac{c}{m}.w)^2}$ and the Amplitude equation becomes,

$$AO = e.(\frac{w}{w_c})^2 : \sqrt{[1 - (\frac{w}{w_c})^2]^2 + [2\zeta(\frac{w}{w_c})]^2} \dots\dots(s1)$$

Remarks: Equation indicates that eccentricity line $e = OA$

Leads the displacement line $OA = O \rightarrow R$ by the phase ϕ , which depends on the amount of damping and the rotation speed ratio $\frac{w}{w_c}$, and in critical ratio $w_c = \sqrt{k/m}$ frequency in lateral vibration, the amplitude is restrained by the damping $\epsilon = \mu = 1$. Point O is always on axis, shaft, and point A rotates about it on circle of radius OA. The existing force is equal to $\rightarrow m.e.w^2 = m.OA.w^2$.

Forces, Pressure, Velocity, Work (Energy Space), equivalence

A- Equations of Elasticity: Principle stresses
 $\sigma_1 = \sigma/2 [1 + \sqrt{5}]$, $\sigma_2 = \sigma/2 [1 - \sqrt{5}]$, $\sigma_1.\sigma_2 = \sigma^2$ where,
 $\sigma_1 = E.\epsilon(u) =$ The inward compressible pressure (in radial displacement distance).
 $\sigma_2 = G.\epsilon(v) =$ The transverse stretchable pressure (the perpendicular to radial displacement distance).
 E = Young's modulus (linear stress/strain)
 G = Shear modulus (transverse stress/strain) and holds $E \perp G$

B- Equations of motion -Viscously Damped Free Vibration - Homogenous equation $m\ddot{x} + c\dot{x} + kx = 0$ is composed of $x = A.\sin.wt$, $\dot{x} = wA.\sin(wt + \pi/2)$, $\ddot{x} = w^2A.\sin(wt + \pi)$, where $m =$ mass = A Reaction coefficient proportional to velocity change and directed to velocity vector \bar{v} ,
 $c =$ The Damping coefficient directional to velocity vector $\bar{v}q$,
 $k =$ The stiffness coefficient directed to velocity vector \bar{v} , and holds between coefficients, $m // k \perp c$.

C- Equations of Maxwell's Displacement Current :Electric Displacement field $D = \epsilon.E + P$, Magnetic field $B = \mu.H$ where, $\epsilon =$ Permittivity = Dielectric constant multiplier, i.e. a measure opposing displacement distance between electric field E and electric flux density D.
 $\mu =$ Dielectric constant multiplier, i.e. a measure opposing the perpendicular to displacement rotation between the inner vortex density H and the external weighted vorticity density B i.e. Dielectric constant multiplier $\Sigma \perp \mu$.

Remark:

Work as Energy is Quantized, converted, in Space monads $\bar{x} = d\bar{s} = \lambda m$, as the Electromagnetic Wave E,P (Displacement current) and moves in Gravity's field medium [MFMF] and is dissipated as Quaternion monads (Particles or Waves, matter or vectors) as Forces (displacements, masses, pressure etc.) using modulus, coefficients, reactions to the motion and all other geometrical indices.

j) Gravity's Displacement Current (S)

It was referred that Fragments $s^2 = \pm |(\bar{w}.r)^2|$ occupying the minimum quantized space $|s^2|$ are deported and fill all [STPL] cylinder which is the Rest Quantized Field $\pm [(\bar{w}.r)^2]$ or it is, the material point in mechanics, as the base of all motions where force $[(\bar{w}.r)^2 \nabla i] = 2.[(\bar{w}.r)^2]$ is vibrating on length $2. |[(\bar{w}.r)^2]| = \lambda$ as a Stationary Wave, and creates the curl Electromagnetic Field $E \perp P$, on which is the Universal Quantized force called Gravity. The Gravity - Force is equal to $F_g = q.[E + \bar{v} \times P]$ and is exerted on any movable particle with charge q . Gravity - Field is $G_f = [E + \bar{v} \times P]$, the unmovable, forced welded spinning dipole, and because jointed with force, means that Newton's laws issue in both, Absolute System [S] and Relative System [R]. (F-11)

On cycloid [Fig-12], Thrust $\rightarrow g =$ Force $F =$ velocity, where Velocity $\bar{v} = [\sqrt{g/4r}].\rho = [\sqrt{g/4r}].|(1)-(2)|$.

Acceleration $\bar{a} = (d^2s/dt^2) = -(g/4r).s$

Trajectory acceleration $\bar{a}q = g.\sin\phi = [g/4r].s$

Centripetal acceleration $\bar{a}r = (v^2/\rho) = [g/4r].\rho = [g/4r].AA$

Ratio $v/\cos.\phi = \sqrt{4gr} =$ constant and velocity of center K of rolling circle is, $\bar{v}k = v.r/PA = (1/2).v/\cos\phi = \sqrt{gr} \rightarrow$ i.e. motion, the velocity, of the rolling circle center is linear.

Force $2.[(\bar{w}.r)^2]$ as velocity \bar{v} is acting at point (1) and since $dF=0$ then is analyzed into the two equal velocity vectors $\bar{v}x = \bar{v}1 = (\bar{w}.r)^2\sqrt{2}$, $\bar{v}y = \bar{v}2 = (\bar{w}.r)^2\sqrt{2}$ as the cross-product $\bar{v} = \bar{v}1 \times \bar{v}2$ i.e. in two perpendicular plane motions.

Energy as the horizontal constant velocity $\bar{v}1 =$ (thrust), is transported at point (2) by following the tangential trajectory A, forming on cycloid the Electric field, E, and for stability the anti-trajectory A' on Evolute, the Anti-Electric field, -E, both decomposed in a velocity $\bar{v}1r$ perpendicular to the trajectory and thus executing zero work .and $v1q$ tangential

Fig.12 : The Moving Electromagnetic Fields of Monads in their Stationary Cycloidal wavelength ($\lambda=2\pi r = |(wr)^2|$)

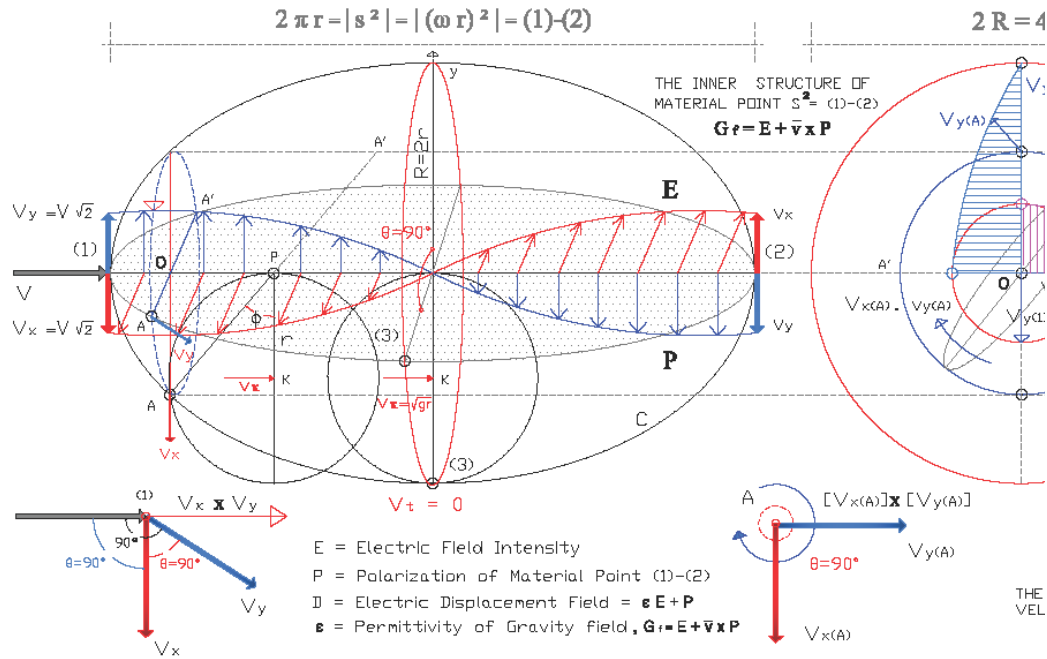


Fig. 12 : The Stationary Velocity's wave-length, $|V|=\lambda$, as the Intrinsic Electromagnetic field $E \perp P$ and for Gravity $\lambda=s^2 = |(wr)^2|$

to the trajectory executing the work. The equation of Gravity's Standing waves E, P is from Wave function, $Y = [2A \sin kx] \cdot \cos wt$ where $A = v_1 = v_2 = |v|/\sqrt{2} \rightarrow$ Wave's Amplitude, $kx = \pi/2, \pi, 3\pi/2, \rightarrow$ The Wave's number, location, $w = 2\pi f = 2\pi/T \rightarrow$ Oscillating frequency, angular frequency and equations become $E = 2A \cdot \sin kx \cdot \cos wt = \sqrt{2} \cdot |(wr)^2| \cdot \sin kx \cdot \cos wt$
 $P = 2A \cdot \sin kx \cdot \cos wt = \sqrt{2} \cdot |(wr)^2| \cdot \sin kx \cdot \cos wt \dots (g_1)$ which consist Monad's Electromagnetic wave equations, and mapping as below,
 At points (1), (2), $\bar{v}_1 r = \bar{v}_1 \cdot \bar{v}_1 q = 0, \bar{a}_1 r = \bar{r}_0 \cdot v^2 / 2r, \bar{a}_1 q =, \bar{q}_0 \cdot v^2 / 2r, CoF = 0$
 At point (A = x), $\bar{v}_1 r = \bar{v}_1 \cdot \sin kx \cdot \cos wt, \bar{v}_1 q = \bar{v}_1 \sin kx \cdot \cos wt, \bar{a}_1 r = \bar{r}_0 \cdot (d/d\bar{r})(v^2/2) \cdot \sin kx, \bar{a}_1 q = \bar{q}_0 \cdot (d/d\bar{r})(v^2/2) \cdot \sin kx, CoF = VP$

Considering Planck's length $L = 1,616 \cdot 10^{-35} m$ filled with the two only breakages $s^2 = \pm |(w \cdot r)^2|$ then $(1) \leftrightarrow (2) = L = \lambda = 2 \cdot |(w \cdot r)^2|$. Using Planck's work equations connecting particles and wave properties $W = \Lambda \cdot ds = p \cdot \lambda = h$ then $p = \frac{h}{\lambda}$ and from Kinetic energy $E = mv^2/2 = (m^2 \cdot v^2) / 2m = \frac{p^2}{2m} = \frac{h^2}{\lambda^2}$, and since also is $E = hf, p = h/\lambda, \bar{v}r = \sqrt{g \cdot r_c}$.
 In gravity level, $\bar{p} = m\bar{v} = (m \cdot v_k)$ and $|\bar{p}|^2 = |m \cdot v_k|^2 = m^2 \cdot g \cdot r_c$ and $E = \frac{p^2}{2m} = m \cdot \frac{g \cdot r}{2} = \frac{h^2}{\lambda^2}$, where $r = r_c$

For a material point, electron, $\lambda = 1,616 \cdot 10^{-9} m$ it is $m \frac{g \cdot r}{2} = \frac{h^2}{\lambda^2} = [6,626 \cdot 10^{-34}]^2 / [1,616 \cdot 10^{-9}]^2 = 1,681 \cdot 10^{-49}$ and for $g = 9,81 m/s^2$ then $r = 1,681 \cdot 10^{-49} \cdot (2/9,81) m = 3,427 \cdot 10^{-50} m$, which is the rolling circle's radius in electron wavelength.

For a material point under Planck's length then $\lambda = L/2 = 2\pi r$ and $r = L/4\pi = 1,616 \cdot 10^{-35} / 4\pi = 1,286 \cdot 10^{-36} m$.

Kinetic energy $E = mv^2/2 = h \cdot f = h/T = h/(4\pi r/v) = hv/(4\pi r)$ and since also $p = h/\lambda = h/(L/2) = 2h/L$ then $p = 2(6,626 \cdot 10^{-34}) / (1,616 \cdot 10^{-35}) = 82$.

From energy relation $p = h/(2\pi r) = m \cdot v = m\sqrt{g \cdot r}$, $h^2 = 4\pi^2 r^2 \cdot (g \cdot r) \cdot m^2 = 4\pi^2 r^3 g \cdot m^2$ then $m^2 = h^2 / [4\pi^2 r^3 g] = (6,626 \cdot 10^{-34})^2 / [4\pi^2 \cdot (1,286 \cdot 10^{-36})^3 \cdot 9,81] = (4,264 \cdot 10^{-4} \cdot 10^{-68}) / 10^{-111} = 5,3303 \cdot 10^{38}$ and $m = 2,3067 \cdot 10^{19} Kg$.

From constancy of $\bar{v}k = \sqrt{g \cdot r}$ then $v^2 = (9,81 \cdot 1,286 \cdot 10^{-36}) = 12,61566 \cdot 10^{-36}$ and $\rightarrow \bar{v}k = 3,552 \cdot 10^{-18} m/s$ Period $T = \lambda/\bar{v}k = (1,616 \cdot 10^{-35}) / (2,3,552 \cdot 10^{-18}) = 2,275 \cdot 10^{-18} s$ Frequency $f = 1/T = 1 / (2,275 \cdot 10^{-18}) = 4,396 \cdot 10^{17}$ Momentum $p = m \cdot v = 2,3067 \cdot 10^{19} \cdot 2,9979 \cdot 10^8 = 6,915 \cdot 10^{27} Kg \cdot m/s$. From energy equations Energy $E = p^2/2m = (6,915 \cdot 10^{27})^2 / (2 \cdot 2,3067 \cdot 10^{19}) = 1,0364 \cdot 10^{36} Kg \cdot m$ and Stability is obtained by the opposite rotational momentum in Anti-cycloid motion.

IX. A SUMMARY OF NEWTON EULER-LAGRANGE EINSTEIN, EQUATIONS OF MOTION

a) Newtonian Mechanics

Start with the three laws that define the behavior of Objects to, *Stand Still, when Moving, and when Forces act upon them.*→

It is required mainly a rectangular coordinate system on which are considered all constraint forces .The laws,

- Everybody persists in its state of Rest or uniform Motion in a straight line unless it is compelled to change that state by forces impressed on it, (The Inertia law),
- Force is equal to the change in momentum (r.m.v →Rotational, mv→ Linear) per change in time. For a constant mass, force equals < mass times acceleration $F = ma >$, or $F = dp/dt = d(mv)/dt = m(dv/dt) = m.a$,
- For every Action, there is an equal and opposite Reaction,

Remarks: In Euclidean logic, Points follow Principles as follows,

- A = B The Principle of Equality,
- A ≠ B The Principle of Inequality,
- PA + PB = 0 The Principle of Stability,
- A ≡ B Principle of infinite Superposition (extreme)
- A/B = C/D The Principle of Proportionality

And in Mechanics one is, $A \leftrightarrow B = \infty$ The Principle of Virtual Displacements $\sum [Pi + Hi] . \delta \vec{r}_i = 0 \rightarrow W = \int P.ds = 0$,

- The state, is the reaction to the change of motion (in magnitude and direction) which presupposes force only.

Applying this logic in Principle of Stability then →

As in geometry the same in Physics, $PAB = -PBA$ or $PAB + PBA = 0$, or as, The Infinite points in [PNS] form infinite Units, monads $A_i B_i = d\vec{s}$, which equilibrium by the Primary Anti-Space by an Inner Impulse (P) at edges A, B where $P_i A + P_i B = 0$, and $ds = 0 \rightarrow N \rightarrow \infty$ and where Monad \overline{AB} is the ENTITY and Elements=Breakages $[|A,B| - P\overline{A}, P\overline{B}]$ is the LAW of monad AB, and also →The {Space, Anti-Space equilibrium, $\pm \overline{A}$, Absolute System [S] } is at Rest, as Angular momentum $\overline{A} = \Omega = m\vec{v}.r$, and is Crushed out into Fragments, becoming the three Breakages $[s^2=(wr)^2]$, $[-s^2=-(wr)^2]$, $[\nabla i=2(wr)^2]$ and after clashed with the velocity vector \vec{v} of [S], (unless succeed escaping un clashed through center O of [S] into[R]=[STPL] and this because $\vec{v} = 0$), are Thrown OFF this System [S], (in order to avoid scattering ,in STPL line) conveyed into the Linear momentum ,the Inertial and Energy-Space, the Relative [STPL] System [R] as the Particles Fermions → $[\vec{v}.s^2]$ and Bosons → $[\vec{v}.\nabla i]$ with momentum, $m\vec{v}$, which behave as Mass and

as Force, in Relative System [R], The Un-clashed through center, O, Fragments $s^2 = \pm |(\vec{w}.r)^2|$ occupying the minimum quantized space $|s^2|$ are deported and fill all [STPL] cylinder which is the Rest Quantized Field $\pm [(\vec{w}.r)^2]$ or, The material point (1) in mechanics, as the base of all motions and the force $[|(\vec{w}.r)^2| \nabla i] = 2.[(\vec{w}.r)^2]$, is vibrating on $[|(\vec{w}.r)^2|] = \lambda$ as an Stationary Wave creating a curl Electromagnetic Field $E \perp P$ which is the Universal Quantized force called Gravity, meaning that Newton's laws issue in both, Absolute System [S] and Relative System [R] .

- Object in mechanics, may be the Material point (1) at Euclidean point (1), which is now Breakage $\pm [(\vec{w}.r)^2]$ magnitude in this Rest Homogenously - Isotropically and, Quantized, mass-less Field $\pm [(\vec{w}.r)^2]$ and consist the required coordinate System and base for all motions and forces . This rest Space system [PNS] (the Base) is the [MFMF] Field with the less space distance $ds = |\vec{w}.\vec{r}|^2$, *Minimum Space-Quanta*.
- Object in mechanics may be also the Material wavelength $\lambda = (1)-(2)$ in the {[Medium-Field Material Fragment] → $[\pm s^2] = |\vec{w}.\vec{r}|^2 =$ [MFMF]Field ←} which is a standing wave in cavity (1)-(2) with scalar breakage $|\pm(\vec{w}.r)^2|$ as medium (1)-(2) field, and (J1) as energy at point (1) and carried to point (2) by following the cycloid motion from (1) to (2) which is isochrones. Velocity \vec{v} , during shifting is analyzed into two velocity vectors \vec{v}_1, \vec{v}_2 , which undergo vibrations causing two waves that represent the two Electric E, and Magnetic P, perpendicular components following the trajectory, $in=(c1)$, $out=(c2)$. On cycloid $= (c) = |A1-A2|$ is needed the isochrones time $T = \pi.\sqrt{Rc/g} = \pi\sqrt{T/\lambda}$ to reach end $A2 < \text{Fermat's Principle of Least time} >$ is the Extreme in <Isochrones Principle > which is embedded in all wavelength vector monads, *Minimum Energy-Quanta* .F-12

b) Einstein's General Relativity [GR]

- The, *Laws of Physics*, are the same for all inertial reference frames
- Light always propagates through a Vacuum at a, *definite velocity* ,c, which is independent of the state of motion of the emitting body.

a. Maxwell's Displacement current → Dc:

Dc is a quantity appearing in Maxwell's equations of Electromagnetism and is defined in terms of the rate of change of, *electric displacement fields* D, in a dielectric medium and is defined as $D = \epsilon .E + P$ where,

- ϵ =The permittivity of the free space,
- E=The electric field intensity,
- P=The polarization of the medium .By differentiating above equation then,

$$dD/dt = JD = \epsilon . (\partial E/\partial t) + (\partial P/\partial z)$$

where, $(\partial E/\partial t)$ = The Magnetic field $\rightarrow B \leftarrow$
 $(\partial P/\partial t)$ = The Electric field $\rightarrow E \leftarrow$
 and in Isotropic dielectric case ($P=0$) then $D = \epsilon \cdot E$ and Maxwell's equations become:

$\nabla \cdot D = \rho \rightarrow$ Gauss's law for Electrostatic

$\nabla \cdot B = 0 \rightarrow$ Gauss's law for Magnetostatic

$\nabla \cdot B = \rho / \epsilon_0 \rightarrow$ Gauss's law for Magnetism.

$\nabla \times D = J \rightarrow$ Ampere's law

$\nabla \times E + (\partial B/\partial t) = 0 \rightarrow$ Faradays' law where

$D = \epsilon \cdot E$, $H = B/\mu \rightarrow$ in SI units,

$\rho =$ The free charge density

$\epsilon_0 =$ Electric constant

For the origin of Maxwell's equations [41].

Relativity considers such a current could be very directly connected to empirical phenomena, <Speculation had proved itself superior to empiricism >

Remarks (a):

Since wavelength, λ , as distance is equal to product velocity (v).period (T) then $\lambda = \bar{v} \cdot T$. Displacement current is a current like the conduction current and produces a magnetic field. It is a stationary wave in individual charges in motion as this is velocity vector $\bar{v} = \bar{\omega} \cdot r$ being wavelength which is connected to angular momentum $\bar{L} = r \cdot m \bar{v} = m \cdot \bar{\omega} \cdot r^2$ in Planck's or beyond Planck's length $L_p = 1,616 \cdot 10^{-35} \times \sqrt{3} = 8,906 \cdot 10^{-35} \text{m}$, decomposed into the two perpendicular velocity vectors, \bar{v}_1, \bar{v}_2 which create Electric (E) and Magnetic field (P). The same also for macroscopic bound current circulation around a material's (monad) surface. [29]

Velocity describes the origin of magnetic in the law field as variation of Electric Flux. Since Dc had never been directly detected, proof is the following reasonable logic.

Displacement current density, D , is Energy in cavity (1)-(2) = λ which is a standing wave following cycloid trajectories in cavity to reach edge (2). Medium of cavity is breakage $|\pm(\bar{\omega} \cdot r)^2|$ of Gravity Field and Energy on (1) is the density velocity vector $\bar{v} = |(D1)|$. In stationary wave conservation of energy (charge) is assembled in Anti-cycloid (Evolute). (7.9)

Force $2 \cdot [(\bar{\omega} \cdot r)^2]$ as velocity \bar{v} is acting at point (1) and since $dF=0$ then is analyzed into the two equal velocity vectors $\bar{v}_x = \bar{v}_1 = (\bar{\omega} \cdot r)^2/\sqrt{2}$, $\bar{v}_y = \bar{v}_2 = (\bar{\omega} \cdot r)^2/\sqrt{2}$ as the cross-product $\bar{v} = \bar{v}_1 \times \bar{v}_2$ in two perpendicular plane motions.

Velocity vector $\bar{v} = \bar{v}_1 \times \bar{v}_2$, with head at point (1) is analyzed, in a perpendicular to $\lambda = (1)-(2)$ directional plane into the two orthogonal velocity vectors, \bar{v}_1, \bar{v}_2 which heads are at point (1), is carried to point (2) by following the cycloid motion (1)-(2). During shifting, velocity vectors \bar{v}, \bar{v}_2 , being vectors, undergo vibrations which causes the two waves that represent the Electric

[E] and the Magnetic [P] perpendicular components until reaching point (2) which is the Reemission of the wave and it is the new head of velocity, \bar{c} , where then mechanism is recycled.

Source is constant Force $2[(\bar{\omega} \cdot r)^2] = \bar{c}$, because of angular velocity vector $\bar{\omega}$, in Stationary wave.

The two velocity vectors $\bar{v}_1 \perp \bar{v}_2$ form the Electrical and Magnetic field, E, P , as sink follow cycloid Isochrones motion. i.e.

Electric Displacement density (field), $D = \epsilon \cdot E + P$, in an dielectric medium, of any moving charge of wavelength, λ , in the rate of change, is alternately in terms of The Electric field ($\partial P/\partial t$) and of The Magnetic field ($\partial E/\partial t$) in phase with each other in the wavelength, λ , \rightarrow and generally means that velocity vector $\bar{v} = \lambda/T = \lambda f$, and for Photon (or any other moving charge) is a Stationary Electromagnetic wave in Photon's wavelength, λ , and a self-propagating transverse oscillating wave producing a changing Magnetic field ($\partial E/\partial t$) around itself and according to the second of Maxwell's equations (Ampere-Maxwell law). The resulting Magnetic field creates an Electric field ($\partial P/\partial t$) around itself according to the first of Maxwell's equations (Faraday's law of the Electromagnetism Induction).

This alternative Electromagnetic wave travels as velocity vector, \bar{v} , (charge = momentum, or the assembled conserved unaltered energy, is internally interchanged on wavelength).

The Duality Principle of Photon is the Intensity of light vector $|\bar{v}| = \text{real part}$, which is Particle and since light is also quaternion $\rightarrow [q = s + \nabla i \times D i]$ then photon is represented as Particle by the intensity (s) of light, and as Wave, by the Electromagnetic fields $\{E, P\} = [\nabla i \times D i]$ in Wavelength $|q|$ as energy, where $\nabla i = \bar{c} = \lambda f = \lambda/T$, and this also occurs for all moving monads.

The fact that speed of light is constant and travels at the same speed regardless of any direction is because rotational energy $\bar{L} = r \cdot m \cdot \bar{v}$ and centrifugal velocity $\bar{v} = \bar{\omega} \cdot r$ are constant and acceleration $[d\bar{v}/dt = d(\bar{\omega} \cdot r)/dt = 0]$ is zero and when exported to STPL is also constant. When tangential velocity $\bar{v} = \bar{\omega} \cdot r$ on circumference of a cave, r , is in another of radius $R > r$, then the new tangential velocity $\bar{v} = \bar{\omega} \cdot R$ is greater than \bar{v} and when \bar{v} is the speed of light, then the new \bar{v} are velocities greater than that of light.

Michelson's-Morley experiments cannot prove reality because in Planck's cave occurs isochrones motions, and Gravity is the force (energy) which is connecting Material points of the Medium with the constant light velocity \bar{c} .

Numerical value, s , and Imaginary $\nabla i = ExP$ are variant in Invariant rotational energy $\bar{L} = r \cdot m \cdot \bar{v} = m \cdot \omega r^2$ as velocity $\bar{v} = \bar{\omega} r$, meaning that quaternion = energy, travels by changing velocity \bar{v} and angular velocity $\bar{\omega} = 2\pi/T$, and the Period T of vibration and because of Isochrones motion of Fields on cycloids trajectories, automatically

distribute themselves uniformly (Electromagnetic wave $E=P$ due to \bar{c}) across the whole wavelength, λ , of monad.

Relativity being confined in Planck's length, { and because Maxwell's Displacement current where Displacement current is equivalent to an Intrinsic Electromagnetic Wave with two perpendicular velocities forming the two Fields}, could not perceive this Intrinsic property of monads or quaternion (velocity vector \bar{v}), to be Wave and Particle. The above experiment and the Non-Euclidean geometries initiated the line to Relativity. The Monads in monads is a characteristic expression of this property.

Einstein failed to see this reality (zero acceleration of rotational velocity $\bar{\omega}$) and to explain the WHY speed of light is constant and where, considering constancy of light as an axiom from which derived the rest of his theory of GR.

Galileo Galilei arguing that the mechanical laws of physics are the same for every inertial observer (those moving uniformly with constant speed in a straight line), and so one cannot distinguish, a state of rest, from, a state of constant velocity, was in reality.

Increasing-Decreasing of a Removal Source F (13)

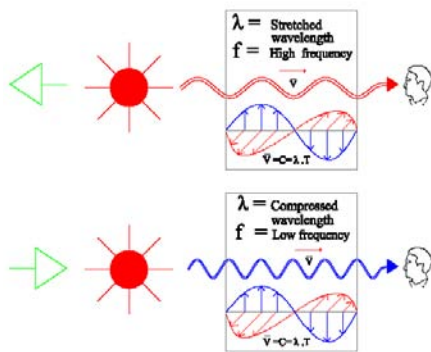


Fig. 13 : Increasing-Decreasing λ of a Removal Source $V(f)$

b. Equivalence Principle

In a uniformly and non-uniformly accelerated reference frame with acceleration, a , situated in a Gravitational field of gravity, g , then $g = -a =$ Intensity of gravity field i.e. All particles have the same acceleration in a gravitational fields and is not possible with experiment to distinguish the effect of gravity from that of an accelerated reference frame using local observations.

This is a fundamental principle of GR and gravitational mass is identical to inertial mass. This implication of the principle is that, since photons have momentum and therefore must be attributed an inertial mass, they must also have a gravitational mass and thus photons should be deflected by gravity and also be impeded in their escape from a gravity field, leading to the gravitational red shift, the concept of a black hole,

and to the gravitational lens effect. Above is, the Why charge of gravity is the Inertia of a body, or equivalency between Inertial mass and Gravitational mass.

Remarks (b):

Galileo's Principle of Equivalence states that Inertial mass is equal to the gravitational mass and acceleration $a = d\bar{v}/dt \rightarrow$ equal to acceleration due to gravity, g , Gravity is the Stationary force $\rightarrow [\nabla i = 2(wr)^2] \leftarrow$ on the base for all motions \rightarrow The Medium-Field Material-Fragment, $|\pm s^2| = (wr)^2 = [MFMF] \leftarrow$ in all universe and so Newtonian theory of gravity, acting instantaneously between two separated masses, is correct.

Maxwell's equations predict Electromagnetic waves in and out of monads, while Einstein's equations of GR predict Gravitational waves that travel at the speed of light in order to explain Simultaneity. GR failed to conceive Gravity force as a Stationary force, restraining the breakages for monads beyond Planck's length $[10^{-62} - 10^{-35}]$.

Breakages acquire different velocities and different energy and because follow cycloid trajectories, thus need the same time (isochrones) to reach [STPL] line.

Fermat's Principle of Least time in Isochrones Principle is embedded in all wavelength, λ , as vector monads.

During Intrinsic Diffraction, $d\bar{s} = \lambda$, of isochronous motion of vectors, frequency, f , doesn't change and only the velocity, \bar{v} , and wavelength, λ , changes so from equation

$$\lambda = \bar{v} \cdot T = \bar{v} / f, \bar{v} = \lambda f \text{ and } a = d\bar{v}/dt = (d\lambda/dt) \cdot f + \lambda(df/dt)$$

then $\rightarrow a = g = d\bar{v}/dt = (d\lambda/dt) \cdot f$ since $f = \text{constant}$, \rightarrow or Let $\lambda \rightarrow$ be the wavelength of a moving monad, $t = \lambda / c \rightarrow$ is the needed time to cross length, λ ,

$$s = at^2 / 2 \rightarrow \text{Deflection due to acceleration, } a,$$

$$H = gt^2 / 2 \rightarrow \text{Deflection due to acceleration of, } g, \dots (h)$$

For $s = \lambda$ then $s = at^2 / 2 = c \cdot T$, where T is the period of Isochrones displacement, and $t^2 = 2 \cdot cT / a \dots (1)$

From equation (h) $t^2 = 2 \cdot H / g \dots (2)$ and by equating (1) and (2) then $cT/a = H/g$ and since in gravity field where cycloid motion (Simultaneity) defines the same displacement, cT, H then $ct = H$ and consequently $a = g$,

Therefore all particles have the same acceleration, g , in our gravitational field with frequency unchanged, and \rightarrow velocity, \bar{v} , with wavelength, λ , to be changed \leftarrow so light being a particle also, is deviated in gravity field.

c. Mercury's Perihelion advance:

The perihelion of the orbit of the planet advances, 2 degrees per century, 80s, accounted by the

perturbations from the other planets and, 43s, by Einstein`s GR theory.

Remarks (c):

The→[Space, Anti-Space equilibrium, ± $\bar{\Lambda}$, Absolute System [S] ←], as Angular momentum $\bar{\Lambda} = \Omega = mvr$, is Crushed out into Fragments and, becoming the three Breakages [$s^2 = (wr)^2$], [$-s^2 = - (wr)^2$], [$\nabla i = 2(wr)^2$], and after clashed with the velocity vector \bar{v} of [S], (unless succeed to escape un-clashed through center O in STPL cylinder and this because of $\bar{v} = 0$), are Thrown OFF this System [S], conveyed into the, Relative [STPL] System [R], with Linear momentum and Inertial Energy-Space, as the Particles Fermions →[± $\bar{v}.s^2$] and Bosons →[$\bar{v}.\nabla i$].

The un-clashed through center, O, Fragments $s^2 = \pm |(\bar{w}.r)^2|$ occupy the minimum quantized space $|s^2|$ and consist the Medium-Field Material-Fragment → [± s^2] = [MFMF] as base for all motions , fill all [STPL] cylinder and thus consist the Rest, Homogenous, Isotropic Base of all motions. On this Base, force [∇i] = [2. |(w.r)^2| ∇i] called Gravity is connecting material points of Medium, while all the other clashed or un-clashed fragments of the cylinder move, consisting the Relative System [R] to Absolute, Space, Anti- Space, ± $\bar{\Lambda}$, System [S]. Un-clashed Fragments through center O, clashed with the constant velocity, \bar{c} , consist the Dark matter [± $\bar{c}.s^2$] and the Dark energy[$\bar{c}.\nabla i$], or in summary,

- A. [± $\bar{v}.s^2$] → Fermions [$\bar{v}.\nabla i$] → Bosons
- B. [± s^2] → [MFMF] Field [∇ i] → Gravity force
- C. [± $\bar{c}.s^2$] → Dark matter[$\bar{c}.\nabla i$] → Dark energy

Since [MFMF] = [± $s^2=(wr)^2$] is the base for all motions and Gravity force [∇i] = [2. |(w.r)^2| ∇i] = 2.(± s^2)= 2(wr)² then forces (from anywhere) is twice the Base, i.e. Base is half (1/2) of Gravity force, (or since perturbations from other planets is 80s), so Base is→ 80 / 2 = 40s, which are the Unaccounted last40 seconds of arc .

d. Gravitational deflection of light by the Sun

In GR indicated that light from a star, which just grazed the sun, should be deflected by1, 75 seconds of arc.

Remarks (d):

Monads, as an Electromagnetic Standing wave move in Field [MFMF] = $s^2 = \pm |(wr)^2|$ which is the smallest quantized space of this level. Let, L, be the length of an undergoing constant acceleration monad in gravity field,

$$t = L/ c \rightarrow \text{is the needed time to cross length } L,$$

$s=at^2 /2 = aL^2/2c^2 \rightarrow$ is Deflection due to acceleration, a,

- 1. For a monad in Planck`s length 10^{-35} m then T

$$= 8,906.10^{-35} / 3.10^8 = 2,968. 10^{-35} \text{ and } s = aT^2 /2 = 9,81.8,809.10^{-70} = 4,32.10^{-69} \text{m}$$

- 2. For Photon wavelength $\lambda = 6,21.10^{-7}$ mas Monadin monad Photons = $9,81(\lambda/c)^2 /2 = 2,101. 10^{-14}$ mcorresponding to an angle $\theta = s/3600 = 5,386. 10^{-18}$ degrees of second.
- 3. For an arc on earth surface $\pi.(Km)^2 = 3142.10^3$ m then $s=9,81.(9,872/9).(10^{12}/10^{16})=5,38.10^{-4} = 0,53810^3$ mm, which corresponds to an angle θ arc-sec → 3600.s=1,883-arc.sec.

e. Gravitational red-shift and Time Dilation

Gravitational red-shift is the Phenomenon where low frequencies of light [long T=620-750 nm] shifted to red (red-shift → f = 400 - 484 THz) and higher frequencies of light [short T=450-495 nm] are shifted to blue (blue-shifted→ f = 606 - 668 THz) and Time Dilation the opposite Phenomenon for time. Both are the included intuitive deductions of the constancy of light.

Remarks (e):

The answer is as below using the intrinsic property of Constant light velocity vector $|\bar{v}|$, which is a Stationary wave in Photon`s wavelength λ , as→ $\bar{v} = \lambda / T = \lambda f$

In a Stress-Strain System , the State of Principle Stresses, ± σ at each point, is the double refraction in Photo-Elasticity and expressed as the Isochromatic lines [($\sigma_1 - \sigma_2$)= J.k/d] or as Isochromatic surfaces, depending on the direction of force (pressure) which is the same in gravity field as length-contracted and length-expanded in a given piece of quantized space .

Stretching Removal of, λ , creates,- σ_1 , while, Compressed Removal of, λ , creates,+ σ_1 , and since velocity, c, is constant, long and short period T, or low and high, f, varies and a vector with Low energy $E=h.f$ at Red, (Red-shift) → low f = 400-484THz , long $\lambda = 620-750$ nm (Blue-shift)→ high f = 606-668THz ,short $\lambda = 450-495$ nm and High energy since $E = h.f$ at Blue.

In this way Light is

- 1) $s = Particle$, is the Photon, and wavelength $s = \lambda = 380-780 \text{ nm} = (3,8-7,8).10^{-7}$ m and as,
- 2) as Wave, is the Stationary Electromagnetic fields $E, P = \nabla i \times D i$ and it is of the Wave nature force where $\nabla i = \bar{v} = \lambda f = \lambda/T$, and since also Light is quaternion → [q = s+∇i]. The Stationary Wave in wavelength, $s = \lambda$, means that, since Photon is the only Electric Displacement field $D=\epsilon.E+P$, then in the rate of change is alternately in terms of The Electric field ($\partial P/\partial t$) and The Magnetic field ($\partial E/\partial t$), i.e. for Low energy Red-shift and for High energy Blue-shift as Wave, and then wavelength $\lambda = s =$ the Particle.

Since also frequency $f = 1/T$ and energy $\bar{v}=E=h.f$, then Cycloid motion Controls constancy of Energy by changing velocity, $\bar{v} = \bar{w}.r$, and period, T, of monads.

Einstein failed to see this reality and to explain the WHY →Wave nature, is the Intrinsic Electromagnetic

Wave of Particles and speed of light is constant in a Stress-Strain System with (Red-shift, as low, f, and-Blue-shift, as high, f,) Photon to be as Particle and Wave also, but considering constancy of light as an axiom from which he derived the rest of his theory of GR. . The Basic reason is the Hyperbolic geometry which defines, great circles as lines, and thus deeply induced in Planck's cavity. [38]

Intrinsic Stationary Wave of a Removal Source F (14)

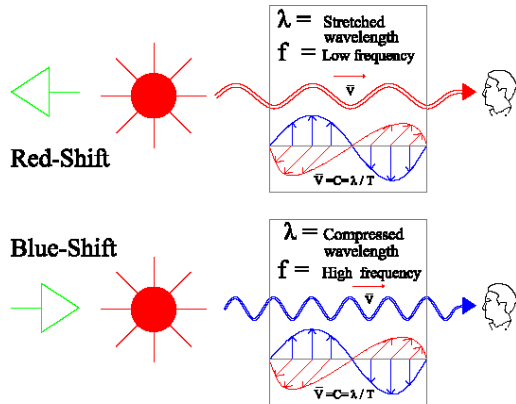


Fig. 14 : Intrinsic Stationary Wave of a Removal Source V(f)

f. Gravity as Curvature

GR of Einstein assimilates gravity as the curvature in space-time and not as Force and this based on Elliptic geometry, by contrast, stating that, all lines through a point M and parallel to a line AB intersect line.

In Elliptic geometry the two lines "curve toward" each other and eventually intersect. The simplest model for Elliptic geometry is a sphere, where lines are "great circles". For any great circle (which is not a straight line) and a point M which is not on the circle all circles through point M will intersect the circle. In elliptic geometry the three angles of a triangle add greater than 180°, without referring that triangle is not in Plane, but in the Sphere (spherical triangle). This omission created the wrong elliptic geometry and all others that follow.

Assuming the postulate of Relativity, c = constant, was valid without restrictions, this would imply that all forces of nature must be invariant under Lorentz transformations in order that principle be rigorously and universally true.

Also say that an object flying pass a massive object, the space time is curved by the massive object.

Remarks (f):

It is was proved in [32-39] that from any point, M, not on line AB can be drawn one and only one parallel to AB, [39] which parallel doesn't intersect line, so the Elliptic Geometry must be revised and also in [36-37] Gravity is force $[\nabla_i = 2(wr)^2]$ in the Medium-Field Material-Fragment $|\pm s^2| = (wr)^2 = [MFMF]$ which is the base for all motions .

This force is acting on Medium Field by having as wavelength the Stationary Breakage $(1-2) = \pm |[(w \cdot r)^2]|$ which consist the Material points, and on all moving Material wavelength $\lambda = (1)-(2)$ massive or not Particles.

- 1) Object in mechanics, may be the Material point (1) at Euclidean point (1), which is now Breakage $\pm [(w \cdot r)^2]$ magnitude in the Rest Homogeneously – Isotropically Quantized mass less Field $\pm |[(w \cdot r)^2]|$ and is the required coordinate System and base for all motions and forces.
- 2) Object in mechanics may be also the Material wavelength $\lambda = (1)-(2)$ in the $\{[Medium-Field Material Fragment] \rightarrow [\pm s^2] = |(\bar{w} \cdot r)|^2 = [MFMF] Field \leftarrow \}$ which is a standing wave in cavity (1)-(2) with scalar breakage $|\pm (\bar{w} \cdot r)^2|$ as medium (1)-(2) field, and (J1) as energy at point (1) and carried to point (2) by following the cycloids motion from (1) to (2) which is isochrones. Velocity, \bar{v} , during shifting is analyzed into two velocity vectors \bar{v}_1, \bar{v}_2 , which undergo vibrations causing two waves that represent the two Electric and Magnetic perpendicular components following the trajectory, in=(c1), out=(c2). On cycloid = (c) = $|A1-A2|$ is needed the isochrones time $T = \pi \cdot \sqrt{Rc/g}$ to reach end A2.

So, Gravity is the minimum attractive and biding Force $\nabla_i = 2(wr)^2$ on $[MFMF] = |(wr)^2|$ Base, which interact with all other particles, and also since acceleration $a = d\bar{v}/dt = (d\lambda/dt) \cdot f$ then for, $\lambda =$ any constant (or zero) and $\bar{v} \rightarrow 0$, then $f \rightarrow \infty$. This is the why the very strong gravitational fields are present and close to black holes where there $\bar{v} = \bar{c} = 0$.

Appealing space-time a Priori accepts the two elements, Space and Time, as the fundamental elements of universe without any proof for it, so anybody can say that this stay on air. It has been proofed [22-26] that any space AB is composed of points A, B which are nothing and equilibrium by the opposite forces $PA = -PB$ following Principle of Virtual Displacement.

Time (t) is the conversion factor between the conventional units (second) and length units (meter) . By considering the moving monads (particles etc. in space) at the speed of light, pass also through Time, this is an widely agreeable illusion.

g. Tidal Forces

Falling between small particles with very small mass and a rigid body with a large mass, change its shape with time, by stretching in the direction of the fall and press in the direction perpendicular to it, are what is called Tidal forces.

Remarks (g):

According to Bernoulli equation of energy conservation in, non-viscous, incompressible fluid in steady flow, Potential and Kinetic Energy per unit volume is constant at any point as, $p + \rho v^2/2 + \rho gh =$ constant, where, p = pressure, ρ = the density, v= the velocity,

h =the elevation and g =the gravitational acceleration, and (1)-(2)points lie on a stream line. The one-dimensional continuity equation gives, $p_1-p_2 = (\rho/2).(v_2^2-v_1^2)$ and $A_1v_1=A_2v_2$, therefore $A_2 < A_1, v_2 > v_1$ and $v_2 > v_1, p_2 < p_1$ or, decreasing area = increasing velocity and increasing velocity = decreasing pressure(Force). Spinning ball in airflow is a characteristic example, where velocity stretches in the velocity direction, and pressures are shrinking in perpendicular to velocity direction.

h. Equilibrium of Forces in monads

RESULTANCE'S EQUILIBRIUM IN EVOLUTE - TRAJE

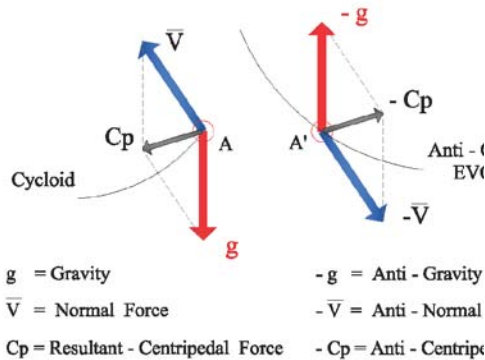


Fig. 15 : Equilibrium of the Resultant Forces ,in the Cycloid Intrinsic motion Wavelength ,and of any Removal Monad

It was shown in [25-30] that The mechanism of Energy Transport as (\bar{v}) through its quantized wavelength $|\lambda| = \bar{v}.T$, is a property of any standing wave, into the Medium $|\lambda| = (1)-(2)$, and involves the Absorption and Reemission of the wave quantized energy $J = (J_1)=(J_2)$ by the two neighbor edges (1) and (2) of the medium. The Absorption of energy causes, J_1 , within edge (1) to undergo vibrations as $[ds^2/dt^2] = -(g/4r).s$ which causes a new wave with the same frequency (because $f=E/h$) as the first wave but delaying the motion through the medium until Reemission by travelling, J_1 to J_2 , through this small region of space between edges (1) and (2) and once the energy of wave is reemitted by its neighbor edge (2) then mechanism is recycled. This mechanism is succeeded by the intrinsic property of the waves (\rightarrow quaternions, monads, vectors, Tensors) which is , the Stationary wave nature of Spaces, and works as follows, It was shown in [27] that on dipole $AB = [\lambda m, \Lambda]$ under the influence of Space Anti-Space forces $dP = PB-PA$ are created from forces $dP \perp$ Space lines the Static Force Field ,E, from forces $dP \perp$ Space lines the Static Force Field, P, where $P \perp E$, which then experience on any moving dipole AB with velocity \bar{v} , a total force $F = F E + F P = (\lambda m).E+(\lambda m).\bar{v} \times P$ which combination of the two types result in a helical motion, with stability demand $\rightarrow E = -(\bar{v} \times P) = -(\bar{v}.P) \perp$ which is the

alternative conservation of momentum $\Lambda^2/2\lambda m$, in the two perpendicular fields E, P .

In case $(\lambda m) = q$ then total force $F = F E + F P = q.E + q\bar{v} \times P = q.[E + \bar{v} \times P] \rightarrow$ which is Lorentz force in the Electromagnetic crossed fields E and P, with electric charge $q = \lambda m$ and both are the two beyond Gravity Fields interpreting the fundamental cause (effect) of motion, in small and large scales.

Remarks :

Since velocity $\bar{v} = \bar{w}.r$ and acceleration for aquaternion $z = (s + \bar{v}.\nabla i)$ is $a = [d^2z/dt^2] = (d/dt, w).(-wz, dz/dt + wxz) = 0$ and, and this because r and \bar{w} are constant , therefore velocity $\bar{v} =$ constant .

When element $d\bar{s} = A.DA = \bar{v}.t = \lambda T =$ constant $= \bar{c}.T$ then $ds^2 = dx^2+dy^2+dz^2 = (cT)^2$ which is the spatial equation of Space{ $d\bar{s}$ } and Energy { $\bar{v}.t = \lambda T = d\bar{s}$ }.

Since quaternion $= (i)^2 = [Energy]^2 = - [Space] =$ Anti-space $= [-(\Lambda \times \Lambda)/m \pm \Lambda \times \nabla i] = [\lambda , \pm \Lambda \times \nabla i] \rightarrow$ it is meaning that the massive mechanism Diffraction, λ , and the Energy mechanism Diffraction, $\pm \Lambda \times \nabla i$, are Interchangable.

A Particle with wavelength $\lambda = (1)-(2)$ and spin say, $h/2$, is consisted of two parts, The one because of the translational motion of speed \bar{v} , and the second of the, common circle, self-rotation velocity $V_c = \lambda^2/T = \lambda^2.f = [\sqrt{1-(v/c)^2}]^2.f = [1-(v/c)^2].f$. Energy $[\Lambda \times \nabla i] = (J_1)$ as velocity vector, \bar{v} , is the cross product of two velocity vectors \bar{v}_1, \bar{v}_2 or $\rightarrow \bar{v} = \bar{v}_1 \times \bar{v}_2$, with head at point (1) and analyzed , in a perpendicular to (1)-(2) directional , plane, into the two orthogonal velocity vectors \bar{v}_1, \bar{v}_2 which heads are at point (1). Energy J_1 is carried to point (2) by following the cycloid motion in $\lambda=(1)-(2)$. Following the above logic, the vector-quaternion Norm is kept constant by an intrinsic (in wavelength norm) isochrone (harmonic oscillation) because of the cycloidal motion, and independently of amplitudes (displacements, or strengths). i.e. Quaternion $q = [\lambda , \pm \Lambda \nabla i]$ with norm, wavelength $|\lambda|$ is a Standing wave (a plane Stationary wave) which preserve the constant position of magnitude $|\lambda|$ with the two edges as nodes independently of amplitude, with a period $T = [y/\Lambda / 2c]$ and $\Lambda = r.m.\bar{v} = r.\bar{p} = r.m.(\bar{w}.r)^2 = mr^2.\bar{w}^2$ depending on, \bar{w} , only (it is the spin) and thus forming the spherical standing waves .

Einstein`s theory of relativity, assumes the equivalence of all Inertial frames as well as that of constancy of light which needs experimental verification of all the intuitive including deductions.

General Relativity is depended on one axiom, that of Galilean Relativity and on non-Euclid geometries without any physical meaning and reality, and this because these are extreme of Euclidean.

The present article using the Euclidean geometry without any assumptions and definitions clearly *shows that*,

- 1) The origin of Space, through the Principle of Virtual Displacements, as the Inner distance of Space and Anti-Space.
- 2) The origin of Energy, through the Principle of Virtual Displacements, as the Work of the Inner Impulse distance of Space and Anti-Space.
- 3) The *minimum Quantized Space, Quantas*², in all quantized spaces, i.e. Particles, [MFMF] Field, moving vectors, free velocity monads, Material lines → Surfaces and bodies .
- 4) The *minimum Quantized Energy, Quanta*, $2s^2$, diffused in all quantized spaces.
- 5) The definition of Material Point as (\pm) Dipole Breakage in [MFMF] medium.
- 6) The definition of Material Object as the Wavelength λ , of the (\pm) Dipole of [MFMF] Field which is a standing Electromagnetic wave in beyond Planck`s cavity .
- 7) The time in Euclidean geometry is not distinguished, because time exists only in its confined -Plank's length level-and neither Space from Energy because -Energy exists as quanta on any first dimensional Unit AB - which connects the only two fundamental elements of Universe, that of points and that of energy.
- 8) The STPL line as the passage of particles from Absolute [S] Frame to all Relative [R] Frames is the Navel cord, the string of galaxies.
- 9) The geometrical Reasoning of Planck Length.
- 10) Time is designated as the meter of changes, or as the conversion factor, between time (s) and space (m) units and not essence of Space-energy Configuration.
- 11) The Geometries related to Euclidean by Lorentz factor, γ , consist, *Geometrical expression of Spaces and Anti-Spaces*.
- 12) The Cause and Events as the Energy quantization and the velocity Breakages as, masses, and velocity, \bar{v} , only as the Thrust of masses, (changes).
- 13) The Origin and the base of Gravity from [S] to[R]frame, and the Equations of the inner Electromagnetic wave.
- 14) The Structure of the Energy - Space Universe with the boundaries of General Relativity.
- 15) The Origin of Particles as velocity-Thrust - on

Breakages and the Breakages as the Fragments of the Space, Anti-Space collision.

- 16) The Origin of Color - forces from the Retardation and the Birefringence of Spaces.
- 17) The Dual nature of Monads, of wavelength $|\lambda|$ as Particle, and Wave as the Stationary Electromagnetic Wave in $|\lambda|$, which is an intrinsic property of the Cycloid motion of velocity, \bar{c} , and Spin, forming the plane and spherical standing waves which are <The Inner structure of Particles> .
- 18) The Cycloidal motion as the intrinsic property of vectors which is a Stationary wave on wavelength of vector, where < Poincot`s ellipsoid > becomes → cycloid Ellipsoid,
- 19) The mechanical relation between the speed of light and principal stresses, guided to, Permittivity, Permeability, in free space medium.
- 20) Michelson`s-Morley experiments cannot prove reality because in Planck`s cave occurs isochrones motions, and Gravity is the force (*energy*) which is connecting the Material points of the Medium with the constant light velocity \bar{c} . The Relative motion of moving systems through Stationary system can be detected only by the Tangential velocities $\bar{v} = \bar{\omega}.r$ on circumference of a cave, r , with radius $R > r$.
- 21) The equations of inners Structure of Gravity field and the stability of the whirling Space, Anti-space, the Spin, extended to monads.
- 22) The immense confusion in the basic ideas regarding the Quantized Energy-Space, *The Quanta*, → vanishes.
- 23) Manifold of mathematics from Astrophysics to Quantum mechanics have been progressively developed on Non-Euclid Geometries, resulting to Relativity`s Space-time confinement, unable to conceive the under Planck`s cavity energy existence is the content of this article.

X. GENERAL REMARKS

Applying all equations of Mechanics and Physics in Common circle (c) of radius, r_c , angular velocity $\bar{\omega}c$, then velocity on radius is $\bar{v}c = \bar{\omega}c.r_c$ and the reaction to this motion which is mass, m_c , is $m_c = v_c .vc = vc^2 = (\omega r)^2$.

Linear momentum $p_c = m_c.\bar{v}c$ and the resultant rotational energy $\Lambda = r_c.p_c = .r_c.m_c.\bar{v}c$ and then since work on circle is $W = p_c.L = p_c.(2\pi.r_c) = m_c.v_c.2\pi.r_c = \Lambda$, by solving to, r_c , and for constant velocity $v_c = c$

$$\text{then, } r_c = \Lambda / 2\pi.m_c.v_c, r_c = \Lambda / 2\pi.m_c.c \dots (a)$$

Applying equation (a) for the fundamental particles (monads) OFF the common circle, then magnitudes are transformed as,

$$\text{mass } (m)m_c \cdot \gamma = m_c \cdot [\sqrt{1-(v/c)^2}] \dots(b)$$

$$\text{radius } ,r_c, \text{ of cycloidal helix } \rightarrow r_c = \Lambda / 2\pi \cdot \gamma \cdot m \cdot c \dots(c)$$

Since, $m = E/c^2 = hf/c^2 = h/Tc^2$ (Einstein's de Broglie's),

$$\text{Radius } R_c = 2 \cdot r_c = 2 \cdot \Lambda / 2\pi \cdot \gamma \cdot m \cdot c = [h / 2\pi \cdot c \cdot \gamma (m = E/c^2 = hf / c^2)] = c / 2\pi \cdot \gamma \cdot f = [c \cdot T / 2\pi \cdot \gamma] = [2c / w \cdot \gamma]$$

$$[2c^3 / w(c^2-v^2)] \text{ and } r_c = c / w \cdot \gamma \dots(d)$$

$$\text{Period } T_c = 4\pi \cdot \sqrt{r_c / g} = \pi \cdot \sqrt{R_c / g} \dots(e)$$

$$\text{Length } L_c = \bar{v} \cdot T_c = [\sqrt{g} \cdot r_c] \cdot [4\pi \cdot \sqrt{r_c / g}] = 4\pi \cdot r_c = 4\pi c / w \cdot \gamma$$

= A1-A2, is the wavelength $\lambda = L_c \rightarrow$ from which Constant velocity $\rightarrow c = w \cdot \gamma \cdot r_c = w \cdot \gamma \cdot \lambda / 4\pi = \gamma \cdot L_c \cdot f_c / 2$

$\Lambda = h =$ Rotational energy (Spin),

where $\rightarrow \bar{v} =$ Velocity of particle in Inertia System [R],

$\bar{v} r = \sqrt{g} \cdot |r| =$ The Rolling circle center const-velocity

$c =$ The constant velocity of the System (and of Light)

$R_c = 2r_c =$ The radius of , Cycloidal helix,

$g =$ Gravity's force $2 \cdot (wr)^2$, acceleration,

$T_c =$ The intrinsic Cycloidal period, $\pi \sqrt{R_c / g}$

$c = \gamma \cdot L_c \cdot f_c / 2 =$ The relation between constancy(c) of Light, Laurence factor (γ), Wavelength ($\lambda = L_c$) and Cycloidal helix rolling circle frequency (f_c) \rightarrow [39].

Monad (Unit) $\bar{A}\bar{B}$ is the Entity and [A, B - $\bar{P}\bar{A}, \bar{P}\bar{B}$] is the Law, so Entities are embodied with the Laws.

Entity is quaternion $\bar{A}\bar{B}$, and law $|AB| =$ length of points A, B and imaginary part forces, $\bar{P}\bar{A}, \bar{P}\bar{B}$ or fields By definition $i = \sqrt{-m \cdot 1}$ and $(-m1)^2 = -1m$ i.e.

$[Energy]^2 = - [Space] =$ Anti-space and since also exists $\Lambda \times \Lambda = -(-m \cdot 1)^2 = \pm \Lambda \cdot \nabla i$, the basic equation of quaternion becomes $[-(\Lambda \times \Lambda) / m \pm \Lambda \times \nabla i] = [\lambda, \pm \Lambda \times \nabla i]$ i.e. wavelength $\lambda = -(\Lambda \times \Lambda) / m$ where $m =$ a constant depending on reactions to present or other conditions.

Applying this in energy cavities then $e^{\wedge} - i$

$$[(\pi/2) \cdot b]^2 = e^{-i \cdot (\frac{2\pi}{2}) \cdot b} = e^{-i \cdot (\pi) \cdot b} = \rightarrow i \cdot e.$$

The massive mechanism Diffraction and the Energy mechanism Diffraction are Interchangeable as follows,

$$e^{-i \cdot [1,78 \cdot 10^{-17}]^2} = e^{-i \cdot [3,56 \cdot 10^{-14}]^2}, \text{ and for Relativity massive Energy } (\Lambda \times \Lambda) = (-m \cdot i) \times (-m \cdot i) = m(i)^2 = -m(\bar{v})^2 = -m\bar{v}^2, \text{ where the imaginary part } i = \bar{v}, \text{ i.e.}$$

a) *Space acquires energy*

Applying quaternion equation $[-\nabla \Lambda, \nabla \times \Lambda] = 0$ for point, O, and constant velocity, \bar{c} , then $[-\nabla c, \nabla \times c] = 0$ where $[-\nabla c] \perp [\nabla \times c]$ meaning that, it is a mechanism that instantly transports breakage masses dynamically and perpendicularly to all Inertial frames Layers. [26]

In extrema, paragraph (7.8), was found the relation $c^2 \cdot \epsilon \cdot \mu = 1$ which is the known relation between the speed of light and, Permittivity, Permeability, in free space medium.

XI. CONCLUSIONS

The dynamics of any system =Work= Total energy, is transferred as generalized force $Fe \rightarrow t \rightarrow$

$Fe = \partial W / \partial (\bar{\delta} \bar{r} \cdot c)$, $(\bar{\delta} \bar{r} \cdot c) = \bar{v} \cdot \bar{\delta} t = [\bar{v} \bar{c} + \bar{w} \cdot \bar{r} \bar{n}] \bar{\delta} t =$ (Translational + rotational velocity) $\cdot \bar{\delta} t$ and $Fe = \bar{v} \bar{c} \cdot (\partial W / \partial \bar{\delta} t) + \bar{w} \cdot \bar{r} \bar{n} \cdot (\partial W / \partial \bar{\delta} t) \rightarrow$ Translational kinetic energy + Rotational kinetic energy \rightarrow

- To the Elastic material Configurations, as Strain energy and is absorbed as Support Reactions and displacement field $[\nabla \epsilon (\bar{u}, \bar{v}, \bar{w})]$ upon the deformed placement, (where these alterations of shape by pressure or stress is the equilibrium state of the Configuration $G \cdot \nabla^2 \epsilon + [m \cdot G / (m-2)] \cdot \nabla [\nabla \cdot \epsilon] = F$), [5] and [14-16].
- To Solid material Configuration, as Kinetic (Energy of motion \bar{v}) and Potential (Stored Energy) energy by displacement (the magnitude of a vector from initial to subsequent position) and rotation, on the principal axis (through center of mass of the Solid) as ellipsoid, which is mapped out, by the nib of vector $(\bar{\delta} \bar{r} \cdot c) = [\bar{v} \bar{c} + \bar{w} \cdot \bar{r} \bar{n}] \bar{\delta} t$, as the Inertia ellipsoid [Poincot' ellipsoid construction] in [S] frame which instantaneously rotates around vector axis $[\bar{w}, \phi]$ with the constant polar distance $\bar{w} \cdot Fe / |Fe|$ and the constant angles θ_s, θ_b , traced on, Reference [R, F] cone and on Absolute frame [S, F] cone, which are rolling around the common axis of \bar{w} vector, without slipping, and if Fe , is the Diagonal of the, *Energy Cuboids*, with dimensions a, b, c following Pythagoras conservation law, where the three magnitudes (J, E, B) of Energy-state follow Cuboids, Plane, or Linear Diagonal direction and If Potential Energy is zero then vector \bar{w} , is on the surface of the Inertia Ellipsoid. From the theory of elasticity the equilibrium of a surface Configuration, in an Isotropic material, obeys the equilibrium equation $\mu \cdot \nabla^2 u + (\lambda + \mu) \cdot \nabla \cdot [\nabla \cdot u] = 0$. [23].
- To Quaternion's Extensive Configuration, as New Quaternion's (with Scalar and Vector magnitudes). Points in Space carry A priori the work $W = \int A \cdot B [P \cdot ds] = 0$, where magnitudes P, dscan be varied leaving work unaltered. Diffusion

(decomposition) of energy follows Pythagoras conservation law where the three magnitudes (J,E,B) of Energy-State follow the Cuboids, Plane, or Linear Diagonal.

4. To Space conserved Extensive property Configuration (Continuum), as Kinetic (3-current motion) and Potential (the perpendicular E,P Stored as curl fields) energy by displacement (the magnitude of a vector from initial to the subsequent position) and rotation. Energy is thus conserved in, E and P, curled Stationary fields of monad's wavelength, and on quaternion's norm. For more extension [40].
5. The STPL line as the passage of particles from Absolute [S] frame to all Relative [R] Frames is the Navel cord, string of galaxies [28].

XII. ACKNOWLEDGMENT

The reason of writing this scanty articles is because *I am Engineer*, and my deep intuition contradicts to some very acceptable conceptions. *The Natural Constants in Physics become from the Laws and Geometry constants are the meters of Laws. Physical constants represent the quantization of Energy in the different levels of Spaces.*

Sequence that Space was created before matter \rightarrow Human mind, in front of this dilemma created the outlet in Religious and the myth of Big-Bang. Because in [S] System Centrifugal velocity is constant, Simultaneity in [R] System is such that is possible to exist in them, the geometrical expression of Lorentz factor, γ , and the related System-Spaces of Relativity to be placed as a part of the whole Euclidean geometry. For a rotating system like the reference [R] with constant velocity, c , is possible to be $c < c' \rightarrow \infty$ and then this would move faster than, c , velocity of light. [27-29]

By Considering breakages as, masses, being off the system [S] and under the constant velocity, c , as Action, then Dark matter and Dark energy is produced and the known formulas of GR for masses and Energy are Geometrically produced without any set restrictions, but from $\rightarrow \sec.\phi = \gamma$ only.

Because break ages travel in [R] = {DA-PA} system (frame) with the constant velocity, c , and so are in rectilinear motion between them, they occupy zero acceleration and thus can be converted to measurements in another by the simple Galilean transformations, because physical laws and electrodynamics take the same form in all inertial systems.

By contrast Inertial frame [R] is the frame of reference which describes the Energy-Space homogeneously and isotropically and in a genius manner, where arbitrary number, t = time is defined as the convention factor between time units (second) and

length units (meter), and this because of geometrical proportionality relation $\rightarrow \sec.\phi = \gamma = (ct/vt)$.

In summary, my personal confidence is that nature is produced from Euclidean Geometry only, following Principle of Virtual work and not any other logical starting point.

The essential difference between Euclidean and the non-Euclidean geometries has been attentive in the very specially written article (ordered) [32] and recently in [38] for the nature of the parallel lines, a unique Postulate directly connected to the physical world. Now, [STPL] line (doubled cylinder in spatial CS) is the creation mould for Particles which are created between all Space-Levels. Since Spaces are directly connected and consist only one, the present article is the proof to what is referred.

REFERENCES RÉFÉRENCES REFERENCIAS

1. Matrix Structure of Analysis by J.L.MEEK library of Congress Catalog 1971.
2. Der Zweck im Rect by Rudolf V. Jhering 1935.
3. The great text of J. L.Heisenberg (1883-1886) and the English translation by Richard Fitzpatrick.
4. Elements Book 1.
5. Wikipedia.org, the free Encyclopedia.
6. Greek Mathematics, Sir Thomas L.Heath – Dover Publications, Inc, New York. 63-3571.
7. [T]Theory of Vibrations by William T. Thomson (Fourth edition).
8. A Simplified Approach of Squaring the circle, <http://www.scribd.com/mobile/doc/33887739>.
9. The Parallel Postulate is depended on the other axioms, <http://vixra.org/abs/1103.0042>.
10. Measuring Regular Polygons and Heptagon in a circle, <http://www.scribd.com/mobile/doc/33887268>.
11. The Trisection of any angle, <http://vixra.org/abs/1103.0119>.
12. The Euclidean philosophy of Universe, <http://vixra.org/abs/1103.0043>.
13. Universe originated not with BIG BANG, <http://www.vixra.org/pdf/1310.0146v1.pdf>.
14. Complex numbers Quantum mechanics spring from Euclidean Universe, <http://www.scribd.com/mobile/doc/57533734>.
15. Zeno's Paradox, nature of points in quantized Euclidean geometry, <http://www.scribd.com/mobile/doc/59304295>.
16. The decreasing tunnel, by Pr. Florentine Smarandashe, <http://vixra.org/abs/111201.0047>.
17. The Six-Triple concurrency line – points, <http://vixra.org/abs/1203.0006>.
18. Energy laws follow Euclidean Moulds, <http://vixra.org/abs/1203.006>.
19. Higgs particle and Euclidean geometry, <http://www.scribd.com/mobile/doc/105109978>.

20. Higgs Boson and Euclidean geometry, <http://vixra.org/abs/1209.0081>.
21. The outside relativity space – energy universe, <http://www.scribd.com/mobile/doc/223253928>.
22. Quantization of Points and of Energy, <http://www.vixra.org/pdf/1303.015v21.pdf>.
23. Quantization of Points with and Energy on Dipole Vectors and on Spin, <http://www.vixra.org/abs/1303.0152>.
24. Quaternion`s, Spaces and the Parallel Postulate, <http://www.vixra.org/abs/1310.0146>.
25. Gravity as the Intrinsic Vorticity of Points, <http://www.vixra.org/abs/1401.0062>.
26. The Beyond Gravity Forced fields, <http://www.scribd.com/mobile/doc/203167317>.
27. The Wave nature of the geometry dipole, <http://www.vixra.org/abs/1404.0023>.
28. The Outside Relativity Space – Energy Universe, <http://www.scribd.com/mobile/doc/223253928>.
29. Planks Length as Geometrical Exponential of Spaces, <http://www.vixra.org/abs/1406.0063>.
30. Universe is built only from Geometry Dipole, <http://www.scribd.com/mobile/doc/122970530>.
31. Gravity and Planck`s Length as the Exponential Geometry Base of Spaces, <http://vixra.org/abs/1406.0063>.
32. The Parallel Postulate and Spaces (IN SciEP).
33. The Origin of the fundamental particles in Planck`s Confinement. On Scribd & Vixra (FUNDAPAR.doc).
34. The fundamental particles of Planck`s Confinement. www.ijesi.com (IJPST14-082601).
35. The origin of The fundamental particles www.ethanpublishing.com(IJPST-E140620-01).
36. The nature of fundamental particles, (Fundapa.doc).www.ijesit.com – Paper ID: IJESIT ID: 1491.
37. The Energy-Space Universe and Relativity IJISM, www.ijism.org – Paper ID: IJISM – 294.
38. The Parallel Postulate, the other four and Relativity (American Journal of modern Physics, Science PG - Publication group USA), 1800978 paper.
39. Space-time OR Space-energy universe (American Journal of modern Physics, science PG – Publication group USA), 1221001 paper.
40. The Origin of, Maxwell`s-Gravity`s, Displacement current.
41. [M] The origin of, Maxwell`s Postulates.
42. [M] The Quantization of Points and Potential and the unification of Space and Energy with the universal principle of Virtual work, on Geometry Primary dipole.

Biography

Markos Georgallides comes from Cyprus and currently resides in the city of Larnaca, after being expelled from his home town Famagusta by the Barbaric Turks in August 1974. He works as a consultant civil and

architect engineer having his own business. He is also the author of numerous scholarly articles focusing on mathematical and physics related subjects. He obtained his degree from the Athens, National Polytechnic University [NATUA] and subsequently studied in Germany with specialization in constructions (WAYSS & FREYTAG – Frankfurt A.M. Neue Mainzer strasse 59, Frankfurt), and Principles of Photoelasticity.



GLOBAL JOURNAL OF SCIENCE FRONTIER RESEARCH: A
PHYSICS AND SPACE SCIENCE
Volume 15 Issue 3 Version 1.0 Year 2015
Type : Double Blind Peer Reviewed International Research Journal
Publisher: Global Journals Inc. (USA)
Online ISSN: 2249-4626 & Print ISSN: 0975-5896

IRNSS Satellite Parameter Estimation using Combination Strategy

By Babu R, Prasanta Mula, S. C. Ratnakara & A S Ganeshan

Indian Space Research Organisation, India

Abstract- Indian regional Navigation Satellite system (IRNSS) is going to be an independent, indigenous navigation satellite system fully controlled by India, planned by ISRO. A system was designed of regional navigation satellite constellation, as an alternate to GPS constellation, for providing space based navigation support to various land, sea and air navigation users over the Indian region. The proposed IRNSS constellation consists of 7 satellites (3 in GEO and 4 in inclined GSO with 29 deg inclination). The continuous visibility of GEO and GSO satellites for near-equator regions provides a promising alternative for regional navigation. The Signal In Space (SIS) broadcasts satellite ephemeris in quasi keplarian elements and satellite clock coefficients which forms the primary navigation parameters generated from navigation software located at INC (ISRO Navigation Centre), bylalu, India. The determination of these parameters is performed by two types of technique, batch least square (BLS) and Extended Kalman Filter (EKF).

Keywords: *batch least square (BLS), extended kalman filter (EKF), signal in space (sis), line of sight (LOS), user equivalent range error (UERE).*

GJSFR-A Classification : FOR Code: 020109



Strictly as per the compliance and regulations of :



IRNSS Satellite Parameter Estimation using Combination Strategy

Babu R ^α, Prasanta Mula ^σ, S. C. Ratnakara ^ρ & A S Ganeshan ^ω

Abstract Indian regional Navigation Satellite system (IRNSS) is going to be an independent, indigenous navigation satellite system fully controlled by India, planned by ISRO. A system was designed of regional navigation satellite constellation, as an alternate to GPS constellation, for providing space based navigation support to various land, sea and air navigation users over the Indian region. The proposed IRNSS constellation consists of 7 satellites (3 in GEO and 4 in inclined GSO with 29 deg inclination). The continuous visibility of GEO and GSO satellites for near-equator regions provides a promising alternative for regional navigation. The Signal In Space (SIS) broadcasts satellite ephemeris in quasi keplarian elements and satellite clock coefficients which forms the primary navigation parameters generated from navigation software located at INC (ISRO Navigation Centre), bylalu, India. The determination of these parameters is performed by two types of technique, batch least square (BLS) and Extended Kalman Filter (EKF). A combination of these strategies is being adopted in IRNSS to broadcast the primary navigation parameters. The BLS based navigation parameters are generated with longer validity period whereas the EKF based outputs are generated with short period validity. The main reason for this combination strategy is to limit the outage duration of satellite as minimal as possible under all circumstances. The events are triggered depending upon the anomalies that occur in SIS, mainly due to onboard frequency jumps and station keeping operations. The most facilitated important fact is that the IRNSS satellite are continuously visible to monitoring and control centre and thus able to uplink the updated navigation parameters as and when required

based on the deviation from User Equivalent Range Error (UERE) as monitored through SIS from IRNSS Reference station's Line of sight (LOS).

In this paper we have discussed the combination strategy and how user equivalent range error is mitigated during anomalous events and results.

Keywords: batch least square (BLS), extended kalman filter (EKF), signal in space (sis), line of sight (LOS), user equivalent range error (UERE).

I. INTRODUCTION

The IRNSS (Indian Regional Navigation Satellite System) is an initiative to build an independent Regional Navigation Satellite System based on a constellation of 3 Geo-stationary (GEO) and 4 Geo synchronous (GSO) satellites. The first satellite (IRNSS-1A) was launched in July 2013 and the second (IRNSS-1B) on April 4, 2014, the third satellite IRNSS-1C on 16 October 2014. Currently three satellites are in space, IRNSS-1A (longitude crossing 55degree, inclination 29degree, Right Ascending Node (RAAN) 130degree), IRNSS-1B (longitude crossing 55degree, inclination 29degree and RAAN 310 degree) and IRNSS-1C (longitude crossing 83 degree with inclination 5degree). The 8 (IRIMS (IRNSS Range and Integrity Monitoring Station) are currently operational. The below plot shows the orbit determination IRIMS stations and IRNSS satellites location.

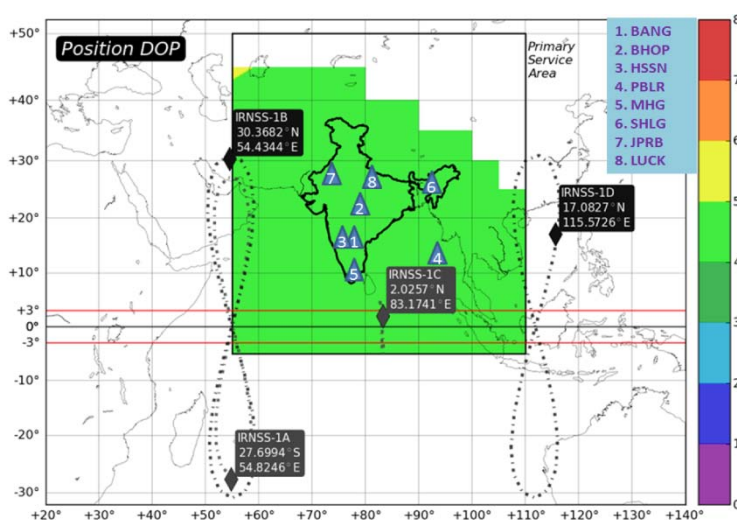


Figure 1 : IRIMS Station and IRNSS satellite location (Typical Snap Shot)

Author ^{α σ ρ ω}: ISRO Satellite Centre (ISAC), Bangalore, India.

e-mail: rbabu@isac.gov.in, prasanta@isac.gov.in,

ratnakar@isac.gov.in, asganesh@isac.gov.in

The IRNSS Network Timing Facility (IRNWT) maintains the precise and stable IRNSS time using an ensemble of atomic clocks that includes Hydrogen Master and Caesium clocks. It will be aiding the user position through 7 IRNSS satellites. The IRIMS (IRNSS Range and Monitoring Stations) continuously provides the one-way ranging of the IRNSS satellites to estimate and monitor the satellite position and satellite clock offset with respect to IRNSS system time. Precise Orbit determination for Geostationary and synchronous satellites from observations remains a key operation for the emerging regional navigation satellite system due to

its minimal relative motion of the satellite with ground reference stations. The challenge is the ability to accurately determine the current position and velocity of the satellite along with onboard clock offset. These estimated state parameters (Ephemeris, clock bias and drift) needs to be predicted for the future which is then broadcast to the users to provide independent navigation solution in the service area of IRNSS, primarily within Indian Land mass. The following figure shows IRNSS satellites location and all the satellite beam points at 85degree longitude with 5 degree latitude.

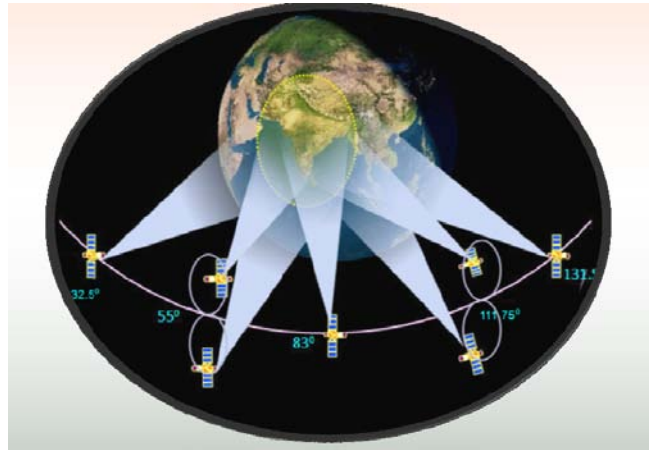


Figure 2 : IRNSS constellation

All useful orbit determination methods produce orbit estimates, and all orbit estimates have estimation error because of input variation. Hence what methods can obtain best solution? There are several choices to make from available orbit determination methods. Should we prefer sequential methods to batch methods? One way to improve Orbit Determination (OD) of IRNSS satellites is to make use of a hybrid estimation techniques, this has been accomplished by applying the both estimation. This strategy provided substantial improvements in accuracy and convergence over the traditional techniques used in the existing orbit determination techniques. This technique is validated with real measurements and operational at INC.

II. ORBIT DETERMINATION METHOD

Two types of technique are used in IRNSS Navigation software for generation of primary parameter estimation. Though both these methods BLS and EKF are commonly used estimation process, here based on the occurrence of events a combination strategy is used were one compliments the other with inputs. In this section we discuss about both the estimation technique employed in IRNSS.

In BLS, we use multi days of data to estimate the parameter. The estimation parameters includes receiver clock coefficients of all reference stations, satellite state vectors, solar radiation pressure

coefficients and satellite clock coefficients with respect to IRNSS system time. During the signal travel from transmitter to receiver, the measurement undergoes different error sources. After modeling and removal of medium errors, the main error contribution remains in each LOS is the error due to onboard and receiver clock. The separation of these errors from each LOS, mainly clock and orbit separation becomes cumbersome in simultaneous estimation. Thus differencing techniques were adopted to overcome.

The differencing techniques used to estimate receiver clock, satellite clock and satellite state vectors along with SRP coefficients, by holding and estimating the other in each of the process. By this method simultaneous estimation is avoided and hence estimation of all parameters is accurate in separation of errors.

But the limitation of the BLS comes in the event of clock jump, since the measurement data used for estimation contains the onboard clock frequency variation as shown in Figure[8-10]. Then the resultant satellite clock coefficients if obtained in this method will be inaccurate, also if parameters uplinked the user solution will also be erroneous.

In such events the new set of uplink parameters is estimated using EKF, since the sequential process depends only on the current measurements. Thus the clock coefficients obtained from this estimation process

is more realistic than the other method. In order to compute the updated clock biases state vector is held fixed and used from previous estimate of BLS. Under nominal conditions both these methods yields results, and at every instant EKF results were compared with BLS estimates and if found to be exceeding certain threshold EKF is reinitialized. Thus EKF is controlled and aligned with BLS, also the uplink parameters are generated and broadcasted with frequent update intervals and validity. The process noise and measurement noises [10] were obtained from adaption process. The limitations of the EKF based estimated solution is assumed to be poorer for long duration propagation because of the slow varying relative motion between the satellite and receiver geometry. Thus the broadcast parameter from EKF solutions is valid for shorter duration of about 900seconds and thus gets updated frequently during such onboard satellite clock anomaly event occurrence.

III. PROPAGATION MODEL

The two estimation techniques uses two types of numerical integration techniques namely Runge Kutta 4th order (RK4) and Adams-Bashforth-Moulton Method 12th order (ABM) method. In EKF for satellite state vector prediction RK4 is employed for simplicity and complexity reduction for real time usage. Whereas BLS uses ABM technique for long duration propagation under normal behaviour of range measurements.

The satellite is usually assumed to be influenced by a variety of external forces, including gravity, solar radiation pressure, third-body perturbations, Earth tidal effects, and general relativity in addition to satellite propulsive manoeuvres. The complex description of these forces results in a highly nonlinear set of dynamical equations of motion. The IRNSS orbits are propagated by numerically integrating, gravitational accelerations due to the Earth, Moon, Sun and other solar planets, together with the accelerations due to solar pressure. The gravity model used is of the order of 20x20 EGM-2008 model. The predicted positions of the Earth, Moon, Sun and other planets such as Venus and Jupiter are from JPL DE405 ephemeris. The solar pressure model used is (SPIRS) Solar pressure model for Indian regional satellite. The figure [3] shows the typical acceleration acting on the IRNSS satellites. The IRNSS satellites orientation is maintained in such a way that the sun is always contained in positive yaw and negative roll plane. The other important mission aspect is that the satellite under goes flipping twice a day and positive roll direction of the satellite never allowed to facing the sun as atomic clocks are mounted in the positive roll panel. The following figure [4] represents the IRNSS spacecraft body axis definition.

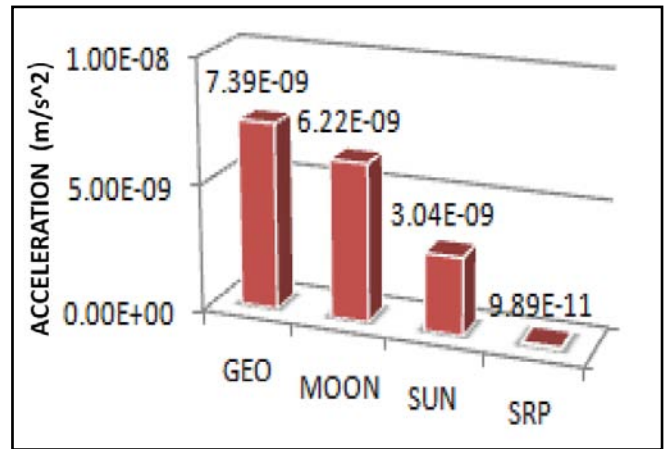


Figure 1: Typical Acceleration Magnitude Acting on IRNSS satellite

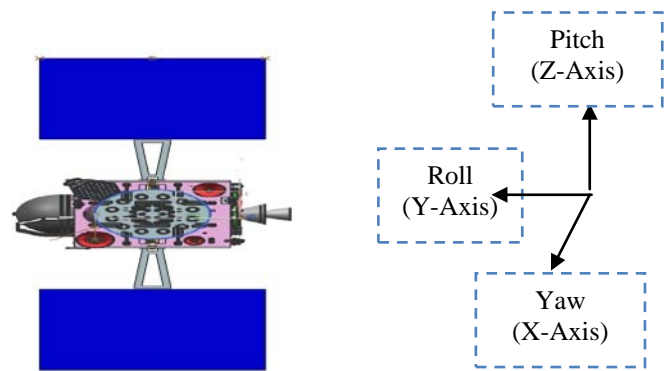


Figure 2: IRNSS Spacecraft Body Axis

IV. RESIDUE COMPUTATION

Estimation technique is based on minimization of residue by iterative update of state parameters. In orbit determination method the residue is difference between observed range measurement and computed range measurements. To compute range residue to the computed range sum of all measurement error models are added. The error includes station displacement, sagnac effect, relativity effect, lonospheric delay, troposphere delay, receiver and satellite clock error, satellite and receiver hardware delay, phase centre offsets. Firstly the smoothed ionospheric free measurements are obtained from observed range using code carrier smoothing technique with dual frequency (L5 and S) measurement combination and ambiguity resolution. The accuracy of the estimation technique depends upon the accuracy of measurement error model and quality of the measurements. Typical range residues from all IRNSS reference stations are shown in figure [5-7].

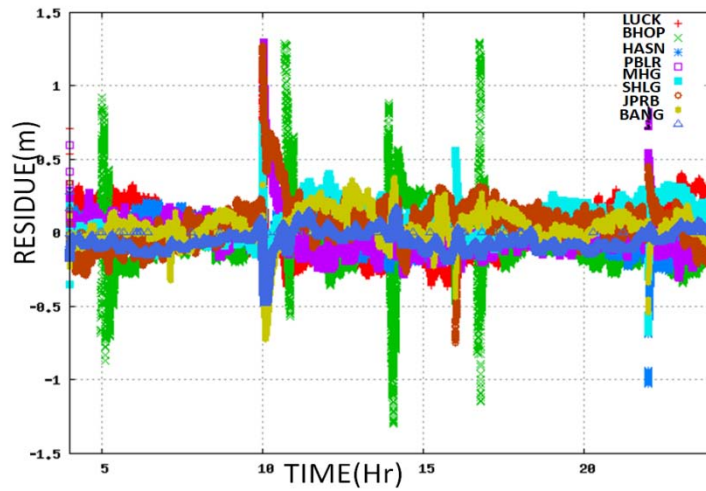


Figure 3 : Range Residue for IRNSS-1A satellite using all IRIMS stations

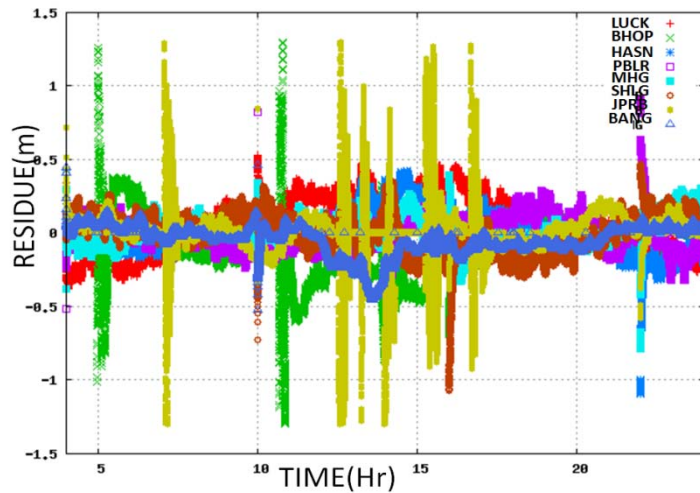


Figure 4 : Range Residue for IRNSS-1B satellite using all IRIMS stations

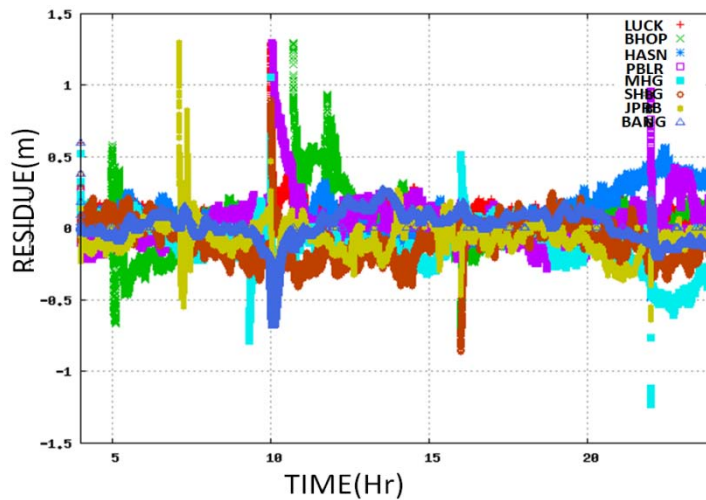


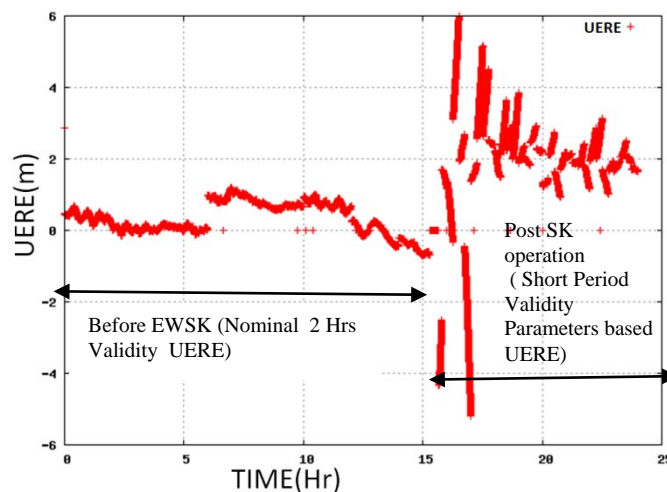
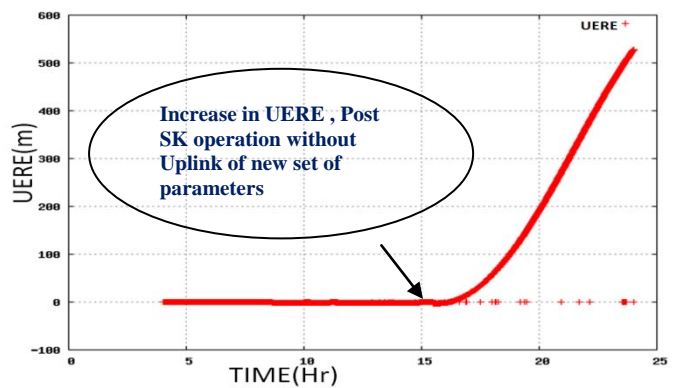
Figure 5 : Range Residue for IRNSS-1C satellite using all IRIMS stations

V. STATION KEEPING OPERATION AND ONBOARD ANOMALIES

The broadcast navigation parameters becomes obsolete during sudden variation in the measurements occurs. In the event of pre-defined station keeping operations and when sudden anomalous behaviour of the clock jumps occurs such as phase or frequency jump happens, the user gets affected due to large measurement variations. On such occasions the user has to receive updated navigation parameters. Like all other satellites, the IRNSS satellite has to be maintained in the window of 0.1 deg Equatorial from its desired longitude location. Since IRNSS works on minimum satellite constellation design (7satellites), outage of single satellite will increase the desired Dilution of Precision (DOP). These make the ground operations challenging in minimisation of the outage duration. In the first part of the section describes the station keeping (SK) operations and estimation strategy. For IRNSS satellites the station keeping operations were carried out regularly within 30-45 days interval. These are East west station keeping (EWSK) operations with very small delta-V corrections. Thus during EWSK the user may experience loss of SIS due to attitude reorientations for SK operations.

In the event of SK operation as soon as the satellite reoriented towards the earth view, in order to limit outage duration as minimal as possible, new set of uplink parameters are uploaded just before the SK operations with appropriate delta-v corrections applied on earlier BLS estimates and on the propagated state

vectors. And when the signal emerges back after re-orientation, the EKF estimates the satellite state vectors holding clock parameters using the received measurements from all reference receivers. Thus the outage is minimised and frequent uplink of navigation parameters are being done with short validity period of about ~900seconds, with Issue of data (IODE) varying between 160 and 255. The uplink process continues in this mode until BLS accumulates sufficient hours of data post SK operations. Then after reception and accumulation of sufficient data BLS estimates updated satellite state vectors holding clock parameters. From there onwards the uplink of navigation parameters will be based on BLS with two hours validity and the process continues and becomes normal until multi days data available for all parameter estimation. The following graphs show the normal user equivalent range error during normal and post SK operations for IRNSS satellites.



The second part of the section deals with anomalous behaviour of onboard clock. The SIS encounters sudden change in range measurement variation in all LOS that emerges from a satellite, called satellite clock jump (in frequency or phase). In the event of this scenario the user using the predicted broadcast clock coefficients may not be valid yielding error in user

solution and increased user equivalent range error [11]. Several such phenomenons had occurred in operational IRNSS satellites. In IRNSS through telemetry, the relative performance of the onboard clock (primary and secondary) is monitored through phase meter data. The following figures [8-10] shows such frequency variations from relative phase meter data of onboard atomic clock.

Through Ground reference receiver measurements the jumps of the onboard were identified whether the jump is on primary or secondary. The figure [8-10] shows occurrence of jump on primary clock and its effect on UERE from one of the IRNSS reference station (IRIMS at Bangalore 13deg N 77 deg E location)

In the below figure [8] shown the relative clock jump variation between onboard RAFS for IRNSS-1C (SAT 03)

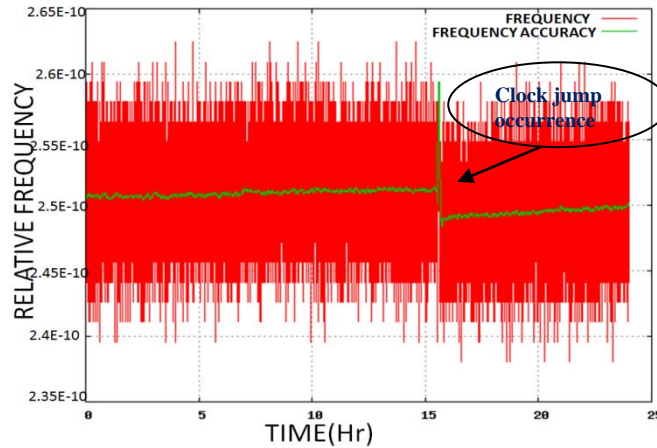


Figure 6 : Frequency jump for IRNSS-1C

The below figure [9] shown the relative clock jump variation between onboard RAFS for IRNSS-1B (SAT 02), In this satellite we can observe a phenomenon

such as the drift variation in the clock was increasing with time.

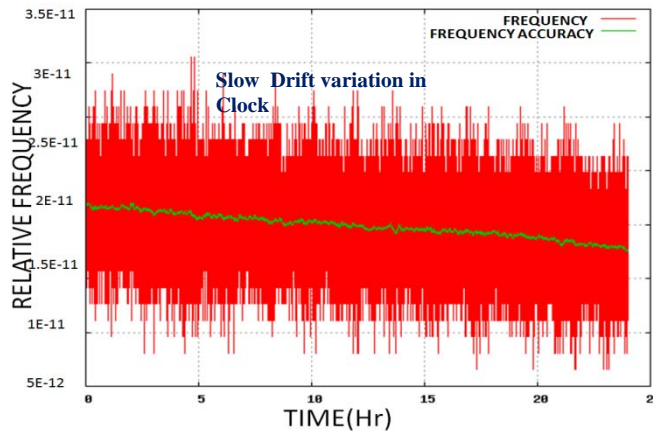


Figure 7 : Frequency Variation for IRNSS-1B

In the below figure [10] shown the relative clock jump variation between onboard RAFS for IRNSS-1A (SAT 01)

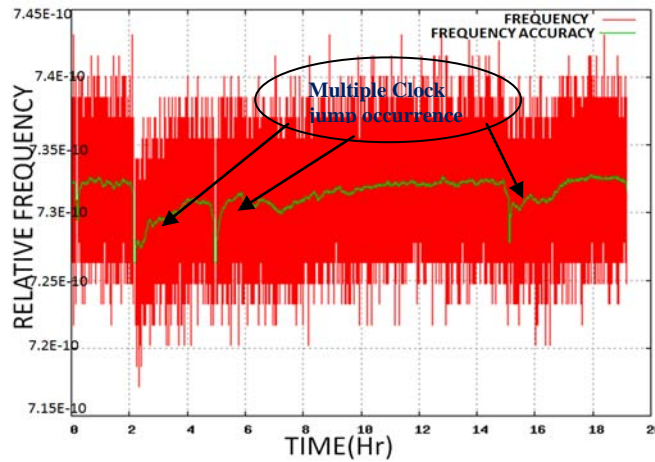


Figure 8 : Frequency Jump for IRNSS-1A

VI. IRIMS BANGALORE UERE

This section deals with accuracy of the IRNSS SIS. To access the accuracy of the IRNSS broadcast parameters measurements from one of the reference receivers (IRIMS Bangalore) were used for demonstration. These are dual frequency receivers at precise surveyed locations. The LOS measurement was treated for various measurement errors as discussed

earlier. The residual error due to broadcast signals is plotted in figures [11-13] over a typical day in nominal conditions and when there is no occurrence of any events. The estimated solution (satellite state vectors and onboard clock coefficients) is based on BLS with previous multi day's data.

Currently, three satellites (IRNSS-1A, IRNSS-1B and IRNSS-1C) are operational and broadcasts SIS.

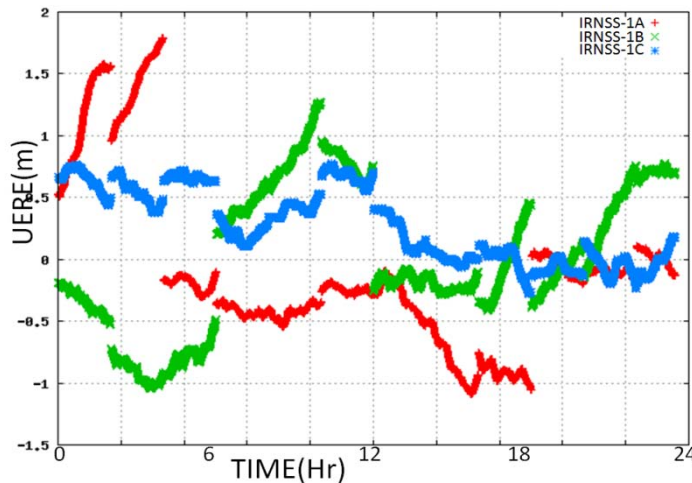


Figure 9 : LOS from BLS estimated state

The below figure shows the UERE variation along IRIMS Bangalore before and after EWSK operations on IRNSS-1A satellite. The satellite undergone SK operations after 11 Hrs. The uplink parameters were EKF based estimates with short period validity.



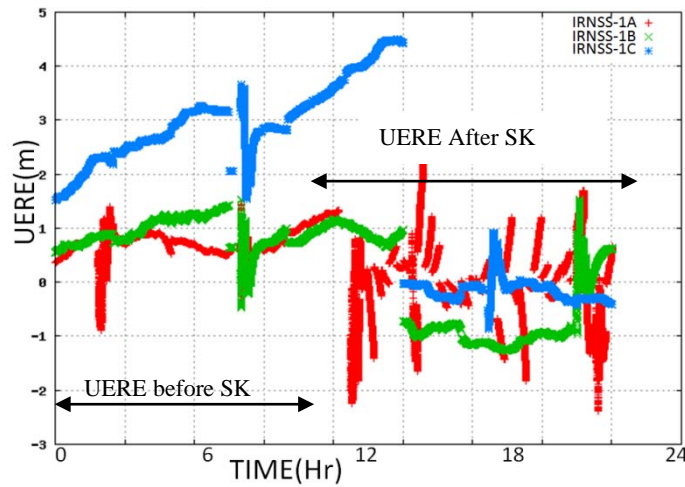


Figure 10 : LOS Error of IRNSS-1A Before and After manoeuvre

The below plots shows typical onboard primary clock jump occurrence on IRNSS-1A . The Jump was occurred at about 3.6 Hrs. The UERE of IRNSS Bangalore shows the effect of frequency jump , resulting

in deviation and sharp increase in UERE. The detection and uplink of new parameters were done from 6Hrs onwards. The updated clock coefficients were based on EKF estimates with short period validity.

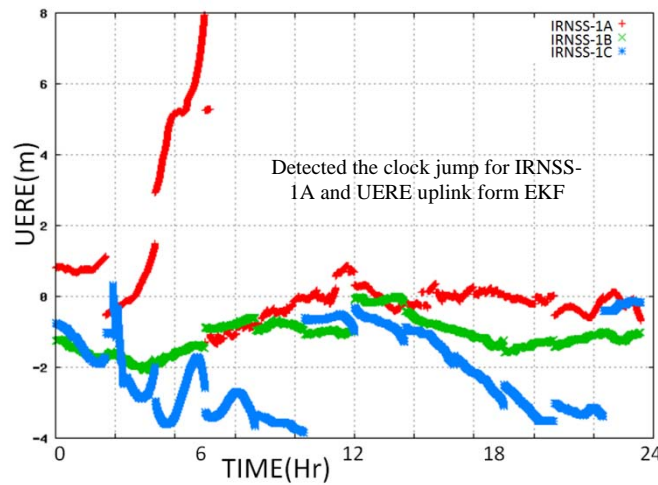


Figure 11 : LOS error after clock jump detection of IRNSS 1A

VII. SUMMARY

In the present paper two different Orbit determination methods were employed in determining the state parameters such as satellite state vectors and onboard clock parameters for IRNSS satellites. The Batch least square techniques is unfavourable during the occurrence and sudden inclusion of clock jump events. On the other hand EKF techniques under considered circumstances yields good solution but cannot be used for longer duration as the propagation error increases. Thus combinations of both the estimation strategies is employed in IRNSS navigation software, thus overcomes and mitigates the anomalous event limiting the user equivalent range error within certain acceptable limit. We have discussed both the technique and its utilization with the results from

operational satellites. Continuous efforts were being made to reduce the SIS error both in modelling, measurement handling and in improved strategy adaptation.

ACKNOWLEDGMENT

This work was supported by IRNSS projects at SNG lab. Wish to acknowledge all the Space Navigation Group members.

REFERENCES RÉFÉRENCES REFERENCIAS

1. IRNSS Comprehensive Review Document , ISRO-ISAC-IRNSS-RR-0992
2. Athans M. and Falb P. L, *Optimal Contro, Mcraw-Hill Book Co., Inc.*, New York, 1966.
3. Gelb A., 1966. Applied Optimal Estimation, Mcraw-Hill Book Co., Inc., New York.

4. Jerome R. Vetter, "Fifty Years of Orbit Determination: Development of Modern Astrodynamics Method", Johns Hopkins APL Technical Digest ,2007, Vol 27, No. 3.
5. James R Wright, Optimal Orbit Determination, 2002, Analytical Graphics, Inc. Printed by the American Astronautical Society.
6. Kalman, R. E., A New Approach to Linear Filtering and Prediction Problems, Journal of Basic Engineering, 1960, Vol 82, pp-35-45.
7. Price C. F., An Analysis of the Divergence Problem in the Kalman Filter, IEEE Trans on Automatic Control, 1968, Vol. AC -13, No. 6, pp. 699-702.
8. Psiaki, M., Backward smoothing Extended Kalman Filter, Journal of Guidance control and Dynamics, sept-Oct 2005, Vol. 28.
9. Sherma S, Non-Mean-Square Error Criteria, Trans. IRE Prof. Group on Information Theory, IT-4,1958, pp-585-589.
10. A. H. Mohamed, K. P. Schwarz, Adaptive Kalman Filtering for INS/GPS, Journal of Geodesy (1999) 73: 193-203.
11. Kavitha S Prasanta Mula Babu R Ratnakara S C Ganeshan A S, "Adaptive Extended Kalman Filter for Orbit Estimation of GEO Satellites" Journal of Environment and Earth Science, Vol.5, No.3, 2015





This page is intentionally left blank



GLOBAL JOURNAL OF SCIENCE FRONTIER RESEARCH: A
PHYSICS AND SPACE SCIENCE
Volume 15 Issue 3 Version 1.0 Year 2015
Type : Double Blind Peer Reviewed International Research Journal
Publisher: Global Journals Inc. (USA)
Online ISSN: 2249-4626 & Print ISSN: 0975-5896

New Type of Hypothetical Venusian Fauna Found at the *Venera-14* Landing Site

By L.V. Ksanfomality, A.S. Selivanov & Yu.M. Gektin

Corporate Values, Hungary

Abstract- The present study deals with one new form of hesperas, hypothetical living objects found on panoramas obtained on the Venus surface by the *VENERA-13* and *VENERA -14* landers in 1982. Novel hypothetical objects of Venusian fauna, called “amisadas”, may belong to terramorphic living forms. At a cursory examination the amisada’s body has the size of 12--15 cm. An amisada has a well-distinguished body that (when observed from above) resembles a fish. However, amisadas have organs of rest (and, probably, of motion) like reptiles. Their motions are very slow, same as of other objects of Venusian fauna. Three amisadas are seen on fragments of the *VENERA -14* panoramas. Despite the *VENERA-13* and *VENERA -14* landing sites separated by a distance of 900 km from each other, amisadas are found in both places. By virtue of a close position of the objects to the TV-camera lens, low noise intrinsic to *VENERA-14* images and sufficient number of the panoramas, relatively detailed images of amisadas were obtained permitting to follow their motion.

Keywords: *planet venus; venera missions ; astrobiology; space vehicles instruments.*

GJSFR-A Classification : *FOR Code: M19*



Strictly as per the compliance and regulations of :



New Type of Hypothetical Venusian Fauna Found at the *Venera-14* Landing Site

L. V. Ksanfomality^α, A. S. Selivanov^σ & Yu. M. Gektin^ρ

Abstract- The present study deals with one new form of hesperas, hypothetical living objects found on panoramas obtained on the Venus surface by the *VENERA-13* and *VENERA-14* landers in 1982. Novel hypothetical objects of Venusian fauna, called "amisadas", may belong to terramorphic living forms. At a cursory examination the amisada's body has the size of 12–15 cm. An amisada has a well-distinguished body that (when observed from above) resembles a fish. However, amisadas have organs of rest (and, probably, of motion) like reptiles. Their motions are very slow, same as of other objects of Venusian fauna. Three amisadas are seen on fragments of the *VENERA-14* panoramas. Despite the *VENERA-13* and *VENERA-14* landing sites separated by a distance of 900 km from each other, amisadas are found in both places. By virtue of a close position of the objects to the TV-camera lens, low noise intrinsic to *VENERA-14* images and sufficient number of the panoramas, relatively detailed images of amisadas were obtained permitting to follow their motion.

Keywords: planet venus; venera missions ; astrobiology; space vehicles instruments.

1. INTRODUCTION

Transmission of TV images is a commonly used modern method in both space research of celestial bodies and the search for extraterrestrial life in the Solar system. Nowadays, this method is intensely applied, e.g., for investigating the planet Mars. However, on the basis of the TV method, already 40 years ago, the Venusian surface was studied by the *VENERA* landers. In 1975, two landers of the Soviet *VENERA* series (missions 9 and 10) landed on the surface of the planet Venus. The TV investigation of the planet surface was one of the most advantageous experiments fulfilled on the planet's surface. Seven years later, in 1982, the *VENERA-13* and *VENERA-14* landers performed even more advanced studies. These experiments were aimed at studies of the most general features of the planet's surface. At that time nobody considered to search for traces of life in the Venusian carbon-dioxide atmosphere free of oxygen at a pressure of 9.2 MPa and temperature of 735 K. Now, the TV images obtained 40 and 33 years ago, were re-processed anew on the basis of modern codes, making images much more distinct. As a result, the images indicate the presence of strange objects that might be hypothetical forms of Venusian flora and fauna. Some of

the found objects are closely reminiscent of the forms of Earth's living organisms. The similarity phenomenon is called terramorphism. Other forms are unfamiliar.

The fundamental question of philosophy of all times is whether there is life outside the Earth. Nevertheless the *VENERA* results are quite sudden. Experiments in *VENERA* television photography [1, 2] yielded in about 40 panoramas (or their fragments) of the Venus surface at 4 landing sites. After re-processing the pictures revealed a dozen previously undetected strange objects that can attest to the fact that Venus does possess hypothetical life. Materials shown in this paper demonstrate experimental results that involve re-processing of the original panoramas, without any retouching or corrections. For the moment, it is impossible to prove that the objects are alive in fact because they cannot be touched. However, the opposite is true also, that nobody can place errors into the processing of the images. A sense of critical arguments boil down to the famous humorous statement of A.P. Chekhov, in his 'Letter to my neighbor-scientist': "this cannot be, because it never can be." Subconsciously, all positions of critics have been based on variations of the statement: only the Earth's conditions are suitable for life. Based on this idea, limited "habitable zones" are drawn in schemes of extra solar planet systems and are under the study of theoreticians. No other possibilities are considered.

During the 40 and 33 years that passed since the time of TV experiments employing *VENERA* landers (1975 and 1982), no similar experiments or missions to Venus have been performed by any space agency. In connection with the renewed interest in what was occurring during the experiment and to the discovery of manifestations of possible life revealed on some of the pictures, the remaining part of panoramas were re-examined too. A train of papers [3, 4 and others] published in 2012-14 presented some data on the hypothetical Venus fauna and flora that survives under physical settings that are radically different from the Earth's.

Author ^α: Space Research Institute of the Russian Academy of Sciences, Mosco. e-mail: ksanf@rssi.ru.

Author ^{σ ρ}: OAO Russian Space Systems, Moscow.

II. ON POSSIBLE EXISTANCE OF NON-TERRESTRIALS LIVING FORMS AND THEIR DETECTION

The existence of life on Venus, at first glance, sounds absurdly. Physical conditions on Venus are incompatible with terrestrial life at all. It may be reminded that the Venusian atmosphere almost entirely is composed of carbon dioxide (CO₂, 96,5%) and nitrogen (N₂, 3.5%). Cloud layers located highly in atmosphere consist of micron-size droplets of concentrated sulfuric acid. Surface temperature of Venus at its mean radius 6051 km is 735 K (462°C), and pressure is 9.2 MPa. In many sites, the planet surface is similar to solidified lava. The daytime illumination attains 5--10 klx and higher; blue light is absorbed by the

atmosphere, and the sky tint is yellowish. The Sun disk usually is not seen through permanently presenting clouds. The duration of both the day and the night is 58.4 Earth days. A typical Venusian landscape (Fig.1) is a waterless, almost red-hot stony or loose surface, mountains, and, sometimes, craters and volcanoes.

A hypothetical waterless Venusian life, if it does exist, has to use biophysical mechanisms of metabolism and photosynthesis, which are distinguished from those of the Earth's life. Panoramic images of the Venusian surface were returned in the course of the Soviet *VENERA* missions in 1975 and 1982. In total, 41 images or their fragments were transmitted by the landers' cameras. Up to now, 11 or 12 unusual objects were found, analyzed, and discussed in relevant publications.



Figure 1 : Images of the planet's surface based on *VENERA-9* and *VENERA-13* panoramas at their landing sites (1975 and 1982) in modern processing

The re-processing of the images made it possible to detect novel unusual objects that could be signs of hypothetical life on the Venus planet. Compared to the *VENERA-13* landing site, the analyzed *VENERA-14* panoramas represent geological provinces of another type [2]. Object found on panoramas of *VENERA-13* were originally referred to as "hesperos" or "hespy" [4] (similarly to the case of the *VENERA-13* landing site). However, described here unusually shaped objects, apparently, represent another hypothetical group of Venusian fauna. Similarly to [3-4] and for convenience of description, the specific nickname "amisadas" was proposed for this group of objects (an abbreviation from the name of ancient Babylonian king Ammizaduqa in Mesopotamia (XVI century BC). His astronomers used clay tablets in which apparitions of Venus were recorded. It should be noted that the processing of primary images to the level required to search for hypothetical forms of Venusian fauna and flora is difficult and a time consuming task. This is the fact that can explain, why the systematic study that began 6 years ago, in 2009, has resulted so

far in 11 or 12 findings only of hypothetical objects. Up to now, the analysis is not completed yet; approximately a half of available images were studied. The amisadas are related to most recent results. Entities found in the present study strongly diverse in their shape so that, as a rule, to classify them to certain groups is impossible. Most easily is detection of terramorphic objects, like a Bear-cub, an Owl, a Mushroom and a Scorpion [4].

Nevertheless, even in these cases, it took long time to recognize an object presented in an insufficiently clear image. Certain kind of support occurred from the atlas of Earth's living forms. However, many objects that strongly differed from surrounding background are unusual so that there was nothing to compare. Of course, the possibility of artifacts associated with the interference of noise cannot be excluded, especially when images are noisy. In these cases, a very thorough analysis was required. An example is an object called Disk [4], which was detected in the BW-6 panorama transmitted from the *VENERA-13* lander on the 87th--100th min upon landing. Panoramas of *VENERA* landers were studied for many years by both Russian and

foreign researchers. However, the amisadas are described for the first time. Therefore, the natural question arises, why no entities, even terramorphic were found previously? This fact can be explained by two reasons. The first one is that nobody was looking for them, although the earliest publication about it is dated by 1978. The second, more important reason is the necessity to develop novel processing methods that did not exist previously and the processing is very labour assuming. It is more difficult to explain, why a certain object could attract attention and be found out. Apparently, this is associated with individual features of the image perception for different persons. These properties are sharpened, e.g., at talent professional photographers of nature, who are capable to notice and fix unusual images or compositions ignored by other people.

III. COLLECTING AND PROCESSING OF EXPERIMENTAL DATA

Images published soon after the completion of the VENERA missions were obtained on the basis of single or combined black-and-white or color-divided

panoramas (Fig.1, left and right parts). There are some primary raw images not studied yet. Detailed information on TV experiments on the VENERA-13 and VENERA-14 landers was published in [2-4] and is not repeated here. Different from cameras 1 of the VENERA-13 and VENERA-14 landers, the cameras 2 transmitted a full black-and-white image and then in turn, colored fragments of right and left parts of the panoramas, 14 fragments taken by each camera. They consist 4 consecutive series of repeated groups of images numbered as 1, 6, 9, and 13. According to the arrangement and positions of noises and defects, series 6 could be a re-transmitted series 1, and series 13 - a retransmitted series 9, although they have certain differences. Each series includes a number of panoramas. On the most successful images, noise is low, which allows using efficient processing methods and combining different images. As a result, the images quality was improved noticeably. Figure 2 show an example of primary processing steps of most successful panoramas for series 1/6 and 9/13 in which identified fragments were selected.

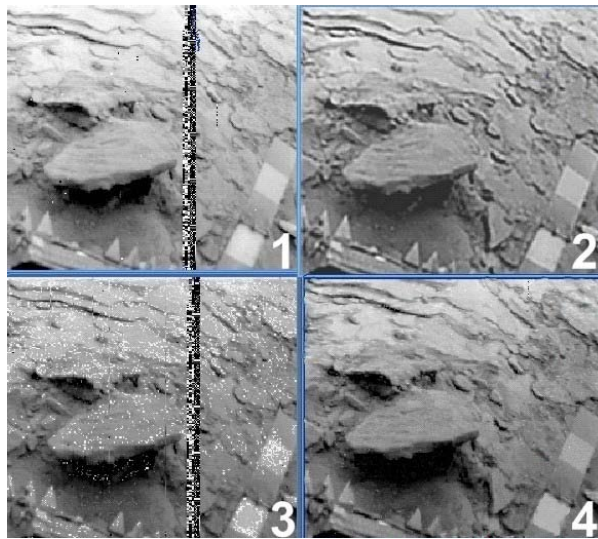


Figure 2 : Illustration of primary-processing methods for selected fragments of Venusian surface panoramas: (1) and (3) are initial images at the VENERA-14 landing point (camera 1); (2) and (4) correspond to the eliminated insets and partly eliminated noise

Images 1 and 3, respectively, correspond to original fragments with a very low (1) and middle (3) noise levels. The vertical band is a telemetry data inserted from other devices. In images 2 and 4, inserts are replaced by sections taken from other panoramas of the same series and noise interferences are removed. The fragments obtained admit further significant improvement of sharpness and clarification of fine details. To this end, four methods were employed: application of an unsharp-mask and the functional-sharpness methods; use of the correlative-stacking operation; and an improvement of the sharpness by

consistent application of the "blur-sharpening" operation of standard WORD and WINDOWS software. All these approaches are known sufficiently well and a significant number of relevant codes are proposed for each of them.

IV. AMISADES

Results of the above operations (and of other less significant ones) are presented in Fig. 3 for series 1/6 (on the left) and for the series 9/13 (on the right). The improved clarity of images made it possible to detect objects not recognized previously. The layered structure

of the surface with numerous cracks is clearly seen. The color-control panel (on the right) provides the scale size with each its field being a square of 10 x 10 cm². The distance between the teeth on the landing buffer is 5 cm. Thus, the size of the large stone in the foreground is about 50 cm.

The amisada-1 object is located on the left to the large stone, in a small alcove at the left edge of the picture and is positioned favorably being close to the

camera lens, at a distance of 1.2 m. The amisada is seen at an angle of about 60° to the horizon and represents an elongated bulky body, 12 cm long, resembling a fish if observed from above. Its frontal part (on the left) terminates by a regular structure. As a result of the first attempt to clarify the amisada's structure, the image shown in Fig. 4 was obtained. The first amisada position is marked by white ring.

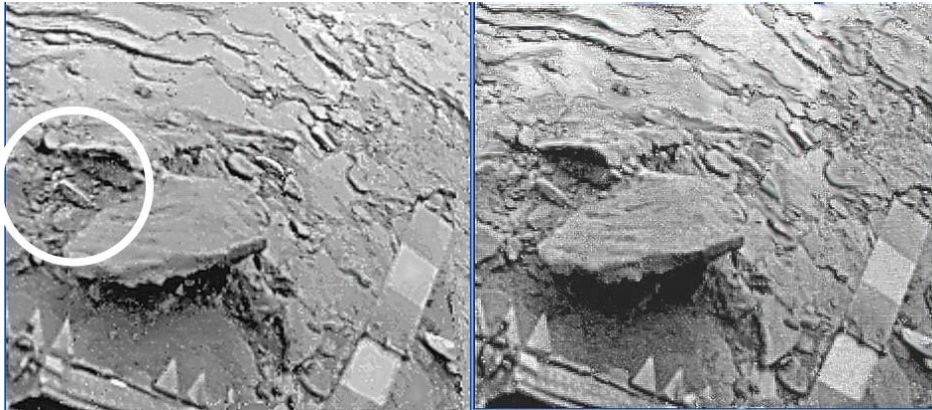


Figure 3 : Advanced methods of processing Venusian surface panoramas improve their sharpness and make it possible to identify objects missed previously. On the left: processed image of the *VENERA-14* panorama fragment (camera 1, series 1/6); on the right: the same fragment on panoramas of series 9/13.

The regular structure of the amisada's "head" (left part) consists of isolated unresolved elements forming a round crown-like semi-circle salient, at 2--3 cm from the amisada's body. At the right, the amisada is terminated by a short narrow appendage similar to the hespy's tail [4]. Of interest is the lower part of the amisada. Combining parts of images obtained independently and presented in Fig. 3. The more detailed view of the fragment is Fig. 4, where geometry

is corrected in part. According to the image, the amisada rests on the projecting parts of its body, their number at this side can attain 3 or 5. The apparent inclined position of the body in Fig.3 is explained by geometry of the image, namely, by the 50° tilt of the camera axis. In Fig.4 under the object a deep shadow is seen, which indicates the volume character of this object.



Figure 4 : Amisada-1: a supposed object of Venusian fauna. Its size is about 12 cm. The left side of the amisada, a "crown", is surrounded by a structure resembling a tilted semi-circle consisting of individual non-resolved elements.

The detailed analysis of Fig. 3 allows to suppose that there is a second amisada located roughly twice as far as the first one. The second amisada is arch-shaped and is seen also in Figs. 3 and 5 (black arrow). Apparently, amisada 2 is a bit larger than the first one. It was found by animation methods that for the observation time, the amisada-1 displaced a bit (for few

cm) and inclination of its "crown" changed. The number of high-resolved BW-images is insufficient for a more detailed conclusion; as for the color-divided panoramas they included only the right part of the amisada 1. In any case, estimates given in [3, 4] for the maximum movement velocity characteristic for Venusian fauna, namely, about 1 mm/s, is not exceeded here. Figs. 3-5

show that both amisadas are located in small depressions.

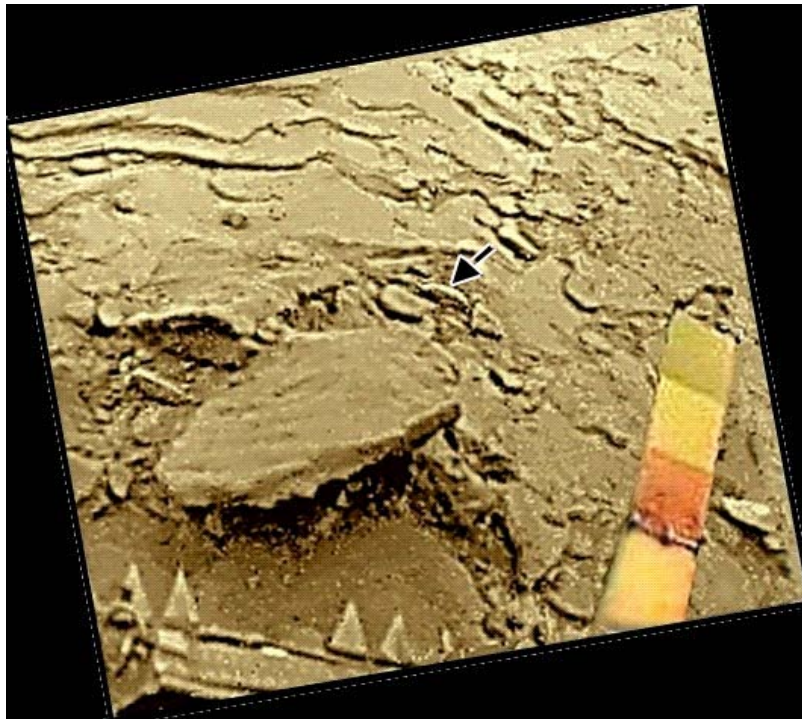


Figure 5 : The high sharpness image stacked of two parts of Fig. 3. The “crown” formed by individual elements is not of a random nature and relates to amisada in itself. A possible second amisada is indicated by black arrow.

Regular and similar shapes of the amisadas and their mutual proximity underline their reality. Due to the larger distance to amisada 2, its lower part is not completely visible. For amisada 2, its total length attains about 15-16 cm.

V. SPOTTY AMISADA

The image resolution is insufficient for attributing it to objects considered above. The most interesting object is a spotty amisada that has been

found at the central part of the *VENERA-14* panorama, left side of fields shown in Figs. 3 and 5. This spotty amisada is located just at the landing buffer, is marked by the white circle in Fig. 6 and is the closest to the lens of camera 1, being observed from above at an angle of about 80° to the horizon. In Fig.6a, a single image of the amisada is presented, which corresponds to about the 30th minute of activity of the TV camera of the *VENERA-14* lander.

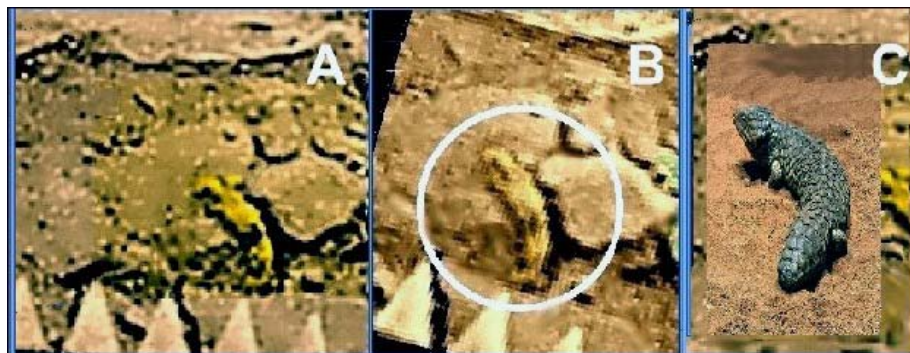


Figure 6 : (a) Amisada climbing up a stone, (b) stacking of 6 original fragments of *VENERA-14* panoramas, (c) sluggish Australian Shingleback lizard whose size and shape resemble the amisada

The distance between the spotty amisada and amisada-1 attains approximately 0.4 m and the spotty amisada is, apparently, seen in motion. Seemingly, it is climbing up or creeping on a 5-8-cm stone. The upper

part of amisada is located on the flat surface of the stone, and the lower part envelops a ledge. Of course, it cannot be excluded that spotty amisada does not go up but comes down from the stone. Its crown is scarcely

seen and manifests itself presumably by an additional processing of initial images both as a semi-circular shadow at the upper part of the amisada and several hardly distinguished points above it. Therefore, if the crown (shown in Figs. 4, 5) is considered as a signature of the amisada's head part, it is actually climbing up onto a stone. Since each image line takes 0.78 s, blurring of the crown image could be caused by the wind above the stone surface (in contrary, the amisadas 1 and 2 were positioned in depressions). Two small protrusions at both sides below the amisada's "head" could be its forelimbs. In general, it resembles actually an Earth lizard climbing up to a rock, which again indicates the surprising terramorphism of Venusian fauna. Spots on the amisada's body in Fig.6 are more

distinctive than in Figs.4 and 5. An oblong spot is seen on the "head", dark spanning bands are visible at its central (at the bend) and lower parts. The length of the amisada is about 10-12 cm (excluding the crown).

The images of the amisada were additionally processed, which made it possible to see the motion of its upper part as a sequence of six sequential positions. Animation of 6 subsequent frames for spotty amisada has made it possible to detect a small displacement of light and dark parts of its "head". Position variation of the upper part of the amisada is shown in Fig.7 as changes in the direction of arrows. Here, fragments of the six available panoramas are given. The images are presented in chronological order, with the intervals between them being, on average, of about 13 min.

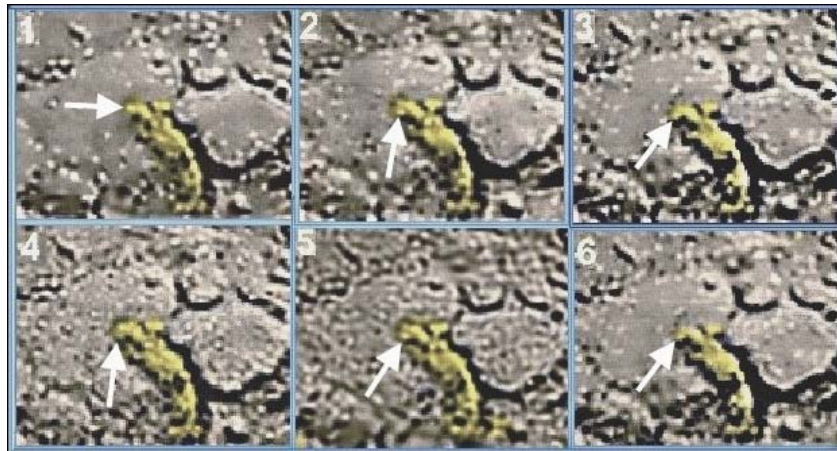


Figure 7 : Amisada at landing buffer of the *VENERA-14* lander. Shown are processed fragments of initial panoramas. Arrows direction indicate and repeat the sequence of positions of the front (upper) part of the amisada, which in size and motions resembles a semibent finger. (All initial images are black-and-white.)

In frame 1 of Fig. 7, the upper part fragment of the amisada is directed to the left (9 h), whereas the shadow under it is almost absent. We should recall that for scattered natural illumination on the Venusian surface, shadows appear only in the case of low positions of an object with respect to the surface. In this case, the altitude of the object above the surface should be comparable to its size. Most likely, the absence of a shadow indicates that the object's part is lifted above the surface. In frame 2, the amisada's upper fragment is displaced along the 7 h direction, and a small shadow is present. Finally, in frame 3, the edge fragment corresponds to, approximately, the 8 h direction with a deep shadow under it. Further variations are given by the frame sequence 4 to 6. The size and displacements of the fragment are close to those of a human finger and its motions. (The procedure of the search for, discovery, and processing of images of terramorphic objects are described in [3, 4].)

For 1.5 hours, the head gradually shifted first for 2 and then - for 2 or 3 image pixels to opposite sides. At a distance of about 85 cm from the camera lens and for a resolution of 11', the displacement corresponds to 1.1

to 1.3 cm. So the displacement, in itself, attains 3 cm. In this case, the speed of the motion is significantly lower than that mentioned in [4]. It is closer to 1 mm/min, rather than 1 mm/s. This value seems may be housekeeping action (looking for food?) of the spotty amisada, rather than its speed of motion that any case, is very slow.

Thus, three amisada-type features were found at the *VENERA-14* landing site. Classification of amisadas as forms of hespies, which had been proposed in [7] for panoramas of *VENERA-14*, likely, was wrong. The body of a hespy is flattened and twice as long as that of an amisada. The amisada's body is thicker and flexible, as can be seen from Figs. 6-7. Apparently, these were amisadas but not hespies that had been shown in [4].

VI. AMISADAS ON *VENERA-13* PANORAMAS

Amisada-like forms were also found in *VENERA-13* panoramas. The object shown in Fig.8 was too far from the camera so that the resolution of the image was insufficient to recognize fine details. The shape of the object was reconstructed by the more rigorous

processing using all available images repeated in successive panoramas.

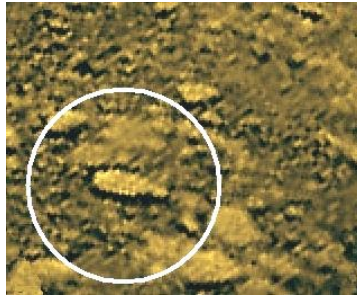


Figure 8 : Fragment of the *VENERA-13* panorama with an object shown that can be identified as an amisada, upon further processing

The above-listed processing methods were applied. A small shift of successive images within a single pixel results in an additional improvement of the resolution.



Figure 9 : Processing of successive images (1-4) of the object shown in Fig. 8 (arrow) and steps of their stacking

Of course, the image cannot be better than that contained in original images. Figure 9 illustrates the step-by-step improvement of images obtained. Frame 1 with an arrow corresponds to the processed version of

Fig.8. Further, the same fragments but taken from other panoramas (2--4) were involved in the processing. The methods employed improve significantly the quality of images, which is demonstrated by final image in Fig.10.

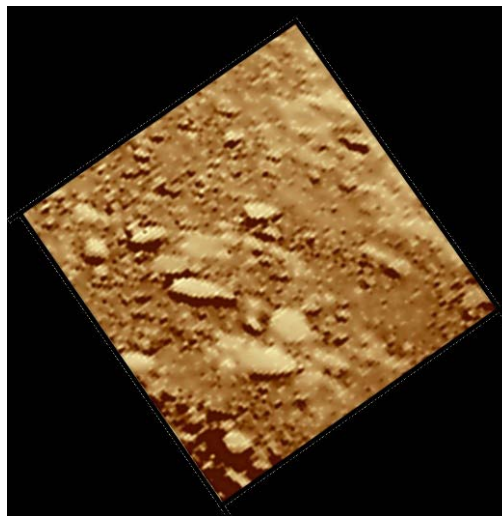


Figure 10 : Result of processing of the fragment of *VENERA-13* panoramas upon employment of all available images

Thus, one may assume that the elongated body shown in Fig.10 actually is an amisada rather than a stone or hespy. However, the resolution is insufficient for detection of fine details such as crown, spots, and other characteristic features of the object, which are more confidently traced on *VENERA-14* panoramas (Figs. 3-7).

VII. CONCLUSION

For thousands of years, humanity has wondered whether there is life outside the Earth. In this paper details are thoroughly described of hypothetical fauna pattern of Venus, found on panoramas of the *VENERA-14* lander, that were returned from the planet

Venus 33 years ago. The objects for which a nickname "amisada" is proposed have terramorphic features and resembles Earth' lizards. The amisadas when viewed from above, are well-distinguished fish-shaped bodies, however, supplied by limbs of support (and, probably, of motion). The amisadas seem are similar to reptiles by their shape. The structure and purpose of the amisada's body part, resembling a crown, is not clear. The crown consisting of isolated elements forms the forward (or may be back) part of an amisada. A limited fragment of the panorama, presented in the text, contains images of three amisadas. Their motion is slow and similar to motions of other objects of Venusian hypothetical fauna. Probably analogous objects were found on panoramas of *VENERA-13* too, that landed at a distance of 900 km from the landing site of *VENERA -14*.

If the hypothetical Venusian fauna is heterotrophic, the source of its existence should be hypothetical autotrophic flora. Direct rays of the Sun, as a rule, do not reach the surface of the planet, nevertheless there is enough light for photosynthesis of the Earth-like type there. In the case of the Earth, a diffuse illumination of 0.5-5 kLux is sufficient for photosynthesis. The measured illuminance on Venus is of the same order, at the range of 0.4 to 9 kLux. Of course, photosynthesis at high temperatures and in a non-oxidizing environment should be based on a completely different, unknown biophysical mechanism. Certain forms of assumed Venusian fauna exhibit surprising similarity to the living world of the Earth. We call this strange repetition of terrestrial forms terramorphism. The discovery of this phenomenon is no less important than that of the extraterrestrial life itself. Certainly, the phenomenon relates to most deep problems of the search for life in the Universe.

Initially, the experiments performed by *VENERA* landers were aimed at accumulating general information on the Venusian surface. However, the results obtained make it possible to consider these experiments as a revolutionary step. The next important problem now becomes the urgent realization of a new special mission to explore the surface of Venus for hypothetical fauna and flora existing on the planet. This mission should be of a particular directivity and significantly more complicated than the previous *VENERA* missions. Nevertheless, progress in science and technology attained during the past 33-40 years, allows the undertaking of this task to be quite realistic.

REFERENCES RÉFÉRENCES REFERENCIAS

1. Selivanov A.S., Gektin Yu.M., Chemodanov V.P. *et al.*, TV Experiment on the Venus Surface // *Kosmicheskiye Issledovaniya*, Vol. 14, No. 5, 1976, pp. 674-677.
2. Selivanov A.S., Gektin Yu.M., Gerasimov M.A. Continuation of the TV Investigation of Venus

surface by means of landers // *Kosmich. Issled.*, Vol. 21, pp.176-182, 1983.

3. Ksanfomality L.V. Possible Detection of Life on the Planet Venus.// ISSN 1028-3358, *Doklady Physics*,57, No. 9, 367-372, 2012.
4. Ksanfomality L.V. Possible Signs of Life on the Planet Venus // *International Journal of Astronomy and Astrophysics (IJAA)*, Vol. 3, pp. 57-79, 2013.



GLOBAL JOURNAL OF SCIENCE FRONTIER RESEARCH: A
PHYSICS AND SPACE SCIENCE
Volume 15 Issue 3 Version 1.0 Year 2015
Type : Double Blind Peer Reviewed International Research Journal
Publisher: Global Journals Inc. (USA)
Online ISSN: 2249-4626 & Print ISSN: 0975-5896

A Physicist Description of Indigenous Telecobalt Machine Bhabhatron-II TAW

By Athiyaman.M, Hemalatha Athiyaman, Neelakandan, Rajasekaran,
Dr.H.S.Kumar & Dr. Ajay Sharma

Acharya Tulsi Regional Cancer treatment and Research Institute, India

Abstract- The newly designed indigenous Bhabhatron-II is installed in our institution. The Telecobalt machines were put into use for Radiotherapy after the possibility of producing High activity sources with smaller dimension which satisfies the ideal requirement of Teletherapy source. The Bhabhatron II head can accommodate nearly 250RMM source strength. Being a computer controlled machine the Bhabhatron machine differs from other conventional Telecobalt machines. This machine has advanced features such as asymmetric collimators, motorized wedge etc. This unit has keypad attached at both sides of the couch that also has digital display. The patient treatment is computer controlled. The plan parameters can be entered in the console computer and the exposure time can be programmed. This unit suits well for developing countries provided the cost of the source shall be maintained cheaper.

Keywords: *bhabhatron ii, asymmetric collimators, indigenous.*

GJSFR-A Classification : *FOR Code: 249999p*



Strictly as per the compliance and regulations of :



© 2015. Athiyaman.M, Hemalatha Athiyaman, Neelakandan, Rajasekaran, Dr.H.S.Kumar & Dr. Ajay Sharma. This is a research/review paper, distributed under the terms of the Creative Commons Attribution-Noncommercial 3.0 Unported License (<http://creativecommons.org/licenses/by-nc/3.0/>), permitting all non commercial use, distribution, and reproduction in any medium, provided the original work is properly cited.

A Physicist Description of Indigenous Telecobalt Machine Bhabhatron-II TAW

Athiyaman. M^α, Hemalatha Athiyaman^σ, Neelakandan^ρ, Rajasekaran^ω, Dr. H. S. Kumar[¥]
& Dr. Ajay Sharma[§]

Abstract- The newly designed indigenous Bhabhatron-II is installed in our institution. The Telecobalt machines were put into use for Radiotherapy after the possibility of producing High activity sources with smaller dimension which satisfies the ideal requirement of Teletherapy source. The Bhabhatron II head can accommodate nearly 250RMM source strength. Being a computer controlled machine the Bhabhatron machine differs from other conventional Telecobalt machines. This machine has advanced features such as asymmetric collimators, motorized wedge etc. This unit has keypad attached at both sides of the couch that also has digital display. The patient treatment is computer controlled. The plan parameters can be entered in the console computer and the exposure time can be programmed. This unit suits well for developing countries provided the cost of the source shall be maintained cheaper.

Keywords: *bhabhatron ii, asymmetric collimators, indigenous.*

I. INTRODUCTION

In the era of advanced radiotherapy (RT) technology development, the telecobalt units (TCU) are still trying to compete with the linear accelerator (LINAC)^[1]. The main reason for the suitability of Telecobalt source for treatment purpose is its high specific activity which can lead to achieve smaller dimension source, an ideal requirement of any Radioactive Source for clinical purpose and also to achieve desirable dose rate at larger distance. The other advantage of the Cobalt 60 source is high energy of 1.25 MeV which lies in the Mega Voltage region. The Megavoltage energy photons interact irrespective of the atomic number and depend only on electron density. Hence the main disadvantage of higher absorption in bone due to Kilovoltage Photons is quashed by introducing the Cobalt 60 source. Even though the Telecobalt units have the above advantage it

Author α: Assistant Professor, Sr. Demonstrator (RSO) Department of Radiation Physics, Acharya Tulsi Regional Cancer treatment and Research Institute, Department of Radiation Physics, Bikaner, Rajasthan, India. e-mails: athi.roja87@gmail.com, hames_medphy@yahoo.co.in.

Author σ: Senior Demonstrator, Department of Radiation Physics, Acharya Tulsi Regional Cancer treatment and Research Institute, Sardar Patel Medical College & Associated Group of Hospitals, Bikaner, Rajasthan, India.

Author ρ ω ¥ §: Acharya Tulsi Regional Cancer treatment and Research Institute, Sardar Patel Medical College & Associated Group of Hospitals, Bikaner, Rajasthan, India.

yields poorer geometrical precision due to larger Penumbra and as a radioactive source it decays when time passes that leads to dose rate reduction. These disadvantages are felt insignificant and they are still preferred in countries where facilities of maintaining Linear Accelerator are so cumbersome.

Acharya Tulsi Regional Cancer Centre has a long history of providing Radiotherapy. At the mid of 1930s this institution is the only centre in North Western India which provided Radiotherapy facility by Radium Sources and Deep Therapy X Ray Units. Presently this institute handles 5000 annual patients every year and majority of the cases are treated in our earlier installed Telecobalt Machines namely 780-E & 780-C; The present Telecobalt Machines approximately handles 100 patients per day and our Varian Linac handles around 50 Patients. To manage this higher workload it was decided to procure a Telecobalt Machine.

It shall be emphasized here that many of the major techniques and advances in physics of External Beam Radiotherapy were developed from Telecobalt Units. Techniques such as Arc Therapy, Measurement of T.A.R and subsequent Scatter Air Ratio and the associated algorithms for treatment planning based on the separation of primary and secondary radiation has evolved from Telecobalt Machine. More recently, Poffenbarger and Podgorask in 1998 have investigated the possibility of using an isocentric unit for S.R.S. Warrington and Adams have shown that conformal Therapy and even IMRT could be adequately delivered with a Cobalt-60 unit except for Deep seated Tumors.

II. MATERIALS AND METHODS

The general characteristics, mechanical characteristics and special features of Bhabhatron-II, are described here. The machine was installed by the regulatory board authorized service engineer of the vendor. All the mechanical quality assurance tests were performed and ensured the mechanical characteristics of the machine is in line with the regulatory board and IEC recommendations. The normal conventional Quality Assurance equipments which are available in our department are used for commissioning the unit. For the measurement of Absolute Dosimetry Farmer Chamber was used along with the water equivalent Phantom. The Victoreen Based Advanced Survey Meter and

Pressurized Ion Chamber are used for the Radiation Protection survey. Additionally we had obtained the Digital Pocket Dosimeters from Rosalina Medical Instruments for the purpose of Source Loading procedures which shall be worn by the personnel involved in source Transfer. The basic construction of the machine, the components of the Head, description of primary collimator and secondary collimator, symmetric and asymmetric properties of Jaws are described here. The machine properties vary significantly from other conventional telecobalt machines. The planning parameter related motions such as field size, collimator rotation and exposure time are programmable in the control console computer. Also we describe here about the computer control console and the facilities available in the console such as visible indicators for source on, transit and OFF position, pressure situation in the compressor, wedge details.

III. BASIC CONSTRUCTION OF BHABHATRON-II TAW MACHINE

a) Head

The basic mechanical construction of Bhabhatron-II is as similar to other commercial Telecobalt Machines. The Bhabhatron-II machine head

can accommodate the maximum source strength of 250RMM^[4]. The Source Head is made up of Tungsten to shield the source in the OFF position which differs from the other machines where the other commercial machine's head are made of Depleted Uranium Figure 1. The Tungsten shield in Bhabhatron-II TAW model forms a conical opening at the source fully exposed condition which forms the primary collimator. The source capsule is mounted in a cavity approximately 2.8cm in diameter and 1.2cm long with an end plug and clip. The source drawer is operated with the pneumatic pressure system with pressure range of 35 - 40 PSI to 60 - 65 PSI. The source drawer slides along a horizontal tube inside the head which places the source from Fully Exposed (ON) position to Fully Shielded (OFF) Position by the piston of air cylinder. The air cylinder is controlled by two air valves, which, under normal conditions, do not permit the source to remain in the fully exposed position when electrical power is removed from the unit. In this case, the valves will return the source to the fully shielded position or will depressurize the system so that the source can be returned manually. The valves are operated by the treatment control system (primary and secondary timers).

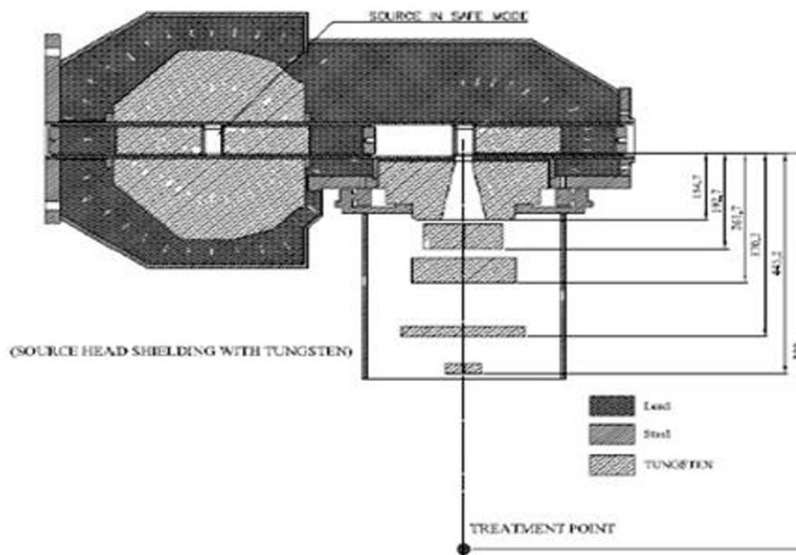


Fig. 1 : Head Characteristics of Bhabhatron-II TAW

The manufacturer of Bhabhatron Telecobalt Machine uses two materials i.e. Tungsten & Depleted Uranium for shielding the source in OFF condition. The models Bhabhatron-II, Bhabhatron-II-A, Bhabhatron-II-AW contain Depleted Uranium. The models Bhabhatron-II T, Bhabhatron-II-TW, Bhabhatron-II-TA, and Bhabhatron-II-TA contain Tungsten. The Suffixes T, A & W are used to identify the models of Bhabhatron. TAW

represents Tungsten, Asymmetric & Motorized Wedges respectively.

Beam limiting devices are made of fixed primary collimator and two secondary collimators. The Y jaws are next to the primary collimator which is parallel and independent to each other as Y1 & Y2 Jaws. The secondary Y Jaws stops at a minimum level of approximately 2x2 cm². The minimum achievable field

size of 0x0 is achieved by the Y jaw Trimmers. Next to Y Jaws the X Jaws are placed which are symmetrical to each other. It shall also be noted that the Y Jaws can be

operated in both the modes (Symmetrical & Asymmetrical mode) with the help of the dedicated switch attached in the Keypad.

Mechanical Parameters	Extension Level
Gantry	360 Degree
Couch Lateral	+/- 20 cm from the Isocentre
Couch Longitudinal	0 to 90cm Range
Couch Rotational	+/- 90 Degree Isocentric Rotation (IEC 61217)
Couch Vertical	60cm to 130cm(70cm Range)
Collimator Rotation	+/- 90 Degree Isocentric Rotation (IEC 61217)
X Jaw (Symmetrical)	0 x 0 cm ² to 35 x 35 cm ²
Y Jaw (Symmetrical)	0 x 0 cm ² to 35 x 35 cm ²
Y1 Jaw Asymmetrical	0 to -17.5 cm (as per IEC Scale 61217)
Y2 Jaw Asymmetrical	0 to +17.5 cm (as per IEC Scale 61217)

As described above are the functional limits of various parameters such as Couch, Gantry, Collimator & Jaws. Apart from the asymmetric feature of Y Jaws in basic construction wise the Bhabhatron-II TAW almost matches with the other commercial Telecobalt Machines. The Gantry shall be rotated to 360 Degree as similar to other Telecobalt machines to support various beam angle treatments. The gantry rotation speed shall be varied by the speed regulatory switch which is provided in the Keypad attached in the couch. Enabling this speed switch shall make all the mechanical motions to happen faster which shall help the Technologist for faster patient setup. A counter weight is designed to take counter the weight of the Head & other parts such as Collimator, Jaws, and Trimmers etc. The posterior counter weight is specially filled with Lead material which weighs almost 2 Tone capacities. The Head also has the source indicator rod as similar to other Telecobalt machines. It is attached with the source drawer and moves with the source that indicates (Through CCTV and/or Mirror) Beam ON condition. The external T-ROD shall be fitted with this indicator rod incase of failure of Automatic source retracting system to push the source to the OFF condition.

b) Collimator

The implementation of Asymmetric Jaws highly differentiates this machine from other Telecobalt Machines. The Asymmetric Jaws will play a vital Role in the Head & Neck cases treatment plan where the Bilateral Field Isocentre will be matched with LAN field which is not possible in other Telecobalt Machines due to the absence of Asymmetric feature. Along with this the asymmetric Jaw feature shall be greatly used in Breast cases where the dependency of Breast Cone to block the rest half of the beam to shield the underlying Lung tissue shall be achieved by independent Y Jaws. The Technologists shall be freed from mounting the

heavy Breast cone in the machine due to this asymmetric Y JAW feature of Bhabhatron-II TAW.

The movement of Asymmetric Jaws can be done by selecting the asymmetric switch provided in the Keypad thereafter the individual movements of Y1 & Y2 shall be controlled by their switches. The other keys to turn ON Lasers, ODI & Field light are also provided. The Emergency Switches are given on both Keypads.

IV. ADVANCED FEATURES OF BABHATRON-II

a) Isowedge

The Isowedge is one of the important features of Bhabhatron model over other conventional Telecobalt machines. Motorized wedge is a single wedge (60°) which could generate desired angle (0 to 60°) with the combination of open and wedged beam^[1-2&3]. Isowedge time calculated by the software depends on the Isowedge Angle, field size and treatment time^[4]. The isowedge is mounted permanently into the treatment head and are automatically driven into the radiation path through programming. By adjusting the proportion of the treatment time the wedge angle can be adjusted. The isowedge treatment time depends on the field size and required wedge angle. The required Isowedge angle shall be selected in the control console and the respective time shall be entered. The isowedge remain in the radiation path till the isowedge timer consumes the programmed time. The isowedge reaches its home position after remaining in the beam path for the programmed time. The motorized wedge shall be used with the help of the Treatment Planning System which helps in accurate calculation of the beam weightage for the wedged and non wedged beams to achieve the desired wedge angle^[1]. The implementation of isowedge has created an advantage of delivering wedged beams without mounting any physical accessories also the reduced the Technologists entry into the Treatment room to mount the accessories in-between.

b) *Couch and Keypad*

The couch is made of carbon fibers which shall withstand the maximum weight of 150kg. In conventional machines the mechanical motions

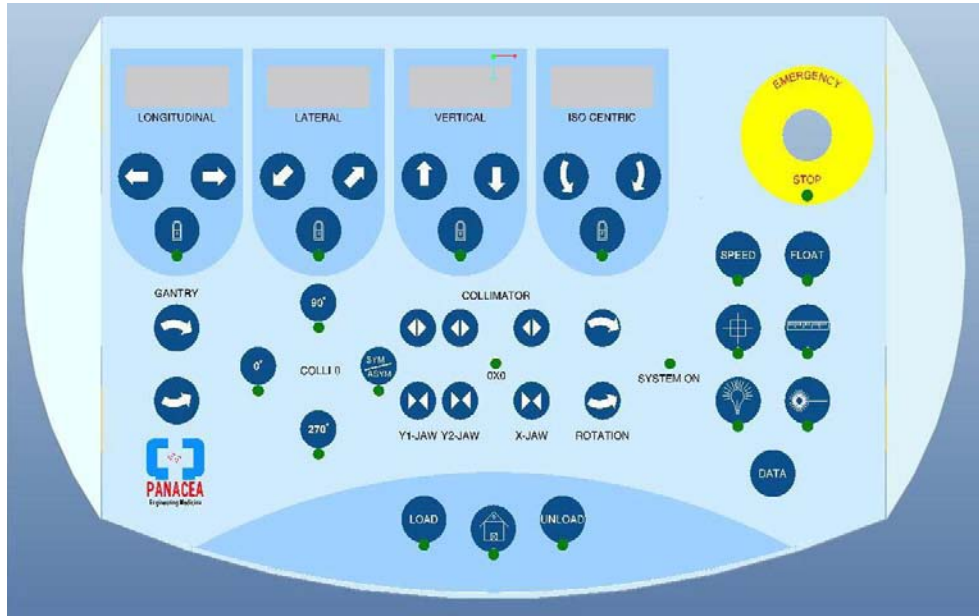


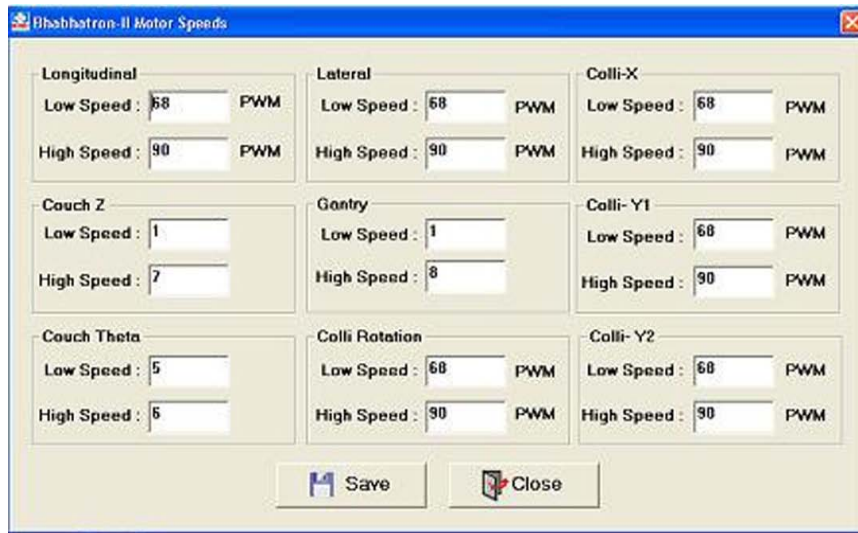
Fig. 2 : Key Pads attached in the Couch

are controlled by Hand Pendant whereas in Bhabhatron the mechanical motions are executed by keypads attached towards both sides of the couch. These Key pads have the digital display of Couch Values such as Longitudinal, Lateral, and Vertical & Isocentric Rotations. These pads control the collimator, Gantry & Couch motions. The first four key sets arranged in order is for controlling the Longitudinal, Lateral, Vertical and Isocentric rotation of the couch movement. Each key has a lock to fix the couch in the desired position which helps for accurate patient immobilization. It is not inevitable to use these motion keys every time since the motion enable key attached at both ends of the keypad restrict the motions of all the parameters unless enabled. Moving downwards there are keys provided for the Gantry rotation for clock and anticlockwise movements. Followed to that the keys for X and Y Jaw movement is provided. The movement of Couch, Gantry can be speeded up by the help of speed up switch provided in the key pad. The keys for field light, ODI scale, laser and room lights are provided in the keypad for easy patient setup.

c) *Accessories velocity adjustment*

The velocity i.e the speed of the mobile accessories, which are part of the machine such as couch, secondary collimator and Jaws, shall be programmed in the control software. The motor speed values shall be modified in the motor speed column by entering the desired PWM (pulse width modulation)

values in the control console. As the mechanical accessories can be displaced in speed mode and normal mode with the help of enabling and disabling the speed switch the PWM values differ for these two modes. Providing the values as described in the figure will control the speed of the DC motors. The entered values will alter the duty cycle of the pulse to control the speed of the motors.



d) Control Console

The Control Console of Bhabhatron-II machine is computer controlled. The Beam On procedure happens through Mouse click which differs this machine a lot from other conventional machines. The treatment shall be given in two methods; they are namely Treatment Mode & Service Mode. The Treatment mode shall mainly be used for daily scheduled fractions. In this

mode the patient treatment shall be programmed; The Collimator values (Field Size), Collimator, Gantry & Couch Rotation shall be entered through a valid id for every patient and be saved. The desired patient shall be opened for every fraction by entering the Valid ID number. The plan parameters will automatically be displayed.

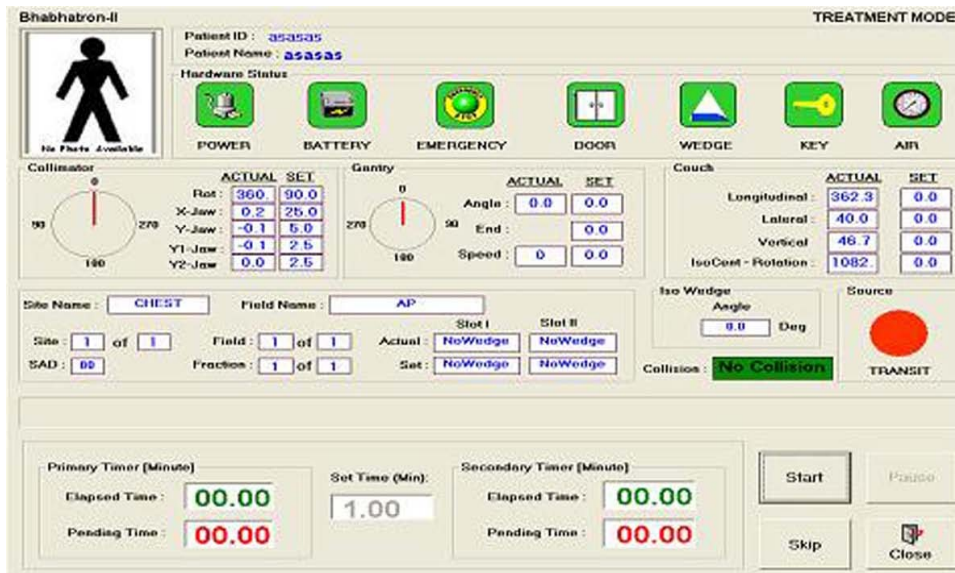


Fig. 3 : The console screen of Bhabhatron-II

The collimator values will automatically be set as entered in the Patient Record. The couch and Gantry shall be moved manually taking the display as reference. The Physicist shall enter all the parameters on the first fraction by creating a Record of individual patient. The patient details such as Name, ID No shall be provided for identification and for subsequent opening for daily fractions. The no of fractions to be delivered shall be entered in the next phase; then

follows the plan parameter phase which demands the values of Filed size, Collimator Angle, Gantry Angle, Name of the Field, details of wedge etc. In case of executing the treatment through computerized 3D planning the couch values shall be entered after completing the CT Isocentre shift to the Treatment Isocenter. Another way of executing the treatment is through service mode. Executing treatment through computer controlled is a remarkable achievement in

Telecobalt Treatment which ensures the patient received proper treatment and manual errors are reduced considerably.

The service mode shall be used for unplanned fractions such as single fractions for palliative cases. There is no provision to enter the plan parameters in the service mode; The plan parameters shall be set in the machine through keyboard. The treatment time of the patient shall only be entered in the service mode and the Beam ON procedure shall be performed through mouse click. From the Treatment Console Screen we can get the details such as Power status of the machine, Battery Status, Door Status (Opened or Closed), placing of wedge, status of key, pressure status and mainly Source Status in color. Once all the parameters are set the treatment shall be executed through Mouse click. The source Transit is indicated in terms of RED color and the source ON position is indicated in terms of yellow color. The Primary timer and secondary timer will start displaying the elapsed time and pending time. The treated patient detail will be stored in the patient history. A detailed History of patients treated daily & weekly wise can be taken out as a printed copy.

V. DISCUSSION & CONCLUSION

The Telecobalt units have disadvantages of penumbra & dose rate decay; But still these machines are preferred in developing countries due to less maintenance cost. For large countries like India based on the incident spectrum of malignancies prevailing, World Health Organization (WHO) recommended telecobalt machines as a simple effective equipment^[5]. Dinshaw advocated the need to revisit the context of cost effectiveness, cost benefit, and cost-utility analysis in Indian perspective and to strike the right balance between the science of technology and the art of medicine, with special relevance to radiotherapy in cancer treatments^[6] Though this machine has advanced features such as asymmetric collimator, motorized wedge etc it can never compete with the Linear Accelerator since fundamentally it is a Telecobalt unit with radioactive source which decays when time passes. This machine stands superior with among other Telecobalt units having the above mentioned features. The Theratron Equinox model has the same features such as asymmetric jaws, motorized wedge etc and stands at par with Bhabhatron. In today scenario the cost of the Telecobalt source has increased to a significant extent which made the Oncology community to rethink the purchase of Telecobalt units. The process of commissioning is always dependent on the availability of the source. This country faces acute shortage of Telecobalt source as so many institutions are waiting in long queue.

This machine shall be configured in the Treatment Planning System for accurate calculation and

dose delivery. The 3D Planning will result in proper usage of asymmetric jaws and motorized wedges etc. The Head & Neck cancer patients shall receive effective lymph node irradiation due to the feasibility of LAN technique with the help of Y1 & Y2 Jaws. The Ca Breast patients will receive single Isocentre Treatment as the MT, LT fields & SCF fields will be treated with simultaneously with single isocentre. Also mounting the heavy Breast cone by the Technologists is eliminated due to the same asymmetric feature.

We conclude that the machine has advanced features from other conventional Telecobalt machines. The use of this machine shall be enhanced by commissioning this unit in the Treatment Planning System. The source cost and its availability still a disadvantage to its progress. Being an indigenous product this unit gives a pride to this Indian country and this country's dependency on foreign nation for radiotherapy units is reduced.

VI. ACKNOWLEDGEMENT

The author would like to thank all the Radiation Oncologists in the Department of Radiation oncology and Radiotherapy Technologist, Acharya Tulsi Regional cancer treatment and Research Institute, Bikaner.

REFERENCES RÉFÉRENCES REFERENCIAS

1. Characterizing and configuring motorized wedge for a new generation telecobalt machine in a treatment planning system, Rajesh A. Kinshikar, Smriti Sharma, Rituraj Upreti, Chandrashekar M. Tambe, Deepak D. Deshpande Department of Medical Physics, Tata Memorial Hospital, Parel, Mumbai - 400012, India.
2. Dai J, Zhu Y, Ji Q. Optimizing beam weights and wedge filters with the concept of the super-omni wedge. *Med Phys* 2000;27:2757-62.
3. Van Dyk J, Barnett RB, Cygler JE, Shragge PC. Commissioning and quality assurance of treatment planning computers. *Int J Radiat Oncol Biol Phys* 1993;26:261-73.
4. Bhabhatron-II User Guide version 4.4, Panacea Medical Technologies.
5. Optimisation of radiotherapy treatment facilities. Technical Report Series 644, World Health Organization (WHO), Geneva, 1980.
6. Has the time come for doing away with Cobalt-60 teletherapy for cancer treatments, Editorial, *Journal of Medical Physics*, Vol 34, No.2, 2009.



GLOBAL JOURNAL OF SCIENCE FRONTIER RESEARCH: A
PHYSICS AND SPACE SCIENCE
Volume 15 Issue 3 Version 1.0 Year 2015
Type : Double Blind Peer Reviewed International Research Journal
Publisher: Global Journals Inc. (USA)
Online ISSN: 2249-4626 & Print ISSN: 0975-5896

The Modified Interfacial Gravity: Unifying CDM, MOG, and MOND

By Ding-Yu Chung

Delta State University, Nigeria

Abstract- The paper posits the modified interfacial gravity (MIG) as the modified gravity in the interfacial region between homogeneous baryonic matter region and homogeneous dark matter region. The MIG model contains both dark matter and modified gravity to unify the CDM (Cold Dark Matter) model, MOG (Modified Gravity), and MOND (Modified Newtonian Dynamics). In MIG, the interfacial repulsive Yukawa force in the interfacial region to separate baryonic matter region and dark matter region is equivalent to the repulsive Yukawa force in outer galaxy in MOG. The modified interfacial gravity is interfacial gravity interacting with the interfacial repulsive Yukawa force. The modified interfacial gravity emerges in the interfacial region between dark matter region and baryonic matter region only when the homogeneous surface density is above the critical homogeneous surface density in both dark matter region and baryonic matter region.

Keywords: *modified interfacial gravity, CDM, MOG, MOND, unified model, repulsive Yukawa force, galaxy evolution, unified model, modified gravity, dark matter.*

GJSFR-A Classification : *FOR Code: 260201*



Strictly as per the compliance and regulations of :



The Modified Interfacial Gravity: Unifying CDM, MOG, and MOND

Ding-Yu Chung

Abstract- The paper posits the modified interfacial gravity (MIG) as the modified gravity in the interfacial region between homogeneous baryonic matter region and homogeneous dark matter region. The MIG model contains both dark matter and modified gravity to unify the CDM (Cold Dark Matter) model, MOG (Modified Gravity), and MOND (Modified Newtonian Dynamics). In MIG, the interfacial repulsive Yukawa force in the interfacial region to separate baryonic matter region and dark matter region is equivalent to the repulsive Yukawa force in outer galaxy in MOG. The modified interfacial gravity is interfacial gravity interacting with the interfacial repulsive Yukawa force. The modified interfacial gravity emerges in the interfacial region between dark matter region and baryonic matter region only when the homogeneous surface density is above the critical homogeneous surface density in both dark matter region and baryonic matter region. The critical homogeneous surface density is derived from the acceleration constant a_0 from MOND. The four separate regions in the galaxy structure in MIG are the core (inner) baryonic matter galaxy with the Newtonian gravity, the interfacial (outer) baryonic matter galaxy with the modified interfacial gravity, the interfacial (inner) external dark matter halo with the modified interfacial gravity, and the core (outer) external dark matter halo with the Newtonian gravity. Dark matter in the external dark matter halo is cold dark matter without electromagnetism as in CDM. CDM and MIG are identical during the very early universe below the critical homogeneous surface density and before the emergence of the modified interfacial gravity. After the emergence of the modified interfacial gravity by dense giant molecular clouds during the early universe, MOND, MOG, and MIG are identical for baryonic matter galaxy structure. MIG explains galaxy evolution, globular clusters, dwarf galaxy plane, dark matter halo in galaxy cluster, the rotation velocities, and the failure to detect directly dark matter on earth.

Keywords: *modified interfacial gravity, CDM, MOG, MOND, unified model, repulsive Yukawa force, galaxy evolution, unified model, modified gravity, dark matter.*

I. INTRODUCTION

The previous paper [1] proposes a repulsive force between baryonic matter and dark matter to explain galaxy evolution. In this paper, the repulsive force is described as the modified interfacial gravity (MIG) which is the modified gravity in the interfacial region between homogeneous baryonic matter region and homogeneous dark matter region. As a result, the MIG model contains both dark matter and

modified gravity to unify the CDM (Cold Dark Matter) model [2], MOG (Modified Gravity) [3,4], and MOND (Modified Newtonian Dynamics) [5,6,7].

The two major models for galaxy are the CDM model and the modified gravity models including MOG and MOND. CDM contains no modified gravity, while the modified gravity models contain no dark matter. Dark matter was originally proposed to account for the asymptotically flat rotation curve in outer galaxy and to keep galaxy together based on only the Newtonian gravity. CDM has the Navarro–Frenk–White (NFW) profile [2] derived from N-body collisionless dark matter simulations based on only the Newtonian gravity. The highest density is at the center as the central cusp. Baryonic matter is dragged along by the gravitationally dominant dark matter, resulting in the first protogalaxies consisting of hydrogen, helium, and dark matter. Modified gravity was originally proposed in MOND and MOG to account for the asymptotically flat rotation curve in outer galaxy and to keep galaxy together based on only baryonic matter. MOND and MOG propose the region (outer galaxy) for modified gravity in addition to the separate region (inner galaxy) for the Newtonian gravity.

CDM explains well and easily large-scale phenomena such as galaxy clusters and the universe evolution, while the modified gravity models explain well and easily small-scale phenomena such as galaxy. However, CDM [8] faces considerable difficulties to explain galaxy-scale phenomena, such as the observed absence of the cusp density in dwarf galaxies, the formation of long thin spiral galaxies, and the continuous failure to detect dark matter directly on earth. The modified gravity models require additional assumptions and complications to explain large-scale phenomena such as the observed dark matter halos in galaxy clusters, the observed gravitational lensing of dark matter, and the observed peaks in CMB (Cosmic Microwave Background) [8]. Furthermore, the modified gravity models essentially are valid only on galactic scales. Extremely low acceleration experiments (below the acceleration constant a_0) have been conducted, finding no departure from Newton's second law in laboratory conditions [9].

A possible solution to the dilemma of CDM and the modified gravity models is to combine both dark matter and modified gravity in a single model for galaxy. The proposed single model is the MIG model. The proposed modified interfacial gravity is the modified

Author: e-mail dy_chung@yahoo.com

gravity in the interfacial region between homogeneous baryonic matter region and homogeneous dark matter region, so MIG contains both modified gravity and dark matter to unify CDM, MOG, and MOND. MIG combines the existence of cold dark matter from CDM, the repulsive Yukawa force from MOG, and the critical homogeneous surface density derived from the acceleration constant a_0 from MOND [10,11]. The repulsive Yukawa force in outer galaxy in MOG is equivalent to the interfacial repulsive Yukawa force in the interfacial region to separate baryonic matter region and dark matter region in MIG. The modified interfacial gravity is interfacial gravity interacting with the interfacial repulsive Yukawa force. The modified interfacial gravity emerges in the interfacial region between dark matter region and baryonic matter region only when the homogeneous surface density is above the critical homogeneous surface density in both dark matter region and baryonic matter region. The critical homogeneous surface density is derived from the acceleration constant a_0 from MOND. CDM and MIG are identical during the very early universe below the critical homogeneous surface density and before the emergence of the interfacial repulsive force. After the emergence of the modified interfacial gravity by dense giant molecular clouds in the universe, MOND, MOG, and MIG are identical for the baryonic matter galaxy structure. As a result, MIG is the unified model of galaxy to unify CDM, MOG, and MOND as the different aspects of MIG. MIG explains both galaxy-scale and large-scale astronomical phenomena.

Section II explains the modified interfacial gravity in the interfacial region between dark matter region and baryonic matter region. Section III describes the evolution of galaxies, dark matter halos, dwarf galaxies, and globular clusters. Section IV describes dark matter halos for galaxy clusters.

II. THE MODIFIED INTERFACIAL GRAVITY

Dark matter in MIG is cold dark matter without electromagnetism as in CDM. The origin of dark matter without electromagnetism is explained in Reference [12]. The paper posits the modified interfacial gravity (MIG) as the modified gravity in the interfacial region between homogeneous baryonic matter region and homogeneous dark matter region. The MIG model contains both dark matter and modified gravity to unify the CDM, MOG, and MOND.

In MIG, the interfacial repulsive Yukawa force in the interfacial region to separate baryonic matter region and dark matter region is equivalent to the repulsive Yukawa force in outer galaxy for MOG. A repulsive Yukawa force was proposed as additional force for baryonic matter in MOG [3]. A Yukawa force appears only in a specific range. In MOG, the modified gravity is gravity interacting with the repulsive Yukawa force. In

Scalar-Tensor-Vector Gravity (STVG) [3] of MOG, the radial acceleration, a , acquires a Yukawa modification as in Equation (1) as explained in Reference [3].

$$a = -\frac{GM}{r^2} + \frac{GM}{r^2} \left\{ \sqrt{\frac{M_0}{M}} \left[1 - \exp(-r/r_0) \left(1 + \frac{r}{r_0} \right) \right] \right\} \tag{1}$$

$$= a_{inner\ galaxy} + a_{outer\ galaxy}$$

where G is the gravitation constant, r is the distance, r_0 is the starting distance for the Yukawa modification, M is the enclosed mass, and M_0 is a coupling constant of the Yukawa modification. The equation shows the two regions consisting of the Newtonian region (inner galaxy) with $a = GM/r^2$ and the repulsive Yukawa force region (outer galaxy) with the acceleration resulted from gravity interacting with the Yukawa vector force field and $r \gg r_0$.

The repulsive Yukawa force in outer galaxy for MOG is equivalent to the interfacial repulsive Yukawa force in the interfacial region to separate baryonic matter region and dark matter region in MIG. (The interfacial repulsive Yukawa force is the repulsive force between baryonic matter and dark matter [1].) The modified interfacial gravity is interfacial gravity interacting with the interfacial repulsive Yukawa force.

The four separate regions in the galaxy structure for MIG are the core (inner) baryonic matter galaxy with the Newtonian gravity, the interfacial (outer) baryonic matter galaxy with the modified interfacial gravity, the interfacial (inner) external dark matter halo with the modified interfacial gravity, and the core (outer) external dark matter halo with the Newtonian gravity as Figure 1.

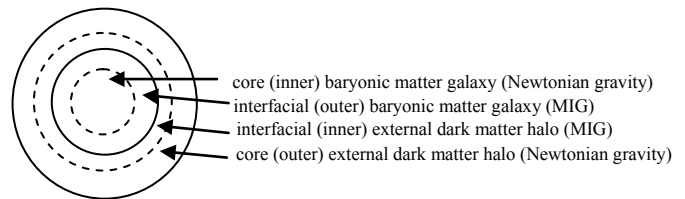


Figure 1 : the dark matter region and the baryonic matter regions

For MIG, from the rotation velocity, $V = (ar)^{1/2}$ and Equation (1), the rotation velocity can be derived as Equation (2).

$$V = \sqrt{\frac{GM}{r} + \frac{GM}{r} \left\{ \sqrt{\frac{M_0}{M}} \left[1 - \exp(-r/r_0) \left(1 + \frac{r}{r_0} \right) \right] \right\}^{1/2}} \tag{2}$$

$$= V_{core} + V_{interfacial}$$

$$= V_{inner\ galaxy} + V_{outer\ galaxy}$$

Equation (2) is the rotation velocity equation for MOG. Equation (2) shows that the rotation velocities are different in the core region with $V = (GM/r)^{1/2}$ and in the interfacial region with the velocity resulted from gravity interacting with the Yukawa vector force field. From the rotation velocities of a number of galaxies, the value of M_0

is found to be $9.6 \times 10^{11} M_{\text{sun}}$ and r_0 is found to be 13.92 kpc. Equation (2) yields a flat rotation curve in the interfacial region (outer galaxy). The rotation velocity equation of MOG as Equation (2) for the inner galaxy and outer galaxy can fit well the observed rotation curves of galaxies.

There are the Newtonian attractive gravity and the interfacial repulsive Yukawa force in the interfacial region. The dominate force is the Newtonian attractive gravity that disrupts the interfacial repulsive Yukawa force. The modified interfacial gravity is interfacial gravity interacting with the interfacial repulsive Yukawa force. The modified interfacial gravity between dark matter region and baryonic matter region emerges only when the homogeneous surface density in both dark matter region and baryonic matter region is above the critical homogeneous surface density to overcome the disruption of the Newtonian gravity. As shown later, the critical homogeneous surface density is derived from the acceleration constant a_0 from MOND.

Such emergence of the modified interfacial gravity is similar to the emergence of superconductivity. Among electrons, there are Coulomb repulsion and phonon attraction to form the Cooper pairs. The dominant force is Coulomb repulsion that disrupts phonon attraction. Superconductivity emerges only when the density of a dense-correlated electron system is above the critical density to overcome the disruption of Coulomb repulsion [13,14]. Superconductivity emerges with Coulomb repulsion in the two different regions: the short-distance superconductivity and the long-distance Coulomb repulsion as in the Hubbard model [15]. In the same way, the modified interfacial gravity emerges with Newtonian gravity in two different regions: the interfacial region for the modified interfacial gravity and the core region for the Newtonian gravity.

The critical homogeneous surface density is derived from the acceleration constant a_0 from MOND [10, 11]. (Below the critical homogeneous surface density, MIG is identical to CDM without modified interfacial gravity.) Milgrom found that the preferred surface density of giant molecular clouds in the galaxy can be derived from a_0 of MOND [10]. The critical homogeneous surface density Σ_0 is such surface density [11],

$$\begin{aligned} \Sigma_0 &= a_0 / 2\pi G \\ &= 138 M_{\text{sun}} \text{pc}^{-2} \end{aligned} \tag{3}$$

where a_0 is the acceleration constant $\approx 1.2 \times 10^{-10} \text{ m s}^{-2}$, a_0 is the acceleration at the critical homogenous surface density and G is the gravitational constant.

The core acceleration a_c ($a_c > a_0$) in the core region is unchanged as Newtonian acceleration a_n . In the interfacial region, the interfacial acceleration a_i is the Newtonian acceleration a_n ($a_n < a_0$) interacting with the interfacial force derived from a_0 at the critical

homogeneous surface density, resulting in the geometric mean [5] as $(a_n a_0)^{1/2}$ in Equation (4).

$$\begin{aligned} a_c &= a_n \\ a_i &= \sqrt{a_n a_0} \\ a_n &= a_i^2 / a_0 \end{aligned} \tag{4}$$

From the Newtonian gravity (GMm/r^2) and the Newtonian acceleration formula ($F = ma$), the core acceleration a_c in the core region is as Equation (5),

$$\begin{aligned} F_c &= ma_n \\ &= ma_c \\ &= \frac{GMm}{r^2} \\ a_c &= \frac{GM}{r^2} \end{aligned} \tag{5}$$

From the Newtonian gravity (GMm/r^2) and the Newtonian acceleration formula ($F = ma$), the interfacial acceleration a_i in the interfacial region is as Equation (6).

$$\begin{aligned} F_i &= ma_n \\ &= ma_i^2 / a_0 \\ &= \frac{GMm}{r^2} \\ a_i &= \frac{\sqrt{GMa_0}}{r} \end{aligned} \tag{6}$$

From $V^2 = ar$, Equation (5), and Equation (6), the rotation velocity V can be expressed as Equation (7).

$$\begin{aligned} V^2 &= V_c^2 + V_i^2 \\ &= V_{\text{inner galaxy}}^2 + V_{\text{outer galaxy}}^2 \\ &= \frac{GM}{r} + \sqrt{GMa_0} \end{aligned} \tag{7}$$

Equation (7) is the rotation velocity equation for MOND. Equation (7) shows that the rotation velocities are different in the core region with $V^2 = GM/r$ and in the interfacial region with $V^2 = (GMa_0)^{1/2}$ resulted from gravity interacting with the interfacial force at the critical homogeneous surface density. The rotation velocity equation of MOND as Equation (7) for the inner galaxy and outer galaxy can fit well the observed rotation curves of galaxies. The calculated rotation curves from MOND (Equation (7) and MOG (Equation (2)) are very similar [3].

III. THE EVOLUTION OF GALAXIES, DARK MATTER HALOS, DWARF GALAXIES, AND GLOBULAR CLUSTERS

Without the emergence of the modified interfacial gravity between dark matter region and baryonic matter region and below the critical homogeneous surface density, the models of galaxy evolution are the same in CDM and MIG in the period from the beginning of the universe to the coexistence of the large baryonic matter region as large dense

primordial molecular cloud and the large dense dark matter region. For the first few hundred thousand years after the Big Bang, the universe was a hot and murky mess, with no light radiating out. About 400,000 years after the Big Bang, temperatures in the universe cooled, electrons and protons joined to form neutral hydrogen as the recombination. The inhomogeneous structure in CMB (cosmic microwave background)[16] was observed as in both CDM and MIG. MOG and MOND without some form of non-baryonic dark matter cannot explain the peaks in CMB easily.

Dark matter halos were formed as in N-body collisionless dark matter simulations. They followed the NFW profile where the highest density is at the center as the central cusp. Baryonic matter was dragged along by the gravitationally dominant dark matter with the highest density at the center. When the temperature dropped to $\sim 1000^\circ\text{K}$, at the center of a dark matter halo, some hydrogen atoms paired up to create the primordial molecular layers. Molecular hydrogen cooled the primordial molecular layers by emitting infrared radiation after collision with atomic hydrogen. The further cosmic cooling reduced the gas pressure and allowing the molecular layers to continue contracting into gravitationally bound baryonic matter dense primordial molecular clouds. This process is the cooling flow for baryonic matter flowing to molecular clouds. The size of a molecular cloud increased by the process of gas accretion of cooling flow as in both CDM[17] and MIG.

In MIG, when the dense baryonic matter cloud and the dark matter region reached the critical homogeneous surface densities [10, 11] the modified interfacial gravity appeared to separate the dense baryonic matter molecular cloud and the dense dark matter region into two completely separate regions, the homogeneous baryonic matter region and the homogeneous dark matter region. Since there was much more dark matter than baryonic matter, the nearly homogeneous baryonic matter region was surrounded by the nearly homogeneous dark matter region. The baryonic matter region became the baryonic matter droplets surrounded by the dark matter medium in the baryonic matter-dark matter emulsion, which is like oil-water emulsion with oil as the oil droplet surrounded by water medium. The homogeneous baryonic matter droplet are shown as A and B in Figure 2.



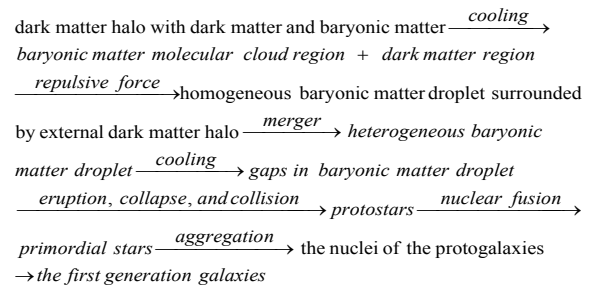
Figure 2 : homogeneous baryonic matter droplets (A, and B), and the heterogeneous baryonic matter droplets (C, D, E, and F)

Initially, the baryonic matter droplets were small. They increased in size by the cooling flow, gravity, and mergers with other small baryonic matter droplets. In MIG, the reduction of the interfacial repulsive Yukawa force between the baryonic droplets and the dark matter medium by the mergers of the droplets increased the rate of the mergers faster than the rate of the mergers of dark matter halos in CDM without the interfacial repulsive Yukawa force. The merger is analogous to the merger of the droplets in an unstable emulsion. The fast rate of the mergers in MIG explains the observation of very massive galaxy clusters at high redshifts sooner than expected in CDM[18]. Gradually, they became large homogeneous baryonic matter droplets. When three or more large homogeneous baryonic matter droplets merged, large dark matter regions were likely trapped in the merged droplet, resulting in heterogeneous baryonic matter droplets. To minimize the interfacial repulsive Yukawa force inside a heterogeneous baryonic matter droplet, dark matter regions inside the baryonic matter droplet merged into one or two dark matter regions inside the baryonic matter droplets, resulting in the heterogeneous baryonic matter droplets (C, D, E, and F in Figure 2). Surrounded by dark matter halo, a heterogeneous baryonic matter droplet contained the dark matter core and the baryonic matter shell. There were two modified interfacial gravities as the pressures between the dark matter core and the baryonic matter shell and between the baryonic shell and the external dark matter halo. In the equilibrium state, the internal pressure between the dark matter core and the baryonic matter shell was same as the external pressure between the baryonic shell and the dark matter halo.

The further cooling and the condensation of the primordial molecular clouds created the gaps and the random distribution of first stars in the baryonic matter shell. The gaps allowed the dark matter in the dark matter core to leak out, resulting in a tunnel between the dark matter core and the external dark matter halo. The continuous leaking of the dark matter expanded the tunnel. Consequently, the dark matter in the dark matter core rushed out of the dark matter core, resulting in the "droplet eruption" with the "ejected dark matter jet". A cause for the droplet eruption is the reduction of the interfacial repulsive Yukawa force by the merger of dark matter in the dark matter core and dark matter in the external dark matter halo. The kinetic energy of the ejected dark matter jet was derived from the interfacial repulsive Yukawa force between the dark matter core and the baryonic matter shell. The droplets acquired their droplet rotations from tidal interactions with other droplets, so the ejected dark matter jet was emitted largely along the rotating droplet's rotation axis, analogous to the jet moving in the same direction as the rotating neutron star's rotation axis.

During the droplet eruption, the ejected dark matter jet inevitably carried some baryonic matter out of the droplet along the droplet rotation axis. The baryonic matter in the ejected dark matter jet resulted eventually in the dwarf galaxies which are observed as satellite galaxies arranged on a plane. The explanation of dwarf galaxies is similar to the explanation by Noam I. Libeskind who proposes that the satellite galaxies did not flock to the Milky Way from all directions, but were shot towards it along cosmic superhighways (filaments) of dark matter, thus giving the satellites a preferred direction and alignment [19]. Under gravity, orbiting a galaxy, the dwarf galaxies from the ejected dark matter jet largely inhabit a single plane analogous to moons around a giant planet. Such dwarf galaxy planes for galaxy systems by MIG are confirmed by Ibata et al [20]. Among 380 galaxy systems in the nearby universe (redshift $z < 0.05$), their finding may indicate that co-rotating planes of satellites, similar to that seen around the Andromeda galaxy, are ubiquitous in nature,

The ejection of the dark matter from the dark matter core left a hole in the core of the droplet. The external pressure (the interfacial repulsive force) from the external dark matter halo caused the collapse of the baryonic matter droplet. The droplet collapse is like the collapse of a balloon as the air (as dark matter) moving out the balloon rapidly. The droplet collapse forced the head-on collisions of the primordial molecular clouds in the baryonic matter shell. In the center of the collapsed baryonic matter droplet, the head-on collisions of the primordial molecular clouds generated the shock wave as the turbulence in the collided primordial molecular clouds. The turbulence triggered the collapse of the core of the primordial cloud. The core fragmented into multiple stellar embryos, in each a protostar nucleated and pulled in gas. Without the heavy elements to dissipate heat, the mass of the primordial protostar was 500 to 1,000 solar masses at about 200°K. The primordial protostar shrank in size, increased in density, and became the primordial massive star when nuclear fusion began in its core. The aggregation of primordial stars formed the nuclei of the the protogalaxies. The star formation from the droplet collapse and head-on collision was highly efficient, which was confirmed by the observation of the completion of the rapid and explosive reionization process by extremely bright and active first galaxies in the period at least 250 million years shorter than expected [21]. The protogalaxies evolved into the first generation galaxies. Reference [1] describes how C, D, E, and F in Figure 2 turn into elliptical, spiral, barred spiral, and irregular galaxies, respectively, as the first generation galaxies that constitute the major part of the observed galaxies as follows.



The galaxy formation of the first generation galaxies in MIG is similar to a top-down formation as proposed by Olin Eggen, Donald Lynden-Bell, and Allan Sandage [22]. They proposed a top-down formation of galaxies through a monolithic collapse of a large gas cloud. The formation of galaxy by the droplet collapse from the droplet eruption allows the central region of a galaxy to produce high angular momentum from the external pressure (the interfacial repulsive Yukawa force) of the external dark matter halo in accordance with the Tully-Fisher relation in MOND[23] and to produce long thin disk for spiral galaxy as observed. The bigger the hole was during the droplet eruption and collapse, the thinner and longer the disk became. In CDM, the galaxy formation is through a bottom-up formation from the mergers of smaller galaxies to form larger galaxies in the manner of hierarchical formation. CDM without extensive modifications and fine tunings cannot produce high angular momentum and long thin disks for spiral galaxies, including numerous bulgeless spiral galaxies [8]. CDM also has the problem with the failure of to detect directly dark matter on earth. Dark matter has not been detected by the contact (interaction) between dark matter and baryonic matter. The absence of dark matter on earth is further confirmed by the study of the detailed set of measurements of planetary orbits by Nikolay Pitjev and Elena Pitjeva [24]. Their conclusion is that the gravitational effect of dark matter on the solar system is negligible. In MIG, galaxy interior is essentially dark matter-free, so it is not possible to detect dark matter on earth by the contact (interaction) between dark matter and baryonic matter.

There were large, medium, and small heterogeneous baryonic matter droplets for the droplet eruption. The timing for the droplet eruption depends on the cosmic temperature and the sizes of the droplets. At the cosmic temperature considerably below 1000°K, the droplet eruption for all different sizes of the droplets occurred within a certain period when the universe was a few hundred million years old. With the shorter distance for the dark matter in the dark matter core to travel to the outside of the droplet, the droplet eruption for smaller droplet occurred earlier. The times for the completed droplet collapse are also different for different sizes of the droplets. The completed droplet collapse took shorter time for a smaller hole left by ejected dark matter in a smaller droplet. The completed



droplet collapse led to the collision that produced the stars for the nuclei of protogalaxy, so the formation of stars in protogalaxy was faster for the smaller droplets. Protogalaxy evolved into galaxy. Consequently, the ages of majority of stars increase with decreasing size of galaxy.

When the universe was a few billion years old, and the galaxies were still in the protogalaxy stage without full development, large protogalaxies accreted the surrounding small and medium protogalaxies, and turned them into metal-poor globular clusters without external dark matter halos [25] in galactic halos. (Some of the accreted protogalaxies had their own accreted protogalaxies.) As a result, the stars in globular clusters derived from medium and small size baryonic matter droplets in general are older than the stars in the host large galaxies. The tidal interactions with the host galaxy stripped off largely outer stars and gases from a globular cluster. A similar approach was proposed by Patrick Cote et al. who proposed the assembly of the globular cluster system via the accretion of metal-poor protogalaxies by the dominant host protogalaxy (protobulge)[26].

The dwarf galaxies in the dwarf galaxy planes of large galaxies are derived from the ejected dark matter jets during the droplet eruption as mentioned before. Without the dark matter cores, these dwarf galaxies did not have droplet collapse, so these dwarf galaxies do not contain nuclei. The star formation came from the turbulences through the movement of the ejected dark matter jet and the gravitational interactions with parent large galaxies. The dwarf galaxies contain both metal-poor stars from the early formation of stars and metal-rich stars from the late formation of stars. Unlike globular clusters, the dwarf galaxies have external dark matter halos. As a result, the rotation velocities in the dwarf galaxies with external dark matter halos follow MOND, while the rotation velocities in globular clusters without dark matter halos follow the Newtonian gravity without dark matter [25].

IV. DARK MATTER HALO IN GALAXY CLUSTER

A galaxy cluster consists of hundreds to thousands of galaxies bound together by gravity. In MIG, in addition to normal galaxies, there are dwarf dark matter halos without baryonic matter droplet and dwarf dark halos with small baryonic matter droplets. When the baryonic matter primordial molecular clouds were formed in some dwarf dark matter halos, the molecular clouds below the critical homogeneous surface density resulted in dwarf dark matter halos without baryonic matter droplet. In some dwarf dark matter halos, baryonic matter droplets formed were too small to develop significant numbers of stars, resulting in the observed ultra-faint dwarf galaxy [27] for dwarf dark matter with small baryonic matter droplets. The

gravitational attraction of dwarf dark matter halos without baryonic matter droplet, ultra-faint dwarf galaxies, and normal galaxies brings about dark matter halos for galaxy clusters.

A recent study of fifty individual galaxy clusters finds that the density is observed to decrease outwards from the center of these galaxy clusters in excellent agreement with the predictions of dark matter halos in CDM models [28]. The method to measure dark matter density consists of measuring the slight distortion of background galaxies induced by the gravitational deformation of space-time along the line of sight. This gravitational lensing locates and measures the amount of dark matter, even though it is transparent on the image. The fifty observed galaxy clusters have individual variations for central concentrations. For all fifty observed galaxy clusters, the obtained map of the mean dark-matter distribution is symmetrical with a central cusp to be consistent with the NFW model. Without the active involvement of the modified interfacial gravity, the models for the evolution of dark matter halo for galaxy cluster are the same in CDM and MIG. MOND without 2eV neutrinos or non-baryonic form cannot explain dynamics and lensing of galaxy clusters.

V. SUMMARY

The paper posits the modified interfacial gravity (MIG) as the modified gravity in the interfacial region between homogeneous baryonic matter region and homogeneous dark matter region. The MIG model contains both dark matter and modified gravity to unify the CDM (Cold Dark Matter) model, MOG (Modified Gravity), and MOND (Modified Newtonian Dynamics). In MIG, the interfacial repulsive Yukawa force in the interfacial region to separate baryonic matter region and dark matter region is equivalent to the repulsive Yukawa force in outer galaxy in MOG. The modified interfacial gravity is interfacial gravity interacting with the interfacial repulsive Yukawa force. The modified interfacial gravity emerges in the interfacial region between dark matter region and baryonic matter region only when the homogeneous surface density is above the critical homogeneous surface density in both dark matter region and baryonic matter region. The critical homogeneous surface density is derived from the acceleration constant a_0 from MOND. The four separate regions in the galaxy structure in MIG are the core (inner) baryonic matter galaxy with the Newtonian gravity, the interfacial (outer) baryonic matter galaxy with the modified interfacial gravity, the interfacial (inner) external dark matter halo with the modified interfacial gravity, and the core (outer) external dark matter halo with the Newtonian gravity. Dark matter in the external dark matter halo is cold dark matter without electromagnetism as in CDM. CDM and MIG are identical during the very early universe below the critical

homogeneous surface density and before the emergence of the modified interfacial gravity. After the emergence of the modified interfacial gravity by dense giant molecular clouds during the early universe, MOND, MOG, and MIG are identical for baryonic matter galaxy structure. MIG explains galaxy evolution, globular clusters, dwarf galaxy plane, dark matter halo in galaxy cluster, the rotation velocities, and the failure to detect directly dark matter on earth.

REFERENCES RÉFÉRENCES REFERENCIAS

1. D. Chung. *Galaxy Evolution by the Incompatibility between Dark Matter and Baryonic Matter*. International Journal of Astronomy and Astrophysics **4**, 374-383(2014).
2. C. Frenk, and S. White. *Dark matter and cosmic structure*. Annalen der Physik **524**, 507-534(2012).
3. J. D. Brownstein and J. W. Moffat. *Galaxy Rotation Curves without Nonbaryonic Dark Matter*. Astrophysical Journal **636**, 721-741 (2006).
4. W. Moffat and S. Rahvar, *The MOG weak field approximation and observational test of galaxy rotation curves*. Monthly Notices of the Royal Astronomical Society **436**, 1439-1451(2013).
5. M. Milgrom. *A modification of the Newtonian dynamics as a possible alternative to the hidden mass hypothesis*. Astrophysical Journal **270**, 365-370 (1983).
6. M. Milgrom. *MOND--theoretical aspects*. New Astronomy Reviews **46**, 741-753 (2002).
7. B. Famaey and S. S. McGaugh. *Modified Newtonian Dynamics (MOND): Observational Phenomenology and Relativistic Extensions*. Living Review Relativity, **15**, 10(2012).
8. B. Famaey and S. S. McGaugh. *Challenges for Λ CDM and MOND*. Journal of Physics: Conference Series **437**, 012001 (2013).
9. J. H. Gundlach, et al. *Laboratory Test of Newton's Second Law for Small Accelerations*. Physical Review Letter **98**, 150801(2007).
10. M. Milgrom. *Concerning the preferred surface density of giant molecular clouds in the Galaxy*. Astronomy and Astrophysics **211**, 37-40(1989).
11. M. Milgrom. *The central surface density of 'dark haloes' predicted by MOND*. Monthly Notices of the Royal Astronomical Society **398**, 1023-1026(2009),
12. D. Chung, and V. Krasnoholovets. *The Space Structure, Force Fields, and Dark Matter*. Journal of Modern Physics **4**, 27-31(2013).
13. P. W. Anderson. *More Is Different*. Science **177**, 393-396(1972).
14. D. Chung. *The Basic Cause of Superconductivity*. Journal of Modern Physics **6**, 26-36(2015)
15. J. Hubbard. *Electron Correlations in Narrow Energy Bands*. Proceedings of the Royal Society A **276**, 237-257(1963).
16. A. Readhead et al. *Extended Mosaic Observations with the Cosmic Background Imager*. Astrophysical Journal **609**, 498-512(2004).
17. Q. Guo et al. *From dwarf spheroidals to cD galaxies: simulating the galaxy population in a Λ CDM cosmology*. Monthly Notices of the Royal Astronomical Society **413**, 101-131(2011).
18. F. Menanteau et al. *The Atacama Cosmology Telescope: ACT-CL J0102-4215 'El Gordo,' A Massive Merging Cluster at Redshift 0.87*. The Astrophysical Journal **748**, 7(2012).
19. N. I. Libeskind et al. *The distribution of satellite galaxies: the great pancake*. Monthly Notices of the Royal Astronomical Society **363**, 146-152(2005).
20. N. G. Ibata, R. A. Ibata, B. Famaey, and G. F. Lewis. *Velocity anti-correlation of diametrically opposed galaxy satellites in the low-redshift Universe*. Nature **511**, 563-566 (2014).
21. O. Zahn et al. *Cosmic Microwave Background Constraints on the Duration And Timing of Reionization from the South Pole Telescope*. The Astrophysical Journal **756**, 65(2012).
22. O. J. Eggen, D. Lynden-Bell, and A. R. Sandage. *Evidence from the motions of old stars that the Galaxy collapsed*. The Astrophysical Journal **136**, 748-766(1962).
23. S. McGaugh. *The Baryonic Tully-Fisher Relation of Gas Rich Galaxies as a Test of Λ CDM and MOND*. The Astrophysical Journal, **143**, 40(2012).
24. N. P. Pitjeu and E. V. Pitjeva. *Constraints on dark matter in the solar system*. Astronomy Letters **39-3**, 141-149(2013).
25. R. Ibata et al. *The Globular Cluster Ngc 2419: A Crucible for Theories of Gravity*. The Astrophysical Journal **738**, 186 (2011).
26. P. Cote et al. *Evidence for the Hierarchical Formation of the Galactic Spheroid*. The Astrophysical Journal **533**, 869-883(2000).
27. T. M. Brown et al. *The Primeval Populations of the Ultra-Faint Dwarf Galaxies*. The Astrophysical Journal Letters **753**, L21 (2012).
28. N. Okabe. et al, *LoCuSS: The Mass Density Profile of Massive Galaxy Clusters at $z=0.2$* . The Astrophysical Journal Letters **769**, L35 (2013).



GLOBAL JOURNAL OF SCIENCE FRONTIER RESEARCH: A
PHYSICS AND SPACE SCIENCE
Volume 15 Issue 3 Version 1.0 Year 2015
Type : Double Blind Peer Reviewed International Research Journal
Publisher: Global Journals Inc. (USA)
Online ISSN: 2249-4626 & Print ISSN: 0975-5896

Electronic Transport Properties in Bulk ZnO and $Zn_{1-x}Mg_xO$ Using Monte Carlo Simulation

By F. Nofeli & H. Arabshahi

Khayyam University, Mashhad, Iran

Abstract- In this paper, an investigation with the application of Monte Carlo simulations to steady-state electron transport and low-field electron mobility characteristics of in bulk ZnO in the wurtzite crystal structure and its alloy $Zn_{1-x}Mg_xO$ with different doping of Mg, $x=0.05, 0.1$ and 0.2 . The Monte Carlo calculations are carried out using a three-valley model for the systems under consideration. The following scattering mechanisms, i.e, impurity, polar optical phonon and acoustic phonon are included in the calculation. The maximum electron drift velocity that is obtained at room temperature for 10^{23} m^{-3} donor concentration is $1.97 \times 10^7 \text{ cms}^{-1}$ for ZnO in threshold field of 400 kV/cm. While the maximum electron drift velocity is $1.62 \times 10^7 \text{ cms}^{-1}$, $1.03 \times 10^7 \text{ cms}^{-1}$ and $0.43 \times 10^7 \text{ cms}^{-1}$ for $Zn_{0.95}Mg_{0.05}O$, $Zn_{0.9}Mg_{0.1}O$ and $Zn_{0.8}Mg_{0.2}O$ in threshold field 700 kV/cm respectively. It can be seen the peak drift velocity for bulk ZnO is $1.97 \times 10^7 \text{ cms}^{-1}$, while for $Zn_{1-x}Mg_xO$ the peak drift velocity decreases due to increasing electron effective mass.

Keywords: *Electron Transport, Monte Carlo Simulation, Wurtzite $Zn_{1-x}Mg_xO$, Effective Mass.*

GJSFR-B Classification : *FOR Code: 030399p*



Strictly as per the compliance and regulations of :



Electronic Transport Properties in Bulk ZnO and Zn_{1-x}Mg_xO Using Monte Carlo Simulation

F. Nofeli ^α & H. Arabshahi ^σ

Abstract- In this paper, an investigation with the application of Monte Carlo simulations to steady-state electron transport and low-field electron mobility characteristics of in bulk ZnO in the wurtzite crystal structure and its alloy Zn_{1-x}Mg_xO with different doping of Mg, x=0.05, 0.1 and 0.2. The Monte Carlo calculations are carried out using a three-valley model for the systems under consideration. The following scattering mechanisms, i.e, impurity, polar optical phonon and acoustic phonon are included in the calculation. The maximum electron drift velocity that is obtained at room temperature for 10²³ m⁻³ donor concentration is 1.97×10⁷ cms⁻¹ for ZnO in threshold field of 400 kV/cm. While the maximum electron drift velocity is 1.62×10⁷ cms⁻¹, 1.03×10⁷ cms⁻¹ and 0.43×10⁷ cms⁻¹ for Zn_{0.95}Mg_{0.05}O, Zn_{0.9}Mg_{0.1}O and Zn_{0.8}Mg_{0.2}O in threshold field 700 kV/cm respectively. It can be seen the peak drift velocity for bulk ZnO is 1.97×10⁷cms⁻¹, while for Zn_{1-x}Mg_xO the peak drift velocity decreases due to increasing electron effective mass.

We find about valley occupancy in this materials that for fields lower than the threshold field, most of the electrons are in the central valley and significant inter valley scattering into the satellite valleys occurs just for fields above the threshold field.

Finally for electron mobility shows the maximum electron mobility for ZnO is 886 cm²/V.s and for Zn_{1-x}Mg_xO in various amount x=0.05, 0.1 and 0.2 is 304, 132 and 33 cm²/V.s respectively. The electron mobility of ZnO is more than ZnMgO alloys at all temperatures because electron mobility behavior dependence on effective mass and ionized impurity concentration.

Keywords: Electron Transport, Monte Carlo Simulation, Wurtzite Zn_{1-x}Mg_xO, Effective Mass.

I. INTRODUCTION

Recently, the material properties of ZnO and Zn_{1-x}Mg_xO has attracted much attention [1-8]. This interest has been fuelled, in large measure, by the considerable promise that these materials offer for novel electronic and optoelectronic device. ZnO possesses material properties that makes it particularly suitable for a number of important electronic and optoelectronic device applications. The important properties for ZnO include its wide and direct energy gap of 3.43 (eV), small effective mass, large inter valley energy separation, and large polar optical phonon energy. ZnO is an exhibit favorable electron transport characteristics, so a number of studies of the electron transport that occurs within this material have been

Author α: Physics Department, Khayyam University, Mashhad, Iran.

e-mail: fariba.nofeli@yahoo.com

Author σ: hadi_arabshahi@yahoo.com

reported over the years. Based on these fundamental properties, ZnO has many applications in the short wavelength region, such as optically pumped lasers, UV light emitting diodes, detectors, solar cells, gas sensor and many other advantages, make ZnO a strong candidate for the next generation of ultraviolet light emitting and lasing devices operating at high temperatures and in harsh environments [9-11]. These material properties suggest that bulk ZnO will exhibit favorable electron transport characteristics, i.e., elevated steady-state electron drift velocities [12].

Of course it should be pointed out that ZnO is a group transparent conductive oxide (TCO) material. The transparent conductive oxide (TCO) materials, such as ZnO, In₂O₃, Ga₂O₃, Al₂O₃ are fundamental components in optoelectronic devices [6,7]. In 1999-now, Albrecht et al. and Arabshahi et al. reported on Monte Carlo simulations of the steady-state electron transport that occurs within bulk wurtzite ZnO [4,5].

Studies indicate that ZnO with ZnMgO alloys like Zn_{1-x}Mg_xO can improve some properties optoelectronic devices [1-6]. The purpose of the present paper studying the steady-state transport in high electric field and in low filed electron mobility within Bulk ZnO and Zn_{1-x}Mg_xO by three-valley Monte Carlo simulation analysis in 10000 electrons. It is organized as follows. Details of the simulation model which is used in this work are presented in Sec. II, and results for simulation are interpreted in Sec. III-1 for steady-state and Sec. III-2 for electron mobility.

II. MODEL DETAILS

In this research for studying of the electron transport within a semiconductor, an ensemble Monte Carlo approach is used in order to solve the Boltzman transport equation (BTE), the BTE describes how the electron distribution function evolves under the action of an applied electric field. In this approach, the motion of a large number of electrons within a semiconductor, under the action of an applied electric field, is simulated. The acceleration of each electron in the applied electric field, and the present of the scattering, are both taken into account. The scattering events that an individual electron experiences are selected randomly, the probability of each such event being selected in proportion to the scattering rate corresponding to that particular event. The analysis of electron transport is restricted within the conduction band. Typically, only the

lowest part of the conduction band contain a significant fraction of the electron population instead of including the entire electron band structure for the conduction band, so only the lowest valleys need to be represented and in this work a three valley model is used. Within the framework of this three valley model, the non parabolicity of each valley is treated through the application of the Kane model, the energy band corresponding to each valley being assumed to be spherical and is the form of:

$$E(k)[1 + \alpha_i E(k)] = \frac{\hbar^2 k^2}{2m^*}$$

Where m^* is the electron effective mass in it valley and α_i is the non parabolicity coefficient in it valley. The scattering mechanisms considered are ionized impurity, polar optical phonon, and acoustic deformation potential and inter valley scattering. For electron transport properties in Bulk ZnO and Zn_{1-x}Mg_xO Materials simulations, the motion of 10000 electrons is examined in three valleys of Γ , U and K. The material parameters and valley parameters that are used in this simulation are mentioned in tables I and II.

Table 1 : Material parameters for wurtzite ZnO [5]

Parameters	Unit	ZnO
Mass density	kg/m	5600
Static relative permittivity	ϵ_0	8.2
High frequency relative permittivity	ϵ_∞	3.7
Polar optical phonon	ev	0.072
Piezoelectric constant	C/m ^y	0.089
Acoustic deformation potential	ev	14
Sound velocity	m/s	6400
Direct energy gap	ev	3.43

Table 2 : Valley parameters for wurtzite ZnO and Zn_{1-x}Mg_xO [5,6]

Valley (ZnO)	Unit	Γ	U	K
Electron effective mass	m^*/m_0	0.318	0.42	0.7
Non parabolicity coefficients	1/ev	0.312	0.059	0.65
Equivalent valley number	-	1	6	2
Valley separation	ev	0	2.1	2.9

Valley (Zn _{1-x} Mg _x O)	Unit	Γ	U	K
Effective mass for x = 0.05	m^*/m_0	0.462	0.61	1.015
Effective mass for x = 0.1	m^*/m_0	0.7338	0.969	1.61
Effective mass for x = 0.2	m^*/m_0	1.5586	2.05	3.4

III. RESULTS

a) Steady-State Electron Transport

Figure 1 shows the velocity-field characteristics that obtained by our model for ZnO wurtzite and Zn_{1-x}Mg_xO with different doping of Mg, x=0.05, 0.1 and 0.2 in 300K temperature and in the 10²³ m⁻³ donor concentration. It can be seen, the electron drift velocity increases by high electric field. As soon as the electrons drift velocity and electric field reached to electrons thermal velocity and threshold field, so the electrons are scattered from Γ valley to satellite valleys with more electrons effective mass. In upper valleys the electrons effective mass increase and scattering rate of electrons increase, so the drift velocity decreases. Therefore this

scattering creates a peak velocity in curve of drift velocity-electric field. The simulations suggest that the peak drift velocity for bulk ZnO is 1.97×10⁷ cm/s in threshold field of 400kV/cm, while the maximum drift velocity for Zn_{0.95}Mg_{0.05}O, Zn_{0.9}Mg_{0.1}O and Zn_{0.8}Mg_{0.2}O is 1.62×10⁷ cm/s, 1.03×10⁷ cm/s and 0.43×10⁷cm/s in threshold field of 700 kV/cm respectively. The results shows that the electrons drift velocity decreases in ZnMgO alloys due to have effective mass more than ZnO in satellite valleys, so the scattering rate of electrons increase and mobility and drift velocity of electrons decreases in this valleys. These results of Monte Carlo simulation are in good agreement with the others calculation [6].

Figure 2 shows the calculated electron drift velocity as a function of high electric field at the different temperature. It can be seen that the temperature increasing causes the drift velocity decreasing. On the other hand the peak velocity occurs in the higher electric fields when the temperature increases.

The valley occupation for the Γ , U and K valleys are shown in Figure 3. It is obvious that the inclusion of satellite valleys in the simulation is important. Significant electron transfer to the upper valleys only begins to occur when the field strength is very close to the threshold value. For electric fields lower than the threshold field, most of the electrons are in the central valley and significant inter valley scattering into the satellite valleys occurs in electric fields above the threshold field for ZnO and each of ZnMgO alloys. The reason can be explained in terms of different electron effective masses for this materials within the central valley. This is important because electrons which are

near a valley minimum have small kinetic energy and therefore strongly scattered. At the threshold field 400 kV/cm in bulk ZnO for Γ the electron valley occupancies at room temperature is 100%. And in electric field more than threshold field like 500 kV/cm the electron valley occupancies are about 95% in Γ valley and 4% in U valley. Also we know, the effective mass in ZnMgO alloys are more than ZnO, so for the ZnMgO alloys intervalley scattering into the satellite valleys occur in stronger electric fields.

The total average electron kinetic energy as a function of electric field is shown in Figure 4. It can be seen that, kinetic energy increases with the electric field due to the large proportion of electrons in the low mass Γ valley. However, as the field increases the electrons transfer to higher valleys with higher mass and increased scattering which causes a substantial reduction in the rate of increasing of energy.

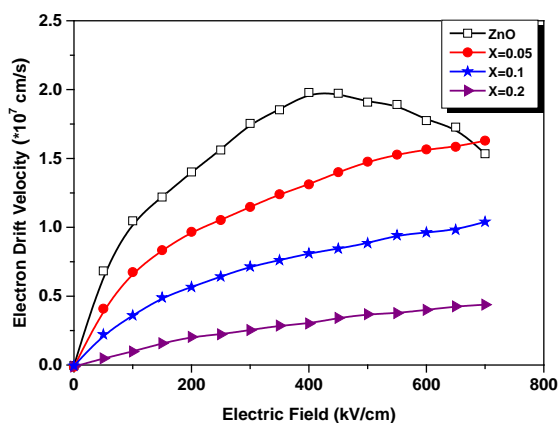


Figure 1 : Calculated electron drift velocity in wurtzite ZnO, Zn_{0.95}Mg_{0.05}O, Zn_{0.9}Mg_{0.1}O and Zn_{0.8}Mg_{0.2}O at T=300 K and 10²³ m⁻³ impurity concentration

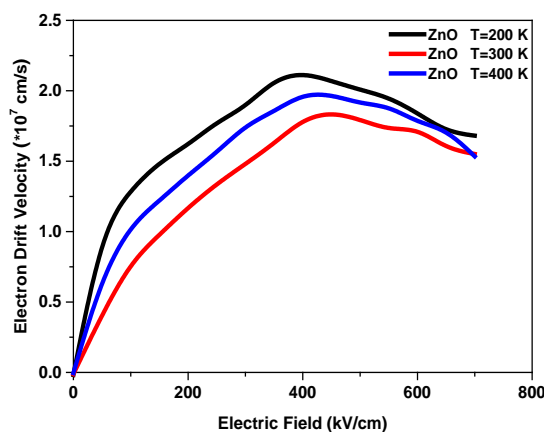


Figure 2 : Calculated electron drift velocity in bulk ZnO at 10²³ m⁻³ impurity Concentration and different temperatures

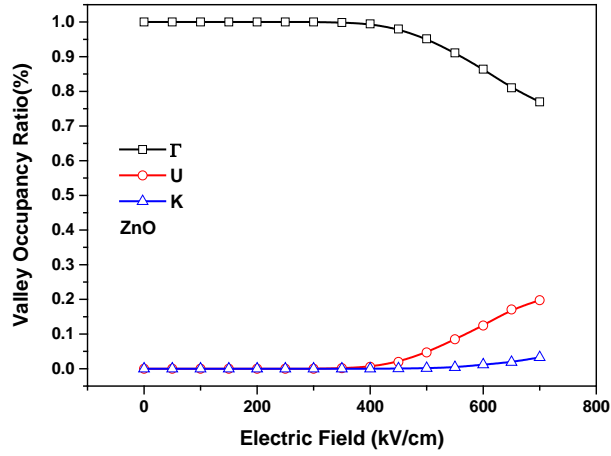


Fig 3 : A

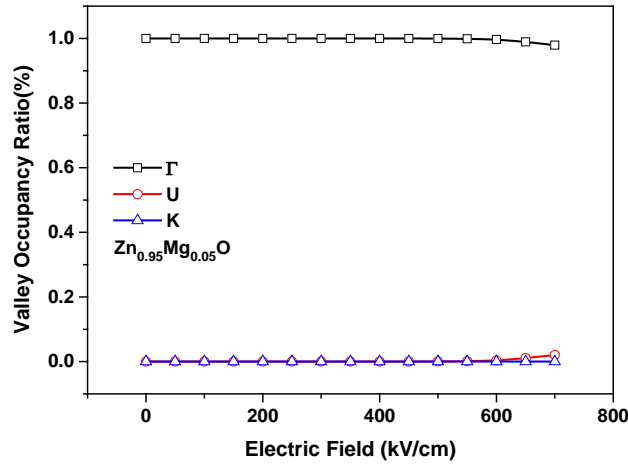


Fig 3 : B

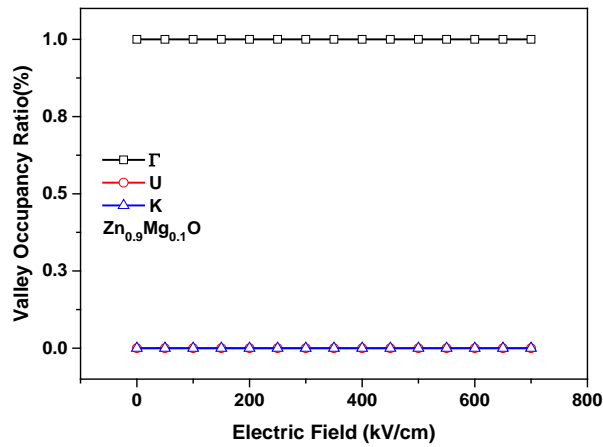


Fig 3 : C

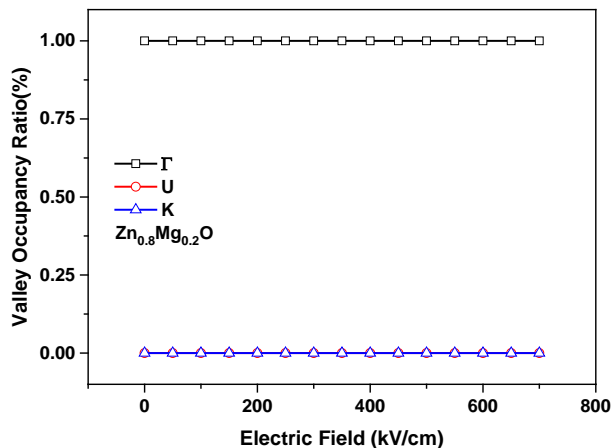
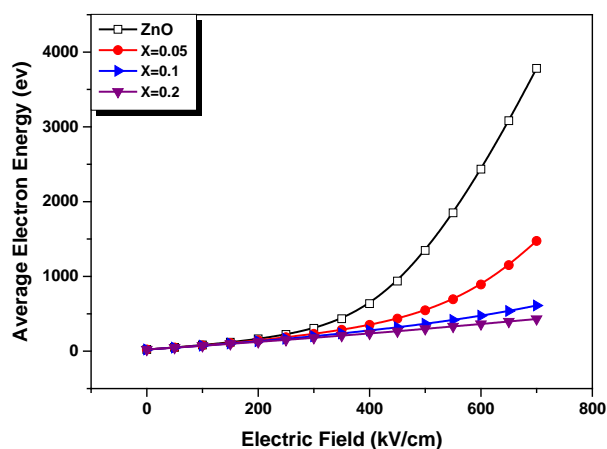


Fig 3 : D

Figures 3 : Calculated valley occupancy ratio in bulk ZnO and ZnMgO alloys at T=300K and 10^{23} m⁻³ impurity concentration



Figures 4 : Total average electron kinetic energy in bulk ZnO and ZnMgO alloys at T=300 K and 10^{23} m⁻³ impurity concentration

b) Electron Mobility

The electron mobility calculates in low field because changing curve drift velocity-electric field is high before threshold field, so the mobility in low field is important. But after threshold field, changing drift velocity in terms of electric field is a little and also the electron mobility decrease. The mobility values are found from each curve of the slope of the linear part of each velocity–field curve.

Figure 5 shows the calculated electron mobility in term temperature in bulk ZnO, Zn_{0.95}Mg_{0.05}O, Zn_{0.9}Mg_{0.1}O and Zn_{0.8}Mg_{0.2}O at the 10^{23} m⁻³ impurity concentration. It can be seen that the electron mobility at room temperature for ZnO is 886 cm²/V.s and for Zn_{0.95}Mg_{0.05}O, Zn_{0.9}Mg_{0.1}O and Zn_{0.8}Mg_{0.2}O is 304, 132 and 33 cm²/V.s respectively. The results indicate that the

electron mobility of ZnO is more than ZnMgO alloys at all temperatures. This is largely due to the higher valley effective mass in the ZnO phase. Increasing temperature is increased phonons scattering rate and energy of phonons, so it causes a strong interaction between electrons and these phonons that its result is increase of electrons scattering rate and finally decrease of the electrons mobility. Figure 6 show that the electron mobility decrease by the electrons concentrations increasing because electrons increasing causes increase of ionized impurity centers in crystals that it causes times more electrons under the influence of the coulomb potential of impurity centers located that its result is increase of electrons scattering rate and finally decrease of electrons mobility.

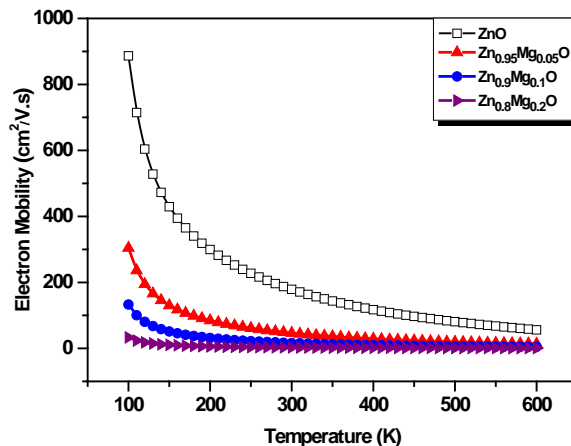


Figure 5 : Changes the electron mobility function in terms of temperature in bulk ZnO and ZnMgO alloys at the 10^{23} m^{-3} impurity concentration

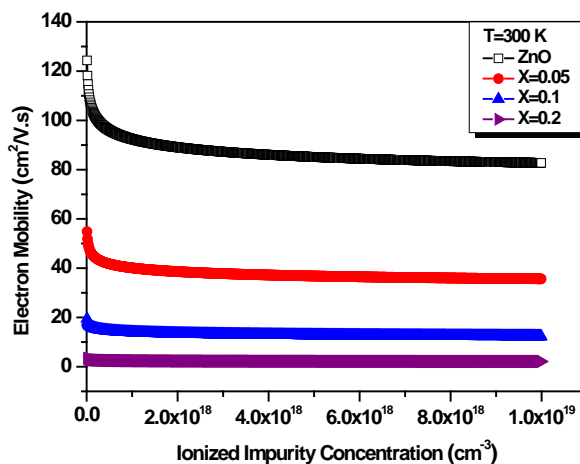


Figure 6 : Changes the electron mobility function in term of ionized impurity concentration in bulk ZnO, Zn_{0.95}Mg_{0.05}O, Zn_{0.9}Mg_{0.1}O and Zn_{0.8}Mg_{0.2}O at room temperature

IV. CONCLUSION

This research presents is about electron transport properties in bulk ZnO and Zn_{1-x}Mg_xO materials performed with ensemble Monte Carlo simulation for different temperatures and ionized impurity concentrations.

These calculations for bulk ZnO and Zn_{1-x}Mg_xO show superior electron transport properties that in this study we obtained some the results for application this materials in device semiconductors:

1. The band gap, drift velocity, mobility and cutoff frequency of bulk ZnO can be controlled by MgO alloys in Zn_{1-x}Mg_xO materials and in this case the electron effective mass increases and the electron mobility decreases. Therefore we can control peak velocity and saturation velocity of threshold field in this materials.

2. The ZnMgO alloys are stronger than ZnO, because the threshold field in ZnMgO alloys is higher than ZnO. Therefore these days in engineering science that use this materials in semiconductors.
3. Comparison of ZnO and ZnMgO alloys show the electrons drift velocity in ZnMgO alloys are less susceptibility to changing temperature. Therefore devices that are made by ZnMgO alloys are more resistant versus high temperature and heat and these devices have more efficiency.
4. The electron mobility in ZnO semiconductor is upper than of ZnMgO alloys because the effective mass in ZnO is lower than Zn_{1-x}Mg_xO. Also the ionized impurity scattering in both the semiconductor ZnO, Zn_{0.95}Mg_{0.05}O, Zn_{0.9}Mg_{0.1}O and Zn_{0.8}Mg_{0.2}O at all temperatures is an important factor in reducing the mobility.

REFERENCES RÉFÉRENCES REFERENCIAS

1. Daqian Ye, Zengxia Mei, Huili Liang, Junqiang Li, Yaonan Hou, Changzhi Gu, Alexander Azarov, Andrej Kuznetsov, Wen-Chiang Hong, Yicheng Lu, and Xiaolong Du, "Enhancement-mode $ZnO/Mg_{0.5}Zn_{0.5}O$ HFET on Si", <http://doi:10.1088/0022-3727/47/25/255101>, 2014.
2. Xu Ji, Yuan Zhu, Mingming Chen, Longxing Su, Anqi Chen, Xuchun Gui, Rong Xiang & Zikang Tang, "The modulation of grain boundary barrier in $ZnMgO/ZnO$ hetero structure by surface polar liquid", *Applied Physics Electronic, Processing Electronic Devices*, Scientific, doi: 10.1038/srep04185, 2014.
3. A. Guen-Bouazza, C. Sayah, B. Bouazza, N. E. Chabane-Sari, "Steady-State and Transient Electron Transport within Bulk InAs, InP and GaAs: An Updated Semiclassical Three-Valley Monte Carlo Simulation Analysis", *Journal of Modern Physics*, <http://dx.doi.org/10.4236/jmp.2013.45089>, 2013.
4. H. Arabshahi, M. R. Ronki-Abadi, and F. B. Bagh-Siyahi, "Comparison of High Field Electron Transport Properties in Wurtzite Phase of ZnO , GaN and SiC", *Research Journal of Applied Sciences*, vol. 5, no. 3, pp. 215-220, 2010.
5. H. Arabshahi and F. Badieian-Baghsiyahi, "Simulation of High Field Electron Transport in Wurtzite Phase of ZnO ", *International Archive of Applied Sciences and Technology*, vol 3, pp. 105 – 111, 2012.
6. Yarar. Z., "Steady-State Electron Transport and Low-Field Mobility of Wurtzite Bulk ZnO and $Zn_{1-x}Mg_xO$ ", Vol. 40, No. 4, 2011. DOI: 10.1007/s11664-011-1516-1.
7. Wei Wei, Chunming Jin, Jagdish Narayan, and Roger J. Narayan, "Optical and electrical properties of gallium doped $Mg_x Zn_{1-x} O$ ", *J Appl Phys*, 10.1063/1.3271415, 2010.
8. Bernhard Laumer, Thomas A. Wassner, Fabian Schuster, Martin Stutzmann, Jörg Schörmann, Marcus Rohnke, Alexej Chernikov, Verena Bornwasser, Martin Koch, Sangam Chatterjee and Martin Eickhoff, "Exciton confinement in homo- and hetero epitaxial $ZnO/Zn_{1-x}Mg_xO$ quantum wells with $x < 0.1$ ", *JOURNAL OF APPLIED PHYSICS* 110, 093513, 2011.
9. Chih-I Huang, Huai-An Chin, Yuh-Renn Wu, Member, IEEE, I-Chun Cheng, Member, IEEE, Jian Z. Chen, Member, IEEE, Kuo-Chuang Chiu, and Tzer-Shen Lin, "Mobility Enhancement of Polycrystalline $MgZnO/ZnO$ Thin Film Layers With Modulation Doping and Polarization Effects", *IEEE Transactions on Electron Devices*, vol. 57, No. 3, 2010.
10. C. Jacoboni and P. Lugli, "The Monte Carlo Method for Semiconductor and Device Simulation", 1998.
11. V. Srikant and D. R. Clarke, "On the optical band gap of zinc oxide," *Journal of Applied Physics*, vol. 83, no. 10, pp. 5447-5451, 1998.
12. Walid Abdul Hadi, "The electron transport within the wide energy gap compound semiconductors gallium nitride and zinc oxide", University of Windsor, Ontario, Canada, 2014.



GLOBAL JOURNALS INC. (US) GUIDELINES HANDBOOK 2015

WWW.GLOBALJOURNALS.ORG

FELLOWS

FELLOW OF ASSOCIATION OF RESEARCH SOCIETY IN SCIENCE (FARSS)

Global Journals Incorporate (USA) is accredited by Open Association of Research Society (OARS), U.S.A and in turn, awards “FARSS” title to individuals. The 'FARSS' title is accorded to a selected professional after the approval of the Editor-in-Chief/Editorial Board Members/Dean.



- The “FARSS” is a dignified title which is accorded to a person’s name viz. Dr. John E. Hall, Ph.D., FARSS or William Walldroff, M.S., FARSS.

FARSS accrediting is an honor. It authenticates your research activities. After recognition as FARSS, you can add 'FARSS' title with your name as you use this recognition as additional suffix to your status. This will definitely enhance and add more value and reputation to your name. You may use it on your professional Counseling Materials such as CV, Resume, and Visiting Card etc.

The following benefits can be availed by you only for next three years from the date of certification:



FARSS designated members are entitled to avail a 40% discount while publishing their research papers (of a single author) with Global Journals Incorporation (USA), if the same is accepted by Editorial Board/Peer Reviewers. If you are a main author or co-author in case of multiple authors, you will be entitled to avail discount of 10%.

Once FARSS title is accorded, the Fellow is authorized to organize a symposium/seminar/conference on behalf of Global Journal Incorporation (USA). The Fellow can also participate in conference/seminar/symposium organized by another institution as representative of Global Journal. In both the cases, it is mandatory for him to discuss with us and obtain our consent.



You may join as member of the Editorial Board of Global Journals Incorporation (USA) after successful completion of three years as Fellow and as Peer Reviewer. In addition, it is also desirable that you should organize seminar/symposium/conference at least once.

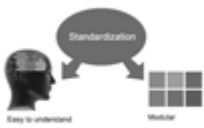
We shall provide you intimation regarding launching of e-version of journal of your stream time to time. This may be utilized in your library for the enrichment of knowledge of your students as well as it can also be helpful for the concerned faculty members.





The FARSS can go through standards of OARS. You can also play vital role if you have any suggestions so that proper amendment can take place to improve the same for the benefit of entire research community.

As FARSS, you will be given a renowned, secure and free professional email address with 100 GB of space e.g. johnhall@globaljournals.org. This will include Webmail, Spam Assassin, Email Forwarders, Auto-Responders, Email Delivery Route tracing, etc.



The FARSS will be eligible for a free application of standardization of their researches. Standardization of research will be subject to acceptability within stipulated norms as the next step after publishing in a journal. We shall depute a team of specialized research professionals who will render their services for elevating your researches to next higher level, which is worldwide open standardization.

The FARSS member can apply for grading and certification of standards of their educational and Institutional Degrees to Open Association of Research, Society U.S.A. Once you are designated as FARSS, you may send us a scanned copy of all of your credentials. OARS will verify, grade and certify them. This will be based on your academic records, quality of research papers published by you, and some more criteria. After certification of all your credentials by OARS, they will be published on your Fellow Profile link on website <https://associationofresearch.org> which will be helpful to upgrade the dignity.



The FARSS members can avail the benefits of free research podcasting in Global Research Radio with their research documents. After publishing the work, (including published elsewhere worldwide with proper authorization) you can upload your research paper with your recorded voice or you can utilize chargeable services of our professional RJs to record your paper in their voice on request.



The FARSS member also entitled to get the benefits of free research podcasting of their research documents through video clips. We can also streamline your conference videos and display your slides/ online slides and online research video clips at reasonable charges, on request.





The FARSS is eligible to earn from sales proceeds of his/her researches/reference/review Books or literature, while publishing with Global Journals. The FARSS can decide whether he/she would like to publish his/her research in a closed manner. In this case, whenever readers purchase that individual research paper for reading, maximum 60% of its profit earned as royalty by Global Journals, will be credited to his/her bank account. The entire entitled amount will be credited to his/her bank account exceeding limit of minimum fixed balance. There is no minimum time limit for collection. The FARSS member can decide its price and we can help in making the right decision.

The FARSS member is eligible to join as a paid peer reviewer at Global Journals Incorporation (USA) and can get remuneration of 15% of author fees, taken from the author of a respective paper. After reviewing 5 or more papers you can request to transfer the amount to your bank account.



MEMBER OF ASSOCIATION OF RESEARCH SOCIETY IN SCIENCE (MARSS)

The ' MARSS ' title is accorded to a selected professional after the approval of the Editor-in-Chief / Editorial Board Members/Dean.

The “MARSS” is a dignified ornament which is accorded to a person’s name viz. Dr. John E. Hall, Ph.D., MARSS or William Walldroff, M.S., MARSS.



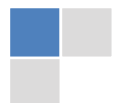
MARSS accrediting is an honor. It authenticates your research activities. After becoming MARSS, you can add 'MARSS' title with your name as you use this recognition as additional suffix to your status. This will definitely enhance and add more value and repute to your name. You may use it on your professional Counseling Materials such as CV, Resume, Visiting Card and Name Plate etc.

The following benefits can be availed by you only for next three years from the date of certification.



MARSS designated members are entitled to avail a 25% discount while publishing their research papers (of a single author) in Global Journals Inc., if the same is accepted by our Editorial Board and Peer Reviewers. If you are a main author or co-author of a group of authors, you will get discount of 10%.

As MARSS, you will be given a renowned, secure and free professional email address with 30 GB of space e.g. johnhall@globaljournals.org. This will include Webmail, Spam Assassin, Email Forwarders, Auto-Responders, Email Delivery Route tracing, etc.





We shall provide you intimation regarding launching of e-version of journal of your stream time to time. This may be utilized in your library for the enrichment of knowledge of your students as well as it can also be helpful for the concerned faculty members.



The MARSS member can apply for approval, grading and certification of standards of their educational and Institutional Degrees to Open Association of Research, Society U.S.A.



Once you are designated as MARSS, you may send us a scanned copy of all of your credentials. OARS will verify, grade and certify them. This will be based on your academic records, quality of research papers published by you, and some more criteria.

It is mandatory to read all terms and conditions carefully.



AUXILIARY MEMBERSHIPS

Institutional Fellow of Global Journals Incorporation (USA)-OARS (USA)

Global Journals Incorporation (USA) is accredited by Open Association of Research Society, U.S.A (OARS) and in turn, affiliates research institutions as “Institutional Fellow of Open Association of Research Society” (IFOARS).



The “FARSC” is a dignified title which is accorded to a person’s name viz. Dr. John E. Hall, Ph.D., FARSC or William Walldroff, M.S., FARSC.

The IFOARS institution is entitled to form a Board comprised of one Chairperson and three to five board members preferably from different streams. The Board will be recognized as “Institutional Board of Open Association of Research Society”-(IBOARS).

The Institute will be entitled to following benefits:



The IBOARS can initially review research papers of their institute and recommend them to publish with respective journal of Global Journals. It can also review the papers of other institutions after obtaining our consent. The second review will be done by peer reviewer of Global Journals Incorporation (USA) The Board is at liberty to appoint a peer reviewer with the approval of chairperson after consulting us.

The author fees of such paper may be waived off up to 40%.

The Global Journals Incorporation (USA) at its discretion can also refer double blind peer reviewed paper at their end to the board for the verification and to get recommendation for final stage of acceptance of publication.

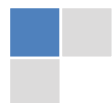


The IBOARS can organize symposium/seminar/conference in their country on behalf of Global Journals Incorporation (USA)-OARS (USA). The terms and conditions can be discussed separately.

The Board can also play vital role by exploring and giving valuable suggestions regarding the Standards of “Open Association of Research Society, U.S.A (OARS)” so that proper amendment can take place for the benefit of entire research community. We shall provide details of particular standard only on receipt of request from the Board.



The board members can also join us as Individual Fellow with 40% discount on total fees applicable to Individual Fellow. They will be entitled to avail all the benefits as declared. Please visit Individual Fellow-sub menu of GlobalJournals.org to have more relevant details.



We shall provide you intimation regarding launching of e-version of journal of your stream time to time. This may be utilized in your library for the enrichment of knowledge of your students as well as it can also be helpful for the concerned faculty members.



After nomination of your institution as “Institutional Fellow” and constantly functioning successfully for one year, we can consider giving recognition to your institute to function as Regional/Zonal office on our behalf. The board can also take up the additional allied activities for betterment after our consultation.

The following entitlements are applicable to individual Fellows:

Open Association of Research Society, U.S.A (OARS) By-laws states that an individual Fellow may use the designations as applicable, or the corresponding initials. The Credentials of individual Fellow and Associate designations signify that the individual has gained knowledge of the fundamental concepts. One is magnanimous and proficient in an expertise course covering the professional code of conduct, and follows recognized standards of practice.



Open Association of Research Society (US)/ Global Journals Incorporation (USA), as described in Corporate Statements, are educational, research publishing and professional membership organizations. Achieving our individual Fellow or Associate status is based mainly on meeting stated educational research requirements.

Disbursement of 40% Royalty earned through Global Journals : Researcher = 50%, Peer Reviewer = 37.50%, Institution = 12.50% E.g. Out of 40%, the 20% benefit should be passed on to researcher, 15 % benefit towards remuneration should be given to a reviewer and remaining 5% is to be retained by the institution.



We shall provide print version of 12 issues of any three journals [as per your requirement] out of our 38 journals worth \$ 2376 USD.

Other:

The individual Fellow and Associate designations accredited by Open Association of Research Society (US) credentials signify guarantees following achievements:

- The professional accredited with Fellow honor, is entitled to various benefits viz. name, fame, honor, regular flow of income, secured bright future, social status etc.



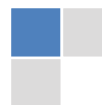
- In addition to above, if one is single author, then entitled to 40% discount on publishing research paper and can get 10% discount if one is co-author or main author among group of authors.
- The Fellow can organize symposium/seminar/conference on behalf of Global Journals Incorporation (USA) and he/she can also attend the same organized by other institutes on behalf of Global Journals.
- The Fellow can become member of Editorial Board Member after completing 3yrs.
- The Fellow can earn 60% of sales proceeds from the sale of reference/review books/literature/publishing of research paper.
- Fellow can also join as paid peer reviewer and earn 15% remuneration of author charges and can also get an opportunity to join as member of the Editorial Board of Global Journals Incorporation (USA)
- • This individual has learned the basic methods of applying those concepts and techniques to common challenging situations. This individual has further demonstrated an in-depth understanding of the application of suitable techniques to a particular area of research practice.

Note :

//

- In future, if the board feels the necessity to change any board member, the same can be done with the consent of the chairperson along with anyone board member without our approval.
- In case, the chairperson needs to be replaced then consent of 2/3rd board members are required and they are also required to jointly pass the resolution copy of which should be sent to us. In such case, it will be compulsory to obtain our approval before replacement.
- In case of “Difference of Opinion [if any]” among the Board members, our decision will be final and binding to everyone.

//



PROCESS OF SUBMISSION OF RESEARCH PAPER

The Area or field of specialization may or may not be of any category as mentioned in 'Scope of Journal' menu of the GlobalJournals.org website. There are 37 Research Journal categorized with Six parental Journals GJCST, GJMR, GJRE, GJMBR, GJSFR, GJHSS. For Authors should prefer the mentioned categories. There are three widely used systems UDC, DDC and LCC. The details are available as 'Knowledge Abstract' at Home page. The major advantage of this coding is that, the research work will be exposed to and shared with all over the world as we are being abstracted and indexed worldwide.

The paper should be in proper format. The format can be downloaded from first page of 'Author Guideline' Menu. The Author is expected to follow the general rules as mentioned in this menu. The paper should be written in MS-Word Format (*.DOC,*.DOCX).

The Author can submit the paper either online or offline. The authors should prefer online submission.Online Submission: There are three ways to submit your paper:

(A) (I) First, register yourself using top right corner of Home page then Login. If you are already registered, then login using your username and password.

(II) Choose corresponding Journal.

(III) Click 'Submit Manuscript'. Fill required information and Upload the paper.

(B) If you are using Internet Explorer, then Direct Submission through Homepage is also available.

(C) If these two are not convenient, and then email the paper directly to dean@globaljournals.org.

Offline Submission: Author can send the typed form of paper by Post. However, online submission should be preferred.

PREFERRED AUTHOR GUIDELINES

MANUSCRIPT STYLE INSTRUCTION (Must be strictly followed)

Page Size: 8.27" X 11"

- Left Margin: 0.65
- Right Margin: 0.65
- Top Margin: 0.75
- Bottom Margin: 0.75
- Font type of all text should be Swis 721 Lt BT.
- Paper Title should be of Font Size 24 with one Column section.
- Author Name in Font Size of 11 with one column as of Title.
- Abstract Font size of 9 Bold, "Abstract" word in Italic Bold.
- Main Text: Font size 10 with justified two columns section
- Two Column with Equal Column with of 3.38 and Gaping of .2
- First Character must be three lines Drop capped.
- Paragraph before Spacing of 1 pt and After of 0 pt.
- Line Spacing of 1 pt
- Large Images must be in One Column
- Numbering of First Main Headings (Heading 1) must be in Roman Letters, Capital Letter, and Font Size of 10.
- Numbering of Second Main Headings (Heading 2) must be in Alphabets, Italic, and Font Size of 10.

You can use your own standard format also.

Author Guidelines:

1. General,
2. Ethical Guidelines,
3. Submission of Manuscripts,
4. Manuscript's Category,
5. Structure and Format of Manuscript,
6. After Acceptance.

1. GENERAL

Before submitting your research paper, one is advised to go through the details as mentioned in following heads. It will be beneficial, while peer reviewer justify your paper for publication.

Scope

The Global Journals Inc. (US) welcome the submission of original paper, review paper, survey article relevant to the all the streams of Philosophy and knowledge. The Global Journals Inc. (US) is parental platform for Global Journal of Computer Science and Technology, Researches in Engineering, Medical Research, Science Frontier Research, Human Social Science, Management, and Business organization. The choice of specific field can be done otherwise as following in Abstracting and Indexing Page on this Website. As the all Global

Journals Inc. (US) are being abstracted and indexed (in process) by most of the reputed organizations. Topics of only narrow interest will not be accepted unless they have wider potential or consequences.

2. ETHICAL GUIDELINES

Authors should follow the ethical guidelines as mentioned below for publication of research paper and research activities.

Papers are accepted on strict understanding that the material in whole or in part has not been, nor is being, considered for publication elsewhere. If the paper once accepted by Global Journals Inc. (US) and Editorial Board, will become the copyright of the Global Journals Inc. (US).

Authorship: The authors and coauthors should have active contribution to conception design, analysis and interpretation of findings. They should critically review the contents and drafting of the paper. All should approve the final version of the paper before submission

The Global Journals Inc. (US) follows the definition of authorship set up by the Global Academy of Research and Development. According to the Global Academy of R&D authorship, criteria must be based on:

- 1) Substantial contributions to conception and acquisition of data, analysis and interpretation of the findings.
- 2) Drafting the paper and revising it critically regarding important academic content.
- 3) Final approval of the version of the paper to be published.

All authors should have been credited according to their appropriate contribution in research activity and preparing paper. Contributors who do not match the criteria as authors may be mentioned under Acknowledgement.

Acknowledgements: Contributors to the research other than authors credited should be mentioned under acknowledgement. The specifications of the source of funding for the research if appropriate can be included. Suppliers of resources may be mentioned along with address.

Appeal of Decision: The Editorial Board's decision on publication of the paper is final and cannot be appealed elsewhere.

Permissions: It is the author's responsibility to have prior permission if all or parts of earlier published illustrations are used in this paper.

Please mention proper reference and appropriate acknowledgements wherever expected.

If all or parts of previously published illustrations are used, permission must be taken from the copyright holder concerned. It is the author's responsibility to take these in writing.

Approval for reproduction/modification of any information (including figures and tables) published elsewhere must be obtained by the authors/copyright holders before submission of the manuscript. Contributors (Authors) are responsible for any copyright fee involved.

3. SUBMISSION OF MANUSCRIPTS

Manuscripts should be uploaded via this online submission page. The online submission is most efficient method for submission of papers, as it enables rapid distribution of manuscripts and consequently speeds up the review procedure. It also enables authors to know the status of their own manuscripts by emailing us. Complete instructions for submitting a paper is available below.

Manuscript submission is a systematic procedure and little preparation is required beyond having all parts of your manuscript in a given format and a computer with an Internet connection and a Web browser. Full help and instructions are provided on-screen. As an author, you will be prompted for login and manuscript details as Field of Paper and then to upload your manuscript file(s) according to the instructions.



To avoid postal delays, all transaction is preferred by e-mail. A finished manuscript submission is confirmed by e-mail immediately and your paper enters the editorial process with no postal delays. When a conclusion is made about the publication of your paper by our Editorial Board, revisions can be submitted online with the same procedure, with an occasion to view and respond to all comments.

Complete support for both authors and co-author is provided.

4. MANUSCRIPT'S CATEGORY

Based on potential and nature, the manuscript can be categorized under the following heads:

Original research paper: Such papers are reports of high-level significant original research work.

Review papers: These are concise, significant but helpful and decisive topics for young researchers.

Research articles: These are handled with small investigation and applications

Research letters: The letters are small and concise comments on previously published matters.

5. STRUCTURE AND FORMAT OF MANUSCRIPT

The recommended size of original research paper is less than seven thousand words, review papers fewer than seven thousands words also. Preparation of research paper or how to write research paper, are major hurdle, while writing manuscript. The research articles and research letters should be fewer than three thousand words, the structure original research paper; sometime review paper should be as follows:

Papers: These are reports of significant research (typically less than 7000 words equivalent, including tables, figures, references), and comprise:

(a) Title should be relevant and commensurate with the theme of the paper.

(b) A brief Summary, "Abstract" (less than 150 words) containing the major results and conclusions.

(c) Up to ten keywords, that precisely identifies the paper's subject, purpose, and focus.

(d) An Introduction, giving necessary background excluding subheadings; objectives must be clearly declared.

(e) Resources and techniques with sufficient complete experimental details (wherever possible by reference) to permit repetition; sources of information must be given and numerical methods must be specified by reference, unless non-standard.

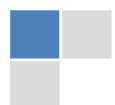
(f) Results should be presented concisely, by well-designed tables and/or figures; the same data may not be used in both; suitable statistical data should be given. All data must be obtained with attention to numerical detail in the planning stage. As reproduced design has been recognized to be important to experiments for a considerable time, the Editor has decided that any paper that appears not to have adequate numerical treatments of the data will be returned un-refereed;

(g) Discussion should cover the implications and consequences, not just recapitulating the results; conclusions should be summarizing.

(h) Brief Acknowledgements.

(i) References in the proper form.

Authors should very cautiously consider the preparation of papers to ensure that they communicate efficiently. Papers are much more likely to be accepted, if they are cautiously designed and laid out, contain few or no errors, are summarizing, and be conventional to the approach and instructions. They will in addition, be published with much less delays than those that require much technical and editorial correction.



The Editorial Board reserves the right to make literary corrections and to make suggestions to improve brevity.

It is vital, that authors take care in submitting a manuscript that is written in simple language and adheres to published guidelines.

Format

Language: The language of publication is UK English. Authors, for whom English is a second language, must have their manuscript efficiently edited by an English-speaking person before submission to make sure that, the English is of high excellence. It is preferable, that manuscripts should be professionally edited.

Standard Usage, Abbreviations, and Units: Spelling and hyphenation should be conventional to The Concise Oxford English Dictionary. Statistics and measurements should at all times be given in figures, e.g. 16 min, except for when the number begins a sentence. When the number does not refer to a unit of measurement it should be spelt in full unless, it is 160 or greater.

Abbreviations supposed to be used carefully. The abbreviated name or expression is supposed to be cited in full at first usage, followed by the conventional abbreviation in parentheses.

Metric SI units are supposed to generally be used excluding where they conflict with current practice or are confusing. For illustration, 1.4 l rather than $1.4 \times 10^{-3} \text{ m}^3$, or 4 mm somewhat than $4 \times 10^{-3} \text{ m}$. Chemical formula and solutions must identify the form used, e.g. anhydrous or hydrated, and the concentration must be in clearly defined units. Common species names should be followed by underlines at the first mention. For following use the generic name should be constricted to a single letter, if it is clear.

Structure

All manuscripts submitted to Global Journals Inc. (US), ought to include:

Title: The title page must carry an instructive title that reflects the content, a running title (less than 45 characters together with spaces), names of the authors and co-authors, and the place(s) wherever the work was carried out. The full postal address in addition with the e-mail address of related author must be given. Up to eleven keywords or very brief phrases have to be given to help data retrieval, mining and indexing.

Abstract, used in Original Papers and Reviews:

Optimizing Abstract for Search Engines

Many researchers searching for information online will use search engines such as Google, Yahoo or similar. By optimizing your paper for search engines, you will amplify the chance of someone finding it. This in turn will make it more likely to be viewed and/or cited in a further work. Global Journals Inc. (US) have compiled these guidelines to facilitate you to maximize the web-friendliness of the most public part of your paper.

Key Words

A major linchpin in research work for the writing research paper is the keyword search, which one will employ to find both library and Internet resources.

One must be persistent and creative in using keywords. An effective keyword search requires a strategy and planning a list of possible keywords and phrases to try.

Search engines for most searches, use Boolean searching, which is somewhat different from Internet searches. The Boolean search uses "operators," words (and, or, not, and near) that enable you to expand or narrow your affords. Tips for research paper while preparing research paper are very helpful guideline of research paper.

Choice of key words is first tool of tips to write research paper. Research paper writing is an art. A few tips for deciding as strategically as possible about keyword search:



- One should start brainstorming lists of possible keywords before even begin searching. Think about the most important concepts related to research work. Ask, "What words would a source have to include to be truly valuable in research paper?" Then consider synonyms for the important words.
- It may take the discovery of only one relevant paper to let steer in the right keyword direction because in most databases, the keywords under which a research paper is abstracted are listed with the paper.
- One should avoid outdated words.

Keywords are the key that opens a door to research work sources. Keyword searching is an art in which researcher's skills are bound to improve with experience and time.

Numerical Methods: Numerical methods used should be clear and, where appropriate, supported by references.

Acknowledgements: Please make these as concise as possible.

References

References follow the Harvard scheme of referencing. References in the text should cite the authors' names followed by the time of their publication, unless there are three or more authors when simply the first author's name is quoted followed by et al. unpublished work has to only be cited where necessary, and only in the text. Copies of references in press in other journals have to be supplied with submitted typescripts. It is necessary that all citations and references be carefully checked before submission, as mistakes or omissions will cause delays.

References to information on the World Wide Web can be given, but only if the information is available without charge to readers on an official site. Wikipedia and Similar websites are not allowed where anyone can change the information. Authors will be asked to make available electronic copies of the cited information for inclusion on the Global Journals Inc. (US) homepage at the judgment of the Editorial Board.

The Editorial Board and Global Journals Inc. (US) recommend that, citation of online-published papers and other material should be done via a DOI (digital object identifier). If an author cites anything, which does not have a DOI, they run the risk of the cited material not being noticeable.

The Editorial Board and Global Journals Inc. (US) recommend the use of a tool such as Reference Manager for reference management and formatting.

Tables, Figures and Figure Legends

Tables: Tables should be few in number, cautiously designed, uncrowned, and include only essential data. Each must have an Arabic number, e.g. Table 4, a self-explanatory caption and be on a separate sheet. Vertical lines should not be used.

Figures: Figures are supposed to be submitted as separate files. Always take in a citation in the text for each figure using Arabic numbers, e.g. Fig. 4. Artwork must be submitted online in electronic form by e-mailing them.

Preparation of Electronic Figures for Publication

Even though low quality images are sufficient for review purposes, print publication requires high quality images to prevent the final product being blurred or fuzzy. Submit (or e-mail) EPS (line art) or TIFF (halftone/photographs) files only. MS PowerPoint and Word Graphics are unsuitable for printed pictures. Do not use pixel-oriented software. Scans (TIFF only) should have a resolution of at least 350 dpi (halftone) or 700 to 1100 dpi (line drawings) in relation to the imitation size. Please give the data for figures in black and white or submit a Color Work Agreement Form. EPS files must be saved with fonts embedded (and with a TIFF preview, if possible).

For scanned images, the scanning resolution (at final image size) ought to be as follows to ensure good reproduction: line art: >650 dpi; halftones (including gel photographs) : >350 dpi; figures containing both halftone and line images: >650 dpi.



Color Charges: It is the rule of the Global Journals Inc. (US) for authors to pay the full cost for the reproduction of their color artwork. Hence, please note that, if there is color artwork in your manuscript when it is accepted for publication, we would require you to complete and return a color work agreement form before your paper can be published.

Figure Legends: Self-explanatory legends of all figures should be incorporated separately under the heading 'Legends to Figures'. In the full-text online edition of the journal, figure legends may possibly be truncated in abbreviated links to the full screen version. Therefore, the first 100 characters of any legend should notify the reader, about the key aspects of the figure.

6. AFTER ACCEPTANCE

Upon approval of a paper for publication, the manuscript will be forwarded to the dean, who is responsible for the publication of the Global Journals Inc. (US).

6.1 Proof Corrections

The corresponding author will receive an e-mail alert containing a link to a website or will be attached. A working e-mail address must therefore be provided for the related author.

Acrobat Reader will be required in order to read this file. This software can be downloaded

(Free of charge) from the following website:

www.adobe.com/products/acrobat/readstep2.html. This will facilitate the file to be opened, read on screen, and printed out in order for any corrections to be added. Further instructions will be sent with the proof.

Proofs must be returned to the dean at dean@globaljournals.org within three days of receipt.

As changes to proofs are costly, we inquire that you only correct typesetting errors. All illustrations are retained by the publisher. Please note that the authors are responsible for all statements made in their work, including changes made by the copy editor.

6.2 Early View of Global Journals Inc. (US) (Publication Prior to Print)

The Global Journals Inc. (US) are enclosed by our publishing's Early View service. Early View articles are complete full-text articles sent in advance of their publication. Early View articles are absolute and final. They have been completely reviewed, revised and edited for publication, and the authors' final corrections have been incorporated. Because they are in final form, no changes can be made after sending them. The nature of Early View articles means that they do not yet have volume, issue or page numbers, so Early View articles cannot be cited in the conventional way.

6.3 Author Services

Online production tracking is available for your article through Author Services. Author Services enables authors to track their article - once it has been accepted - through the production process to publication online and in print. Authors can check the status of their articles online and choose to receive automated e-mails at key stages of production. The authors will receive an e-mail with a unique link that enables them to register and have their article automatically added to the system. Please ensure that a complete e-mail address is provided when submitting the manuscript.

6.4 Author Material Archive Policy

Please note that if not specifically requested, publisher will dispose off hardcopy & electronic information submitted, after the two months of publication. If you require the return of any information submitted, please inform the Editorial Board or dean as soon as possible.

6.5 Offprint and Extra Copies

A PDF offprint of the online-published article will be provided free of charge to the related author, and may be distributed according to the Publisher's terms and conditions. Additional paper offprint may be ordered by emailing us at: editor@globaljournals.org .



Before start writing a good quality Computer Science Research Paper, let us first understand what is Computer Science Research Paper? So, Computer Science Research Paper is the paper which is written by professionals or scientists who are associated to Computer Science and Information Technology, or doing research study in these areas. If you are novel to this field then you can consult about this field from your supervisor or guide.

TECHNIQUES FOR WRITING A GOOD QUALITY RESEARCH PAPER:

1. Choosing the topic: In most cases, the topic is searched by the interest of author but it can be also suggested by the guides. You can have several topics and then you can judge that in which topic or subject you are finding yourself most comfortable. This can be done by asking several questions to yourself, like Will I be able to carry our search in this area? Will I find all necessary recourses to accomplish the search? Will I be able to find all information in this field area? If the answer of these types of questions will be "Yes" then you can choose that topic. In most of the cases, you may have to conduct the surveys and have to visit several places because this field is related to Computer Science and Information Technology. Also, you may have to do a lot of work to find all rise and falls regarding the various data of that subject. Sometimes, detailed information plays a vital role, instead of short information.

2. Evaluators are human: First thing to remember that evaluators are also human being. They are not only meant for rejecting a paper. They are here to evaluate your paper. So, present your Best.

3. Think Like Evaluators: If you are in a confusion or getting demotivated that your paper will be accepted by evaluators or not, then think and try to evaluate your paper like an Evaluator. Try to understand that what an evaluator wants in your research paper and automatically you will have your answer.

4. Make blueprints of paper: The outline is the plan or framework that will help you to arrange your thoughts. It will make your paper logical. But remember that all points of your outline must be related to the topic you have chosen.

5. Ask your Guides: If you are having any difficulty in your research, then do not hesitate to share your difficulty to your guide (if you have any). They will surely help you out and resolve your doubts. If you can't clarify what exactly you require for your work then ask the supervisor to help you with the alternative. He might also provide you the list of essential readings.

6. Use of computer is recommended: As you are doing research in the field of Computer Science, then this point is quite obvious.

7. Use right software: Always use good quality software packages. If you are not capable to judge good software then you can lose quality of your paper unknowingly. There are various software programs available to help you, which you can get through Internet.

8. Use the Internet for help: An excellent start for your paper can be by using the Google. It is an excellent search engine, where you can have your doubts resolved. You may also read some answers for the frequent question how to write my research paper or find model research paper. From the internet library you can download books. If you have all required books make important reading selecting and analyzing the specified information. Then put together research paper sketch out.

9. Use and get big pictures: Always use encyclopedias, Wikipedia to get pictures so that you can go into the depth.

10. Bookmarks are useful: When you read any book or magazine, you generally use bookmarks, right! It is a good habit, which helps to not to lose your continuity. You should always use bookmarks while searching on Internet also, which will make your search easier.

11. Revise what you wrote: When you write anything, always read it, summarize it and then finalize it.



12. Make all efforts: Make all efforts to mention what you are going to write in your paper. That means always have a good start. Try to mention everything in introduction, that what is the need of a particular research paper. Polish your work by good skill of writing and always give an evaluator, what he wants.

13. Have backups: When you are going to do any important thing like making research paper, you should always have backup copies of it either in your computer or in paper. This will help you to not to lose any of your important.

14. Produce good diagrams of your own: Always try to include good charts or diagrams in your paper to improve quality. Using several and unnecessary diagrams will degrade the quality of your paper by creating "hotchpotch." So always, try to make and include those diagrams, which are made by your own to improve readability and understandability of your paper.

15. Use of direct quotes: When you do research relevant to literature, history or current affairs then use of quotes become essential but if study is relevant to science then use of quotes is not preferable.

16. Use proper verb tense: Use proper verb tenses in your paper. Use past tense, to present those events that happened. Use present tense to indicate events that are going on. Use future tense to indicate future happening events. Use of improper and wrong tenses will confuse the evaluator. Avoid the sentences that are incomplete.

17. Never use online paper: If you are getting any paper on Internet, then never use it as your research paper because it might be possible that evaluator has already seen it or maybe it is outdated version.

18. Pick a good study spot: To do your research studies always try to pick a spot, which is quiet. Every spot is not for studies. Spot that suits you choose it and proceed further.

19. Know what you know: Always try to know, what you know by making objectives. Else, you will be confused and cannot achieve your target.

20. Use good quality grammar: Always use a good quality grammar and use words that will throw positive impact on evaluator. Use of good quality grammar does not mean to use tough words, that for each word the evaluator has to go through dictionary. Do not start sentence with a conjunction. Do not fragment sentences. Eliminate one-word sentences. Ignore passive voice. Do not ever use a big word when a diminutive one would suffice. Verbs have to be in agreement with their subjects. Prepositions are not expressions to finish sentences with. It is incorrect to ever divide an infinitive. Avoid clichés like the disease. Also, always shun irritating alliteration. Use language that is simple and straight forward. put together a neat summary.

21. Arrangement of information: Each section of the main body should start with an opening sentence and there should be a changeover at the end of the section. Give only valid and powerful arguments to your topic. You may also maintain your arguments with records.

22. Never start in last minute: Always start at right time and give enough time to research work. Leaving everything to the last minute will degrade your paper and spoil your work.

23. Multitasking in research is not good: Doing several things at the same time proves bad habit in case of research activity. Research is an area, where everything has a particular time slot. Divide your research work in parts and do particular part in particular time slot.

24. Never copy others' work: Never copy others' work and give it your name because if evaluator has seen it anywhere you will be in trouble.

25. Take proper rest and food: No matter how many hours you spend for your research activity, if you are not taking care of your health then all your efforts will be in vain. For a quality research, study is must, and this can be done by taking proper rest and food.

26. Go for seminars: Attend seminars if the topic is relevant to your research area. Utilize all your resources.



27. Refresh your mind after intervals: Try to give rest to your mind by listening to soft music or by sleeping in intervals. This will also improve your memory.

28. Make colleagues: Always try to make colleagues. No matter how sharper or intelligent you are, if you make colleagues you can have several ideas, which will be helpful for your research.

29. Think technically: Always think technically. If anything happens, then search its reasons, its benefits, and demerits.

30. Think and then print: When you will go to print your paper, notice that tables are not be split, headings are not detached from their descriptions, and page sequence is maintained.

31. Adding unnecessary information: Do not add unnecessary information, like, I have used MS Excel to draw graph. Do not add irrelevant and inappropriate material. These all will create superfluous. Foreign terminology and phrases are not apropos. One should NEVER take a broad view. Analogy in script is like feathers on a snake. Not at all use a large word when a very small one would be sufficient. Use words properly, regardless of how others use them. Remove quotations. Puns are for kids, not grunt readers. Amplification is a billion times of inferior quality than sarcasm.

32. Never oversimplify everything: To add material in your research paper, never go for oversimplification. This will definitely irritate the evaluator. Be more or less specific. Also too, by no means, ever use rhythmic redundancies. Contractions aren't essential and shouldn't be there used. Comparisons are as terrible as clichés. Give up ampersands and abbreviations, and so on. Remove commas, that are, not necessary. Parenthetical words however should be together with this in commas. Understatement is all the time the complete best way to put onward earth-shaking thoughts. Give a detailed literary review.

33. Report concluded results: Use concluded results. From raw data, filter the results and then conclude your studies based on measurements and observations taken. Significant figures and appropriate number of decimal places should be used. Parenthetical remarks are prohibitive. Proofread carefully at final stage. In the end give outline to your arguments. Spot out perspectives of further study of this subject. Justify your conclusion by at the bottom of them with sufficient justifications and examples.

34. After conclusion: Once you have concluded your research, the next most important step is to present your findings. Presentation is extremely important as it is the definite medium through which your research is going to be in print to the rest of the crowd. Care should be taken to categorize your thoughts well and present them in a logical and neat manner. A good quality research paper format is essential because it serves to highlight your research paper and bring to light all necessary aspects in your research.

INFORMAL GUIDELINES OF RESEARCH PAPER WRITING

Key points to remember:

- Submit all work in its final form.
- Write your paper in the form, which is presented in the guidelines using the template.
- Please note the criterion for grading the final paper by peer-reviewers.

Final Points:

A purpose of organizing a research paper is to let people to interpret your effort selectively. The journal requires the following sections, submitted in the order listed, each section to start on a new page.

The introduction will be compiled from reference matter and will reflect the design processes or outline of basis that direct you to make study. As you will carry out the process of study, the method and process section will be constructed as like that. The result segment will show related statistics in nearly sequential order and will direct the reviewers next to the similar intellectual paths throughout the data that you took to carry out your study. The discussion section will provide understanding of the data and projections as to the implication of the results. The use of good quality references all through the paper will give the effort trustworthiness by representing an alertness of prior workings.



Writing a research paper is not an easy job no matter how trouble-free the actual research or concept. Practice, excellent preparation, and controlled record keeping are the only means to make straightforward the progression.

General style:

Specific editorial column necessities for compliance of a manuscript will always take over from directions in these general guidelines.

To make a paper clear

- Adhere to recommended page limits

Mistakes to evade

- Insertion a title at the foot of a page with the subsequent text on the next page
- Separating a table/chart or figure - impound each figure/table to a single page
- Submitting a manuscript with pages out of sequence

In every sections of your document

- Use standard writing style including articles ("a", "the," etc.)
- Keep on paying attention on the research topic of the paper
- Use paragraphs to split each significant point (excluding for the abstract)
- Align the primary line of each section
- Present your points in sound order
- Use present tense to report well accepted
- Use past tense to describe specific results
- Shun familiar wording, don't address the reviewer directly, and don't use slang, slang language, or superlatives
- Shun use of extra pictures - include only those figures essential to presenting results

Title Page:

Choose a revealing title. It should be short. It should not have non-standard acronyms or abbreviations. It should not exceed two printed lines. It should include the name(s) and address (es) of all authors.



Abstract:

The summary should be two hundred words or less. It should briefly and clearly explain the key findings reported in the manuscript-- must have precise statistics. It should not have abnormal acronyms or abbreviations. It should be logical in itself. Shun citing references at this point.

An abstract is a brief distinct paragraph summary of finished work or work in development. In a minute or less a reviewer can be taught the foundation behind the study, common approach to the problem, relevant results, and significant conclusions or new questions.

Write your summary when your paper is completed because how can you write the summary of anything which is not yet written? Wealth of terminology is very essential in abstract. Yet, use comprehensive sentences and do not let go readability for brevity. You can maintain it succinct by phrasing sentences so that they provide more than lone rationale. The author can at this moment go straight to shortening the outcome. Sum up the study, with the subsequent elements in any summary. Try to maintain the initial two items to no more than one ruling each.

- Reason of the study - theory, overall issue, purpose
- Fundamental goal
- To the point depiction of the research
- Consequences, including definite statistics - if the consequences are quantitative in nature, account quantitative data; results of any numerical analysis should be reported
- Significant conclusions or questions that track from the research(es)

Approach:

- Single section, and succinct
- As an outline of job done, it is always written in past tense
- A conceptual should situate on its own, and not submit to any other part of the paper such as a form or table
- Center on shortening results - bound background information to a verdict or two, if completely necessary
- What you account in an abstract must be regular with what you reported in the manuscript
- Exact spelling, clearness of sentences and phrases, and appropriate reporting of quantities (proper units, important statistics) are just as significant in an abstract as they are anywhere else

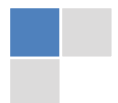
Introduction:

The **Introduction** should "introduce" the manuscript. The reviewer should be presented with sufficient background information to be capable to comprehend and calculate the purpose of your study without having to submit to other works. The basis for the study should be offered. Give most important references but shun difficult to make a comprehensive appraisal of the topic. In the introduction, describe the problem visibly. If the problem is not acknowledged in a logical, reasonable way, the reviewer will have no attention in your result. Speak in common terms about techniques used to explain the problem, if needed, but do not present any particulars about the protocols here. Following approach can create a valuable beginning:

- Explain the value (significance) of the study
- Shield the model - why did you employ this particular system or method? What is its compensation? You strength remark on its appropriateness from a abstract point of vision as well as point out sensible reasons for using it.
- Present a justification. Status your particular theory (es) or aim(s), and describe the logic that led you to choose them.
- Very for a short time explain the tentative propose and how it skilled the declared objectives.

Approach:

- Use past tense except for when referring to recognized facts. After all, the manuscript will be submitted after the entire job is done.
- Sort out your thoughts; manufacture one key point with every section. If you make the four points listed above, you will need a least of four paragraphs.



- Present surroundings information only as desirable in order hold up a situation. The reviewer does not desire to read the whole thing you know about a topic.
- Shape the theory/purpose specifically - do not take a broad view.
- As always, give awareness to spelling, simplicity and correctness of sentences and phrases.

Procedures (Methods and Materials):

This part is supposed to be the easiest to carve if you have good skills. A sound written Procedures segment allows a capable scientist to replacement your results. Present precise information about your supplies. The suppliers and clarity of reagents can be helpful bits of information. Present methods in sequential order but linked methodologies can be grouped as a segment. Be concise when relating the protocols. Attempt for the least amount of information that would permit another capable scientist to spare your outcome but be cautious that vital information is integrated. The use of subheadings is suggested and ought to be synchronized with the results section. When a technique is used that has been well described in another object, mention the specific item describing a way but draw the basic principle while stating the situation. The purpose is to text all particular resources and broad procedures, so that another person may use some or all of the methods in one more study or referee the scientific value of your work. It is not to be a step by step report of the whole thing you did, nor is a methods section a set of orders.

Materials:

- Explain materials individually only if the study is so complex that it saves liberty this way.
- Embrace particular materials, and any tools or provisions that are not frequently found in laboratories.
- Do not take in frequently found.
- If use of a definite type of tools.
- Materials may be reported in a part section or else they may be recognized along with your measures.

Methods:

- Report the method (not particulars of each process that engaged the same methodology)
- Describe the method entirely
- To be succinct, present methods under headings dedicated to specific dealings or groups of measures
- Simplify - details how procedures were completed not how they were exclusively performed on a particular day.
- If well known procedures were used, account the procedure by name, possibly with reference, and that's all.

Approach:

- It is embarrassed or not possible to use vigorous voice when documenting methods with no using first person, which would focus the reviewer's interest on the researcher rather than the job. As a result when script up the methods most authors use third person passive voice.
- Use standard style in this and in every other part of the paper - avoid familiar lists, and use full sentences.

What to keep away from

- Resources and methods are not a set of information.
- Skip all descriptive information and surroundings - save it for the argument.
- Leave out information that is immaterial to a third party.

Results:

The principle of a results segment is to present and demonstrate your conclusion. Create this part a entirely objective details of the outcome, and save all understanding for the discussion.

The page length of this segment is set by the sum and types of data to be reported. Carry on to be to the point, by means of statistics and tables, if suitable, to present consequences most efficiently. You must obviously differentiate material that would usually be incorporated in a study editorial from any unprocessed data or additional appendix matter that would not be available. In fact, such matter should not be submitted at all except requested by the instructor.



Content

- Sum up your conclusion in text and demonstrate them, if suitable, with figures and tables.
- In manuscript, explain each of your consequences, point the reader to remarks that are most appropriate.
- Present a background, such as by describing the question that was addressed by creation an exacting study.
- Explain results of control experiments and comprise remarks that are not accessible in a prescribed figure or table, if appropriate.
- Examine your data, then prepare the analyzed (transformed) data in the form of a figure (graph), table, or in manuscript form.

What to stay away from

- Do not discuss or infer your outcome, report surroundings information, or try to explain anything.
- Not at all, take in raw data or intermediate calculations in a research manuscript.
- Do not present the similar data more than once.
- Manuscript should complement any figures or tables, not duplicate the identical information.
- Never confuse figures with tables - there is a difference.

Approach

- As forever, use past tense when you submit to your results, and put the whole thing in a reasonable order.
- Put figures and tables, appropriately numbered, in order at the end of the report
- If you desire, you may place your figures and tables properly within the text of your results part.

Figures and tables

- If you put figures and tables at the end of the details, make certain that they are visibly distinguished from any attach appendix materials, such as raw facts
- Despite of position, each figure must be numbered one after the other and complete with subtitle
- In spite of position, each table must be titled, numbered one after the other and complete with heading
- All figure and table must be adequately complete that it could situate on its own, divide from text

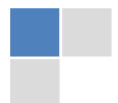
Discussion:

The Discussion is expected the trickiest segment to write and describe. A lot of papers submitted for journal are discarded based on problems with the Discussion. There is no head of state for how long a argument should be. Position your understanding of the outcome visibly to lead the reviewer through your conclusions, and then finish the paper with a summing up of the implication of the study. The purpose here is to offer an understanding of your results and hold up for all of your conclusions, using facts from your research and generally accepted information, if suitable. The implication of result should be visibly described. Infer your data in the conversation in suitable depth. This means that when you clarify an observable fact you must explain mechanisms that may account for the observation. If your results vary from your prospect, make clear why that may have happened. If your results agree, then explain the theory that the proof supported. It is never suitable to just state that the data approved with prospect, and let it drop at that.

- Make a decision if each premise is supported, discarded, or if you cannot make a conclusion with assurance. Do not just dismiss a study or part of a study as "uncertain."
- Research papers are not acknowledged if the work is imperfect. Draw what conclusions you can based upon the results that you have, and take care of the study as a finished work
- You may propose future guidelines, such as how the experiment might be personalized to accomplish a new idea.
- Give details all of your remarks as much as possible, focus on mechanisms.
- Make a decision if the tentative design sufficiently addressed the theory, and whether or not it was correctly restricted.
- Try to present substitute explanations if sensible alternatives be present.
- One research will not counter an overall question, so maintain the large picture in mind, where do you go next? The best studies unlock new avenues of study. What questions remain?
- Recommendations for detailed papers will offer supplementary suggestions.

Approach:

- When you refer to information, differentiate data generated by your own studies from available information
- Submit to work done by specific persons (including you) in past tense.
- Submit to generally acknowledged facts and main beliefs in present tense.



THE ADMINISTRATION RULES

Please carefully note down following rules and regulation before submitting your Research Paper to Global Journals Inc. (US):

Segment Draft and Final Research Paper: You have to strictly follow the template of research paper. If it is not done your paper may get rejected.

- The **major constraint** is that you must independently make all content, tables, graphs, and facts that are offered in the paper. You must write each part of the paper wholly on your own. The Peer-reviewers need to identify your own perceptives of the concepts in your own terms. NEVER extract straight from any foundation, and never rephrase someone else's analysis.
- Do not give permission to anyone else to "PROOFREAD" your manuscript.
- **Methods to avoid Plagiarism is applied by us on every paper, if found guilty, you will be blacklisted by all of our collaborated research groups, your institution will be informed for this and strict legal actions will be taken immediately.)**
- To guard yourself and others from possible illegal use please do not permit anyone right to use to your paper and files.



CRITERION FOR GRADING A RESEARCH PAPER (COMPILATION)
BY GLOBAL JOURNALS INC. (US)

Please note that following table is only a Grading of "Paper Compilation" and not on "Performed/Stated Research" whose grading solely depends on Individual Assigned Peer Reviewer and Editorial Board Member. These can be available only on request and after decision of Paper. This report will be the property of Global Journals Inc. (US).

Topics	Grades		
	A-B	C-D	E-F
<i>Abstract</i>	Clear and concise with appropriate content, Correct format. 200 words or below	Unclear summary and no specific data, Incorrect form Above 200 words	No specific data with ambiguous information Above 250 words
<i>Introduction</i>	Containing all background details with clear goal and appropriate details, flow specification, no grammar and spelling mistake, well organized sentence and paragraph, reference cited	Unclear and confusing data, appropriate format, grammar and spelling errors with unorganized matter	Out of place depth and content, hazy format
<i>Methods and Procedures</i>	Clear and to the point with well arranged paragraph, precision and accuracy of facts and figures, well organized subheads	Difficult to comprehend with embarrassed text, too much explanation but completed	Incorrect and unorganized structure with hazy meaning
<i>Result</i>	Well organized, Clear and specific, Correct units with precision, correct data, well structuring of paragraph, no grammar and spelling mistake	Complete and embarrassed text, difficult to comprehend	Irregular format with wrong facts and figures
<i>Discussion</i>	Well organized, meaningful specification, sound conclusion, logical and concise explanation, highly structured paragraph reference cited	Wordy, unclear conclusion, spurious	Conclusion is not cited, unorganized, difficult to comprehend
<i>References</i>	Complete and correct format, well organized	Beside the point, Incomplete	Wrong format and structuring



INDEX

A

Alterations · 93, 95, 97, 104, 129

E

Eddington · 40, 50

F

Ferromagnetic · 13, 24, 25, 30, 31, 39, 40, 41, 42, 52

G

Giancoly · 4, 53

I

Inconsistence · 4

Interferometry · 6, 36, 44, 52, 53

M

Macroscopic · 2, 4, 6, 31, 34, 46, 96, 118

O

Oscillations · 20, 99, 103

P

Pseudomomentum · 36

U

Unambiguously · 3, 8, 17, 41



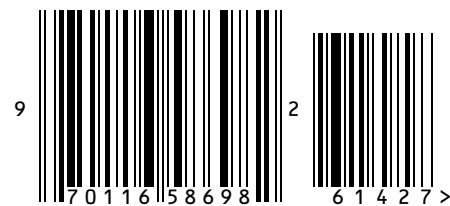
save our planet



Global Journal of Science Frontier Research

Visit us on the Web at www.GlobalJournals.org | www.JournalofScience.org
or email us at helpdesk@globaljournals.org

ISSN 9755896



© Global Journals